# NATIONAL HURRICANE RESEARCH PROJECT

REPORT NO. 38

# On Quantitative Precipitation Forecasting

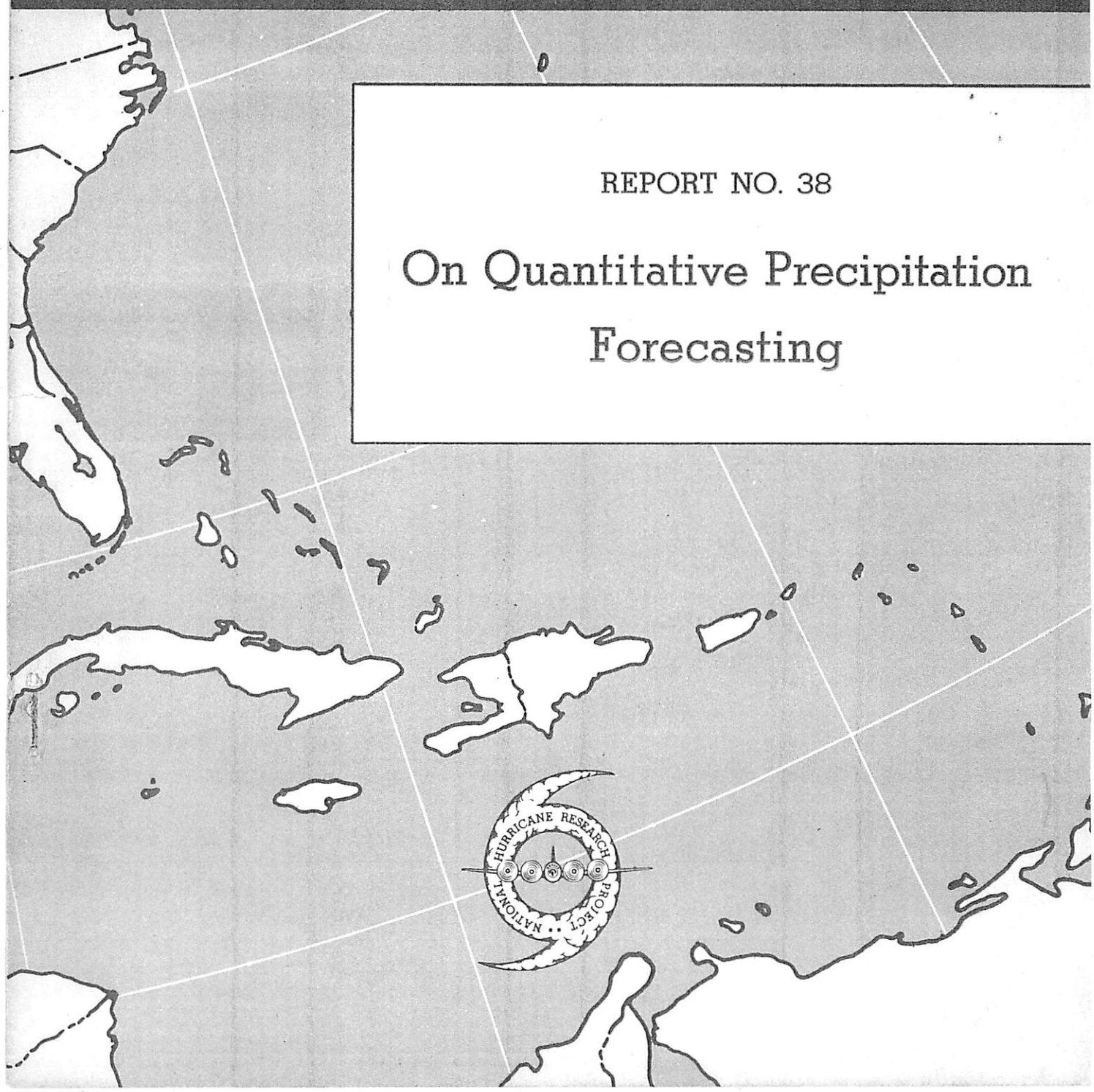

U. S. DEPARTMENT OF COMMERCE
Frederick H. Mueller, Secretary
WEATHER BUREAU
F. W. Reichelderfer, Chief

NATIONAL HURRICANE RESEARCH PROJECT

REPORT NO. 38

# On Quantitative Precipitation Forecasting

by

C. S. Gilman, K. R. Peterson, C. W. Cochrane, and S. Molansky
Hydrologic Services Division, U. S. Weather Bureau

Washington, D. C.
August 1960

## NATIONAL HURRICANE RESEARCH PROJECT REPORTS

Reports by Weather Bureau units, contractors, and cooperators working on the hurricane problem are pre-printed in this series to facilitate immediate distribution of the information among the workers and other interested units. As this limited reproduction and distribution in this form do not constitute formal scientific publication, reference to a paper in the series should identify it as a pre-printed report.

No. 1. Objectives and basic design of the NHRP. March 1956.
No. 2. Numerical weather prediction of hurricane motion. July 1956.
Supplement: Error analysis of prognostic 500-mb. maps made for numerical weather prediction of hurricane motion. March 1957.
No. 3. Rainfall associated with hurricanes. July 1956.
No. 4. Some problems involved in the study of storm surges. December 1956.
No. 5. Survey of meteorological factors pertinent to reduction of loss of life and property in hurricane situations. March 1957.
No. 6. A mean atmosphere for the West Indies area. May 1957.
No. 7. An index of tide gages and tide gage records for the Atlantic and Gulf coasts of the United States. May 1957.
No. 8. Part I. Hurricanes and the sea surface temperature field.
Part II. The exchange of energy between the sea and the atmosphere in relation to hurricane behavior. June 1957.
No. 9. Seasonal variations in the frequency of North Atlantic tropical cyclones related to the general circulation. July 1957.
No.10. Estimating central pressure of tropical cyclones from aircraft data. August 1957.
No.11. Instrumentation of National Hurricane Research Project aircraft. August 1957.
No.12. Studies of hurricane spiral bands as observed on radar. September 1957.
No.13. Mean soundings for the hurricane eye. September 1957.
No.14. On the maximum intensity of hurricanes. December 1957.
No.15. The three-dimensional wind structure around a tropical cyclone. January 1958.
No.16. Modification of hurricanes through cloud seeding. May 1958.
No.17. Analysis of tropical storm Frieda, 1957. A preliminary report. June 1958.
No.18. The use of mean layer winds as a hurricane steering mechanism. June 1958.
No.19. Further examination of the balance of angular momentum in the mature hurricane. July 1958.
No.20. On the energetics of the mature hurricane and other rotating wind systems. July 1958.
No.21. Formation of tropical storms related to anomalies of the long-period mean circulation. September 1958.
No.22. On production of kinetic energy from condensation heating. October 1958.
No.23. Hurricane Audrey storm tide. October 1958.
No.24. Details of circulation in the high energy core of hurricane Carrie. November 1958.
No.25. Distribution of surface friction in hurricanes. November 1958.
No.26. A note on the origin of hurricane radar spiral bands and the echoes which form them. February 1959.
No.27. Proceedings of the Board of Review and Conference on Research Progress. March 1959.
No.28. A model hurricane plan for a coastal community. March 1959.
No.29. Exchange of heat, moisture, and momentum between hurricane Ella (1958) and its environment. April 1959.
No.30. Mean soundings for the Gulf of Mexico area. April 1959.
No.31. On the dynamics and energy transformations in steady-state hurricanes. August 1959.
No.32. An interim hurricane storm surge forecasting guide. August 1959.
No.33. Meteorological considerations pertinent to standard project hurricane, Atlantic and Gulf Coasts of the United States. November 1959.
No.34. Filling and intensity changes in hurricanes over land. November 1959.
No.35. Wind and pressure fields in the stratosphere over the West Indies region in August 1958. December 1959.
No.36. Climatological aspects of intensity of typhoons. February 1960.
No. 37. Unrest in the upper stratosphere over the Caribbean Sea during January 1960. April 1960.

USCOMM-WB-DC

CONTENTS

# ON QUANTITATIVE PRECIPITATION FORECASTING

C. S. Gilman, K. R. Peterson
C. W. Cochrane and S. Molansky

Hydrologic Services Division, U. S. Weather Bureau

## ABSTRACT

A basis for quantitative precipitation forecasting is developed which when combined with synoptic experience, particularly in regard to sea level prognostic charts, enables the preparation of 6- and 24-hour precipitation forecasts. Surface isobaric configurations and dynamic trajectories are used to locate regions of convergence and precipitation. The concept of volumetric control is used to determine specific precipitation amounts.

In Part 1, through theoretical and empirical considerations, it is shown that (1) conditions where cyclonic shear and/or curvature of the geostrophic wind is greater than anticyclonic shear and/or curvature of the real wind are convergence producing; (2) convergence of an air parcel occurs downstream after the parcel encounters a favorable isobaric configuration; and (3) a high percentage of the volume of moisture entering a region of convergence falls as precipitation.

Part 2 is concerned with the development and application of a method of short range (6-hour)precipitation forecasting. Synoptic evidence which supports the results of Part 1 is given. It is brought out that large regions of moist air enter smaller regions of cyclonicity and that these areas of cyclonicity can indicate regions of heavy precipitation. It is further indicated that the present observational network provides a sufficiently detailed analysis to locate closely many precipitation areas.

Part 3 describes the development and field testing of a longer range (24-hour) quantitative precipitation forecasting technique. The results of the field testing further support the hypotheses set forth in Part 1. The results of using day-to-day maps show that sufficiently accurate sea level prognostic charts can be prepared and that the technique can be applied in a short time with enough accuracy to be of synoptic value.

Part 4 describes the development and application of a 6-hour precipitation forecasting technique for hurricanes. Observed sea level pressure maps for past hurricanes were used. The results are encouraging and indicate that the technique is valuable, provided that a reasonably accurate short range forecast of the sea level pressure field can be made. It is generally concluded that the application of the results of Part 1 to 6-hour and 24-hour forecasts shows a considerable degree of skill at quantitative precipitation forecasting.

ACKNOWLEDGMENTS

The authors wish to express their gratitude to Mr. Hugo V. Goodyear of the Hydrometeorological Section for his assistance in the application of dynamic trajectories to precipitation forecasting and for his helpful suggestions throughout the development of the procedures. Thanks are also due the Messrs. Vance A. Myers of Hydrometeorological Section, Jack C. Thompson of the Office of Planning, and Ferdinand C. Bates formerly of Severe Local Storms Research, Kansas City for their review of and helpful suggestions concerning the manuscript. The authors are also indebted to Mr. David F. Templeton, formerly of the Hydrometeorological Section, for his assistance in the numerical solution of the divergence development equation. Thanks go to Mr. Earnest A. Rodney of Forecasts and Synoptic Reports who took part in the field testing of the 24-hour forecasts. Finally, the authors thank the Meteorological Technicians and secretarial staff of the Hydrometeorological Section for assistance throughout the preparation of this report.

# PART 1. PHYSICAL AND EMPIRICAL BASES

C. S. Gilman, K. R. Peterson,
and S. Molansky
Hydrologic Services Division, U. S. Weather Bureau,[1] Washington, D. C.

[Manuscript received January 27, 1959; revised April 13, 1959]

## 1. INTRODUCTION

To forecast precipitation quantitatively it is necessary to estimate, explicitly or implicitly, the vertical motion and the moisture content of the rising air. Most attempts to deal with the problem have attacked these problems directly; the present paper deals with each in a more indirect manner. The vertical motion is not computed explicitly but is inferred from the relationship that it must be associated with large-scale horizontal convergence in the lower atmosphere. The hypothesis is developed that, in many cases, large-scale convergence must be associated with cyclonicity in the isobaric or contour patterns in the lower atmosphere. The problem of where cyclogenesis will occur is approached in two ways: (1) From the contraction of horizontal areas as shown by dynamic trajectories and (2) by numerical integration of the divergence development equation. It turns out, subject to these hypotheses, that the intensities of the cyclonicity can be estimated from the synoptic scale now in use. The moisture is handled volumetrically - that is, the total volume of atmospheric moisture (area times precipitable water) entering a region is related to the volume of rainfall (area times depth) over the region.

## 2. COMPUTATIONS WITH DYNAMIC TRAJECTORIES

Studies by Bjerknes [1] and Petterssen [2] have established that if a current of air blows through a quasi-stationary pressure pattern in which the shear of the geostrophic wind becomes more cyclonic downstream, convergence should tend to develop. Such ideas can be investigated quantitatively by computing dynamic trajectories from the four corners of an original rectangle on a horizontal or constant pressure surface and determining the change of the horizontal area with time. For example, figure 1 shows the dynamic trajectories computed from an original square blowing into a region of cyclonic geostrophic wind shear. It will be noted that the area shrinks to nothing in 7 hours.

---

[1]This work was prosecuted under P. L. 71, 84th Congress as part of Subproject III.

4

The same effect can be observed if the air current blows into a region of cyclonic curvature of the isobars (or contour lines). Figure 2 shows the shrinkage of an original area to zero when it blows into and through a region of cyclonic curvature. For the frictionless dynamic trajectories, the line AB which is originally south of the line CD, crosses it in 7 hours and is north of it thereafter. It is, of course, impossible that this crossing should actually occur.

Figures 3 and 4 show similar shrinking of area when the winds possess anticyclonic shear and curvature, respectively, but the pressure field is linear.

The vorticity equation may be used to explain these illustrations. That equation states that as the vorticity of the wind becomes more cyclonic with time, convergence occurs. Now, other things being equal, the vorticity of the actual wind will change toward the vorticity of the geostrophic wind. Thus if the pressure gradients change with time on an air current in such a way that the later geostrophic vorticity is more cyclonic than the initial actual vorticity, convergence will develop.

It may be noted that in these cases the convergence develops after the cyclonicity has appeared and reaches its maximum somewhat downstream from the maximum cyclonicity.

## 3. THE DIVERGENCE DEVELOPMENT EQUATIONS

In the preceding section simple illustrations were given of the development of convergence under certain simplifying assumptions. The purpose of this section is to establish the mathematics on a firm basis and thus make possible the quantitative study of varying the assumptions. A solution for the non-frictional case is always obtainable by using the trajectory methods described by Goodyear [3] on three or more corners of an original polygon. Moreover this method has the advantage that it also gives the location of the region of convergence. However, the mathematical approach to be described has the advantage that it permits a quantitative evaluation of the mutual effects of certain characteristics in a much simpler manner than could be obtained by repeated use of the trajectory technique. The approach was first suggested to one of the authors by Bellamy's [4] "convergenesis" approach used at the Institute of Tropical Meteorology in 1944. The methods are simple amplifications of the equation developed by Bellamy. They are also closely related to the "Balance Equation" of Charney [5].

The divergence development equations relate divergence to the vorticity of the real wind ($\eta$). In the following development a pair of simultaneous equations are presented which express divergence as a function of the geostrophic vorticity ($\eta_g$), the vorticity of the real wind ($\eta$) being implicitly contained within the equations.

The average horizontal velocity divergence, $\overline{\text{Div } \mathbf{V}}$, over a substantial horizontal area of size A, may be defined by

$$A\,\overline{\text{Div}\ \mathbb{V}} = \frac{dA}{dt} = \oint (u\,dy - v\,dx) \tag{1}$$

Differentiating equation (1) with respect to time

$$\frac{d}{dt}\overline{\text{Div}\ \mathbb{V}} + \left(\overline{\text{Div}\ \mathbb{V}}\right)^2 = \frac{1}{A}\left[\oint\left(\frac{du}{dt}\,dy - \frac{dv}{dt}\,dx\right) + \oint (u\,dv - v\,du)\right] \tag{2}$$

The frictionless equations of horizontal motion on the rotating earth are

$$\frac{du}{dt} = fv' \tag{3}$$

$$\frac{dv}{dt} = -fu' \tag{4}$$

where u' and v' are the components of the geostrophic deviation. Therefore the first term on the right of equation (2) may be written

$$\frac{1}{A}\left[\oint\left(\frac{du}{dt}\,dy - \frac{dv}{dt}\,dx\right)\right] = \frac{1}{A}\oint f(v'\,dy + u'\,dx) \tag{5}$$

$$= \overline{\text{curl}\ f\ \mathbb{V}'}$$

where $\mathbb{V}'$ is the total geostrophic deviation. If the variation of the Coriolis parameter is neglected,

$$\overline{\text{curl}\ f\ \mathbb{V}'} = \overline{f\eta'} \tag{6}$$

The second term on the right of equation (2) is equal to twice the average value of the Jacobian of (u,v) with respect to (x,y) over the area A or twice the number of intersections of unit isotachs of u and v per unit area. Although this term could be evaluated for a specific case, it will be neglected for simplicity. However, this point will be discussed further after the derivation of equation (7) has been completed.

Since only the horizontal divergence over a horizontal area is being considered, equation (2) does not include the changing inclination of the area A with respect to the horizontal. This term is somewhat analogous to the turning of the vortex tubes in the vorticity equation. Equation (2) may be rewritten as

$$\frac{d}{dt}\overline{\text{Div}\ \mathbb{V}} + \left(\overline{\text{Div}\ \mathbb{V}}\right)^2 = \overline{f\eta'} \tag{7}$$

Another means of arriving at equation (7) whereby the neglected terms will appear in a more familiar form is through the frictionless equations of motion for horizontal flow,

$$\frac{du}{dt} = \frac{\partial u}{\partial t} + u\frac{\partial u}{\partial x} + v\frac{\partial u}{\partial y} + w\frac{\partial u}{\partial z} = -\frac{1}{\rho}\frac{\partial p}{\partial x} + fv \tag{8}$$

$$\frac{dv}{dt} = \frac{\partial v}{\partial t} + u\frac{\partial v}{\partial x} + v\frac{\partial v}{\partial y} + w\frac{\partial v}{\partial z} = -\frac{1}{\rho}\frac{\partial p}{\partial y} - fu \tag{9}$$

Differentiating equation (8) partially with respect to x and equation (9) partially with respect to y and adding,

$$\frac{d}{dt}\,\mathrm{Div}\,\mathbf{V} + (\mathrm{Div}\ \mathbf{V})^2 = \frac{1}{\rho}\nabla^2 p + f\eta + 2J - T - \beta u \tag{10}$$

where $J = \frac{\partial u}{\partial x}\frac{\partial v}{\partial y} - \frac{\partial v}{\partial x}\frac{\partial u}{\partial y}$, $T = \frac{\partial w}{\partial x}\frac{\partial u}{\partial z} + \frac{\partial w}{\partial y}\frac{\partial v}{\partial z}$, and $\beta = \frac{\partial f}{\partial y}$

These terms will be neglected as before, However, Shuman [12] using Charney's [5] "balance equation", which is a form of equation (2) neglecting the divergence terms, computed the magnitude of the Jacobian term at 500 mb. for various synoptic examples and found that the term is sometimes of the same order of magnitude as $-f\eta'$ and that both are characteristically larger than the first two terms of equation (2). A logical consequence of his work would be that it would be impossible in general over most areas to use equation (2) without treating the Jacobian term. There is, however, justification for believing that equation (2) might give valuable results in cases involving the development of areas of intense convergence. In the Lagrangian frame of reference used here, a characteristic situation is as follows: A current of air, say a moist tongue, moves within a few hours from a situation where all the terms in equation (10) are very small into an area where the first term on the right in equation (10) is quite large (geostrophic vorticity). Then in the initial stages the dominant terms in equation (10) must be the first terms on the left and the right. When convergence becomes large the second term on the left becomes important. Characteristically, the more intense values of convergence occur over areas too small for it to be measured by our wind networks. However, we know from recorded values of rainfall and elemental reasoning with the equation of continuity that the values must be several orders of magnitude larger than those which have been measured. Thus there are many cases where it would seem that the first few hours of the development of intense convergence can be adequately described by equation (7).

It may be noted that

$$2J = \frac{1}{2}\left(\frac{\partial v}{\partial x} - \frac{\partial u}{\partial y}\right)^2 + \frac{1}{2}\left(\frac{\partial u}{\partial x} + \frac{\partial v}{\partial y}\right)^2 - \frac{1}{2}\left(\frac{\partial v}{\partial x} + \frac{\partial u}{\partial y}\right)^2 - \frac{1}{2}\left(\frac{\partial u}{\partial x} - \frac{\partial v}{\partial y}\right)^2$$

Since the second term is $\frac{1}{2}(\text{Div } \mathbb{V})^2$, equation (7) might be written with the second term on the left reduced by one-half just as logically as the equation actually solved here. It will be impossible to tell which solution has the most practical justification until the value of the other terms constituting the Jacobian has been investigated in detail for these cases.

From taking the vorticity of the geostrophic wind equation

$$\frac{1}{\rho} \nabla^2 p = f\eta_g \tag{11}$$

By definition

$$\eta' = \eta - \eta_g \tag{12}$$

where $\eta'$ is the vorticity of the geostrophic deviation, $\eta$ is the absolute vorticity of the real wind, and $\eta_g$ is the absolute vorticity of the geostrophic wind. Therefore equation (10) is equivalent to equation (7).

Now, by differentiating equation (8) partially with respect to y and equation (9) partially with respect to x and subtracting

$$\frac{d\eta'}{dt} + \frac{d\eta_g}{dt} = -(\eta' + \eta_g) \text{ Div } \mathbb{V} \tag{13}$$

This is the well-known vorticity equation. It should be noted that the solenoid term, the "twisting term," the frictional term, and the variation of the Coriolis parameter have been neglected.

Equations (7) and (13) are non-linear equations relating the growth of divergence to the time rate of change of the geostrophic vorticity. They can be solved simultaneously by means of a numerical integration technique to be explained later. They will be referred to in the future as the non-Jacobian equations.

A simplified solution to these equations can be obtained by differentiating equation (7) with respect to time. Thus,

$$\frac{d^2}{dt^2}\overline{\text{Div } \mathbb{V}} + 2\,\overline{\text{Div } \mathbb{V}}\,\frac{d}{dt}\,\overline{\text{Div } \mathbb{V}} = \frac{d}{dt}\,\overline{f\eta'} \tag{14}$$

$$= \frac{d}{dt}\,\overline{f}\,\overline{(\eta - \eta_g)}$$

Substituting from the vorticity equation (13) for the $\frac{d\eta}{dt}$ term, equation (14) becomes,

$$\frac{d^2}{dt^2}\overline{\text{Div}\,\mathbf{V}} + 2\,\overline{\text{Div}\,\mathbf{V}}\;\frac{d}{dt}\overline{\text{Div}\;\mathbf{V}} + \overline{\eta\, f\ \text{Div}\;\mathbf{V}} = \overline{-f\frac{d\eta_g}{dt}} \qquad (15)$$

By neglecting the second term on the left for a first approximation and taking $\eta = f$ we obtain the following, which will be called the comparison equation,

$$\frac{d^2}{dt^2}\overline{\text{Div}\;\mathbf{V}} + \overline{f^2\ \text{Div}\;\mathbf{V}} = \overline{-f\frac{d\eta_g}{dt}} \qquad (16)$$

Since in equation (7) the second term on the left is never negative, it is obvious that when the divergence is positive and increasing, its rate of growth as given by equation (15) will always be less than the rate of growth given by equation (16). When the divergence is positive and decreasing its rate of decay will be greater for equation (15) than for the comparison equation. Therefore the divergence from any given initial conditions will be overestimated and the convergence will be underestimated by the comparison equation. Moreover, the greater the absolute value of divergence, the greater the percent of overestimation or underestimation.

Equation (16) is of a well-known, much-studied type in mathematical physics. Its solution along with numerical examples is given later in this paper.

## 4. EFFECT OF FRICTIONAL AND VISCOUS FORCES

Although the laws concerning frictional and viscous forces in the atmosphere are not known with sufficient accuracy to provide exact solutions to the equations of motion with these forces included, still, useful qualitative information may be obtained from a consideration of how the frictional forces affect the development of convergence. A comparison between actual precipitation patterns and patterns predicted from the frictionless equations may furnish gross information on the frictional characteristics of the atmosphere.

### Frictional force proportional to and directed against velocity

One of the simplest hypotheses concerning the frictional force is expressed quantitatively by the equations of motion in the form

$$\frac{du}{dt} = fv' - ku \qquad (17)$$

$$\frac{dv}{dt} = -fu' - kv \qquad (18)$$

where k is a constant for any level in the atmosphere.

Repeating the steps leading up to equation (7), one obtains the following

$$\frac{d\overline{\text{Div}\;\mathbf{V}}}{dt} + \overline{\text{Div}\;\mathbf{V}^2} = \overline{f\eta'} - k\,\overline{\text{Div}\;\mathbf{V}} \qquad (19)$$

the terms, J and T, and the variation of f being neglected as before. Thus the frictional effect is to inhibit the development of either divergence or convergence. If the constant k is much larger in the surface layer than aloft, as certainly must be the case, then the convergence or divergence in that layer will be inhibited much more than in higher layers. For example, consider only the terms

$$(\overline{\text{Div } \mathbf{V}})^2 = -k\,\overline{\text{Div } \mathbf{V}}$$

then

$$\overline{\text{Div } \mathbf{V}} = -k$$

Now if k decreases with height the convergence also decreases with height and the effect of the frictional term becomes less important.

Even though the factor k of equations (17) and (18) is sufficiently accurate as an approximation for computing the wind velocity, small variations in k may cause large errors in the last term of equation (19).

Frictional force proportional to a higher power of and directed against velocity

A somewhat more complicated hypothesis regarding the frictional force may be expressed by writing the equations of motion in the form

$$\frac{du}{dt} = fv' - ku^n \tag{20}$$

$$\frac{dv}{dt} = -fu' - kv^n \tag{21}$$

where k is a constant for any level and $n > 1$.
Repeating a similar derivation as above

$$\frac{d\overline{\text{Div } \mathbf{V}}}{dt} + (\overline{\text{Div } \mathbf{V}})^2 = \overline{f\,\eta'} - k\left[\,\overline{u^{n-1}\frac{\partial u}{\partial x} + v^{n-1}\frac{\partial v}{\partial y}}\,\right] \tag{22}$$

Navier-Stokes stress

The Navier-Stokes form of the equations of motion (See Lamb [6] and Haurwitz [7]) are written as

$$\frac{du}{dt} = f\,v' + \frac{\mu}{\rho}\left(\nabla_h^2 u + \frac{\partial^2 u}{\partial z^2}\right) \tag{23}$$

$$\frac{dv}{dt} = -fu' + \frac{\mu}{\rho}\left(\nabla_h^2 v + \frac{\partial^2 v}{\partial z^2}\right) \tag{24}$$

where $\mu$ is the coefficient of eddy viscosity, where the variation of the expansion $\left(\frac{\partial u}{\partial z} + \frac{\partial v}{\partial y} + \frac{\partial w}{\partial z}\right)$ with x and y has been neglected, and where the notation in the last term has been selected to emphasize the distinction between variations in the horizontal and the vertical.

Repeating a similar derivation as before and neglecting the same terms

$$\frac{d}{dt}\overline{\text{Div } \mathbf{V}} + (\overline{\text{Div } \mathbf{V}})^2 = \overline{f\,\eta'} + \frac{\mu}{\rho}\left(\nabla_h^2 \text{ Div } \mathbf{V} + \frac{\partial^2}{\partial z^2} \text{Div } \mathbf{V}\right) \qquad (25)$$

Considering first the second term on the right, one may see that the value of the term is positive near a maximum of convergence and negative near a maximum of divergence. Thus the effect of this term is always to tend to slow down the development.

The result of the last term in equation (25) from analogy with similar expressions in other physical relationships would be to equalize differences in convergence from level to level. For example, Byers [8] gives analogies with the vertical transport of water vapor, the downward transport of heat, and the vertical transport of momentum.

## 5. THE VOLUMETRIC EQUATION

The volume of precipitation that falls over an area A of changing size can be computed from forms of equations (7) and (13)

$$\frac{d}{dt}\overline{\text{Div } \mathbf{V}}A = \overline{f\,\eta'}\,A \qquad (26)$$

$$\frac{d\eta'A}{dt} = -\frac{d\eta_g A}{dt} \qquad (27)$$

Now, assume, as was done by Peterson [9], that the rainfall rate over an area A is determined by the surface convergence and dewpoint, provided that no subarea of A has a positive value of surface divergence and that the air rises pseudoadiabatically. If these two conditions are satisfied and if initially $\eta'$, $\eta_g$, and Div $\mathbf{V}$ are small, from equation (27), $\eta' = -\eta_g$ and substitution into equation (26) gives

$$\frac{d\overline{\text{Div } \mathbf{V}}A}{dt} = \overline{-f\eta_g}A \qquad (28)$$

If V is the total volume of precipitation that falls from an area of changing size A

$$\frac{dV}{dt} = -\int \overline{\text{Div } \mathbf{V}}A\, dW \qquad (29)$$

where W is the precipitable water. Substituting from equation (28)

$$\frac{dV}{dt} = \int\int \overline{f\eta_g} A\, dW dt \qquad (30)$$

and

$$V = \int\int\int \overline{f\eta_g}\, A\, dW dt dt \qquad (31)$$

This equation may be used to give an overall estimate of the volume of precipitation falling from a column as related to the average value of the Laplacian of pressure over a large area, provided that no subarea of surface divergence is included within the area and that the assumptions made are valid.

## 6. THE LINEAR PRESSURE FIELD EQUATION

If $\eta_g$ is negligible the divergence development equation (7) takes the form

$$\frac{d\,\overline{\text{Div}\ \mathbb{V}}}{dt} + (\overline{\text{Div}\ \mathbb{V}})^2 = \overline{f\eta} \tag{32}$$

where as before the Jacobian, turning, Rossby parameter, and friction terms have been neglected.

With the vorticity equation (13),

$$\frac{1}{\eta}\frac{d\eta}{dt} = -\text{Div}\ \mathbb{V},$$

given initial values of $\eta$ and Div $\mathbb{V}$, these two equations can be solved numerically by a technique similar to that used in the next section. An example of how convergence could develop in a field of strong shear when the pressure field becomes weak is presented in figures 3 and 4.

## 7. NUMERICAL SOLUTIONS OF THE DIVERGENCE DEVELOPMENT EQUATIONS

This section is concerned primarily with numerical solutions of the comparision equation (16) and the non-Jacobian equations (7) and (13). Curves of convergence vs. time computed by assigning various durations and intensities to $\eta_g$ in both the comparison and non-Jacobian equations are presented, and an analysis of these is made in order to investigate the effect of the time-duration of $\eta_g$ on the development of convergence.

### Solution of comparision equation

The solution of the comparision equation (16) (dropping the notation for averages) is

$$\text{Div}\ \mathbb{V} = \left[\frac{1}{f}\left(\frac{d}{dt}\text{Div}\ \mathbb{V}_o\right) + \int_o^t \cos ft \frac{d\eta_g}{dt}\,dt\right] \sin ft + \left[\text{Div}\ \mathbb{V}_o - \int_o^t \sin ft \frac{d\eta_g}{dt}\,dt\right]\cos ft \tag{33}$$

or

$$\text{Div}\ \mathbb{V} = A_o\cos(ft-\alpha_o) + \left[\left(\int_o^t \cos ft \frac{d\eta_g}{dt}\,dt\right) \sin ft - \left(\int_o^t \sin ft \frac{d\eta_g}{dt}\,dt\right)\cos ft\right] \tag{33a}$$

where $A_o^2 = [\frac{1}{f}(\frac{d}{dt}\ \text{Div}\ V_o)]^2 + \text{Div}\ V_o^2$ ; $\alpha_o = \tan^{-1}\left[\frac{\frac{1}{f}(\frac{d}{dt}\ \text{Div}\ V_o)}{\text{Div}\ V_o}\right]$

and the subscript o refers to initial conditions.
Thus in equation (33a), the divergence starting at any time is the sum of two terms, the first term on the right being a sinusoidal function defined by the initial conditions, and the second term a function defined by the duration and behavior of $\eta_g$.

A sinusoidal variation of $\eta_g$ with time was assumed. While other hypotheses might have been adopted, this one has two characteristics which recommend its use. First, individual parcels in the atmosphere sometimes tend to assume successive values of positive and negative geostrophic vorticity in an approximate sinusoidal fashion, and secondly the function thus defined lends itself readily to computation. Then, proceeding with this hypothesis, let

$$\eta_g = f + k(1 - \cos nft). \tag{34}$$

where f is the Coriolis parameter, k is the amplitude, a constant of proportionality equal to unity in these particular considerations, and n is the ratio of the period of the $\eta_g$ curve to the length of a half-pendulum day. A latitude of 30°N. is used throughout this analysis. Differentiating (34) with respect to time, neglecting the variation of the Coriolis parameter

$$\frac{d\eta_g}{dt} = knf \sin nft \tag{35}$$

In order to investigate the effect of one period of $\eta_g$ upon Div $V$, $\eta_g$ and $\frac{d\eta_g}{dt}$ are allowed to vary from t = 0 to t = $\frac{2\pi}{nf}$. Substituting (35) into (33) and collecting terms,

$$\text{Div}\ V = \frac{1}{f}(\frac{d}{dt}\ \text{Div}\ V_o)\sin ft + \text{Div}\ V_o \cos ft + [knf \int_o^t \cos ft \sin nft\, dt] \sin ft$$

$$- [\, knf \int_o^t \sin ft \sin nrt\, dt\, ] \cos ft \tag{36}$$

Integrating equation (36) with initial conditions of Div $V_o = 0$ and $\frac{d}{dt}\text{Div}\ V_o = 0$, values of negative divergence are computed for various durations of one period of $\eta_g$. The duration of $\eta_g$ is the duration on the moving air parcel. This is done by assigning different values to n, where, for example, when n = 12, the duration of $\eta_g$ is 2 hours. Figure 5 shows the distributions of negative divergence with time which were computed for one period of $\eta_g$ varying from 1/2 hour to 24 hours. The curve of $\eta_g$ is not illustrated but always reaches a maximum half-way through its period due to the assumptions made in equation (34) and

the maxima of convergence shown in figure 6 lag behind the corresponding maxima of $\eta_g$ from as little as 1/4 hour when the duration of $\eta_g$ is 1/2 hour, up to about 2-1/3 hours when $\eta_g$ lasts almost 10 hours. The values of convergence computed from the comparison equation are usually less than those calculated from the numerical solutions of the non-Jacobian equations which are discussed next. This characteristic of the comparison equation is due to its neglect of the factor $(\text{Div } \mathbb{V})^2$.

Solution of non-Jacobian equations

The non-Jacobian equations are

$$\frac{d}{dt} \text{Div } \mathbb{V} + \text{Div } \mathbb{V} = f\eta' \tag{37}$$

$$\frac{d\eta'}{dt} + \frac{d\eta_g}{dt} = -(\eta' + \eta_g) \text{ Div } \mathbb{V} \tag{38}$$

These are non-linear differential equations which are solved simultaneously using a modified Euler technique explained in Scarborough [10] and outlined below.

Establishing the initial conditions for (37) and (38) such that when time $t = 0$, then $\text{Div } \mathbb{V}_o = 0$, $d/dt \text{ Div } \mathbb{V}_o = 0$ and using (34) and (35) wherein the definitions of f and n remain unchanged but with k equal to $\frac{1}{2}(\eta_g - f)_{max}$, values of negative divergence for various durations and intensities of $\eta_g$ are computed. The stepwise time-incremental approximations made in these computations are as follows:

For the initial trial after time $t = 0$, since $\eta_g$, $\frac{d\eta_g}{dt}$, and f are known, the equation used to approximate Div $\mathbb{V}$ and $\eta'$ is

$$(\ )_{t_{n+1}} = (\ )_{t_n} + \Delta t \frac{d}{dt} [\ (\ )_{t_n}] \tag{39}$$

Where Div $\mathbb{V}$ and $\eta'$ are alternately substituted within the parentheses, and $t_n$ refers to values at initial time, $t_{n+1}$ to values being currently approximated, and $\Delta t$ is the particular time interval being used. To correct this and all other approximations for a particular t the equation used is

$$(\ )_{t_{n+1}} = (\ )_{t_n} + \Delta t \frac{d}{dt} (\ )_{Avg(t_{n+1})} \tag{40}$$

where

$$\frac{d}{dt} (\ )_{Avg(t_{n+1})} = \frac{1}{2} [\frac{d}{dt} (\ )_{t_{n+1}} + \frac{d}{dt} (\ )_{t_n}] \tag{41}$$

Using (40) and (41) successive values of Div $\mathbb{V}$ and $\eta'$ are computed until the

respective values converge. Then to approximate initially all succeeding states for a particular $\Delta t$, the equation used is

$$( \quad )_{t_{n+1}} = ( \quad )_{t_{n-1}} + 2 \Delta t \frac{d}{dt} ( \quad )_{t_n} \qquad (42)$$

where $t_n$ and $t_{n+1}$ have the same definition as before, and $t_{n-1}$ refers to the values of Div and $\eta'$ for the time interval prior to the initial time, $t_n$. To correct this approximation, (42), (40), and (41) are used as described above, and this process is repeated for each time interval until the computed values of negative divergence change sign. Whenever successive approximations of $\eta'$ and Div $V$ at any time do not converge within four trials, $\Delta t$ is made smaller to avoid errors in computing convergence. Using the above technique, values of negative divergence were computed for durations of $\eta_g$ lasting 1/2 hr., 1 hr., 2 hr., 4 hr., and 8 hr., and with values of $(\eta_g - f)_{max}$ varying from 0.10 hr.$^{-1}$ to an extreme value of 30.0 hr.$^{-1}$. These results are shown in figures 6-10.

The values of k used may be related to the observed pressure field as follows: The factor k is approximately

$$\frac{1}{2 \rho f} \left( \frac{p_1 + p_2 + p_3 + p_4 - 4p_o}{L^2} \right)$$

If L = 100 miles, $\rho$ = 1.20 kg. m.$^{-3}$, and f equals its value at 35°N., then a departure of linearity of 1.0 millibar will give a k value of 0.0693 hr.$^{-1}$.

In figure 6 where the duration of $\eta_g$ is 1/2 hr. and a large value of 6.0 hr.$^{-1}$ is assigned to $(\eta_g - f)_{max}$ (which equals 2k), the convergence curve tends to negative infinity in little over an hour after inception, whereas assigning another large value of $(\eta_g - f)_{max}$ of 3.0 hr.$^{-1}$ results in convergence of an average magnitude spread out over a period of 6 hours, while a lesser value of $(\eta_g - f)_{max}$ of 1.0 hr.$^{-1}$ develops convergence closely approaching the comparison equation curve. Reviewing these results, it would seem that intense, short-lived values of $(\eta_g - f)_{max}$ would produce infinite convergence over small areas in a very brief time. Since friction precludes such an occurrence in the atmosphere, this mathematical result is comparable to the extreme intense small-area rainfall. For an equal duration of $\eta_g$, values of $(\eta_g - f)_{max}$ of an order of magnitude greater than a commonly observed value merely produce average convergence. The curves in figure 7 indicate somewhat similar results for $\eta_g$ having a duration of 1 hour, but in figure 8 where the duration is 2 hours, the boundary between infinite and measurable convergence lies between $(\eta_g - f)_{max}$ of 1.4 hr.$^{-1}$ and 1.0 hr.$^{-1}$. This boundary is decreased as duration of $\eta_g$ is increased, and the lower limit of $(\eta_g - f)_{max}$ approaches more closely to commonly observed values, say 0.3 hr.$^{-1}$.

Figure 9, where the duration of $\eta_g$ is 4 hours, demonstrates some interesting results along this line. Consider the curve where k = 0.15 or $(\eta_g - f)_{max} = 0.30$ hr.$^{-1}$. This curve is fairly symmetrical about a maximum convergence development of approximately 0.174 hr.$^{-1}$ and shows no signs of instability or tendency to become infinite. As k is increased the peaks of the curves of convergence become more skewed until when k = 0.28 or $(\eta_g - f)_{max} = 0.56$ hr.$^{-1}$, a point is reached where the boundary between measurable convergence (in this case 0.7 hr.$^{-1}$) and infinite convergence is very critical. A similar condition is shown in figure 10 where the duration of $\eta_g$ is 8 hours.

In light of these results, the following conclusions are suggested. First, short-lived and even intense anomalies of $\eta_g$ should not be followed by large values of convergence. Then given a field in which these brief, intense variations do occur, their combined effects, while they cannot be discounted, do not produce as intense or prolonged values of convergence as do longer durations but weaker intensities of $\eta_g$. A comparison of figures 6 and 10 will demonstrate this argument. In figure 6, with a duration of $\eta_g$ of 1/2 hour, and a value of $(\eta_g - f)_{max} = 2.0$ hr.$^{-1}$, then the maximum convergence = 0.27 hr.$^{-1}$, and the duration of convergence is about 6 hours. In figure 10 with a value or $(\eta_g - f)_{max}$ = 0.3 hr.$^{-1}$, then the maximum convergence is 0.43 hr.$^{-1}$, and the duration of convergence is almost 10 hours. Figures 11 through 16 demonstrate this further. In each case, the intensity of $\eta_{g(max)}$ is the same and the only argument in the resulting distribution of convergence is the duration of $\eta_g$. In all cases it can be seen that the longer the duration of $\eta_g$, the greater the time difference between maximum $\eta_g$ and maximum convergence. Therefore, while brief durations of intense $\eta_g$ exist, an analysis of a potential rain-producing field may be evaluated by utilizing the appreciable lag in convergence resulting from smaller values of $\eta_g$ lasting from 2 to 8 hours which have been demonstrated to be the predominant contributors to convergence in the over-all situation. Part 2 of this report will be concerned with the application of these techniques to synoptic situations.

## 8. VOLUMETRIC APPROACH TO MOISTURE

Empirical studies have shown that, in heavy rainfall situations, a very high percentage of the volume of moisture entering the cyclonic region of a pressure system falls out as precipitation. In a winter month it was found that the volume of precipitation was equal to 80 percent of the volume of moisture flowing into the country across the Gulf Coast between San Antonio and Tallahassee [11]. In Part 2 of this report it was found that on a more limited time and areal basis an even higher percentage of the moisture entering a cyclonic region falls out as precipitation. It is proposed that these relationships can be used to forecast the average depth of precipitation over an area provided that the area can be approximated by the use of dynamic trajectories and the divergence development equations.

## 9. SUMMARY AND CONCLUSIONS

Three results seem to be in agreement:(1) if dynamic trajectories are constructed for four corners of a square area in a current entering a cyclonic region of moderate intensity the area frequently shrinks to zero; (2) numerical integration of the divergence development shows that with certain moderate values of cyclonicity in the horizontal pressure field the values of divergence approach negative infinity; (3) in many intense rainfall situations the volume of precipitation is nearly equal to the volume of moisture entering the cyclonic portion of the system.

Numerical integration of the divergence development equations suggest the following conclusions: (1) Intense low-level convergence develops at times, after cyclonic features have formed in the horizontal pressure field and somewhat downstream from such features; (2) short-lived cyclonic features - say those that last only a half-hour or so - or those that move rapidly across a moving current have a very small effect on the development of convergence; (3) very large values of cyclonicity lasting an hour or so can produce very large values of convergence within a very short time.

## REFERENCES


1. J. Bjerknes, "Theorie der Ausser Tropischen Zyklonenbildung," Meteorologische Zeitschrift, vol. 54, No. 12, Dec. 1927, pp. 462-466.
2. S. Petterssen, Weather Analysis and Forecasting, McGraw-Hill Book Co.,Inc., New York and London, 1940, pp. 326-332.
3. H. V. Goodyear, "Graphical Solution of Horizontal Velocity Equations and Use in Horizontal Trajectories in the Atmosphere," Monthly Weather Review, vol. 87, No. 5, May 1959, pp. 188-195.
4. J. C. Bellamy, Dynamic Meteorology, University of Chicago Institute of Tropical Meteorology Lecture Notes, University of Puerto Rico, Rio Piedras, Puerto Rico, 1944.
5. J. Charney, "The Use of the Primitive Equations of Motion in Numerical Forecasting," Tellus, vol. 7, No. 1, Feb. 1955, pp. 22-26.
6. H. Lamb, Hydrodynamics, 6th Edition, Dover Publications, New York, 1945, p. 577.
7. B. Haurwitz, Dynamic Meteorology, McGraw-Hill Book Co., Inc., New York and London, 1941, p. 190.

8. H. Byers, General Meteorology, 2d Edition, McGraw-Hill Book Co., Inc., New York and London, 1944, pp. 587-594.
9. K. Peterson, "Precipitation Rate as a Function of Horizontal Divergence," Monthly Weather Review, vol. 85, No. 1, Jan. 1957, pp. 9-10.
10. J. Scarborough, Numerical Mathematical Analysis, 3d Edition, Johns Hopkins Press, Baltimore, Md., 1955, pp. 235-240.
11. G. Lott and V. Myers, "Meteorology of Flood-Producing Storms in the Mississippi River Basin," Hydrometeorological Report No. 34, U. S. Weather Bureau, Washington, D. C., 1956.
12. F. G. Shuman, Personal Communication, 1957.

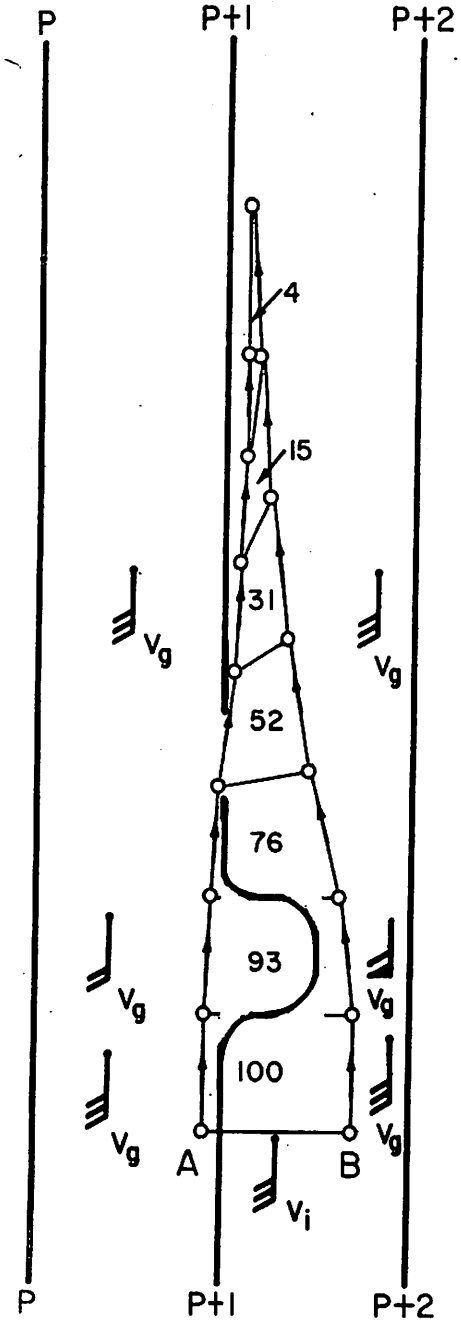


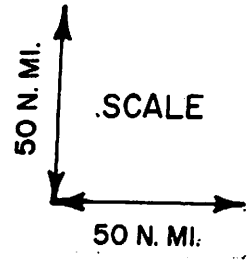


Figures in polygons are percentages of initial area.
Distances between o's represent one hour's travel.
Pressure in millibars.
$V_g$ = geostrophic wind.
$V_i$ = initial actual wind.

Figure 1. - Development of convergence as shown by dynamic trajectories in a pressure field with cyclonic shear lasting one hour.

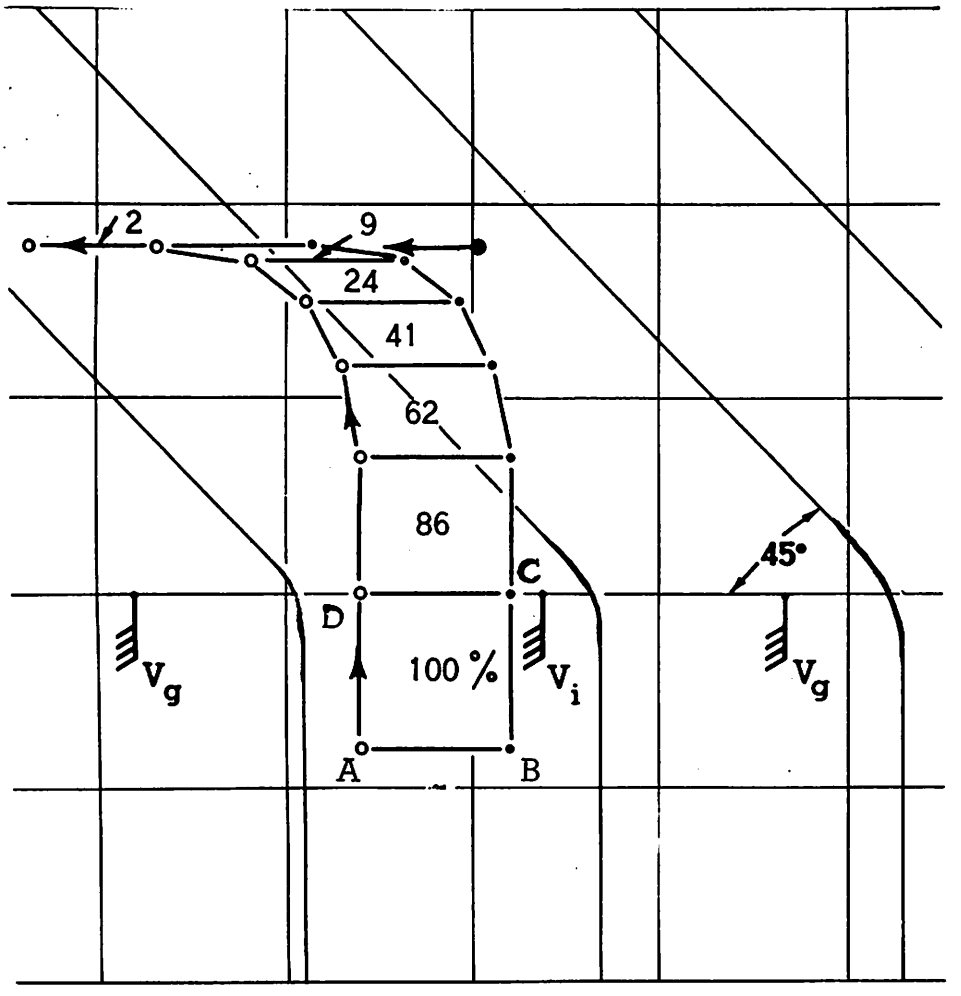


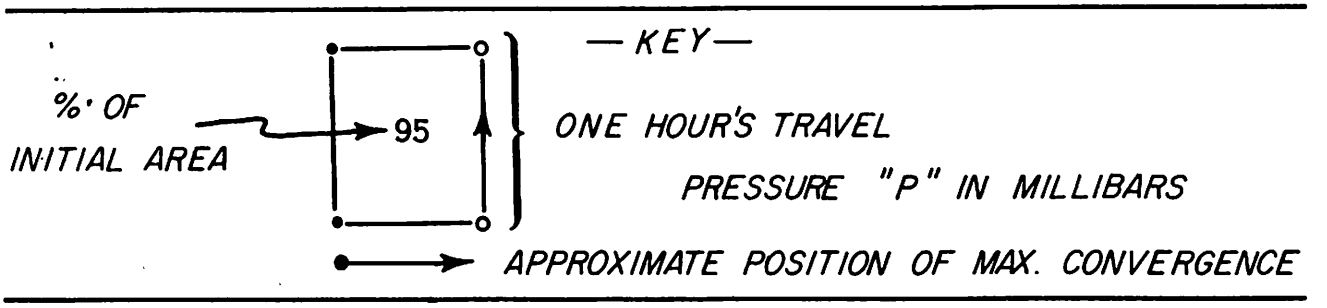


Figure 2. - Development of convergence as shown by dynamic trajectories in a pressure field with cyclonic curvature.

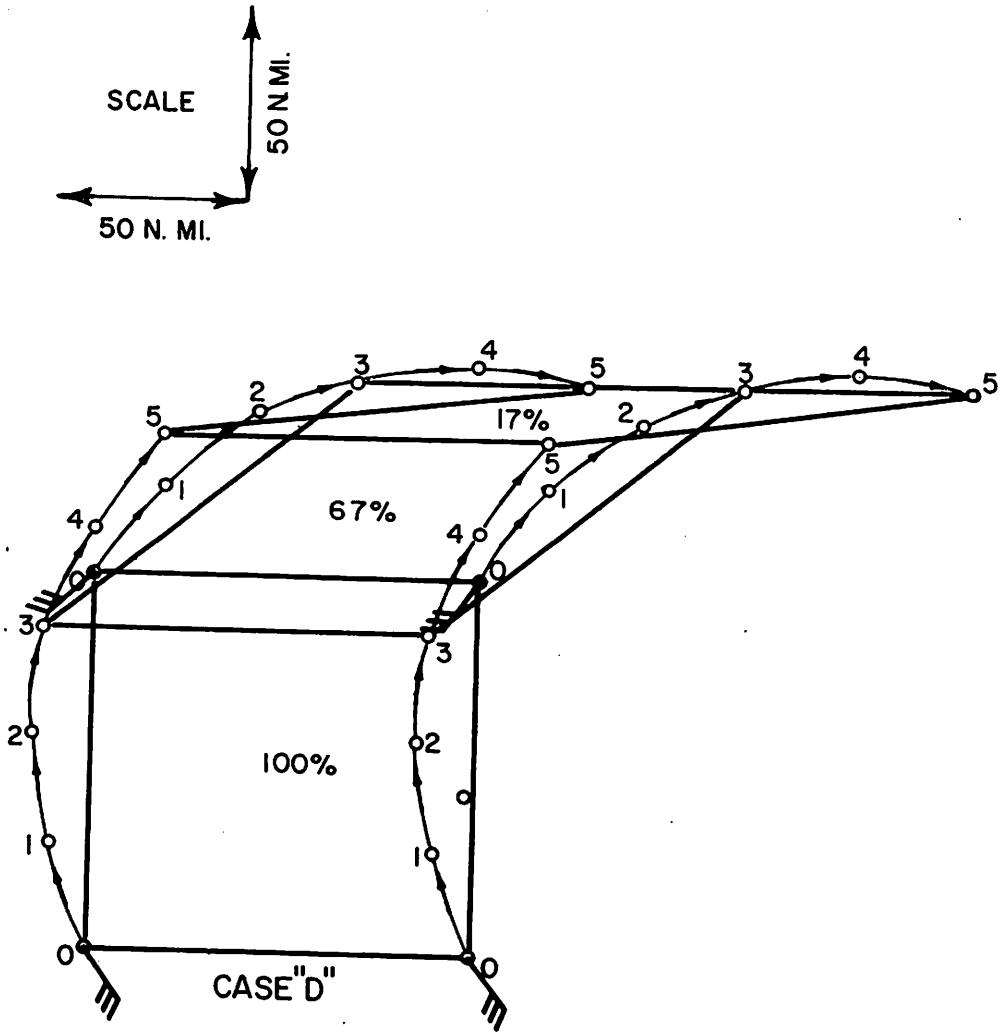


Figure 3. - Development of convergence in wind fields with initially anticyclonic rotation (D). ($\phi$ = 30°N. Pressure gradient = 0)

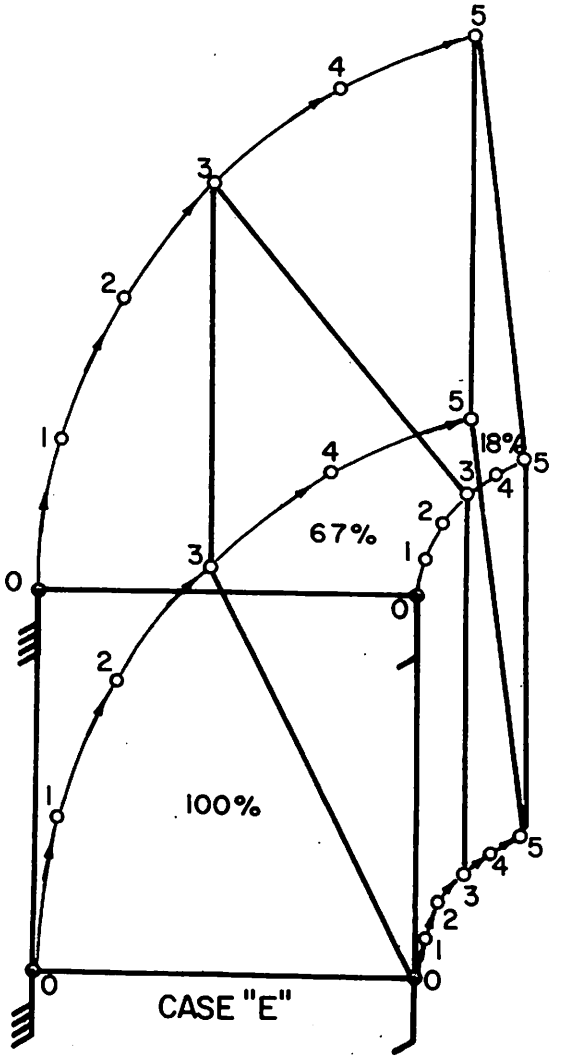


Figure 4. - Development of convergence in wind fields with anticyclonic shear (E). ($\phi$ = 30°N. Pressure gradient = 0)

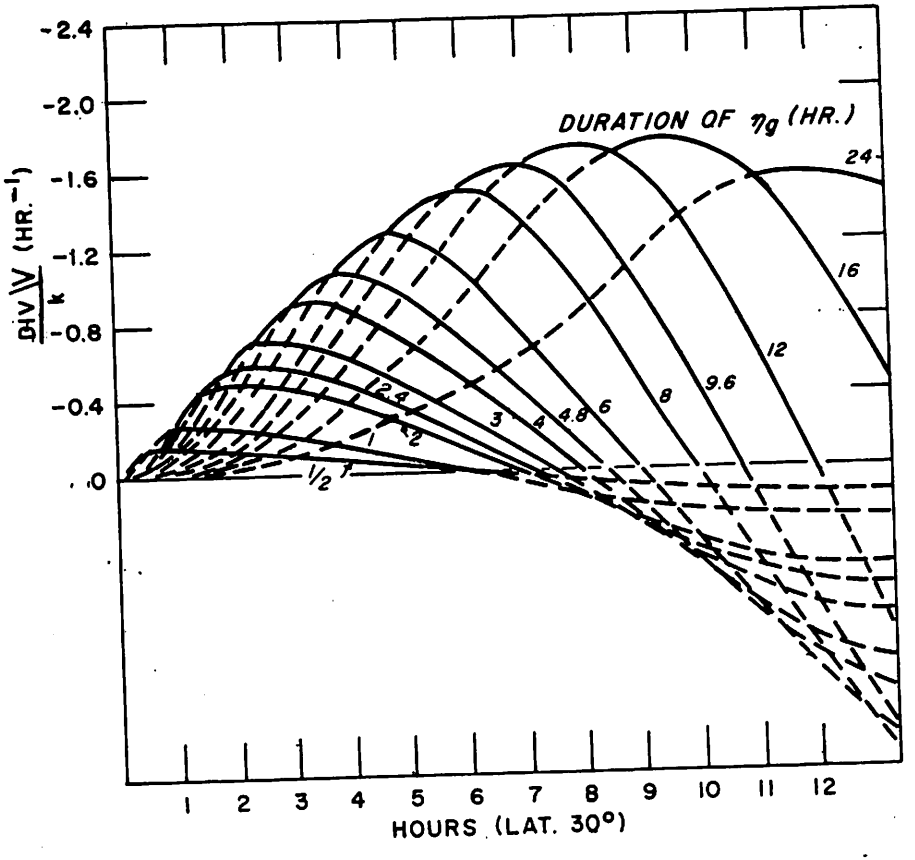


Figure 5. - Solutions of comparison equation, divergence vs. time, for various durations of $\eta_g$.

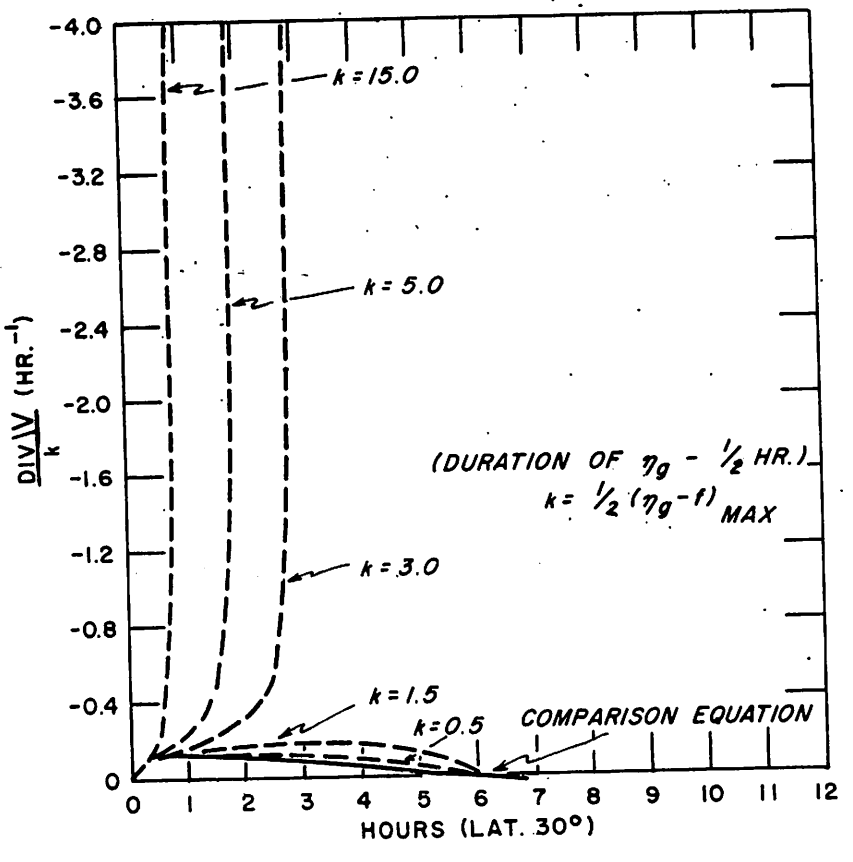


Figure 6

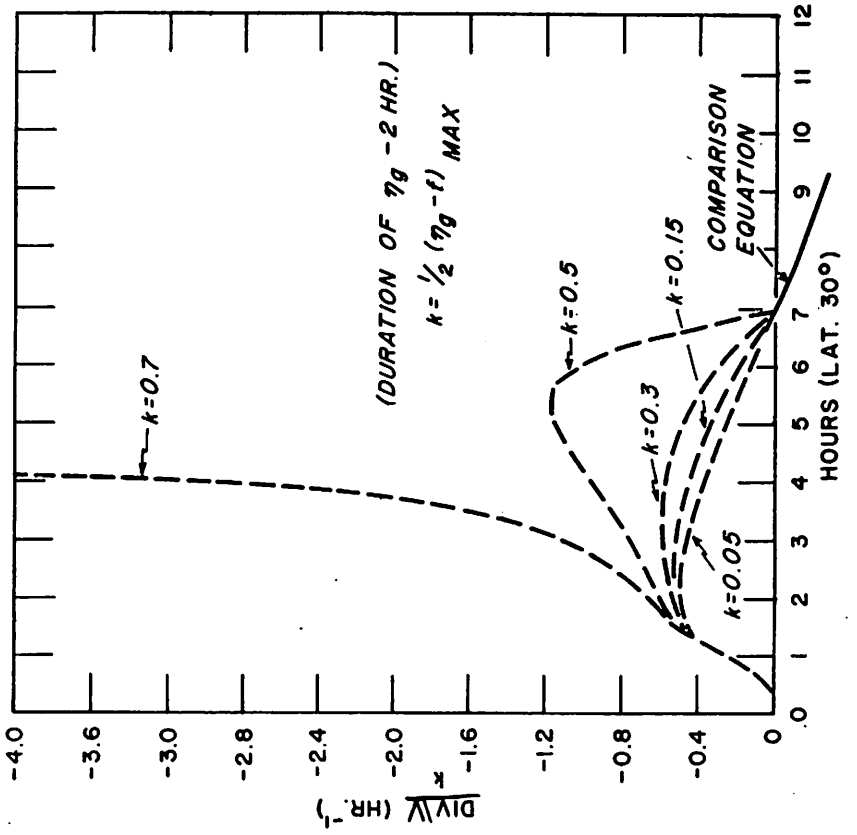


Figure 8

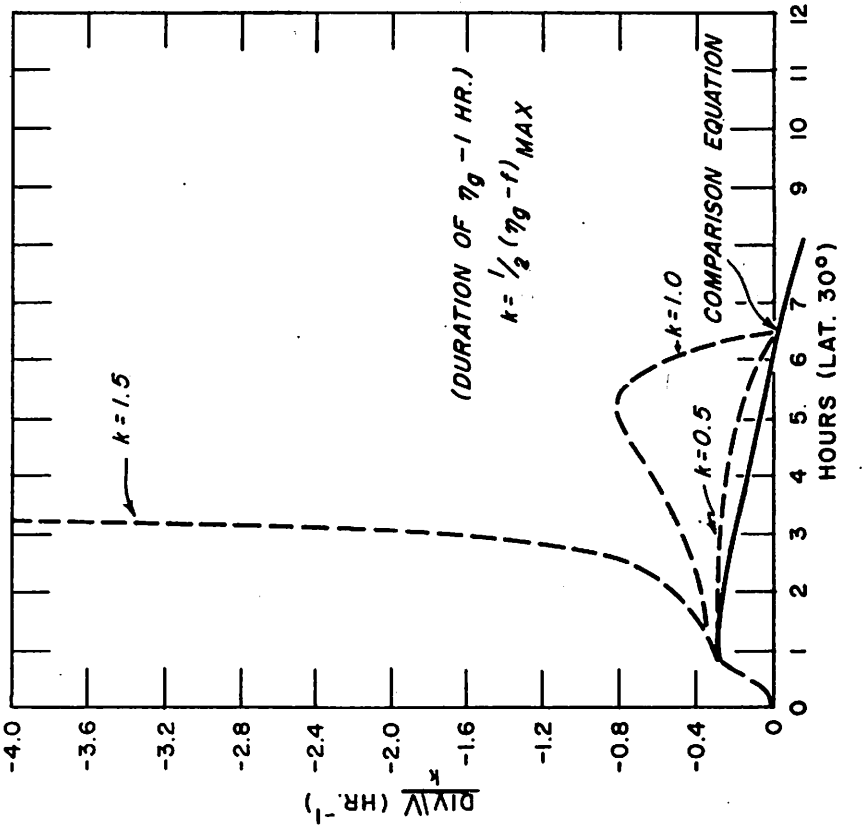


Figure 7

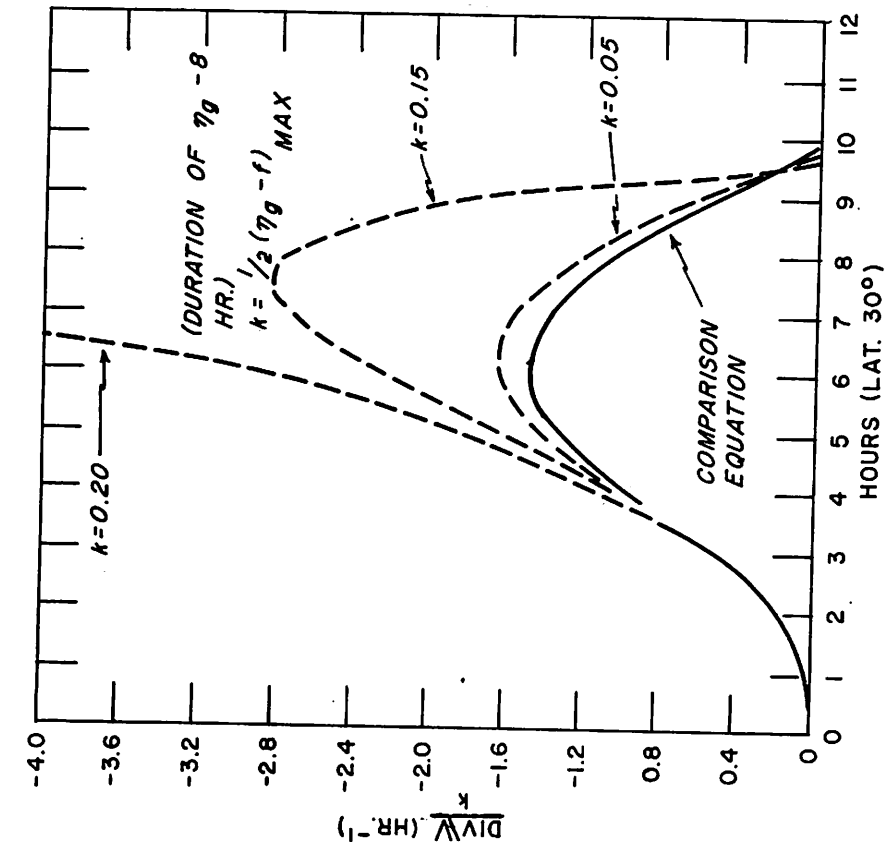


Figure 10

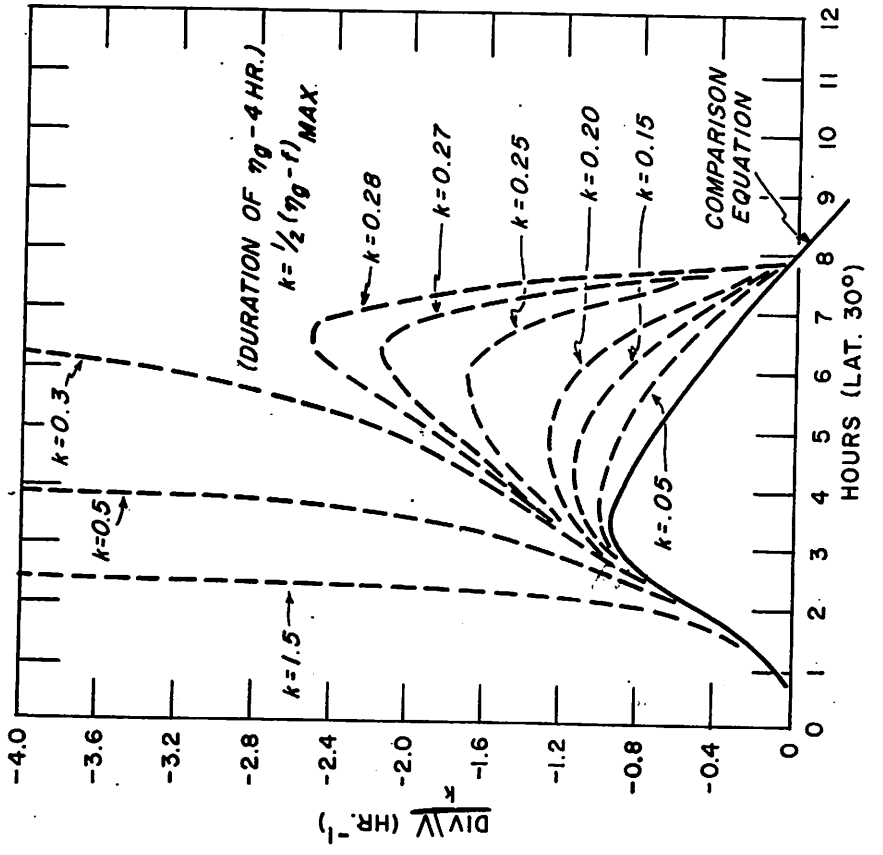


Figure 9

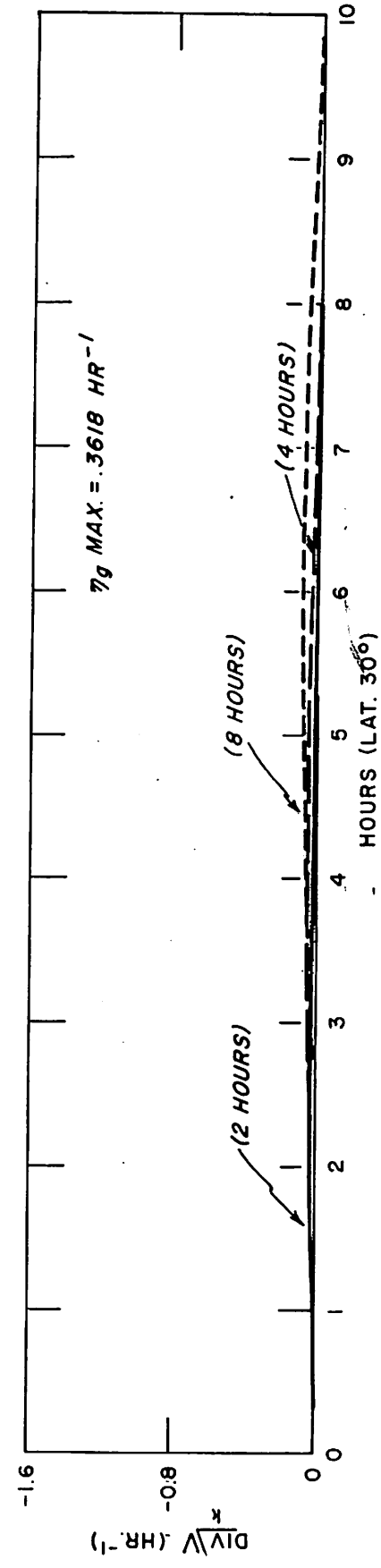


Figure 11. - Divergence as a function of duration of $\eta_g$.

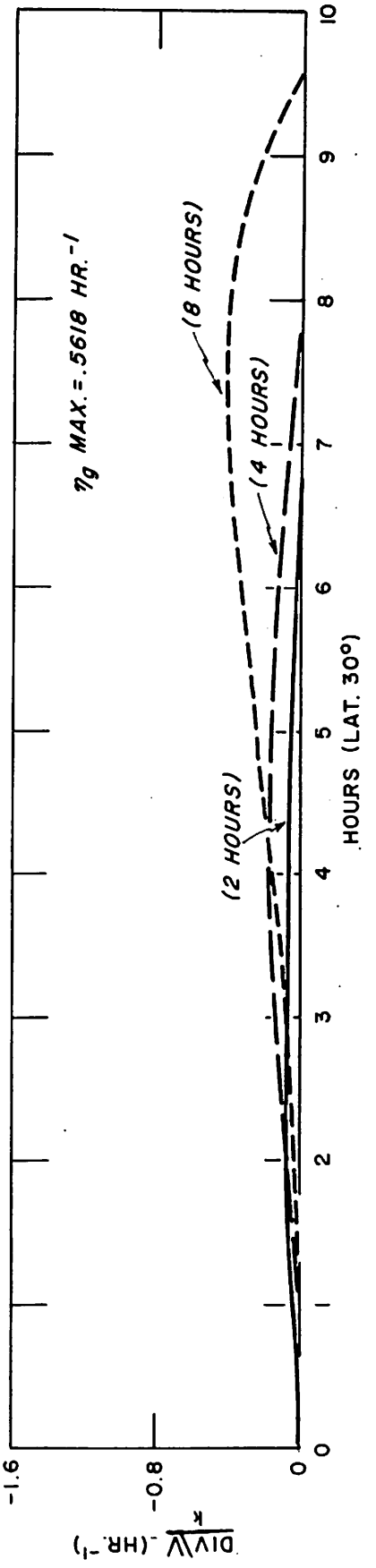


Figure 12

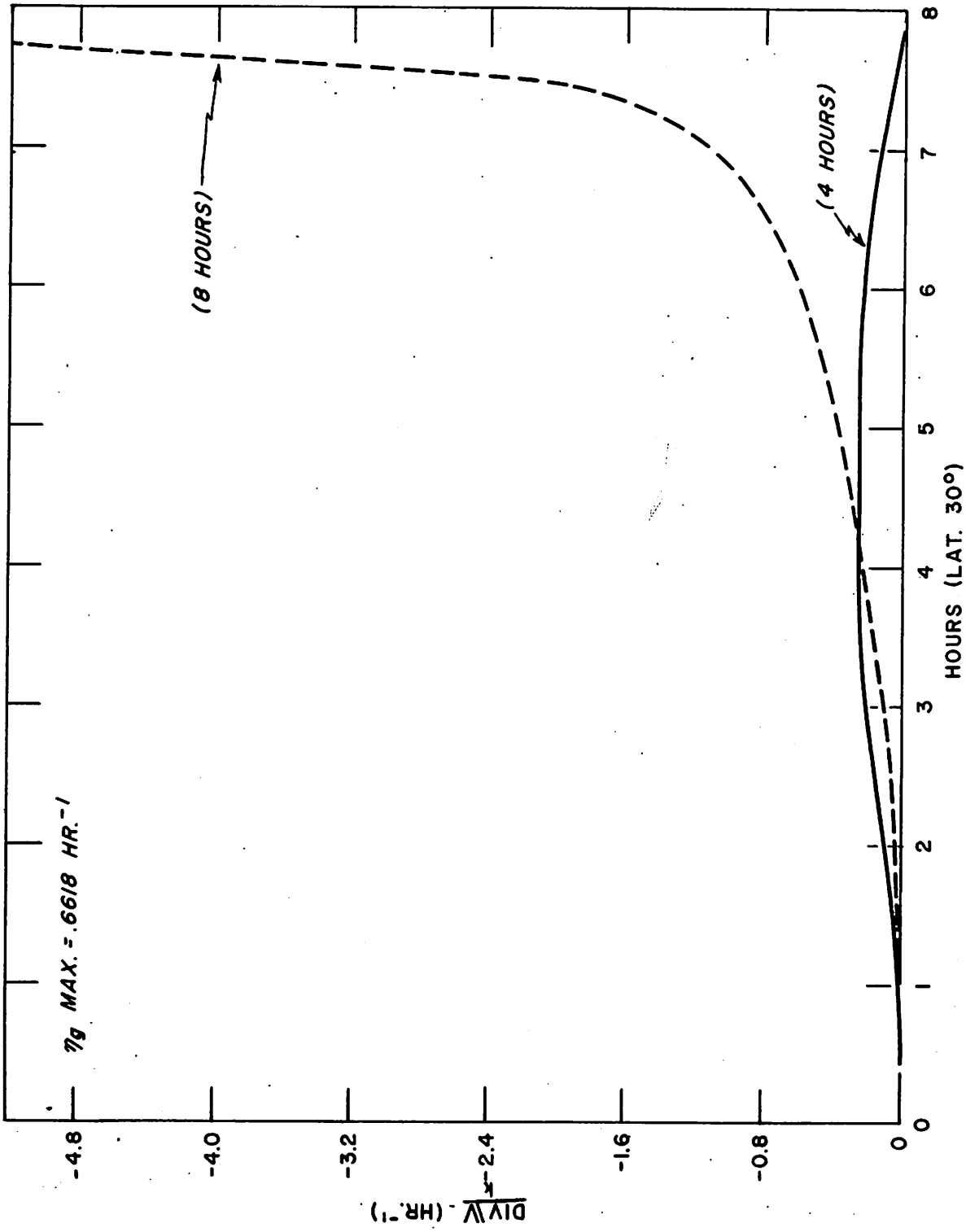
(8 HOURS)
(4 HOURS)
$\eta_g$ MAX. = .66/8 HR.$^{-1}$
$\frac{DIV\,V}{\pi}$ - (HR.$^{-1}$)
-4.8
-4.0
-3.2
-2.4
-1.6
-0.8
0
1
2
3
4
5
6
7
8
HOURS (LAT. 30°)

Figure 13

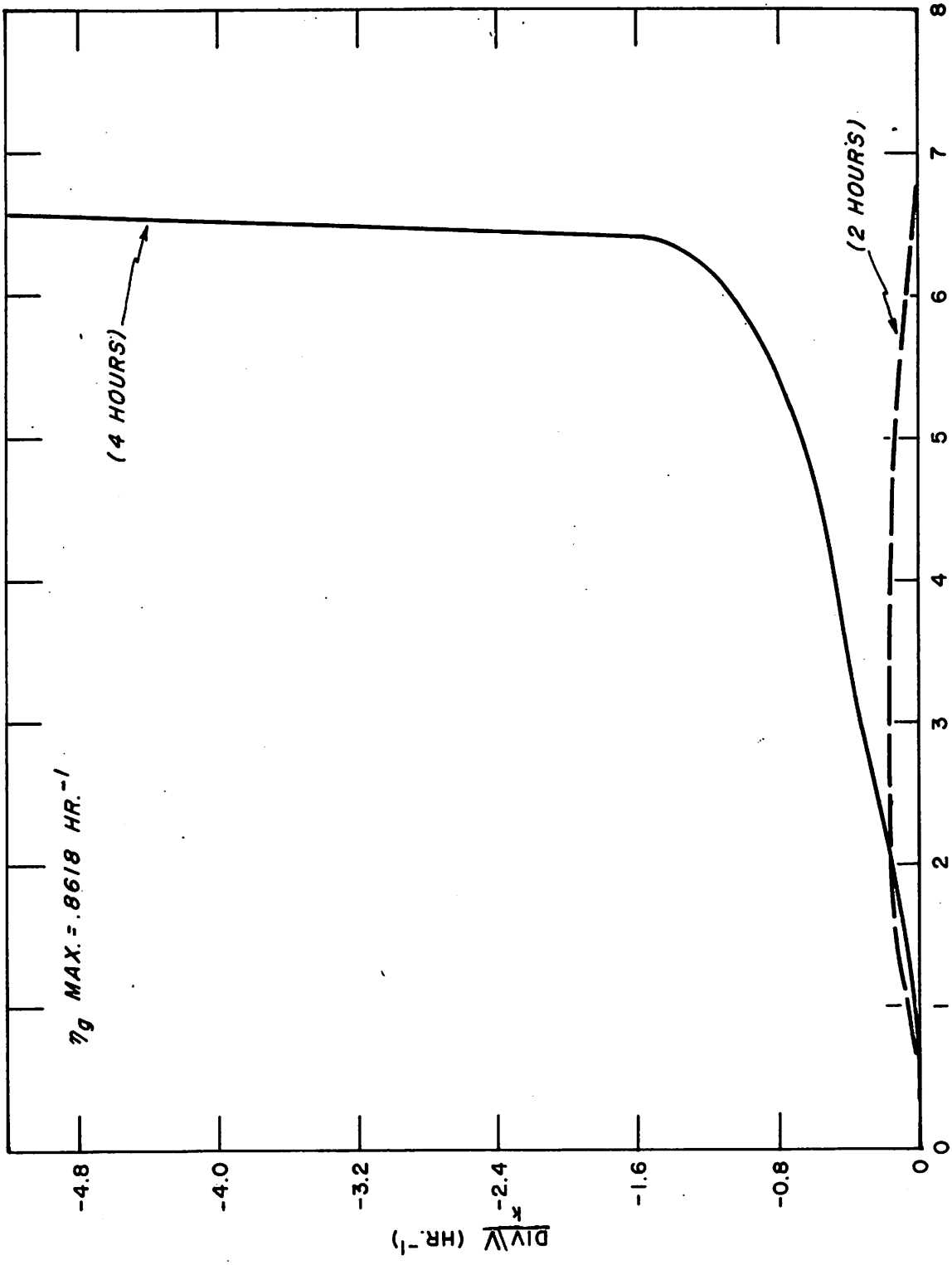
(4 HOURS)
(2 HOURS)
$\eta_g$ MAX. = .8618 HR.$^{-1}$
$\frac{DIV_K V}{V}$ (HR.$^{-1}$)
-4.8
-4.0
-3.2
-2.4
-1.6
-0.8
0
1
2
3
4
5
6
7
8
HOURS (LAT. 30°)

Figure 14

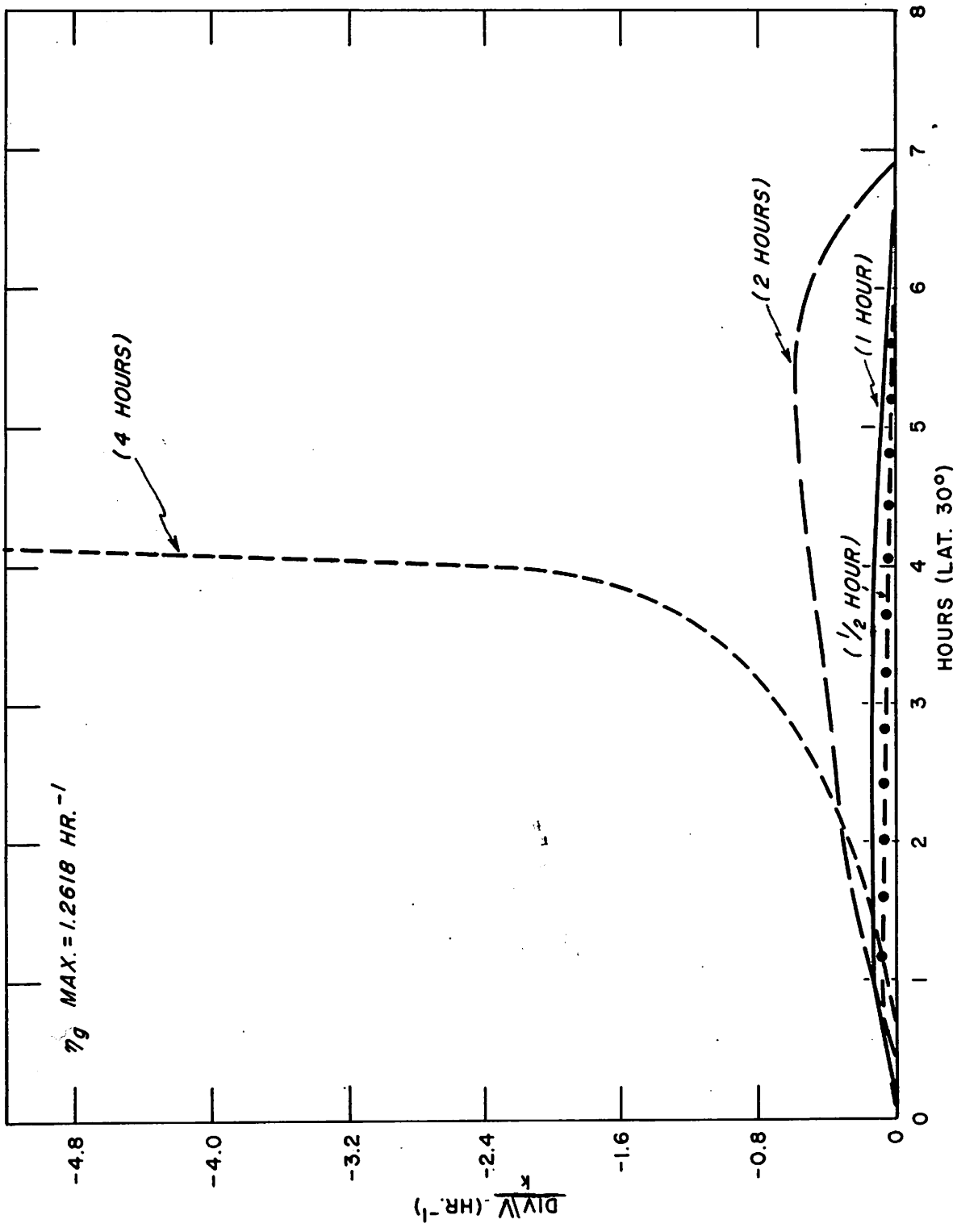
(4 HOURS)
(2 HOURS)
(1 HOUR)
(½ HOUR)
$\eta_g$ MAX. = 1.2618 HR.$^{-1}$
$\frac{DIV}{K}$ (HR.$^{-1}$)
HOURS (LAT. 30°)
-4.8
-4.0
-3.2
-2.4
-1.6
-0.8
0
1
2
3
4
5
6
7
8

Figure 15

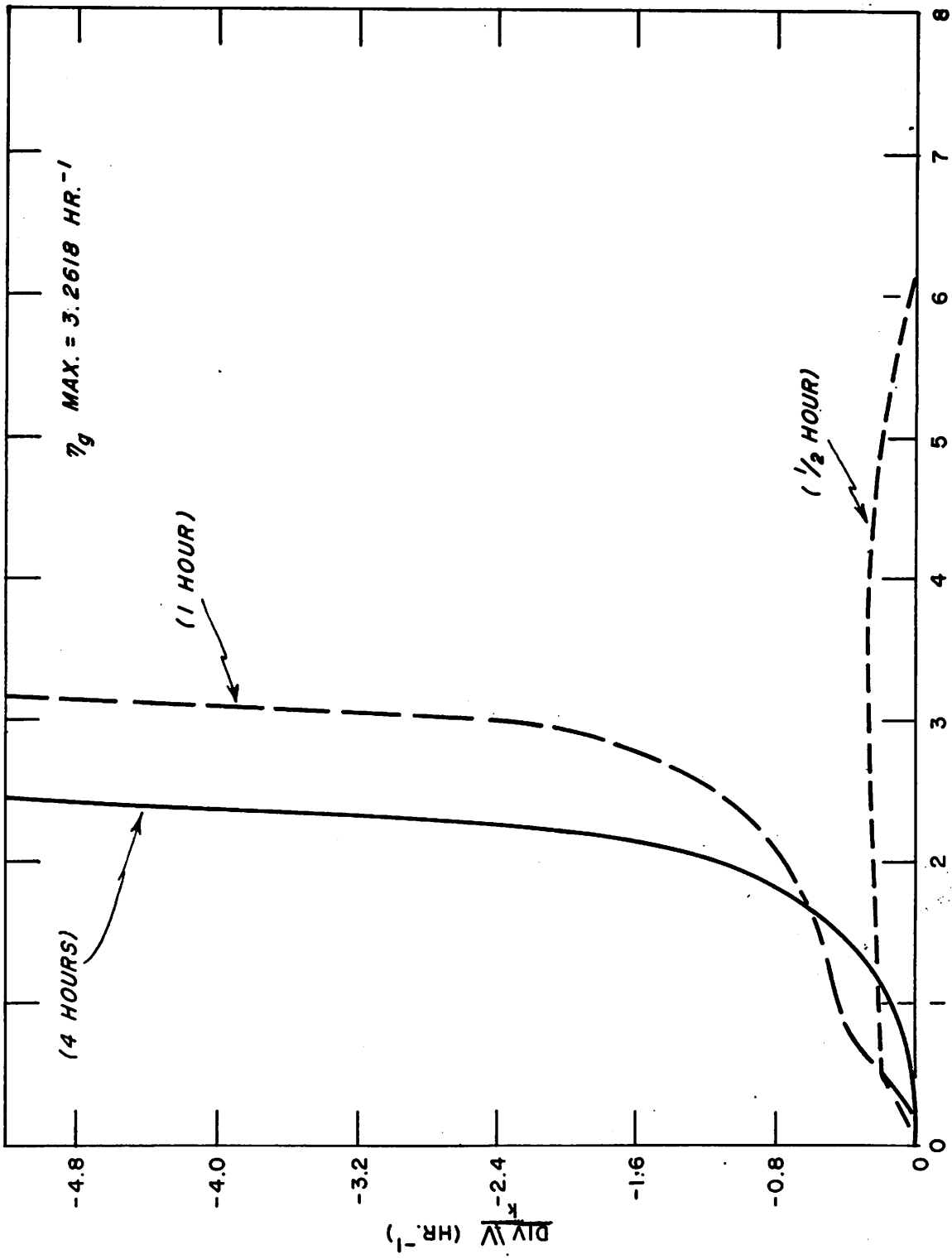
$\eta_g$ MAX. = 3.2618 HR.$^{-1}$
(1 HOUR)
(½ HOUR)
(4 HOURS)
HOURS (LAT. 30°)
$\frac{DIV\,V}{k}$ (HR.$^{-1}$)
0
1
2
3
4
5
6
7
8
-4.8
-4.0
-3.2
-2.4
-1.6
-0.8

Figure 16

# PART 2. SYNOPTIC STUDIES ILLUSTRATING THE PRINCIPLES

K. R. Peterson, C. W. Cochrane, and S. Molansky

Hydrologic Services Division, U. S. Weather Bureau, Washington, D. C.

[Manuscript received January 27, 1959; revised November 13, 1959]

## 1. INTRODUCTION

Part 2 is concerned with the synoptic evidence for the hypothesis developed in Part 1. In particular it is desired to see whether in observed heavy rainfall situations: (1) the rainfall was preceded by cyclonicity in the surface pressure field, (2) if by computations of dynamic trajectories it is possible to explain the location of the heavy rainfall, and (3) what portion of the volume of moisture flowing into the cyclonic portion of a system fell as precipitation.

Other questions that enter the discussion are: (1) whether the present network of stations and the present quality of pressure observations are good enough to determine the cyclonicity even if it exists, (2) how detailed an analysis of the data is needed.

Studies confined to cases where it is known that heavy rainfall has occurred provide, of course, verification only for the minimization of Type I statistical errors. A later and more time-consuming stage in such investigations is that of whether the cyclonic and moisture characteristics are always followed by heavy rainfall and of the magnitude indicated. The latter question is answered to some extent by the skill shown in routine application of the concepts to forecasting, which will be reported in Part 3 of this report.

Quantitative precipitation "forecasts" were made for the following storms: (a) Hurricane Diane, Aug. 17-19, 1955; (b) Holt, Mo. storm, June 22, 1947; and (c) Hallett, Okla. storm, Sept. 3-4, 1940. These storms were selected because they produced heavy concentrated rainfall of an intensity not predicted using standard macro-analytic techniques. The "forecasts" were made using actual analyses of the pressure and moisture fields.

The maps prepared for studying these storms were: (a) hourly or 3-hourly sea level pressure analyses for a 1-millibar isobar interval plotted on one to five million map bases; (b) gradient level or 2,000-foot wind charts; and (c) 3-hour isohyetal maps. With the exception of the Holt, Mo. storm the data for the surface maps are from original observers' records. Data for the Holt storm were obtained from WBAN Analysis Center maps. The isohyetal map data were obtained from U. S. Weather Bureau Hydrologic Bulletins and Hourly Precipitation Data.

It was shown in Part 1 that if the variation of geostrophic vorticity, $\eta_g$, of a subtantial quantity of air, passing through a pressure field is assumed to be sinusoidal with time, such as is shown by the curves on the left in figures 1 and 2, the solution of the divergence-development equations of Part 1 gives a time distribution of convergence similar to the curves shown on the right in the diagrams, the exact shape of the curves being dependent upon the duration and amplitude of the $\eta_g$ curve. Figure 1 shows how a variation in duration of $\eta_g$ affects the convergence, while figure 2 shows the effect of a variation in the amplitude of $\eta_g$ upon the convergence. An increase in duration or amplitude of $\eta_g$ causes an increase in convergence. On the weather map this shows up as a decrease in the areal extent or an increase in the magnitude of a region of geostrophic shear or curvature. In developing the forecast procedure, initially an attempt was made to apply these results directly to the synoptic examples. In order to accomplish this the variation of geostrophic vorticity of individual parcels must be determined. An attempt was made to measure the duration and amplitude of $\eta_g$ of actual air parcels and compare these with the theoretical cases, thereby giving the time and space distribution of convergence. Actually, the variation of vorticity along trajectories in the vicinity of vorticity maxima for the storms being studied was closely sinusoidal, as was determined by several plots of $\eta_g$ vs. time. Therefore it was possible to compare these cases with the theoretical cases. (Laplacians of pressure taken from surface maps or b-values where $b = \ell^2 \nabla^2 p$ were used in place of vorticity.) In Part 1 the solution of the comparison equation indicated convergence values which were much too small, that is, an extremely large $b_{max}$ would be required to produce only light or moderate precipitation. Therefore the solutions to the non-Jacobian equations were applied. However, most of these cases gave infinite convergence within a few hours, even with a relatively small $b_{max}$. This condition is represented by the solid curve in figure 1 and the dashed curve in figure 2.

It was decided to develop a prediction technique using the basic results of the theory; i.e., that a geostrophic vorticity maximum is followed by a convergence maximum downstream and that the time lag is of the order of hours. Geostrophic vorticity presents itself on the surface map in the form of shear of the geostrophic wind or of curvature in the isobars. Therefore if an air current passes through a region of cyclonic shear or curvature, precipitation can be expected downstream, provided that the air is sufficiently moist. The location of this rainfall is determined by the intensity and configuration of the pressure field and by trajectories obtained from the arc-strike technique developed by Goodyear [1]. The amount of rainfall is determined from the moisture transport inflow.

## 2. FORECASTING PROCEDURE

### Initial map time and forecast length

The first steps in the forecasting procedure are to select the initial map time and the length of the forecast. The forecast can begin at any time,

but in practice this would probably be when the isobars at a particular time indicate an increase in geostrophic wind shear or in curvature over the preceding map. The length of the forecast, i.e., the time from beginning to end of precipitation should be long enough for the convergence of parcels to reach a maximum and return close to zero downstream. From the theoretical results of Part 1 this length of time should be 9 hours for a weak vorticity maximum and 3 to 6 hours for strong to moderate vorticity maxima.

Prognostic maps

In order to determine the trajectories throughout the forecast period it is necessary to prepare prognostic maps for the length of the forecast period. These maps should be for at least 3-hour periods or for 1-hour periods in cases of sharp shear or curvature. Particular attention should be paid to the regions of shear and curvature. In the examples presented in this chapter, actual verifying pressure maps have been used in order to eliminate prognostic map errors.

Regions of shear or curvature

Isobars are examined for regions of shear and curvature. At this point, with some experience at constructing trajectories as described in [1], it is possible to make a qualitative forecast of where precipitation will occur by making trajectories by eye and thereby determining the approximate location of precipitation. The next steps in the procedure are to locate more closely where the rain will fall out and then to determine the volume of precipitation.

Trajectories

First, it is necessary to determine the region of future convergence downstream from the shear and curvature. This is done by taking a sufficient number of trajectories to define the field of flow through this region. The trajectories should begin upstream from the region of shear and/or curvature and should extend beyond the forecast time. In the cases presented, trajectories have been taken at 1 or 1-1/2 hour intervals, and the actual winds used in the procedure have been taken from 2000-foot or second standard level pibal charts while the geostrophic winds have been taken from sea level charts. From these trajectories it is possible to delineate the left and right or lateral boundaries of the convergence region. The boundaries of the convergence region are defined by two trajectories within which there is a decrease of area during equal periods of time.

The upstream and downstream boundaries of the convergence region are determined by the intensity and configuration of the shear or curvature of the isobars and by the dewpoint depression in the inflow region. These boundaries are shown in figure 3 along with the lateral boundaries of the convergence region. The solid lines are trajectories, while the dashed lines indicate the inflow boundary, the line of maximum shear and/or curvature, and the boundaries of the convergence region. In the synoptic studies presented, the exact relation between the upstream and downstream boundaries is not known. This relation must be determined empirically; however, such a relation cannot be developed using a limited number of cases but will be presented after more storms have been investigated. For the purpose of this report these

boundaries were chosen from the actual isohyetal maps. From Part 1 and also from the cases studied, the upstream boundary is 0 to 3 hours, while the downstream boundary is 4 to 10 hours travel time from the region of maximum shear and/or curvature.

Moisture transport

The moisture transport across a boundary or inflow volume can be expressed by the equation

$$I_v = L\, V_n\, W\, t \qquad (1)$$

where

$I_v$ = inflow volume (mi.$^2$in.)

$L$ = distance between A and A' (mi.) (fig. 3)

$V_n$ = mean inflow wind speed at gradient wind level during forecast period

$W$ = precipitable water (inches of depth) during forecast period

$t$ = duration of forecast (hours from beginning to end of precipitation)

This equation gives the volume of moisture which will be transported across L and will enter the inflow region during the time of the forecast. L should be measured in the maximum shear or curvature region or slightly upstream and should be oriented so that it is perpendicular to $V_n$. $V_n$ is computed from the observed mean gradient wind speed normal to L during the forecast period. This wind should be the same as the wind determined from the trajectories across L. The precipitable water, W, is computed in 100-mb. layers from the surface to 400 mb. The value of W should be taken as closely as possible to the forecast time and also from one or more stations in the vicinity of the boundary L. The duration, t, of the forecast is determined by the upstream and downstream boundaries of the inflow region, which, in turn are determined by the configuration of the isobars, as was indicated in the previous section.

Efficiency

Admittedly, all of the moisture transported across L does not fall out as precipitation. The continuity equation between precipitation volume and inflow volume can be written

$$P_v = W_b + I_v - O_v - W_e \qquad (2)$$

where

$P_v$ = precipitation

$W_b$ = moisture initially within inflow region

$I_v$ = inflow

$O_v$ = outflow

$W_e$ = moisture within inflow region at end of time period

A quantity which is a measure of the efficiency of the precipitation process can be defined by

$$E = \frac{P_v}{I_v} \tag{3}$$

The efficiency as defined assumes that the moisture which does not precipitate within the inflow area is either transported out of the area as outflow or causes an increase in the precipitable water within the area. This efficiency cannot be determined from such a small number of cases. Theory shows that the efficiency is dependent upon the magnitude and configuration of the geostrophic vorticity or the shear of the geostrophic wind and curvature of the isobars. (See Part 1.) This relation may be determined after more storms have been investigated.

The remainder of Part 2 is concerned with the application of these forecast techniques to the three synoptic examples mentioned previously.

## 3. HURRICANE DIANE

### Storm features

The first storm studied was hurricane Diane which entered the United States mainland near Wilmington, N. C. on August 17, 1955 and passed out to sea on August 19, 1955 south of New England. A detailed track of the storm, based upon hourly pressure analyses, is shown in figure 4. A decrease of storm speed in northern Virginia is noticeable from 0130 EST to 0730 EST August 18 as the storm changed direction and began to move toward the northeast. The track of a secondary center which formed about 60 nautical miles northeast of the primary center during the morning of August 18 is also shown. The squares show the location of cities mentioned in the text.

Hurricane Diane was notable for the heavily concentrated precipitation which fell in the Northeast after the center had filled and moved a considerable distance inland (Aug. 18). However, the 24-hour volume of rainfall within the 1-inch isohyet on the day the storm moved inland (Aug. 17) was almost the same as the volume of rainfall on August 18. Using Schoner's and Molansky's [2] isohyetal maps shown in figures 5 and 6 and applying a 50-mile-square grid within the 1-inch isohyet, 172,000 mi.$^2$in. of precipitation were obtained from midnight to midnight August 17 while 181,000 mi.$^2$ in. of rain occurred during the same time interval on August 18. An examination of figure 5 indicates that the 1-inch isohyet extends over the ocean. No attempt has been made to approximate this extension; therefore the volume of rainfall on August 17 can reasonably be adjusted upwards, closer to the value on August 18. Such an analysis indicates that the volume of precipitation on August 17 was about the same as the volume which caused serious flooding in the Northeast on August 18, the difference between the two days being that the rainfall on the latter day was more concentrated.

The pressure profile of the center with respect to time is given in figure 7. A general filling is evident from the time the hurricane crossed the coast (at 0730 EST Aug. 17) until 1330 EST August 18, after which time the center began to deepen slowly.

Figure 8 illustrates several pressure profiles taken from the center of the storm toward the northeast, the region of maximum curvature. These indicate a slightly curved profile at 0730 EST August 17, becoming nearly linear by 0730 EST August 18. At 1330 EST the effect of the secondary center is evident as a dip in the profile about 80 miles from the primary center. By 1930 EST the central pressure has decreased and the profile has returned to approximate linearity.

Maps indicating the times of beginning and ending of heavy rainfall are shown in figures 9 and 10. The isochrones are drawn for every 3 hours and are for Eastern Standard Time. In order to eliminate small, unimportant amounts, the time of beginning of precipitation was defined as the time when the rainfall rate began to equal or exceed 0.20 in. $hr.^{-1}$ and remained above this amount for at least two consecutive hours. The time of ending of precipitation was the hour when the succeeding hourly rainfall amounts were less than 0.20 in. for two hours or more. The heavy New England rainfall on the morning of the 18th is not shown. The isochrones indicate the time of beginning and ending of only the major bursts. The duration of the heavy rainfall was obtained from the above figures and is shown in figure 11.

Precipitation forecasts for Diane were made for initial map times of 0130 EST and 1030 EST August 18, and 0130 EST August 19, 1955. These times were selected because they were followed (during the succeeding 6-9 hours) by light, moderate, and heavy rain, respectively.

Forecast beginning 0130 EST August 18

Consider first the surface map for 0130 EST August 18 (fig. 12). The hurricane center was located near Lynchburg, Va. with a line of maximum curvature extending toward the north-northeast. Also there was some cyclonic shear between Lynchburg and Blackstone and between Richmond and Urbana, Va. A forecast of rainfall in the vicinity of the low center was made first. From a qualitative examination of the isobars, rain during the next 6-9 hours could be expected to fall in northern Virginia and eastern West Virginia.

Figures 13 and 14 show the surface maps for 0430 EST and 0730 EST August 18. It can be seen from these maps that the trough line (cyclonic curvature) had sharpened while the regions of shear diminished somewhat.

In order to make a quantitative forecast, trajectories were taken east of the hurricane center (fig. 15). All trajectories were taken beginning at the initial time and it was assumed that they remained constant for the full period of the forecast. A sufficient number of trajectories was taken to define the convergent region (shown by the hatched area). The arc strike interval was 1-1/2 hours. Initial winds were selected from 2000-ft. wind charts for 2200 EST August 17 and 0400 EST August 18. From the figure, AA' was chosen for L (120 nautical miles), the line across which inflow is to take place. Convergence was forecast to take place within the interpolated trajectories between A and A'. The starting points of the trajectories were chosen so that they formed a line, L, perpendicular to $V_n$. $V_n$ (18 knots) was measured by interpolation from 2000-foot wind charts. W (2.12 inches) was measured at Hatteras, N.C. at 2200 EST August 17. The time interval chosen was 6 hours.

The moisture transport was equal to 27,500 mi.$^2$ in. The duration of rainfall was taken from the verifying isohyetal map (fig. 17) but is related to the magnitude of the shear and curvature and the dewpoint depression in the vicinity of the shear and curvature.

The dashed line in figure 17 indicates the inflow area. The actual volume of rain which fell within this area was 10,700 mi.$^2$ in. The total volume of rain in this area and surrounding region was 28,500 mi.$^2$ in. These results give a rainfall efficiency of 39 percent within the inflow area and 104 percent for the inflow vs. total area. With the exception of some rainfall to the right of the inflow area (in the vicinity of Washington, D. C.), all of the appreciable rain fell well within the inflow area. By dividing the volume of precipitation as determined by inflow considerations by the inflow area, one obtains the average computed rainfall. In this case this was 1.7 in., while the observed average precipitation within the inflow area was 0.7 in.

The observed isohyetal pattern (fig. 17) indicates a second area of rainfall in the Northeast. A forecast of this rainfall was also made for the same initial map time (0130 EST Aug. 18.) From the surface maps during the forecast period (figs. 12 through 14) it can be seen that there is weak cyclonic shear and curvature extending from Philadelphia, Pa. to Nantucket, Mass. On this basis, a qualitative forecast of rainfall in southern New York and southern New England was attempted. Trajectories for this area taken for 1-1/2 hour arc-strikes and with initial winds selected from extrapolation of 2000-ft. winds are shown in figure 16. The trajectories show isolated regions of convergence separated by areas of divergence with no indication of a large-scale precipitation area. Figure 17 shows the observed isohyetal map for the 6-hour period. It can be seen that moderate precipitation occurred in a band from northeastern Pennsylvania to eastern Massachusetts. The inability of the trajectories to indicate this precipitation possibly may be attributed to the following:

1. Incorrect initial winds obtained by extrapolation over water of a few coastal observations.

2. Incorrect analysis of the sea level pressure fields. Although a number of ship observations were available, some discrepancy was noted between adjacent ship's pressures, making a consistent analysis difficult. Most of the ships failed to send a sufficient number of observations to determine systematic errors which could have been corrected. Those ships that did, gave some evidence that the curvature of the isobars offshore could have been greater than shown.

3. Precipitation effects not discernible by the technique presented in this section.

Forecast beginning 1030 EST August 18

The second initial forecast time was 1030 EST, August 18. At this time, Diane's primary center was in northern Virginia while a secondary center had begun to develop to the west of Baltimore, Md. (see fig. 18). Considerable shear and curvature was present to the east of this center. By 1330 EST

(fig. 19) the secondary center had developed further and the curvature to the east was still present. At 1630 EST (fig. 20) the secondary center had practically vanished but the curvature was still present. From this shear and curvature, a qualitative forecast of rainfall downstream from this region, i.e., in central and eastern Pennsylvania, is indicated. In order to make a quantitative forecast, trajectories were taken to the east and west of the secondary center (fig. 21). Again, the arc-strike interval was 1-1/2 hours and initial winds were selected from 2000-ft. wind charts for 1000 EST and 1600 EST August 18. Line AA' on figure 21 was chosen for L (120 nautical miles) since the end points of this line represented the lateral bounds of the convergent region. $V_n$ (18 knots) was measured by interpolation from the 2000-ft. wind charts. W (2.12 inches) was taken at Washington, D. C. for the 1000 EST observation. The inflow was measured for a 6-hour period. The moisture transport was equal to 27,500 $mi.^2$ in. The upstream and downstream boundaries were selected from the observed isohyetal map. The upstream boundary was one hour's travel time from the line of maximum curvature while the downstream boundary was 6 hours' travel time later. The inflow area is designated by cross-hatching.

The verifying isohyetal map is shown in figure 22. On this map, the dashed line indicates the inflow area. The actual precipitation volume was 17,600 $mi.^2$ in., giving an efficiency of 67 percent. It can be seen that most of the rain fell within the inflow area, the main exception being to the south. This rain was probably due to the fact that some upstream cyclonic vorticity was occurring prior to 1030 EST. The average moisture inflow computed over the inflow area amounted to 3.1 in. while the average actual precipitation over the same area was 2.1 in.

One interesting feature of the surface maps during this time period was the change in the isobars and wind field southeast of the storm center between 1030 EST and 1630 EST (figs. 18 and 20). At 1030 EST the isobars in the Chesapeake Bay and Lower Potomac region were oriented NNE-SSW; by 1630 EST they had become more nearly NE-SE. This shift caused a change in the trajectories, moving the maximum precipitation region eastward with time. Figure 9, showing the time of beginning of persistent rainfall greater than 0.20 in. per hour shows a rapid eastward spread of the rainfall maximum in the vicinity of Philadelphia (Point Breeze) with that station receiving 1.60 inches between 1700 EST and 1900 EST. Another effect was to shift abruptly the rainfall maximum from eastern Pennsylvania to southwestern Massachusetts shortly before midnight of the 18th. Although not used directly, the surface maps for 1930 EST and 2230 EST, August 18 are shown in figures 23 and 24.

Forecast beginning 0130 EST August 19

The third time period studied began at 0130 EST August 19. At this time, the center of Diane was near Philadelphia, moving east-northeastward (fig. 25). Figure 26 for 0430 EST and figure 27 for 0730 EST show this progression and also indicate a region of geostrophic wind shear near the center and geostrophic curvature extending outward from the center through Long Island and along the southern coast of New England. From a qualitative viewpoint, rainfall can be expected downstream from this region of cyclonic vorticity, or over central and southern New England.

In order to make a quantitative determination of the location and magnitude of the inflow area, trajectories were taken beginning south of the region of shear and curvature as shown in figure 28. The eastern convergence boundary is well defined since the trajectory to the left curves sharply westward, while that to the right curves eastward. The western convergence boundary is located at the point where the parcels begin to curve around the back side of the Low. From the observed isohyetal map the beginning of precipitation was set at 1 hour downstream from the line of maximum curvature. The time of ending of precipitation was set at 6 hours. These boundaries set off the area over which the transport of moisture was expected to occur. The moisture transport was equal to 28,100 mi.$^2$in.

The verifying isohyetal map is shown in figure 29. The dashed line indicates the inflow area. The observed volume within this area was 23,200 mi.$^2$ in., giving an efficiency of 83 percent. It can be seen that practically all the rain fell within the inflow area and that the maximum rainfall of over 7 inches is near the center of the area. The average precipitation computed from moisture inflow over the inflow area was 3.3 in. while the observed average rainfall over the same area was 2.8 in.

## 4. THE HOLT, MO. STORM

### Storm features

Twelve inches of rain fell in 42 minutes on the evening of June 22, 1947 at Holt, Mo., 27 miles northeast of Kansas City. A synoptic analysis of the storm was made by Lott [3]. The sea level pressure analyses for 1230 CST, 1530 CST, and 1830 CST presented in Lott's article, together with another 1-mb. analysis prepared from the WBAN manuscript map for 2130 CST, were used in this study (see solid lines in figs. 30-33). All times given in this study are Central Standard.

The technique used in this storm to outline the area of horizontal convergence is somewhat different from the method used in the hurricane Diane study. This is because the sea level pressure pattern in this storm was changing rapidly and the length of the baseline across which the moisture inflow was taking place decreased considerably during the storm period.

The heavy rain at Holt was associated with a meso-Low which developed in northeastern Kansas between 1230 CST and 1530 CST June 22. This meso-Low, which does not appear on the WBAN maps with 3-mb. isobar spacing, moved eastward into central Missouri and weakened considerably by 2130 CST.

### Area of horizontal convergence

The southern boundary of the area of horizontal convergence was taken as a straight line approximately normal to the moist southerly current east of the meso-Low center and, as nearly as possible, through the mean line of maximum curvature of the sea level isobars between 1530 CST and 2130 CST. This line will be called the baseline.

Trajectories were constructed, beginning on the baseline at 1530 CST and 1830 CST (figs. 34 and 35). The arc-strike technique (see [1]) was used,

starting with winds taken from streamline and isotach analyses of winds at about 2000 ft. above sea level at 1530 CST and 2130 CST. The geostrophic winds used in the arc-strike technique were obtained from the 3-hourly sea level maps mentioned above. Trajectories were drawn in 1-1/2 hour segments where possible. Half-hour segments were necessary where marked changes in the pressure gradient occurred along 1-1/2 hour segments of a trajectory.

Figure 34 shows trajectories of air parcels starting on the baseline at 1530 CST. Also shown is the approximate area of convergence of these parcels during the period 1530-2130 CST. The length of the baseline at 1530 CST is 172 nautical miles. Figure 35 shows the trajectories of air parcels starting on the baseline at 1830 CST, together with the area of convergence of these parcels for 1830-2130 CST. The baseline length at 1830CST is 147 nautical miles.

Note that the western boundaries of these two areas of convergence lie just to the west of the meso-low trough at 1530 CST and 1830 CST. The largest positive values of the Laplacians of sea level pressure are found in this trough, with large negative values just to the west. The dashed lines in figures 31-33 show the values of $\ell^2 \nabla_h^2 p_{sl} = p_1 + p_2 + p_3 + p_4 - 4 p_o$ where $\ell$ = 30 n.mi. is the grid size. The eastern boundaries of the areas of convergence are not as clearly related to the Laplacian field since values of the Laplacians become rather small a short distance east of the principal trough.

The western boundary of the area of convergence at 2130 CST was taken just to the west of the 2130 CST trough position. The eastern boundary at 2130 CST was taken just to the east of its position at 1830 CST. The Laplacian map for 2130 CST (fig. 33) provides some justification for this. The baseline length at 2130 CST is 105 nautical miles. The average of the baseline lengths at 1530, 1830, and 2130 CST is 141 nautical miles.

The areas of convergence outlined for 1530-2130 CST and 1830-2130 CST were drawn on the same map, together with the 2130 CST baseline. A smooth envelope inclosing these areas was then drawn to show the total area of horizontal convergence north of the baseline between the west end of the 1530 CST baseline and the east end of the 2130 CST baseline. The area for 1500-2100 CST was extrapolated from this envelope to make the time period coincide with that for the isohyetal map (fig. 36). The latter area is 19,700 $(n.mi.)^2$.

Inflow volume

The streamline and isotach charts were used to obtain the mean wind velocity $V_n$ across the baseline between 1530 CST and 2130 CST. The component of the mean baseline normal to $V_n$ was then computed. This was 137 nautical miles and is the value of L used to compute moisture inflow.

The results of precipitable water (W) computations are given in table 1. The value of W chosen as most representative of the moist current crossing the area baseline between 1500 and 2100 CST is 1.54 in., from the 2100 CST sounding at Columbia, Mo. For forecasting, it would have been necessary to use an

Table 1. - Precipitable water (in.) SFC-400 mb. June 22, 1947

| Station | Time (CST) | |
|---|---|---|
| | 0900 | 2100 |
| Omaha, Nebr. | 1.74 | 1.01 |
| Columbia, Mo. | 1.63 | 1.54 |
| Oklahoma City, Okla. | 1.50 | 1.11 (2200 CST) |
| Ft. Worth, Tex. | 1.70 | 1.70 |
| Little Rock, Ark. | 1.80 (1000 CST) | 2.02 |

earlier sounding, e. g., the average of the values at Columbia, Mo. and Oklahoma City at 0900 CST. That would have been 1.57 in.

From equation (1), the moisture inflow was found to equal 36,700 $(n. mi.)^2$ in.

Precipitation volume

A 6-hour isohyetal map (fig. 36) was constructed for the period 1500-2100 CST, using only recording-gage data, except for the 12-in. amount at Holt. From this map the total volume of precipitation within the total area of horizontal convergence determined above was computed. This amounted to 27,400 $(n.mi.)^2$in., which is an average of 1.39 in. for the 19,700 $(n.mi.)^2$ area.

Comparison of precipitation with inflow

From equation (2), if W = 1.54 in., $W_b$ = 30,300(n. mi.)$^2$ is the volume of precipitable water suspended over the 19,700 $(n.mi.)^2$ area in vapor form at the beginning of the period. This is nearly equal to the computed inflow volume for the following 6 hours. Assuming $W_e = W_b$, $O_v = I_v - P_v$ = 36,700 - 27,400 = 9300 $(n.mi.)^2$in. is the outflow volume. On the other hand, if $O_v = 0$, $W_e - W_b = I_v - P_v$ = 9300 $(n.mi.)^2$in. is the increase in volume of precipitable water over the area during the period.

In this study,

$$E = \frac{P_v}{I_v} = \frac{27,400}{36,700} = 0.747$$

This ratio might have been somewhat higher if all available reports had been used in constructing the isohyetal map instead of just recording-gage data.

# 5. THE HALLETT, OKLA. STORM

## Storm features

On September 4, 1940 a 24-inch rainfall occurred at Hallett, Okla., located 35 miles WNW of Tulsa. This unusual storm which has been studied extensively by Lott [4] constituted a record for Oklahoma since the 24-inch rainfall at Hallett, as established and verified by Corps of Engineers bucket-survey teams, occurred during the 11 hours between 0000 and 1030 CST of the 4th

## Data

Since the usual macro-analysis techniques did not account for this intense rainfall, it was decided to seek an explanation using the methods proposed in this paper. First, a series of hourly surface maps from 1800 CST September 3 through 1200 CST September 4 were analyzed for 1-millibar intervals. Most of the data for these maps were obtained from original observers' records and barograph traces, although some data were obtained from WBAN Analysis Center maps. Maps at 3-hour intervals during this time period are shown in figures 37-43. The star on each of these diagrams denotes the location of Hallett.

## Shear and curvature

An examination of the map for 1800 CST Sept. 3 (fig. 37), 6 hours prior to the start of heavy rain at Hallett, showed slight cyclonic shear and curvature present in eastern Oklahoma. Despite small pressure rises occurring east and north of Oklahoma, this pattern persisted until 2100 CST of the 3d with little change in the configuration of the isobars. However, at this time the map (fig. 38) showed a substantial increase in cyclonic shear and curvature in eastern Oklahoma. Further examination of the maps from 2100 CST of the 3d to 0900 CST of the 4th (all figs. 38-43) showed continuing cyclonic shear and curvature present over eastern Oklahoma of a sufficient magnitude to indicate that the rain at Hallett might be explained by this earlier upstream shear and curvature. In order to eliminate bias in the isobaric analysis, a simple finite-difference computation of the geostrophic shear from Oklahoma City, Okla. to Fort Smith, Ark. for the entire series of maps was made, using the observed pressures at Oklahoma City, McAlester and Fort Smith. These results, shown in table 2, indicated an abrupt increase in the geostrophic wind shear at 2100 CST of the 3d which lasted until 0400 CST of the 4th. After 0400 CST, the region of shear shifted westward and was not picked up by the fixed pressure values used to assess the shear.

## Trajectories

In order to investigate fully the effect of the shear line on air parcels crossing it, and thereby establish areas of convergence and divergence downstream, a number of trajectories were taken from points south and southeast of the shear line. Using the arc-strike technique [1] these were started at 1900 and 2200 CST of the 3d, and 0200 and 0500 CST of the 4th where initial winds for each trajectory were interpolated from 6-hourly 2000-ft.

winds-aloft charts. Figure 44 shows a composite of these trajectories. It may be seen that they tend to follow a somewhat similar pattern for the entire period of the trajectories. The dots are at 1-hour intervals. The heavy lines are the boundaries of the convergent area, and thus establish a general area within which precipitation was expected to occur.

## Inflow volume

The techniques outlined in the introduction to this chapter were then employed to delineate this inflow area, shown in figure 45, and to determine the volume of moisture inflow. The components of the moisture transport equation were obtained as follows. L was drawn at the region of maximum shear as the mean perpendicular between the bounding trajectories and was 80 statute miles. $V_n$ was the interpolated mean wind normal to L for the entire forecast period and was taken from 2000-ft wind charts. $V_n$ measured in this manner equaled 27 m.p.h. and agreed with the mean $V_n$ taken from the trajectories. The precipitable water, W, was computed using the raob for Brownsville, Tex. at 0000 CST Sept. 3, and gave a value of 2.02 in. While the flow of moisture across the central Gulf of Mexico, particularly in the vicinity of New Orleans, might have been more representative of the air reaching Oklahoma during the rainfall period, the limited upper air network of 1940 did not provide this data. The raob report closest to the inflow area and in the warm air was Brownsville. A comparison of the Brownsville raob for 0000 CST of the 3d with that of Oklahoma City (which was adjacent to the inflow area) for 0000 CST of the 4th indicated that the Brownsville raob was representative of the amount of precipitable water in the inflow area. Finally, the boundaries of the inflow area where rain would start and where the rain burst would end were taken from the isohyetal maps. The upstream boundary was taken 1 hour downstream from the shear region. Since the geostrophic wind shear in this storm was exceptionally large, these boundaries follow the hypothesis that strong cyclonic vorticity over a small area is followed by heavy short-duration rainfall bursts downstream. Since the shear held for 12 hours, the 3-hour volumetric amount of moisture within this region was quadrupled. In this manner, the inflow area was delineated and the 12-hour inflow volume beginning at 2200 CST of the 3d was measured by solving the moisture transport equation for the above data, giving an inflow volume of 52,400 $mi.^2 in.$ Dividing the initial inflow volume by the inflow area (8600 $mi.^2$), gave an average depth of 6.1 inches.

## Precipitation volume

The depth-duration-area curve for the Hallett storm as prepared by Lott [4] was used to obtain the observed precipitation volume. Using an area of 8600 $mi.^2$ and a duration of 12 hours, the observed average precipitation of the storm is 5.8 in., which means a volume of 49,900 $mi.^2 in.$ over the inflow area. Thus the area under consideration received 95 percent of the volume of rain computed from inflow considerations. It is felt that this method of verification was valid for this case of an intense, short-lived storm within which the area of interest received almost all its rain within 12 hours since the depth-duration-area curves are drawn on the basis of the maximum average depth of rainfall over an area for given time increments, usually 6 hours.

The total rainfall for the Hallett, Okla. storm is also shown in [4]. This map is for a 90-hour period, but almost all the rainfall occurred between 0000 and 1030 CST, September 4, 1940. Comparing the region of precipitation with the inflow area (fig. 45) it can be seen that except for small areas in the vicinity of Wichita, Kans. and southwest of Tulsa, Okla., all important rain is encompassed by the inflow area, and accordingly depth-duration-area values for the storm were derived for the most part from within the inflow area.

## 6. SUMMARY AND CONCLUSION

The three cases studied all show agreement to a large degree with the hypotheses developed in the conclusion of Part 1. Cyclonicity developed in the surface pressure field before the occurrence of the heavy rainfall. The heavy rainfall occurred downstream from the cyclonic region according to the wind direction at 2,000-3,000 feet above the surface and/or the geostrophic wind. The total volume of precipitation was, in all cases, a fairly large fraction (50-100 percent) of the volume of atmospheric moisture flowing into the cyclonic area.

Table 2. - Geostrophic wind shear between Fort Smith, Ark. and Oklahoma City, Oklahoma based upon observed pressures

| Time (CST) | Geostrophic wind Ft.Smith-McAlester (mi. hr.$^{-1}$) | Geostrophic wind McAlester-Okla. City (mi. hr.$^{-1}$) | Geostrophic wind shear between Ft.Smith and Oklahoma City (hr.$^{-1}$) |
|---|---|---|---|
| Sept.3,1940 | | | |
| 1800 | 41.2 | 24.5 | 0.18 |
| 1900 | 32.0 | 24.5 | 0.08 |
| 2000 | 30.6 | 22.1 | 0.09 |
| 2100 | 35.2 | 4.9 | 0.32 |
| 2200 | 39.8 | 6.2 | 0.36 |
| 2300 | 41.2 | 4.9 | 0.39 |
| Sept. 4,1940 | | | |
| 0000 | 41.2 | 8.6 | 0.35 |
| 0100 | 41.2 | 8.6 | 0.35 |
| 0200 | 39.8 | 9.9 | 0.32 |
| 0300 | 38.1 | 11.1 | 0.29 |
| 0400 | 35.2 | 17.2 | 0.19 |
| 0500 | 29.1 | 22.1 | 0.07 |
| 0600 | 18.2 | 30.7 | -0.13 |
| 0700 | 21.4 | 30.0 | -0.09 |
| 0800 | 22.8 | 32.0 | -0.10 |
| 0900 | 21.4 | 28.3 | -0.07 |
| 1000 | 19.9 | 30.0 | -0.11 |
| 1100 | 22.8 | 32.0 | -0.10 |
| 1200 | 32.0 | 36.9 | -0.05 |

## REFERENCES

1. H. V. Goodyear, "A Graphical Method for Computing Horizontal Trajectories in the Atmosphere," Monthly Weather Review, vol. 87, No. 5, May 1959, 188-195.
2. R. W. Schoner and S. Molansky, "Rainfall Associated with Hurricanes," National Hurricane Research Project Report No. 3, U. S. Weather Bureau, July 1956, pp. 201, 265.
3. G. A. Lott, "The World Record 42-Minute Holt, Missouri Rainstorm," Monthly Weather Review, vol. 82, No. 2, Feb. 1954, pp. 50-59.
4. G. A. Lott, "An Extraordinary Rainfall Centered at Hallett, Oklahoma," Monthly Weather Review, vol. 81, No. 1, Jan. 1953, pp. 1-10.

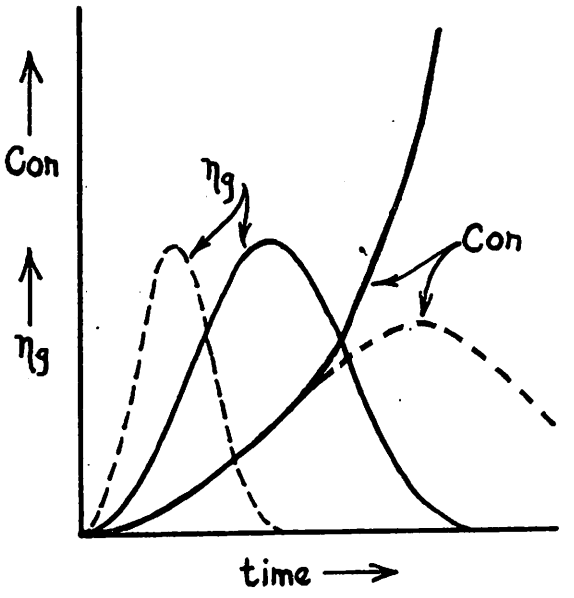


Figure 1. - Showing the effect of a variation of duration of $\eta_g$ upon convergence.

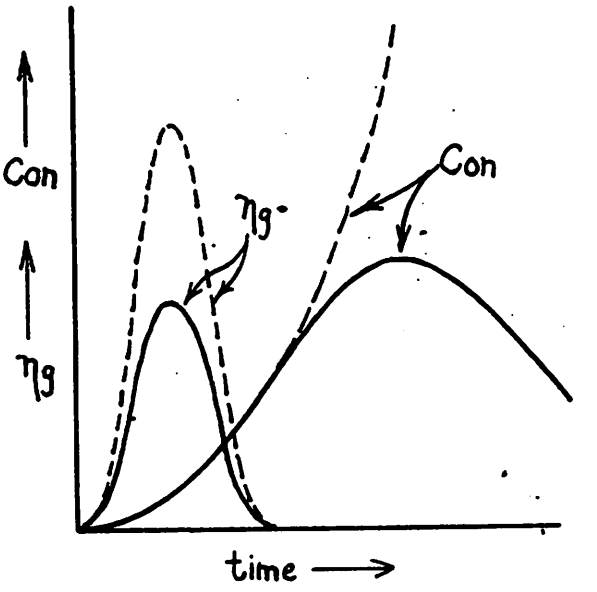


Figure 2. - Showing the effect of a variation of amplitude of $\eta_g$ upon convergence.

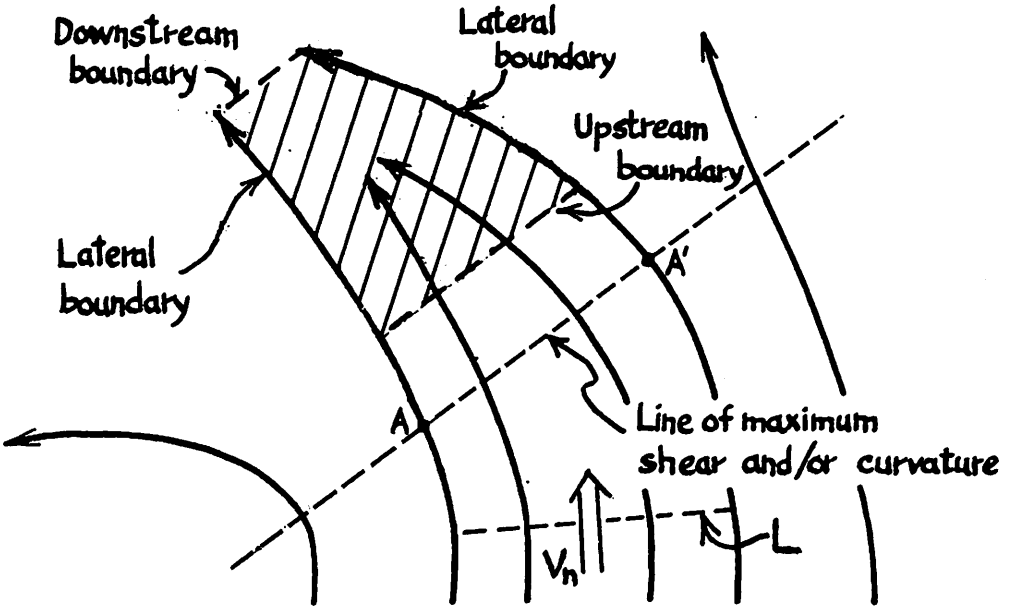


Figure 3. - Showing the inflow boundary (L), line of maximum shear and/or curvature, and bounds of convergence region (inflow area).

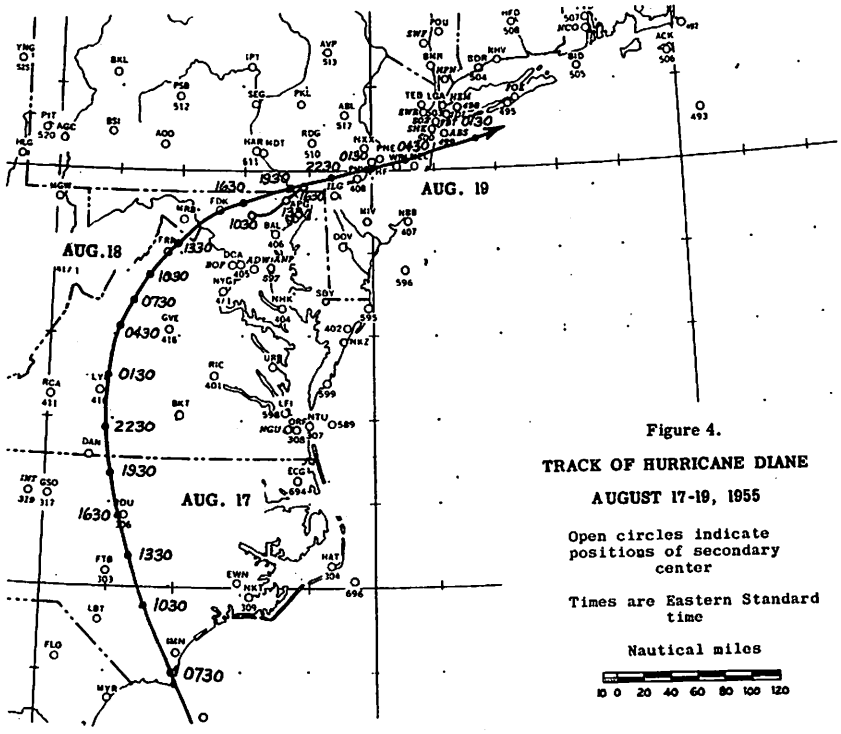


Figure 4.

TRACK OF HURRICANE DIANE

AUGUST 17-19, 1955

Open circles indicate positions of secondary center

Times are Eastern Standard time

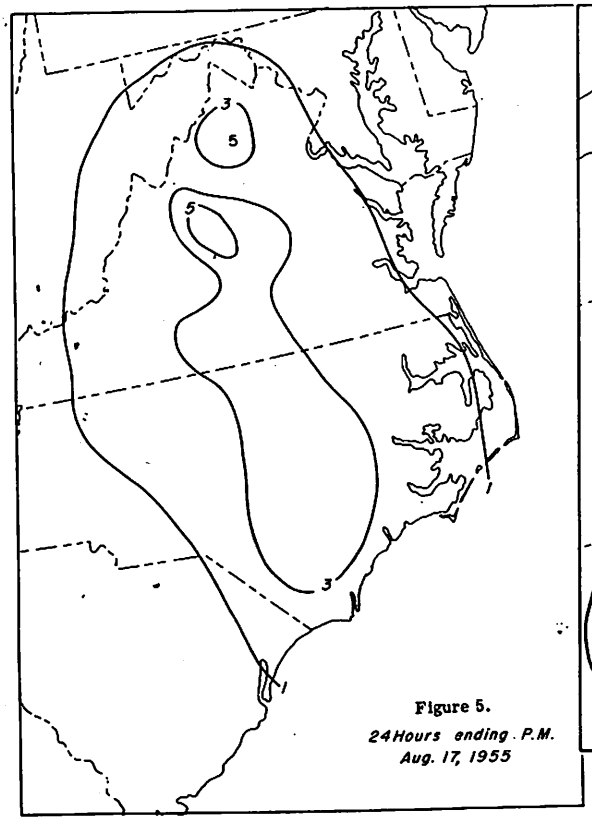


Figure 5.

*24 Hours ending P.M. Aug. 17, 1955*

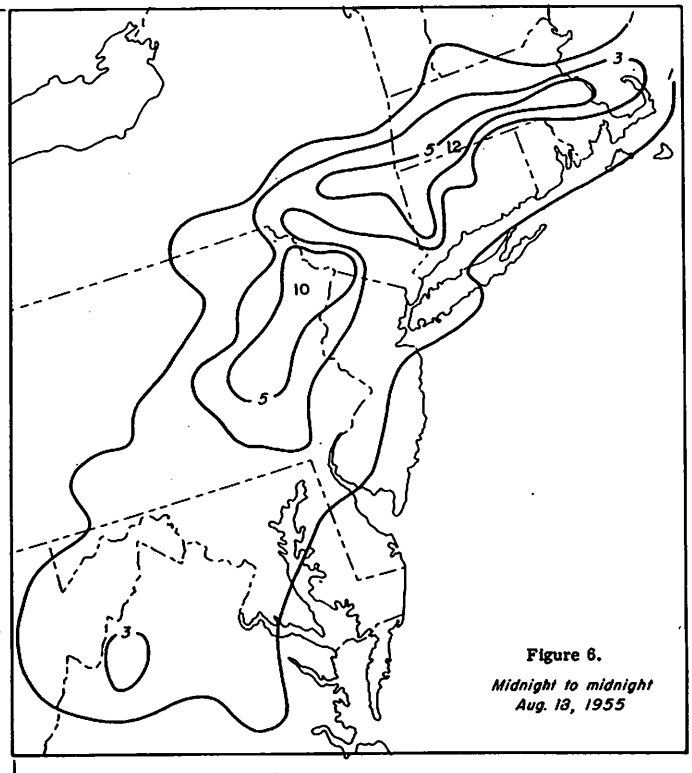


Figure 6.

*Midnight to midnight Aug. 18, 1955*

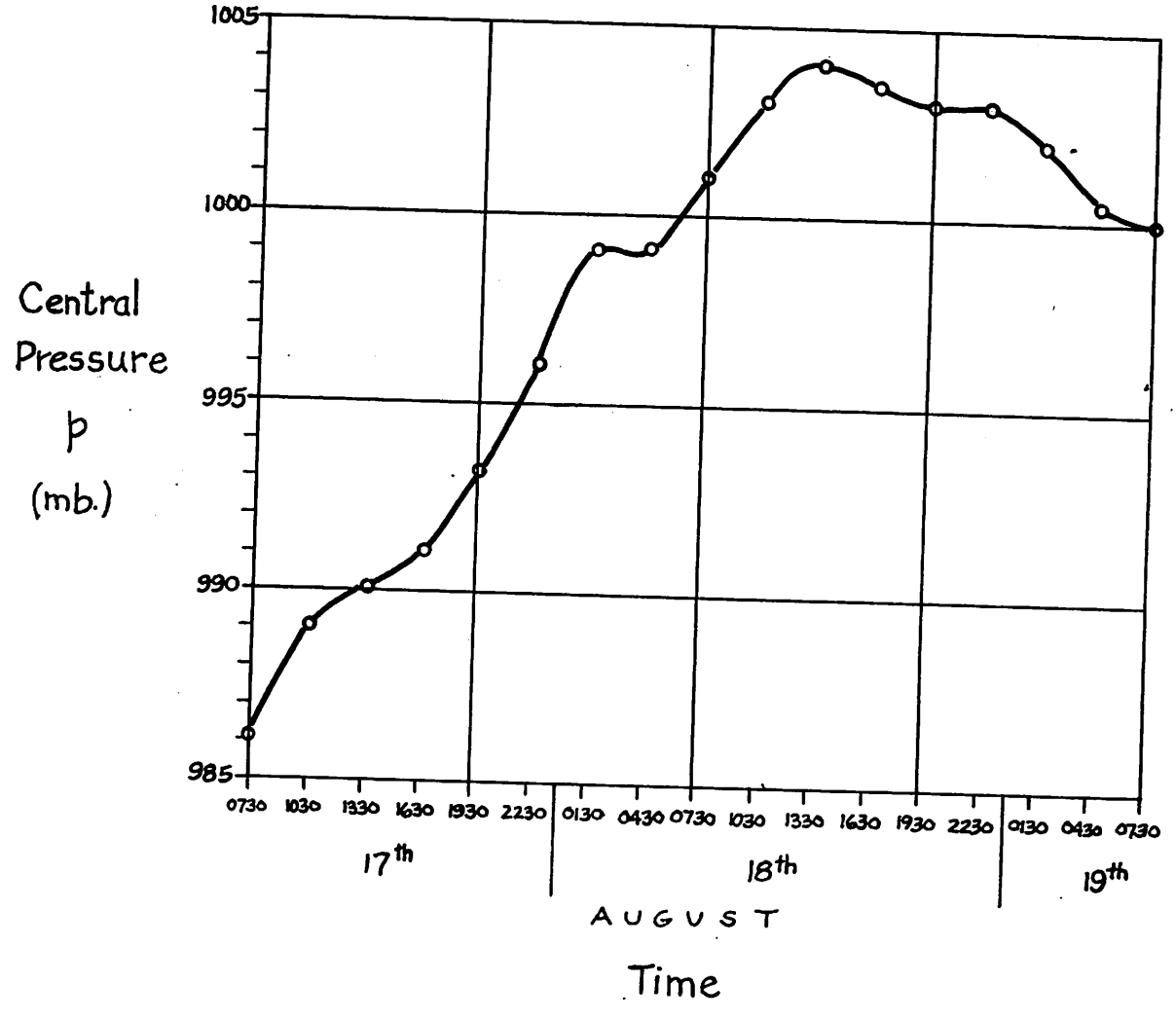


Figure 7. - Central pressure profile of hurricane Diane, August 17019, 1955.

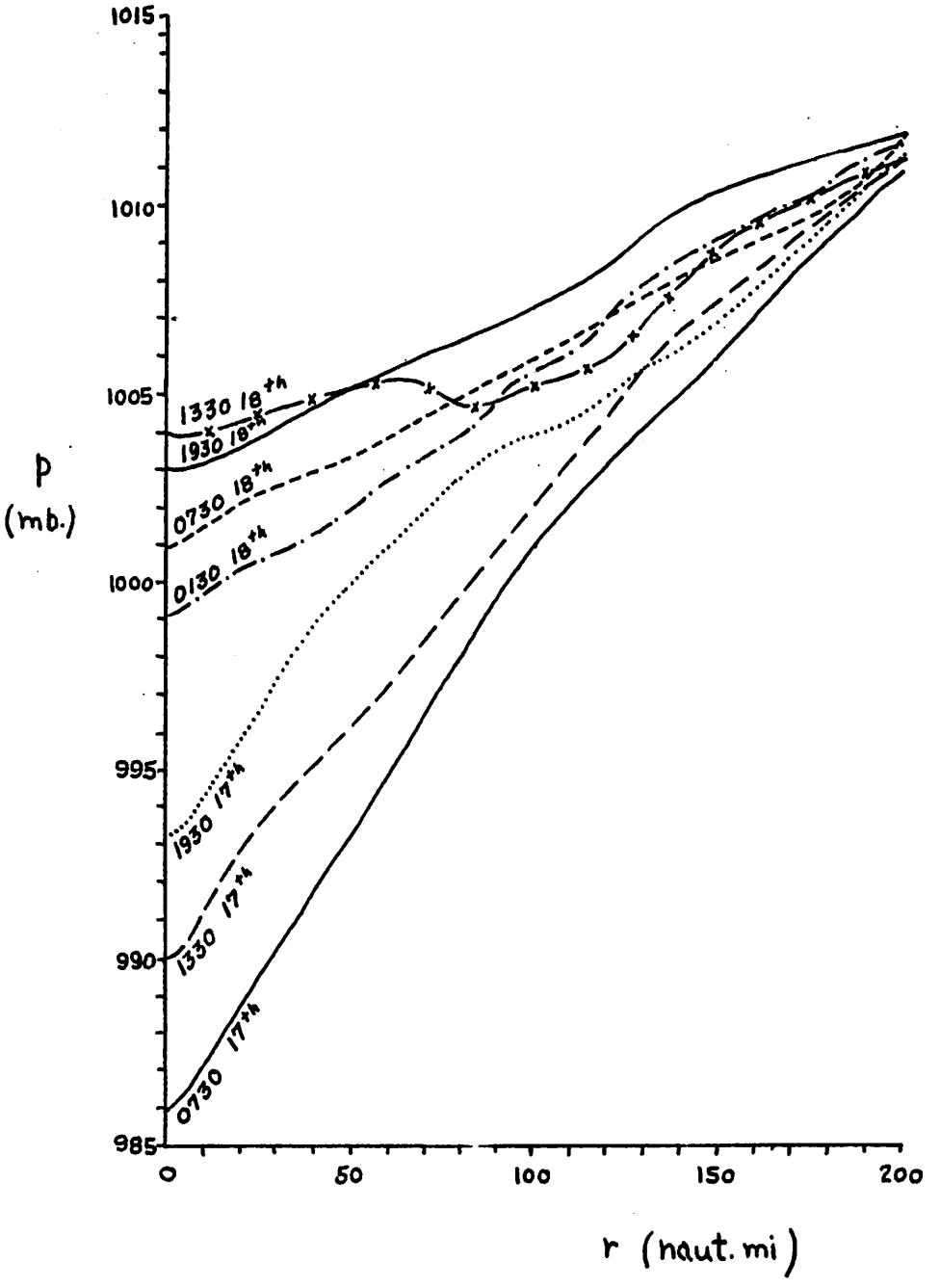


Figure 8. - Pressure profiles of hurricane Diane.

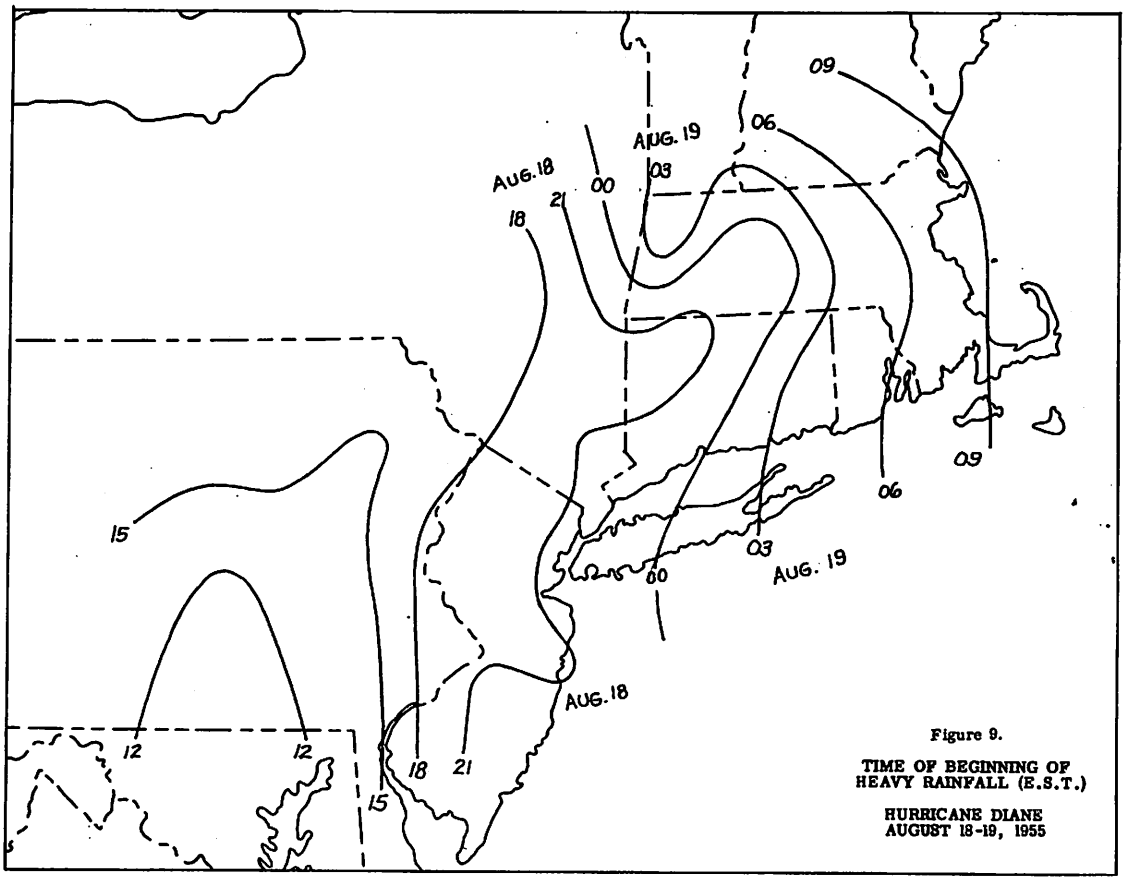


Figure 9.

TIME OF BEGINNING OF HEAVY RAINFALL (E.S.T.)

HURRICANE DIANE
AUGUST 18-19, 1955

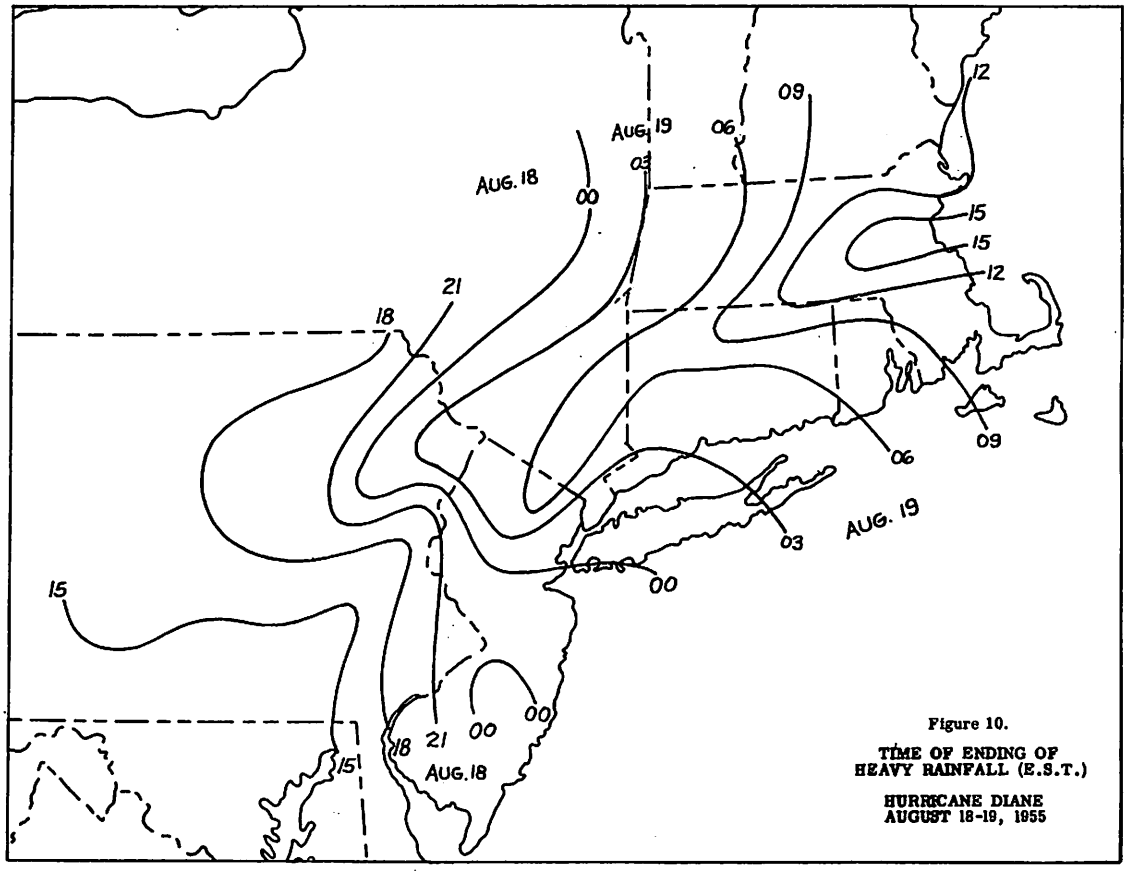


Figure 10.

TIME OF ENDING OF HEAVY RAINFALL (E.S.T.)

HURRICANE DIANE
AUGUST 18-19, 1955

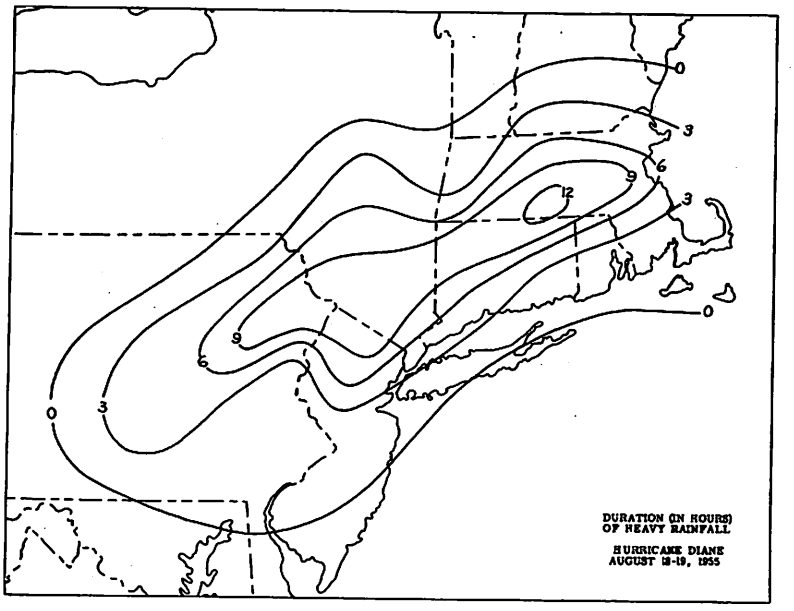


Figure 11.

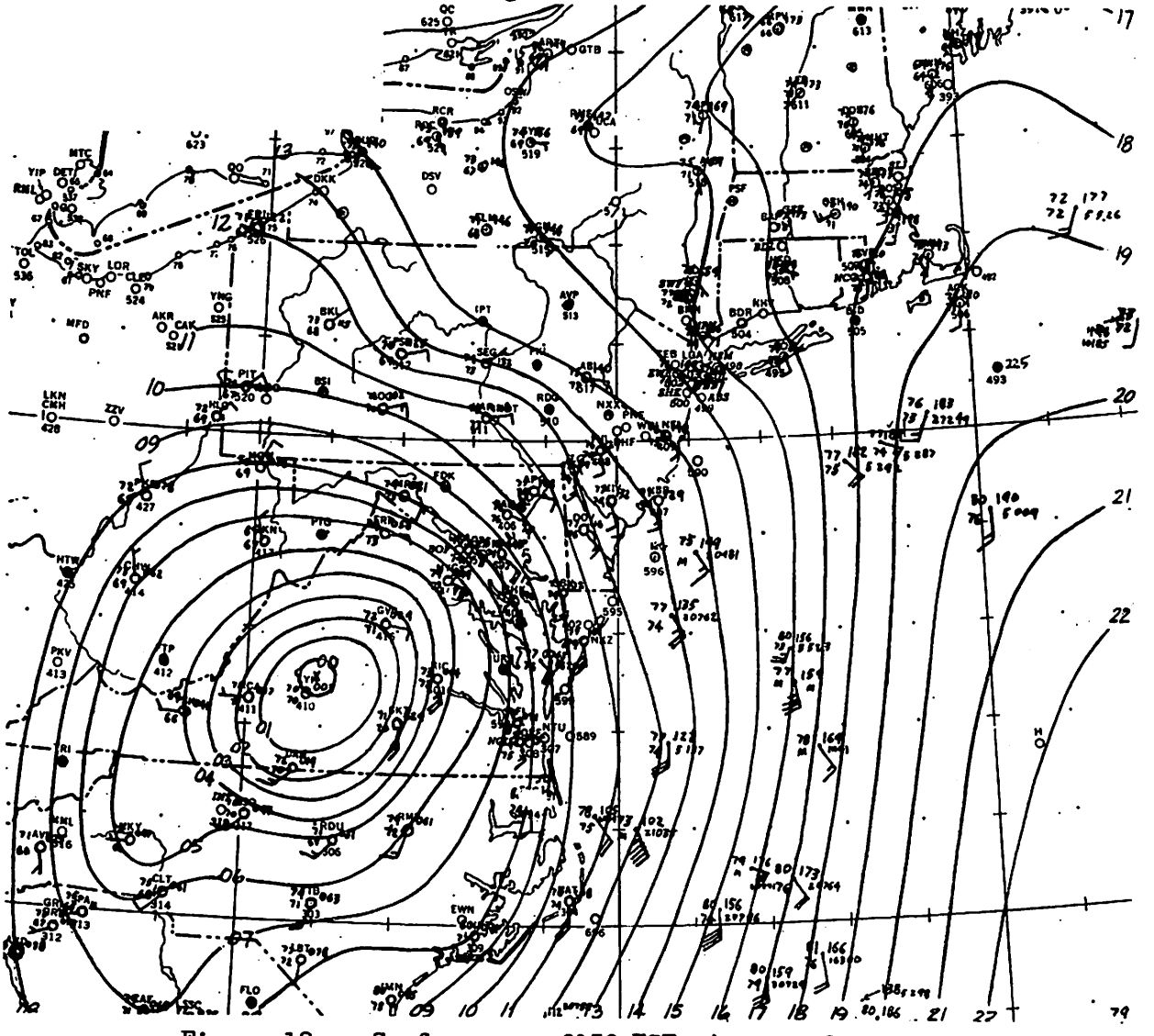

Figure 12. - Surface map, 0130 EST, August 18, 1955.

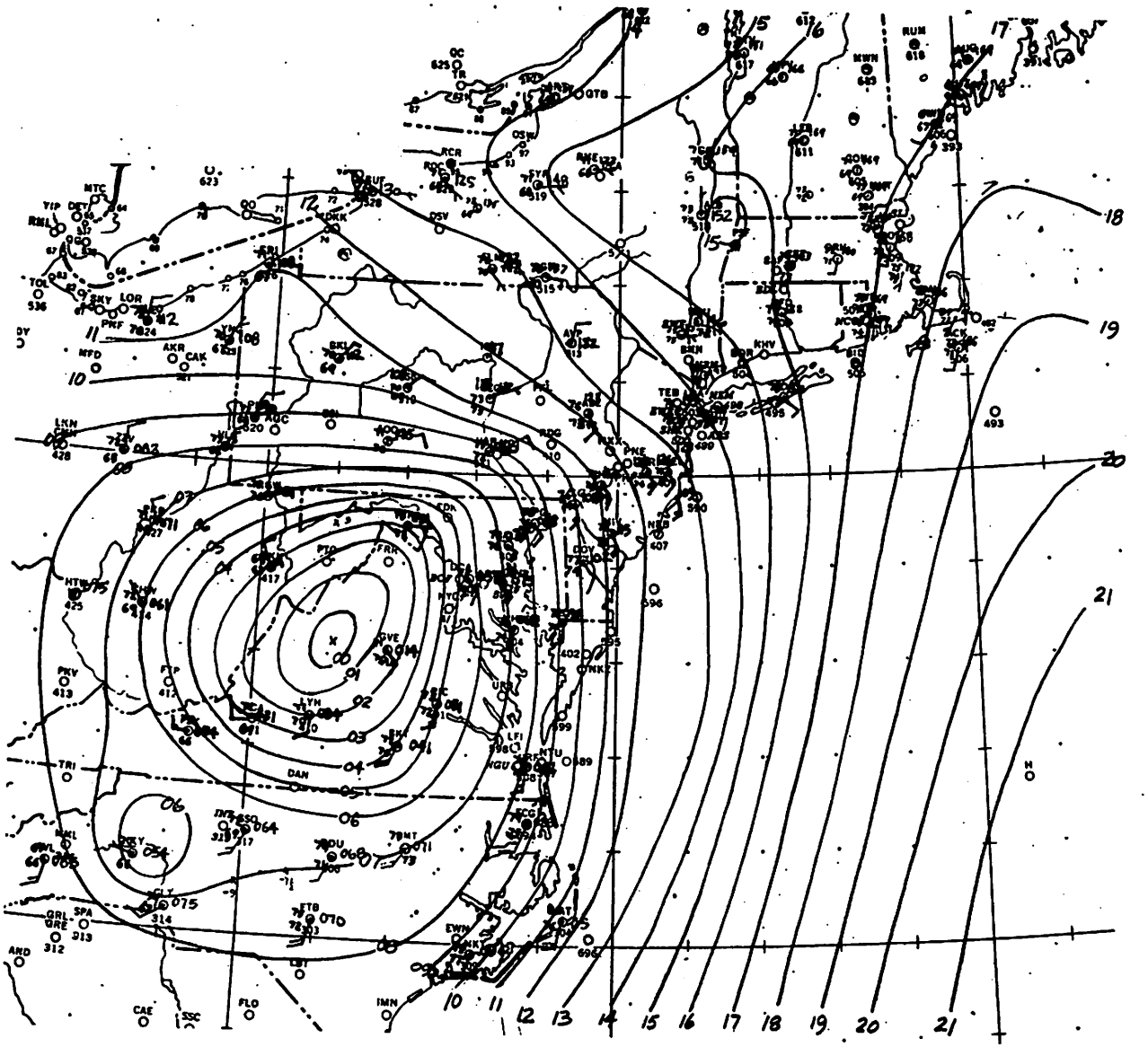

Figure 13. - Surface map, 0430 EST, August 18, 1955

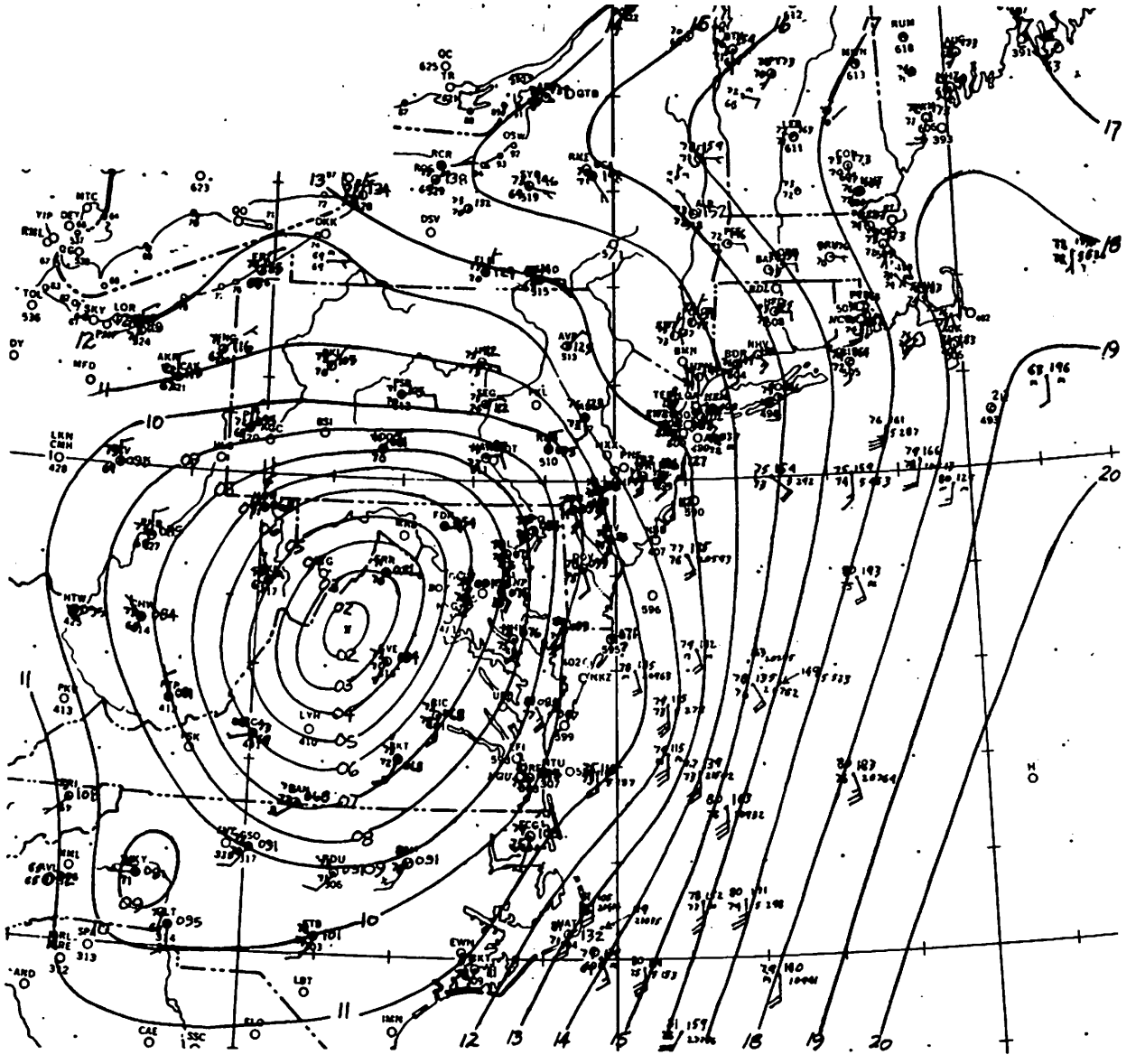

Figure 14. - Surface map, 0730 EST, August 18, 1955.

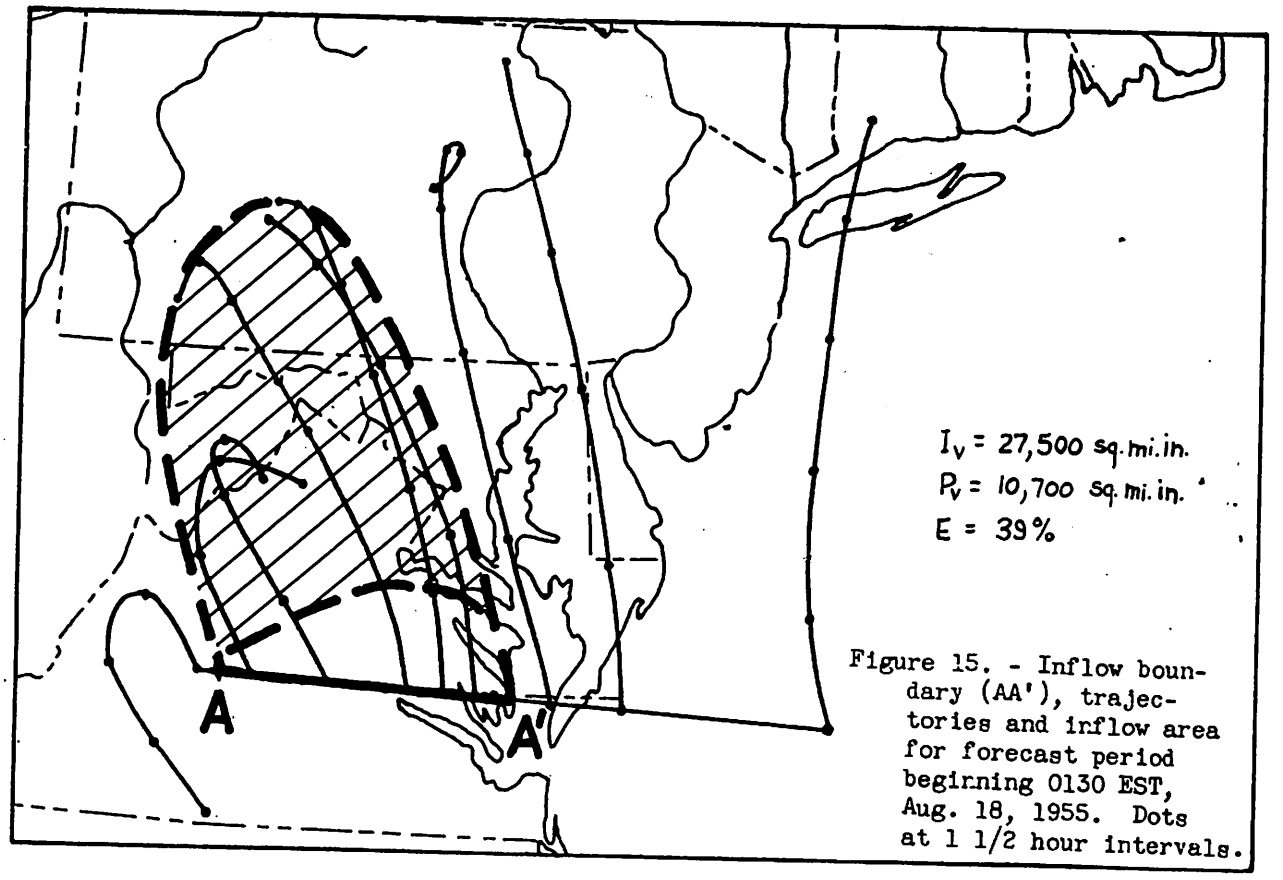


Figure 15. - Inflow boundary (AA'), trajectories and inflow area for forecast period beginning 0130 EST, Aug. 18, 1955. Dots at 1 1/2 hour intervals.

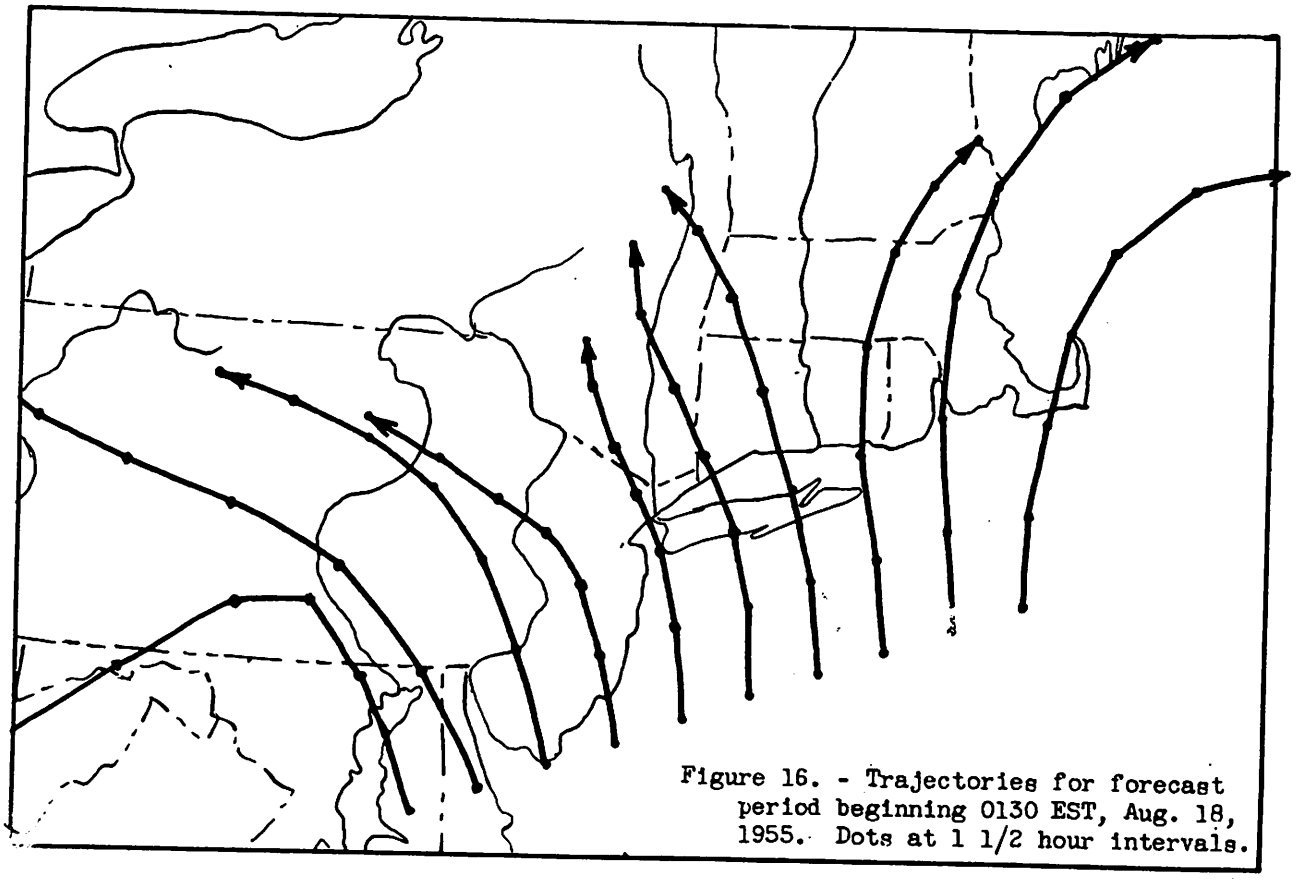

Figure 16. - Trajectories for forecast period beginning 0130 EST, Aug. 18, 1955. Dots at 1 1/2 hour intervals.

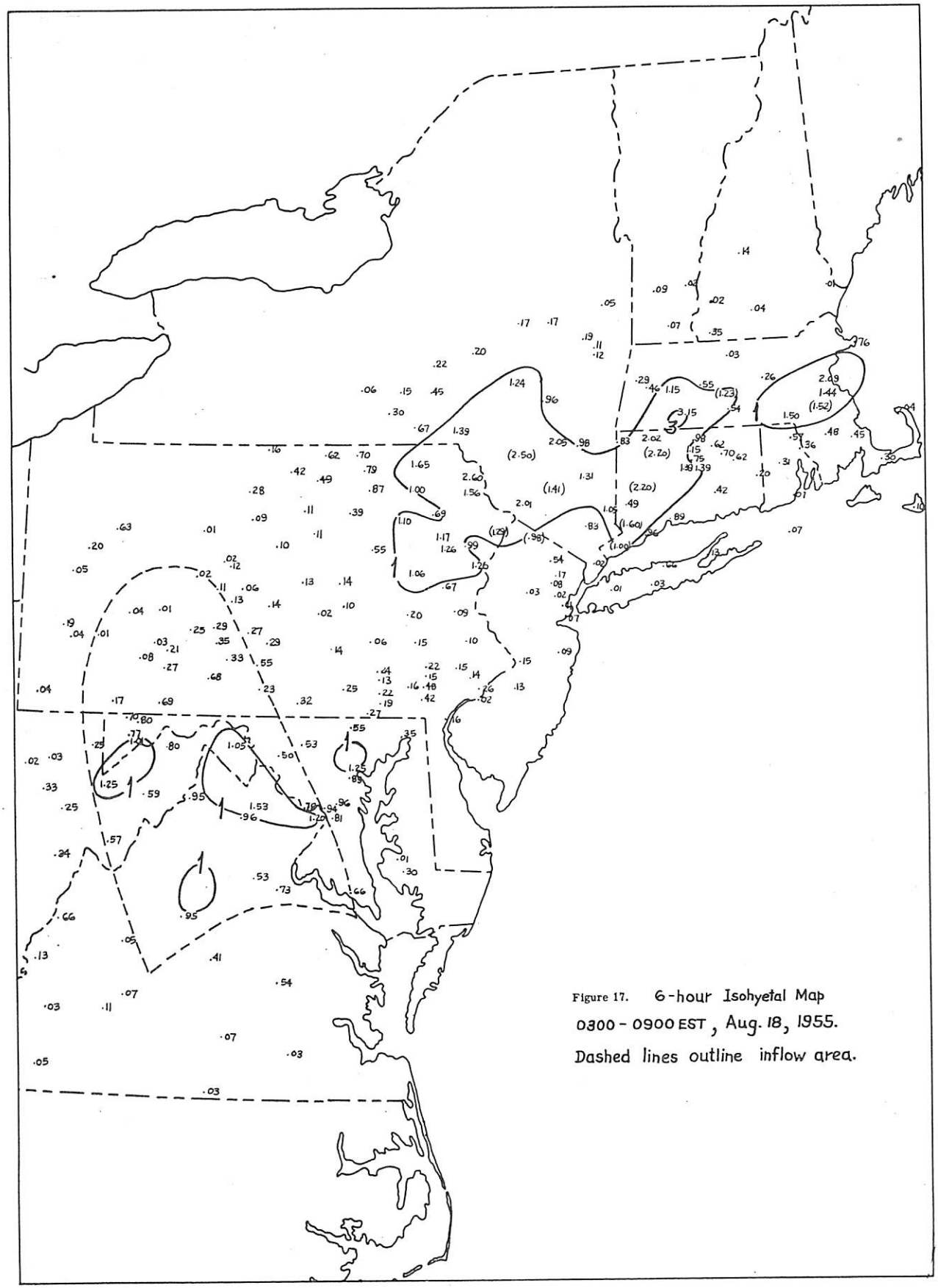

Figure 17. 6-hour Isohyetal Map
0300 - 0900 EST, Aug. 18, 1955.
Dashed lines outline inflow area.

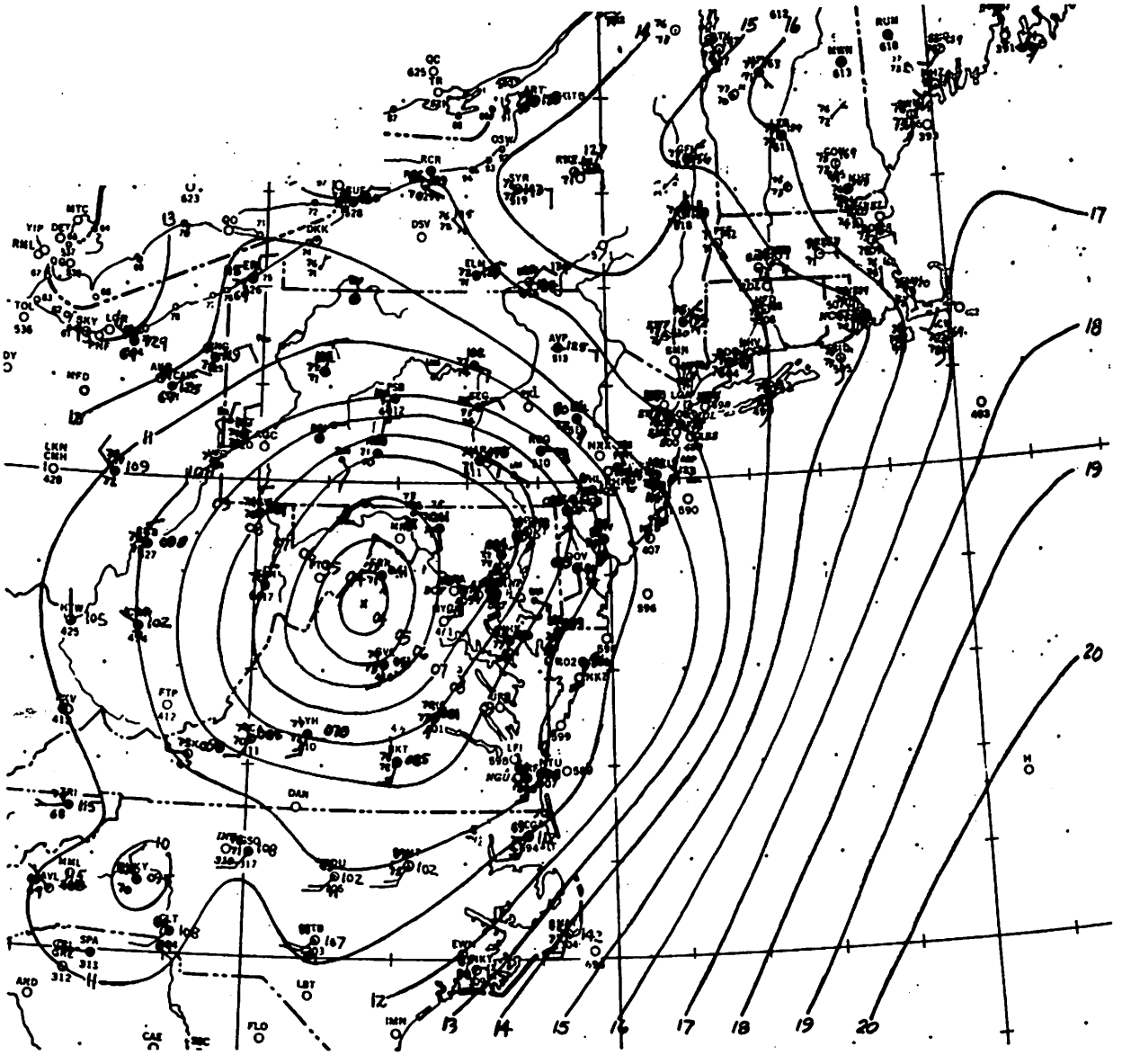

Figure 18. - Surface map, 1030 EST, August 18, 1955.

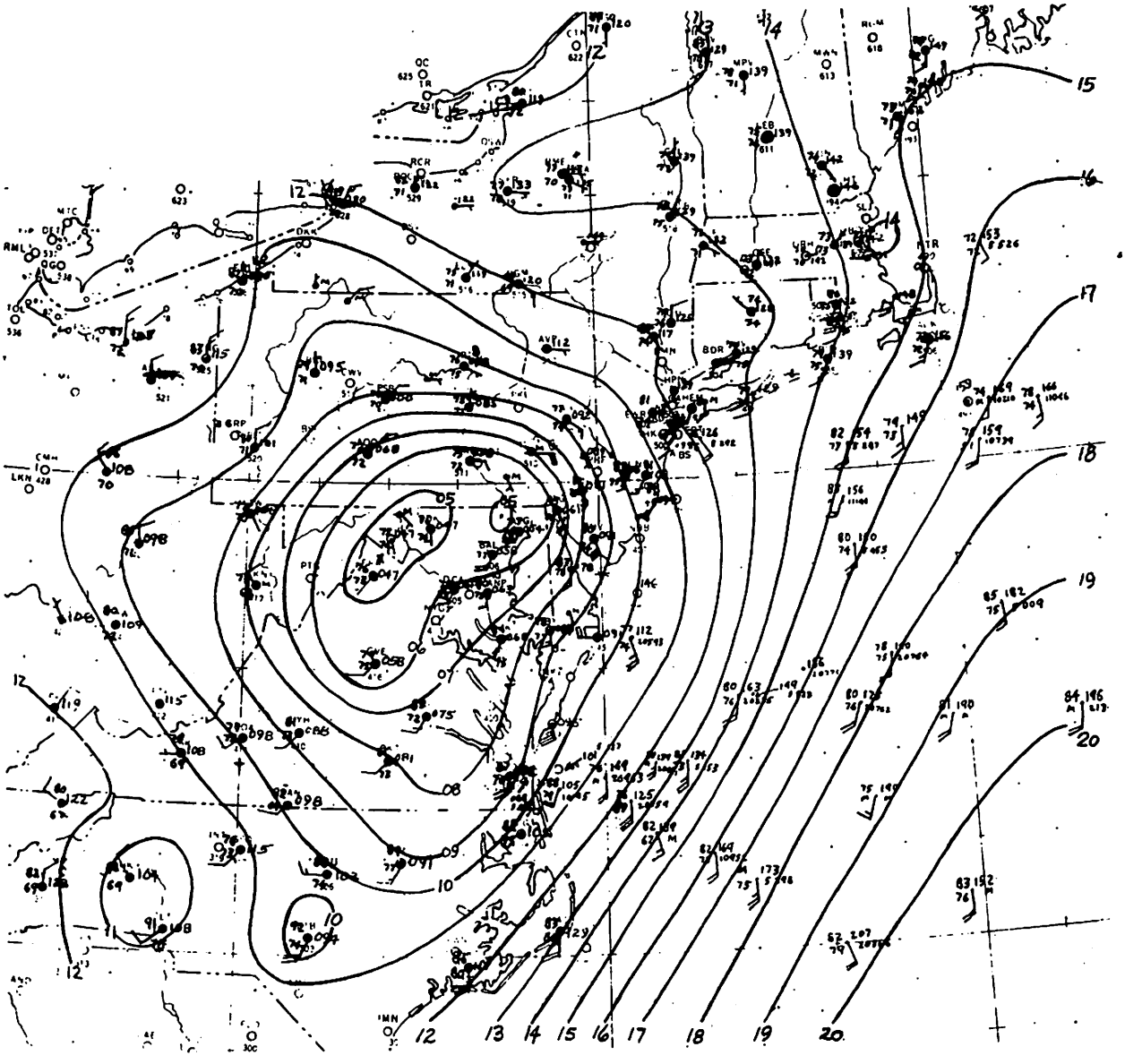

Figure 19. - Surface map, 1330 EST, August 18, 1955.

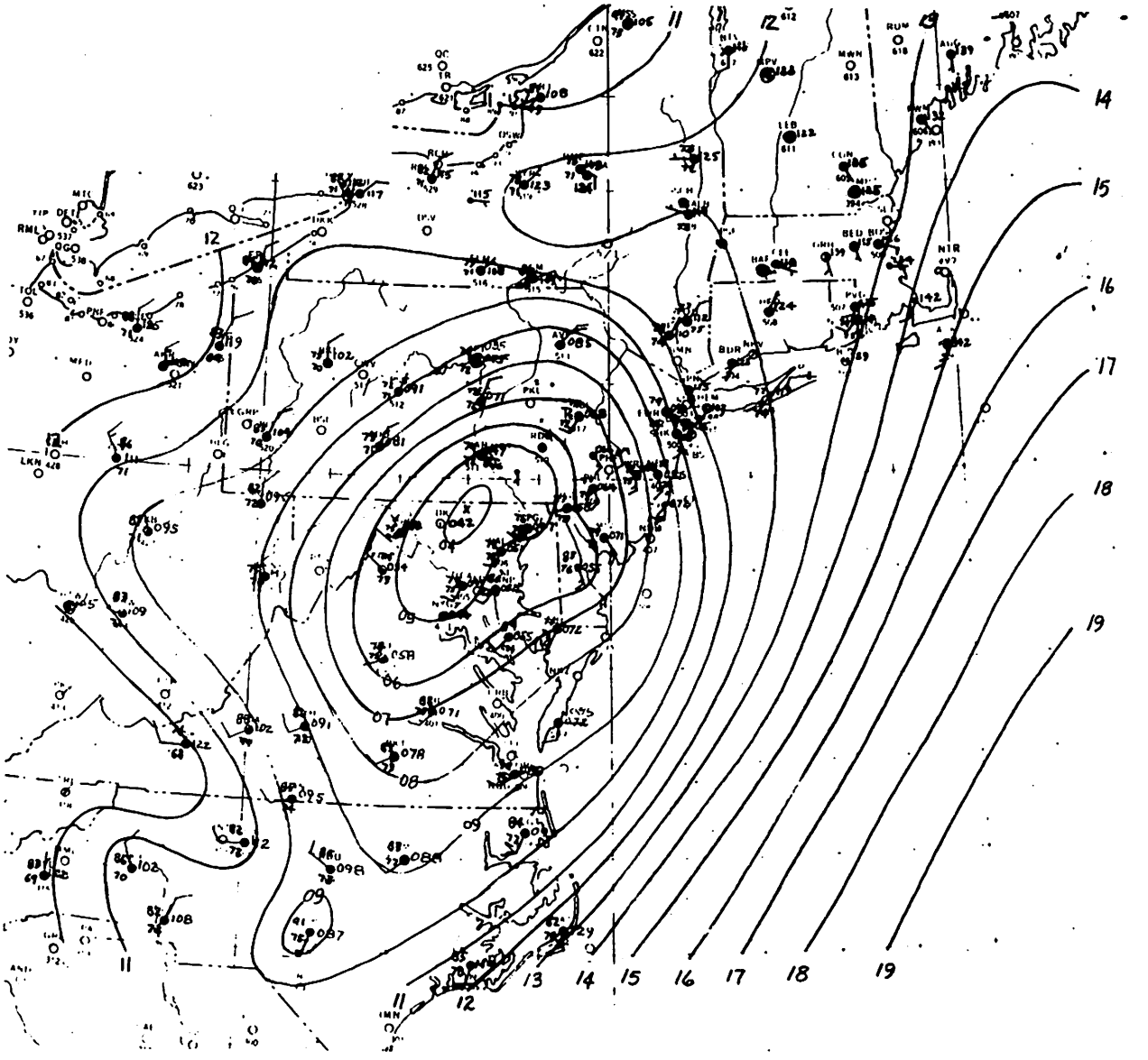


Figure 20. - Surface map, 1630 EST, August 18, 1955.

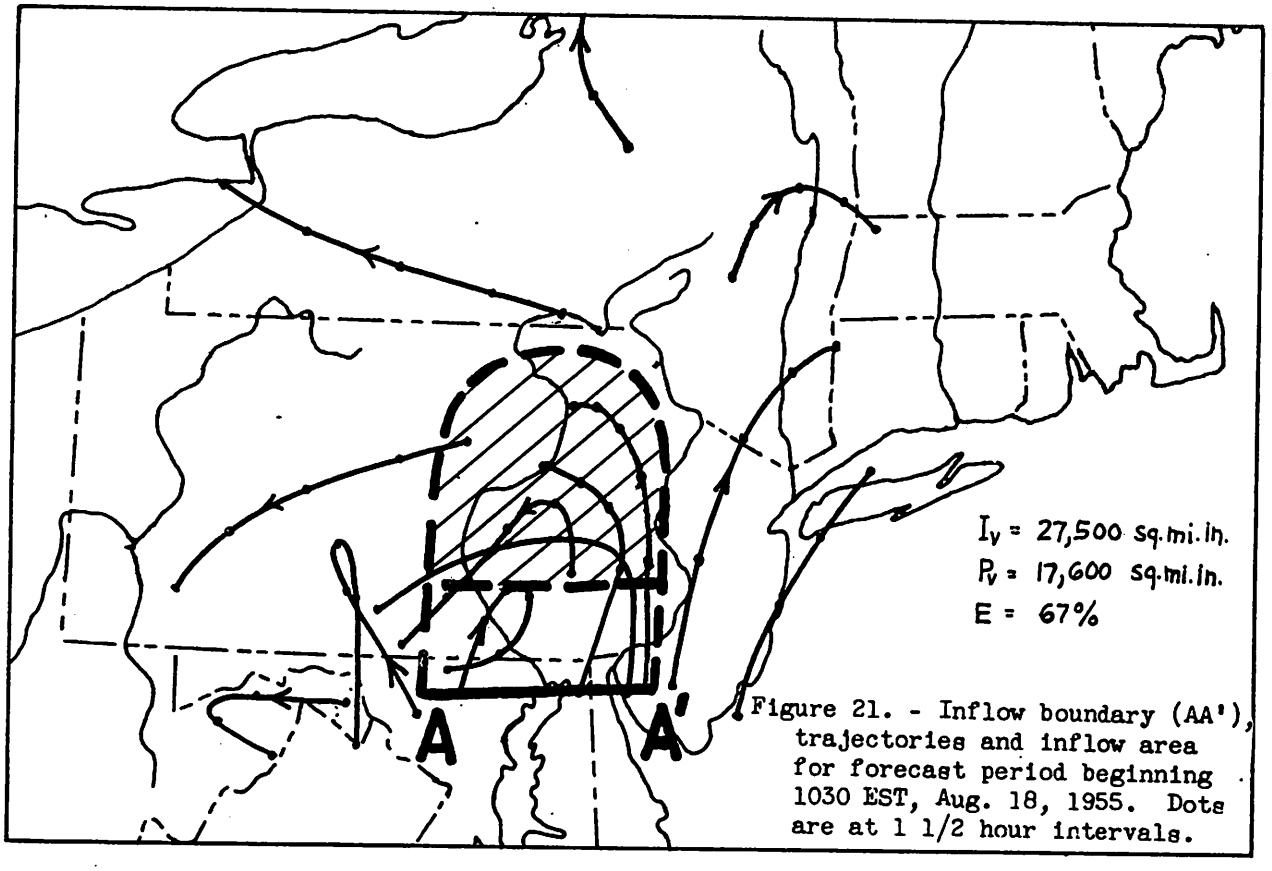


Figure 21. - Inflow boundary (AA'), trajectories and inflow area for forecast period beginning 1030 EST, Aug. 18, 1955. Dots are at 1 1/2 hour intervals.

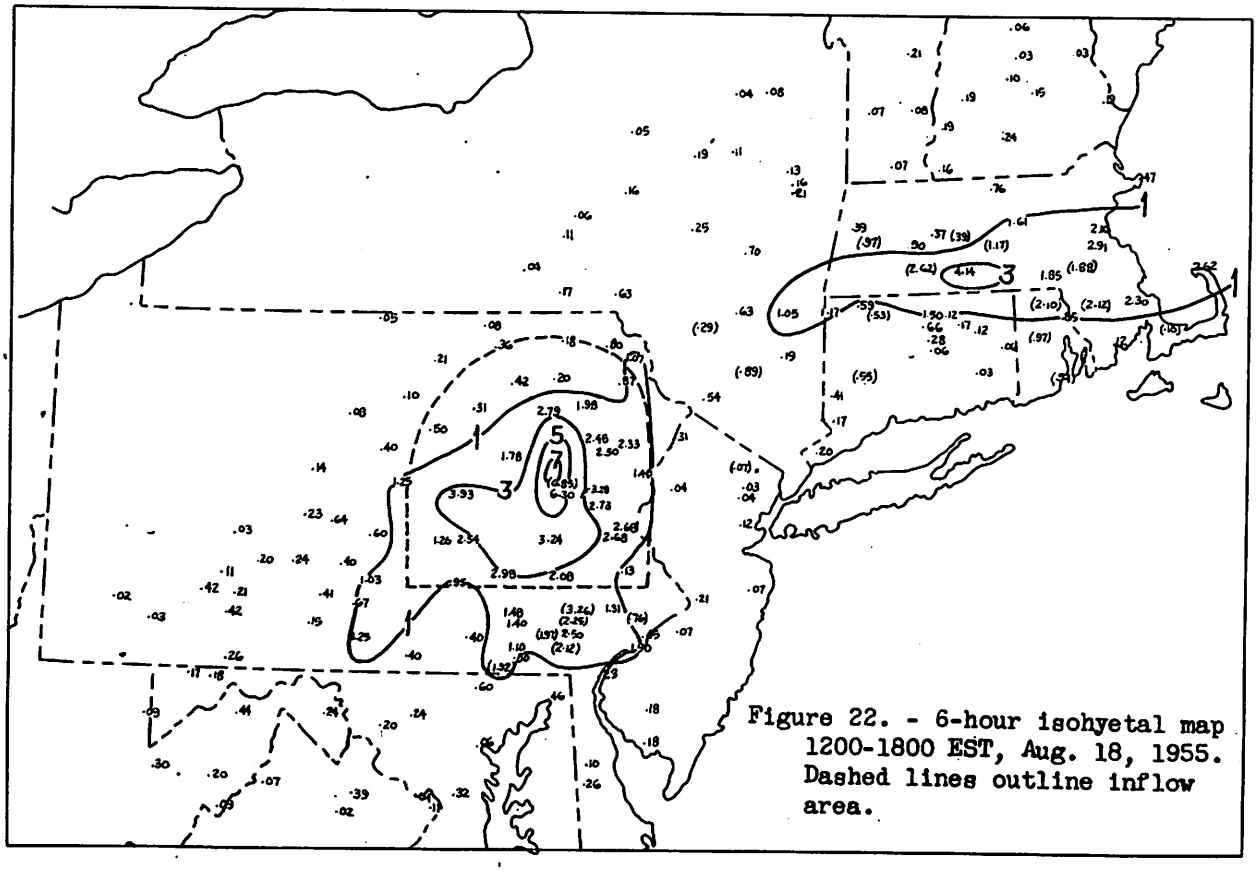

Figure 22. - 6-hour isohyetal map 1200-1800 EST, Aug. 18, 1955. Dashed lines outline inflow area.

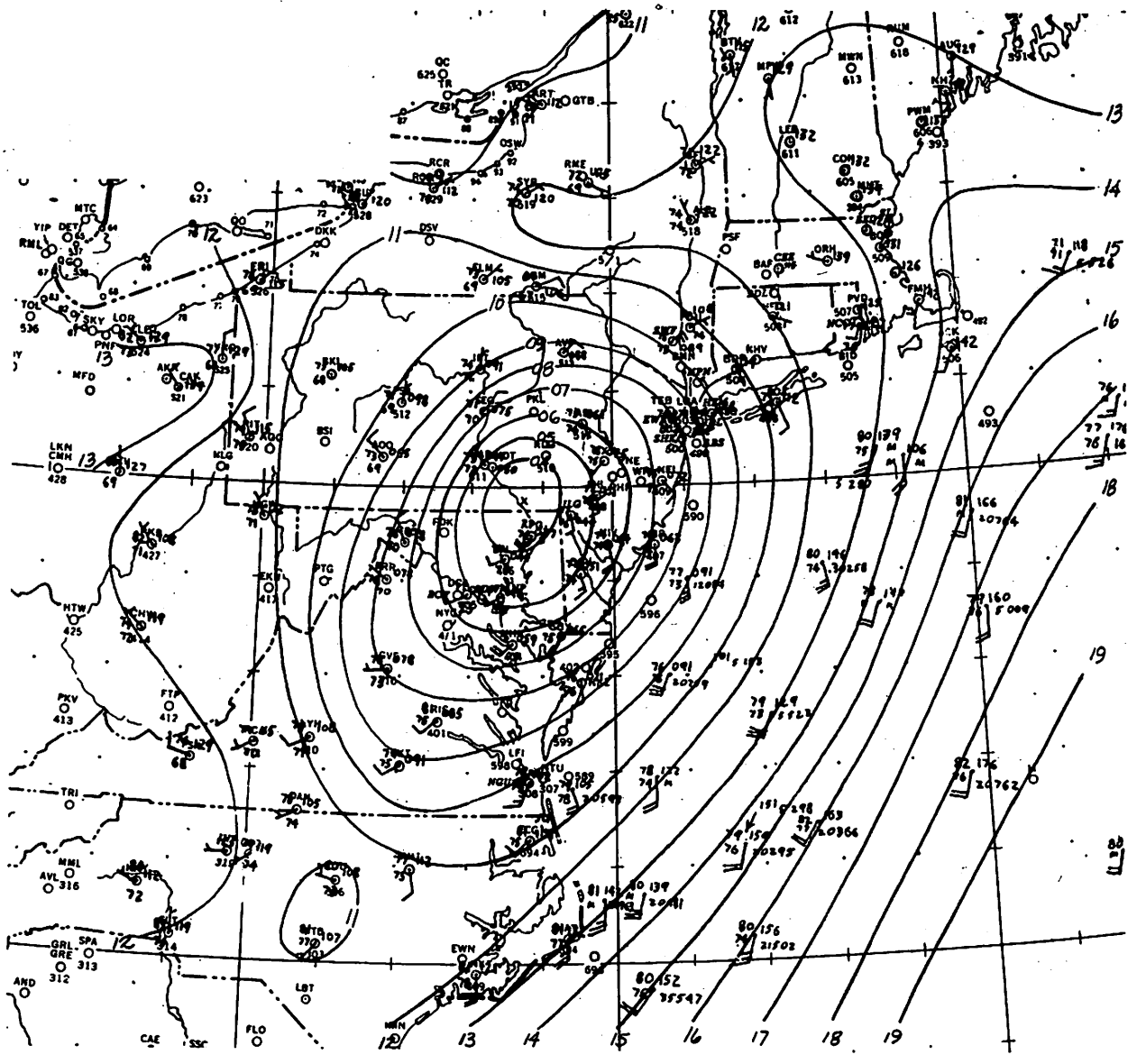

Figure 23. - Surface map, 1930 EST, August 18, 1955.

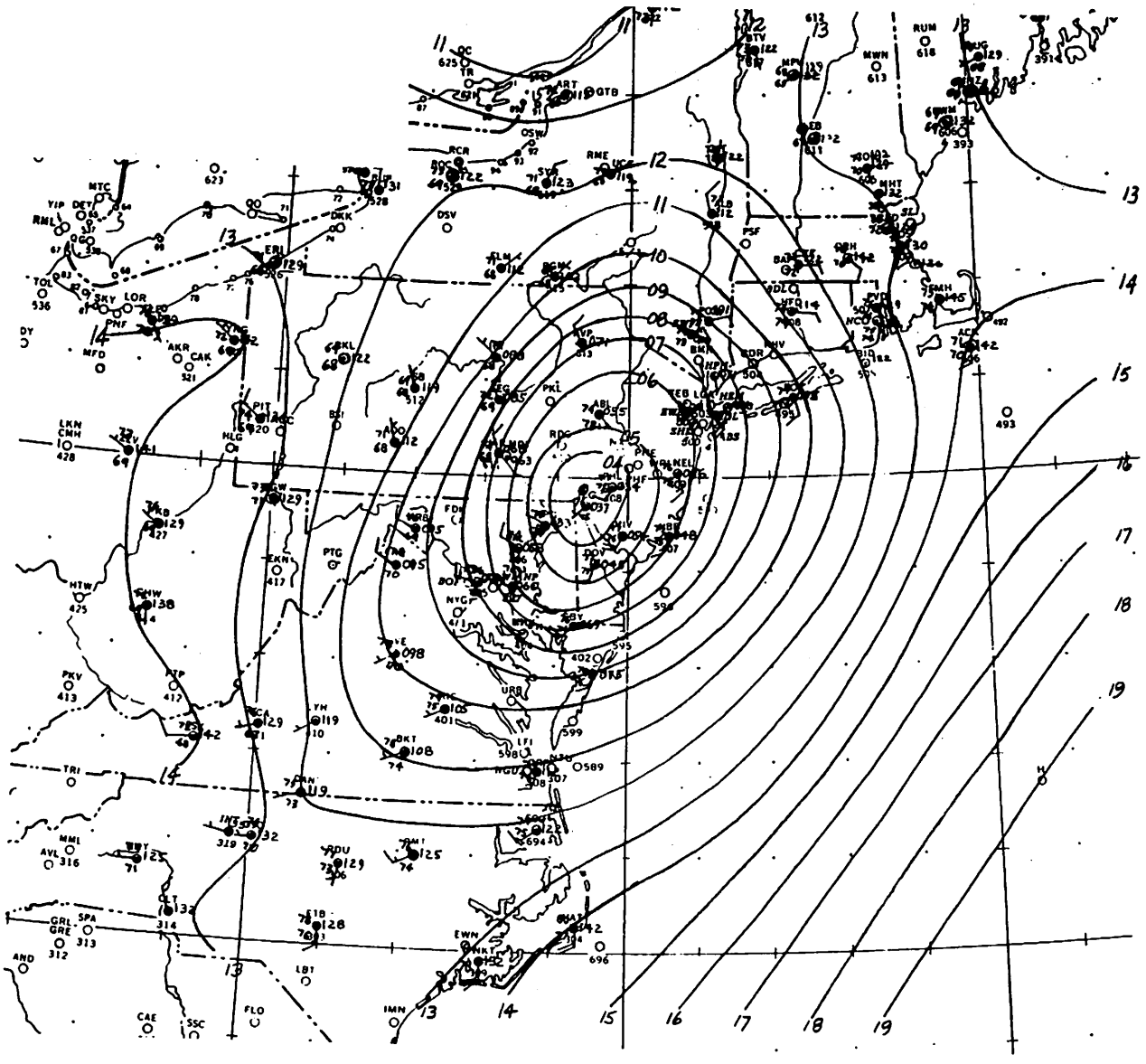

Figure 24. - Surface map, 2230 EST, August 18, 1955.

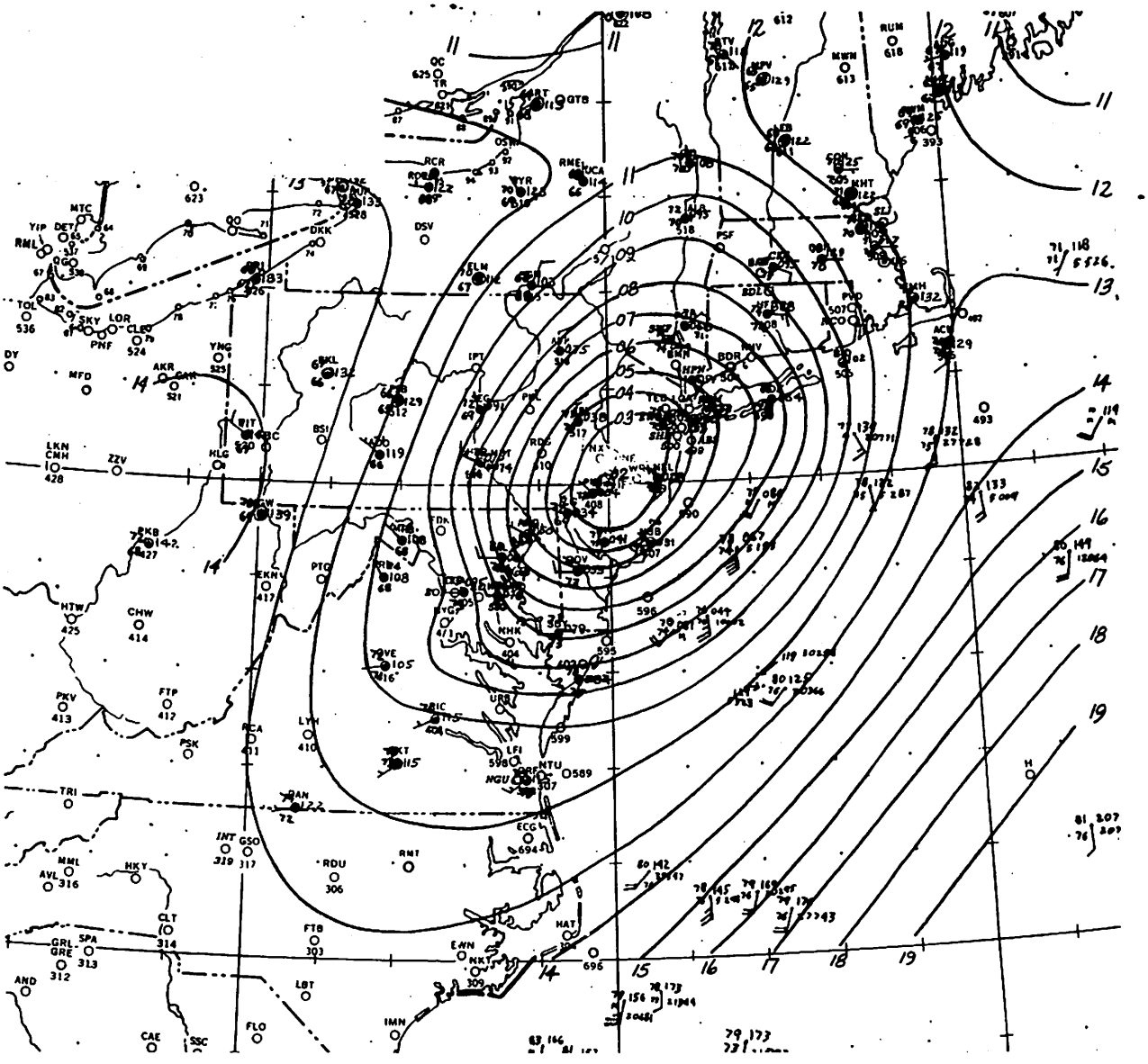

Figure 25. - Surface map, 0130 EST, August 19, 1955.

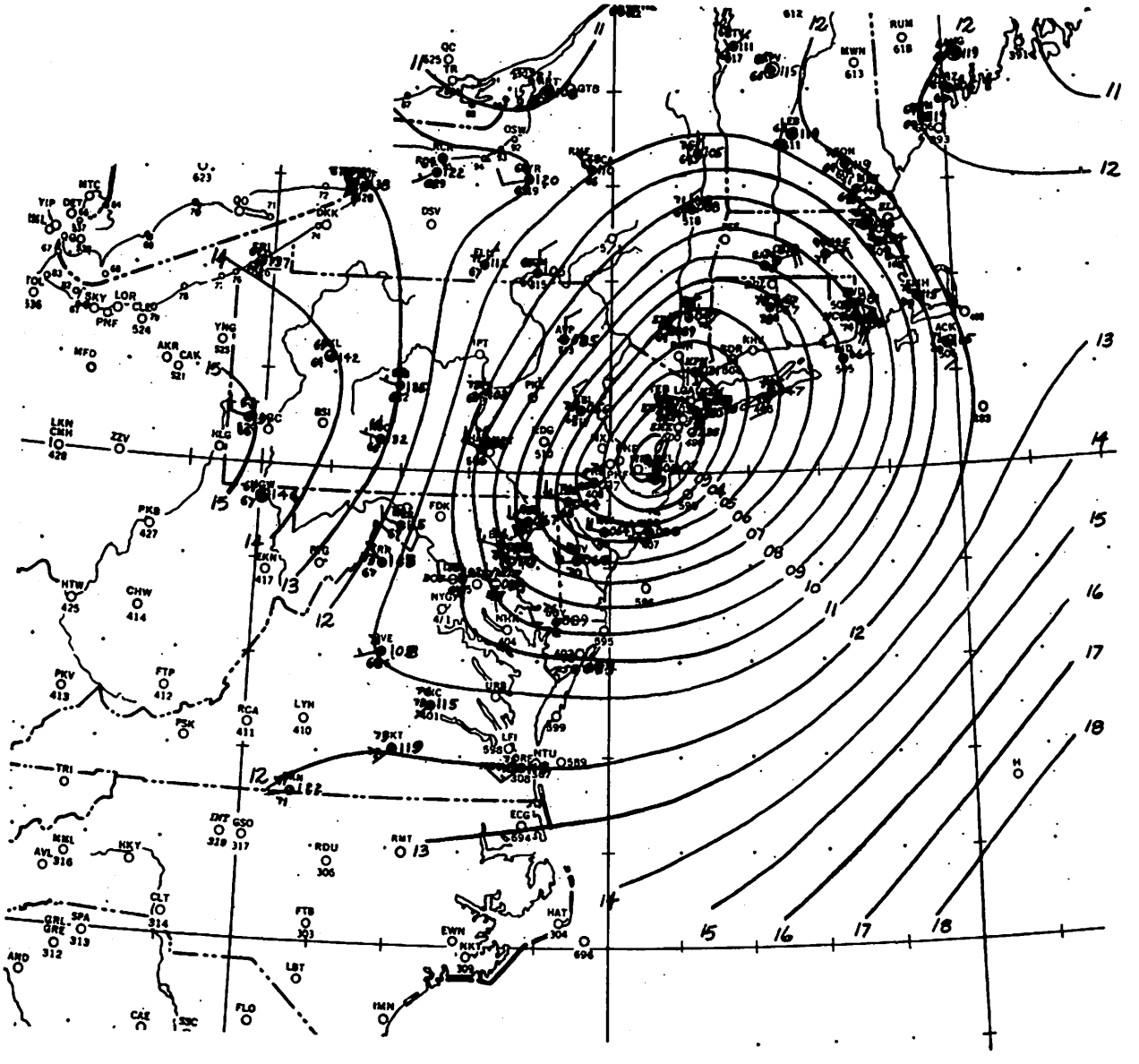

Figure 26. - Surface map, 0430 EST, August 19, 1955.

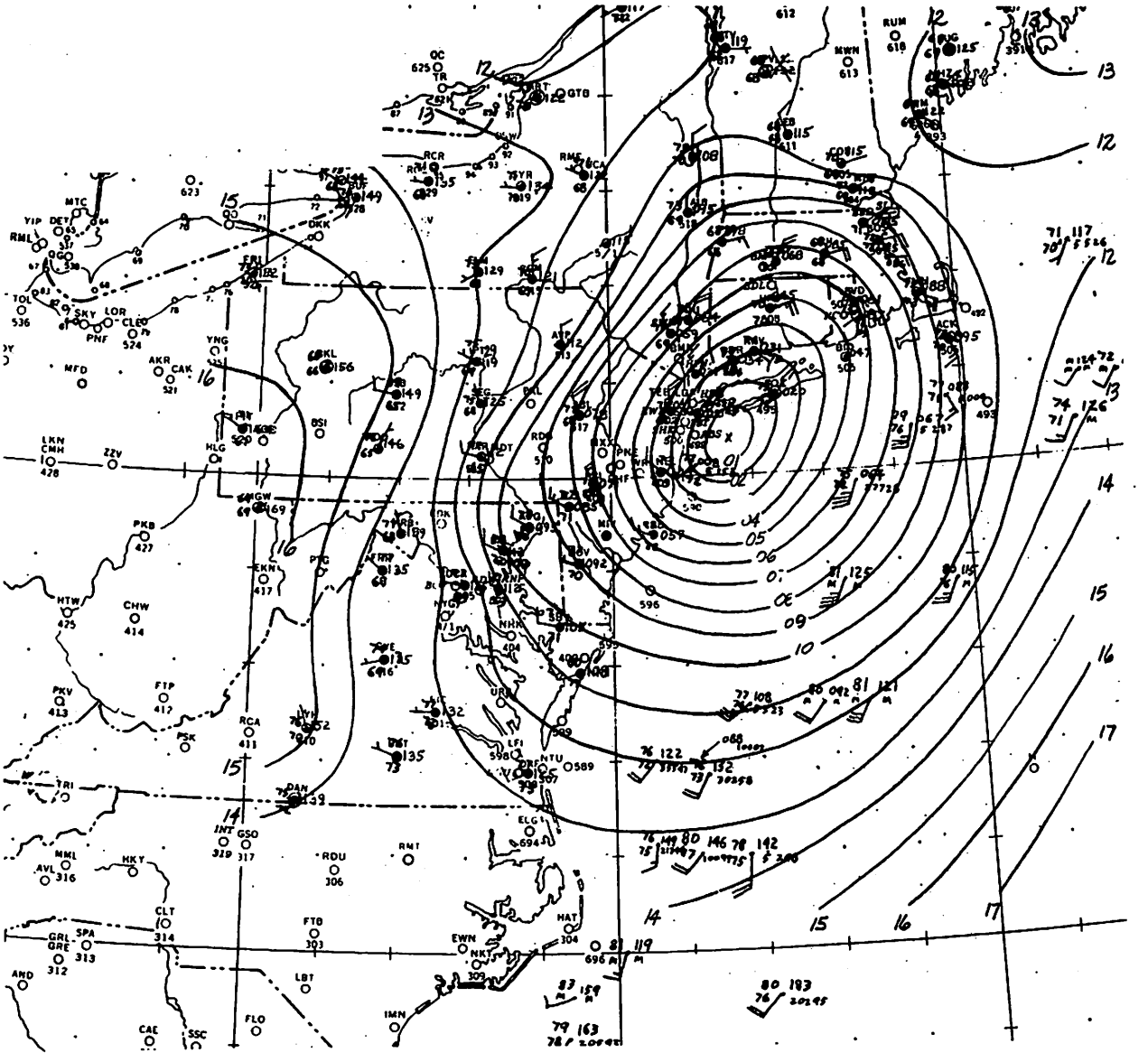

Figure 27. - Surface map, 1730 EST, August 19, 1955.

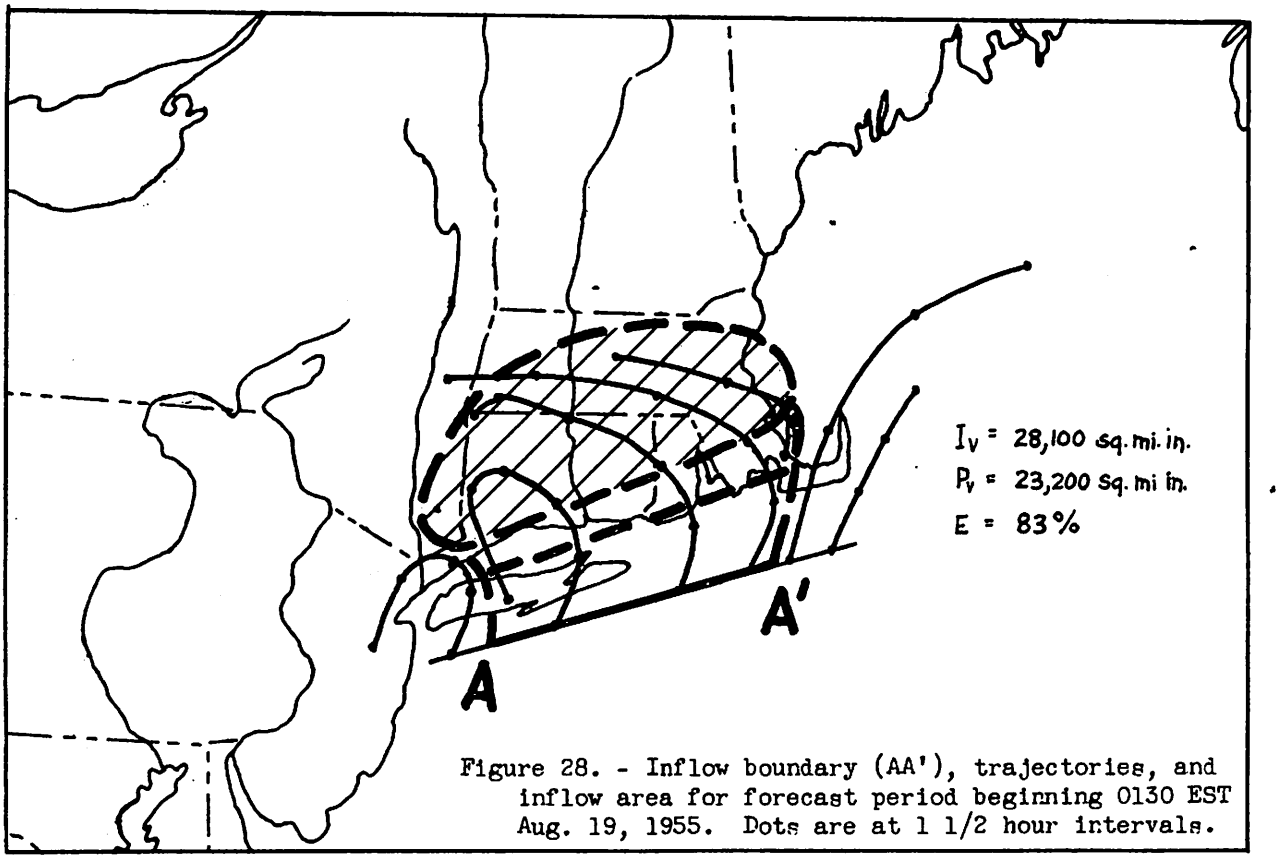


Figure 28. - Inflow boundary (AA'), trajectories, and inflow area for forecast period beginning 0130 EST Aug. 19, 1955. Dots are at 1 1/2 hour intervals.

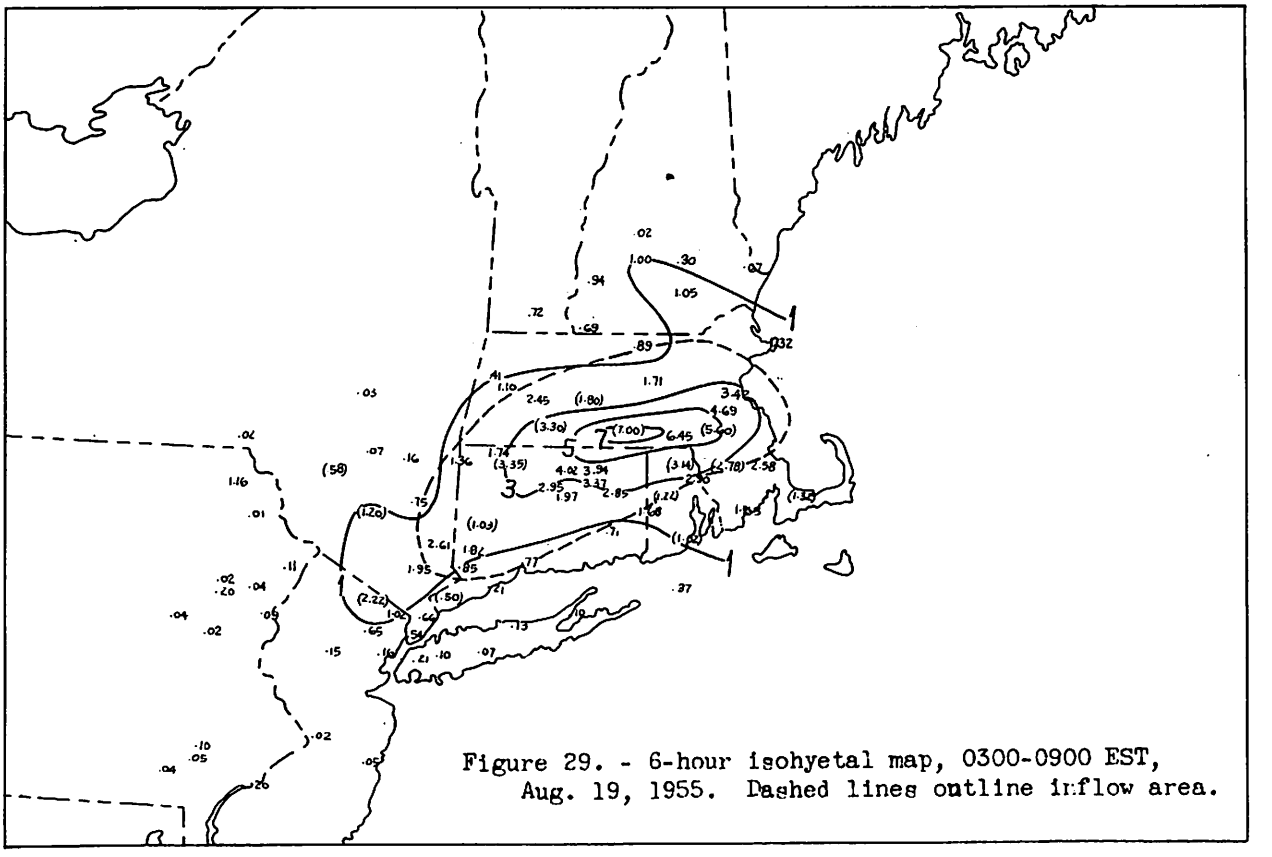

Figure 29. - 6-hour isohyetal map, 0300-0900 EST, Aug. 19, 1955. Dashed lines outline inflow area.

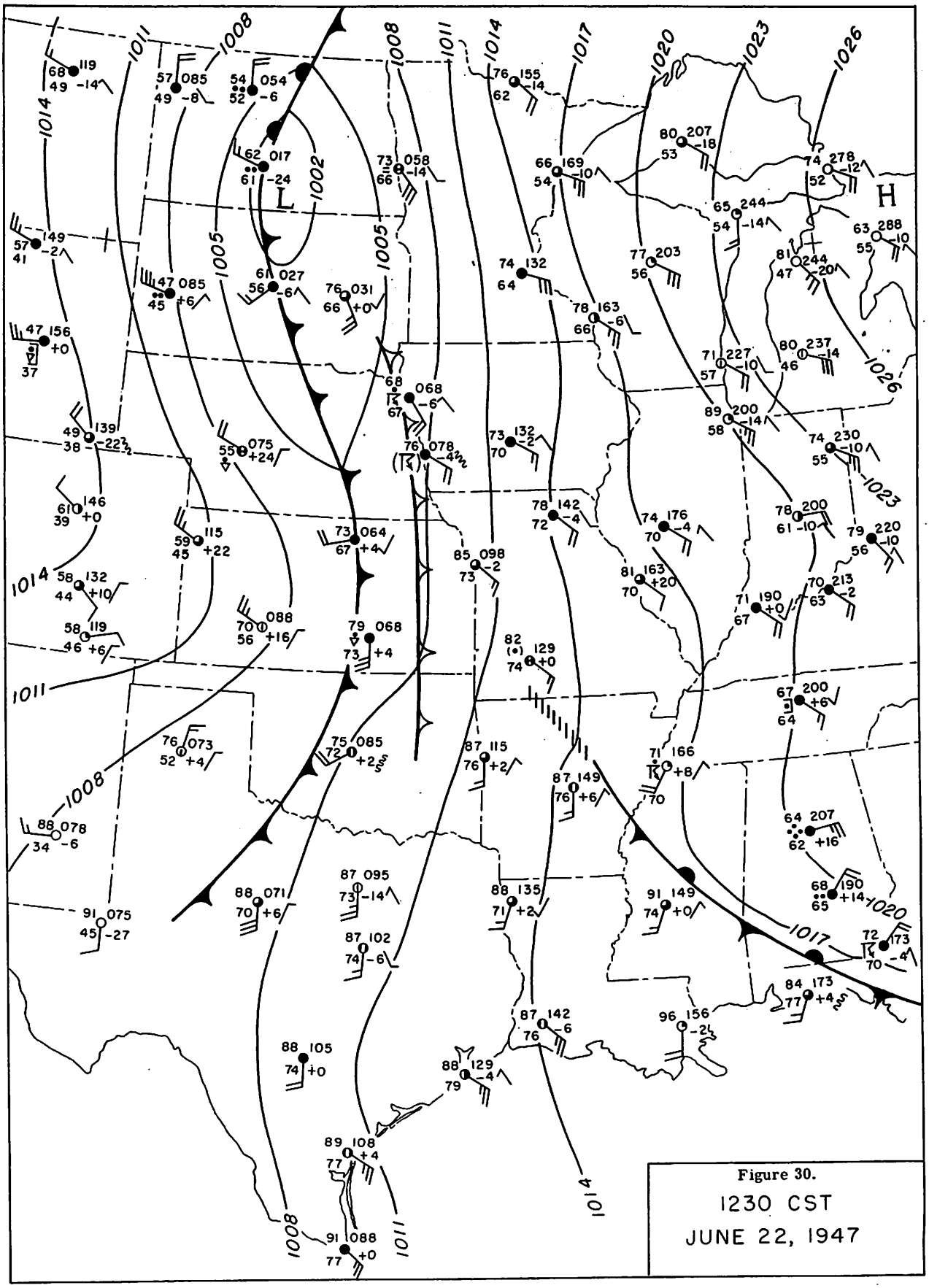


Figure 30.
1230 CST
JUNE 22, 1947

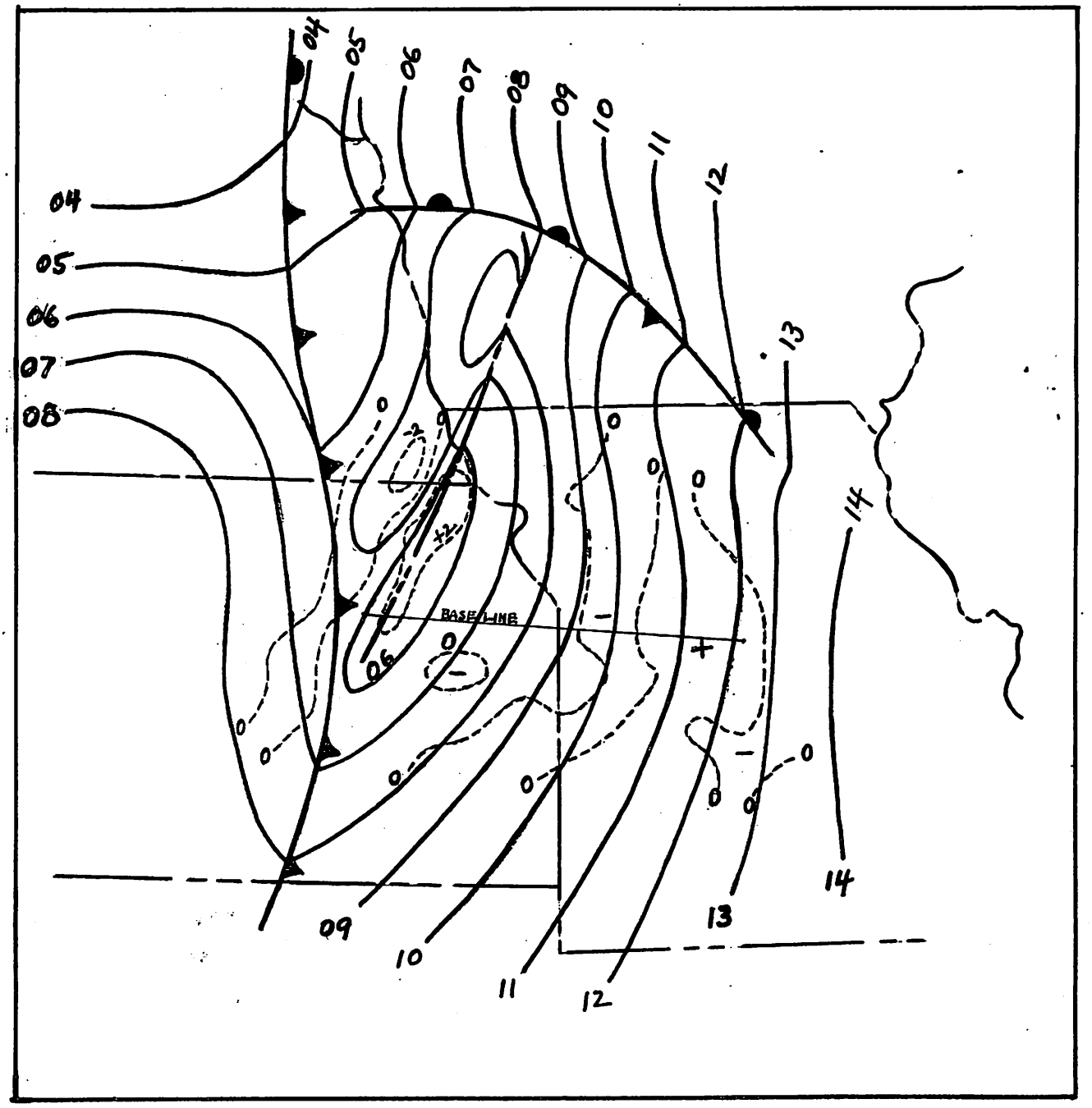


Figure 31. - Sea level chart, 1530 CST, June 22, 1947.

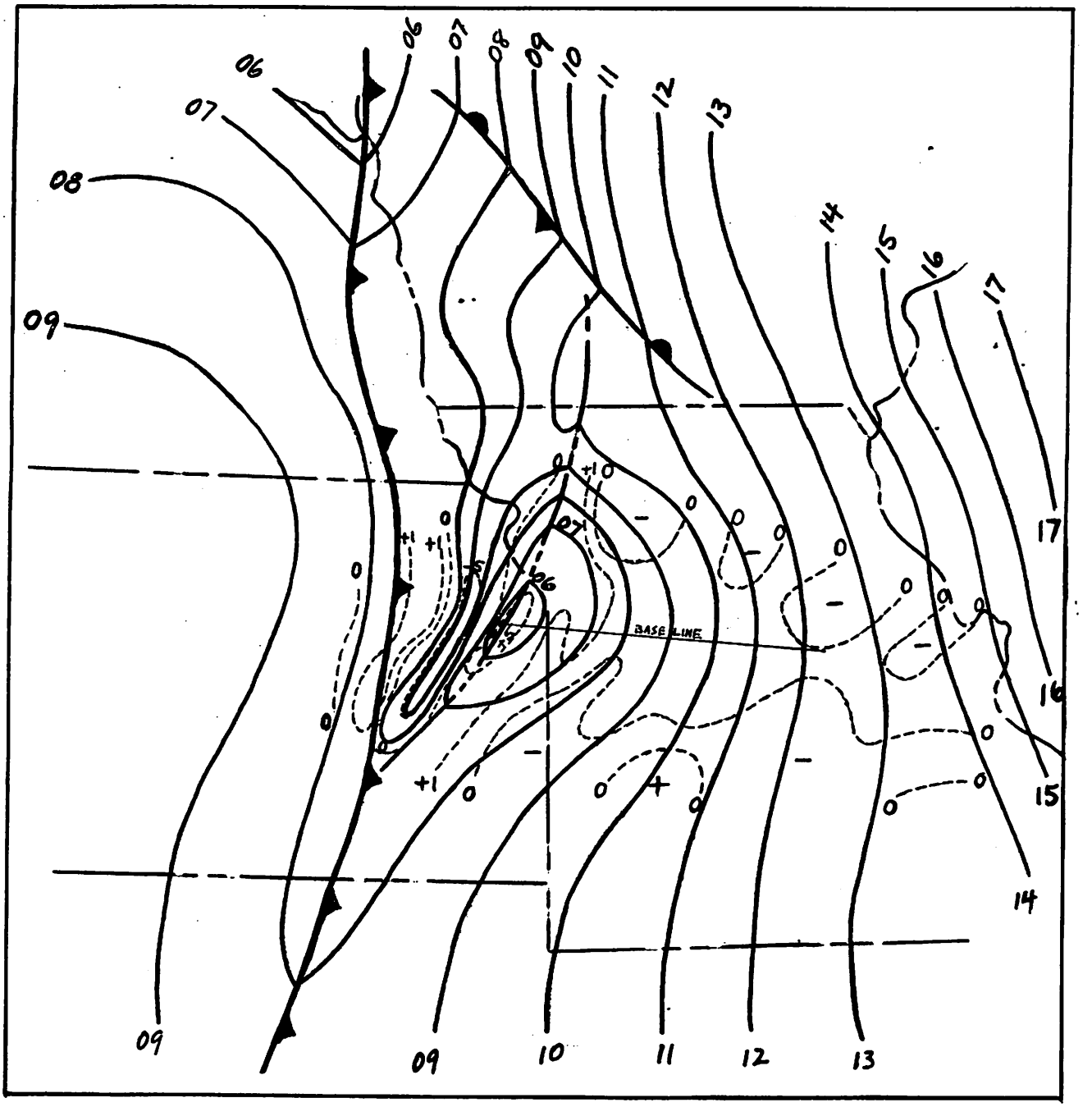


Figure 32. - Sea level chart, 1830 CST, June 22, 1947

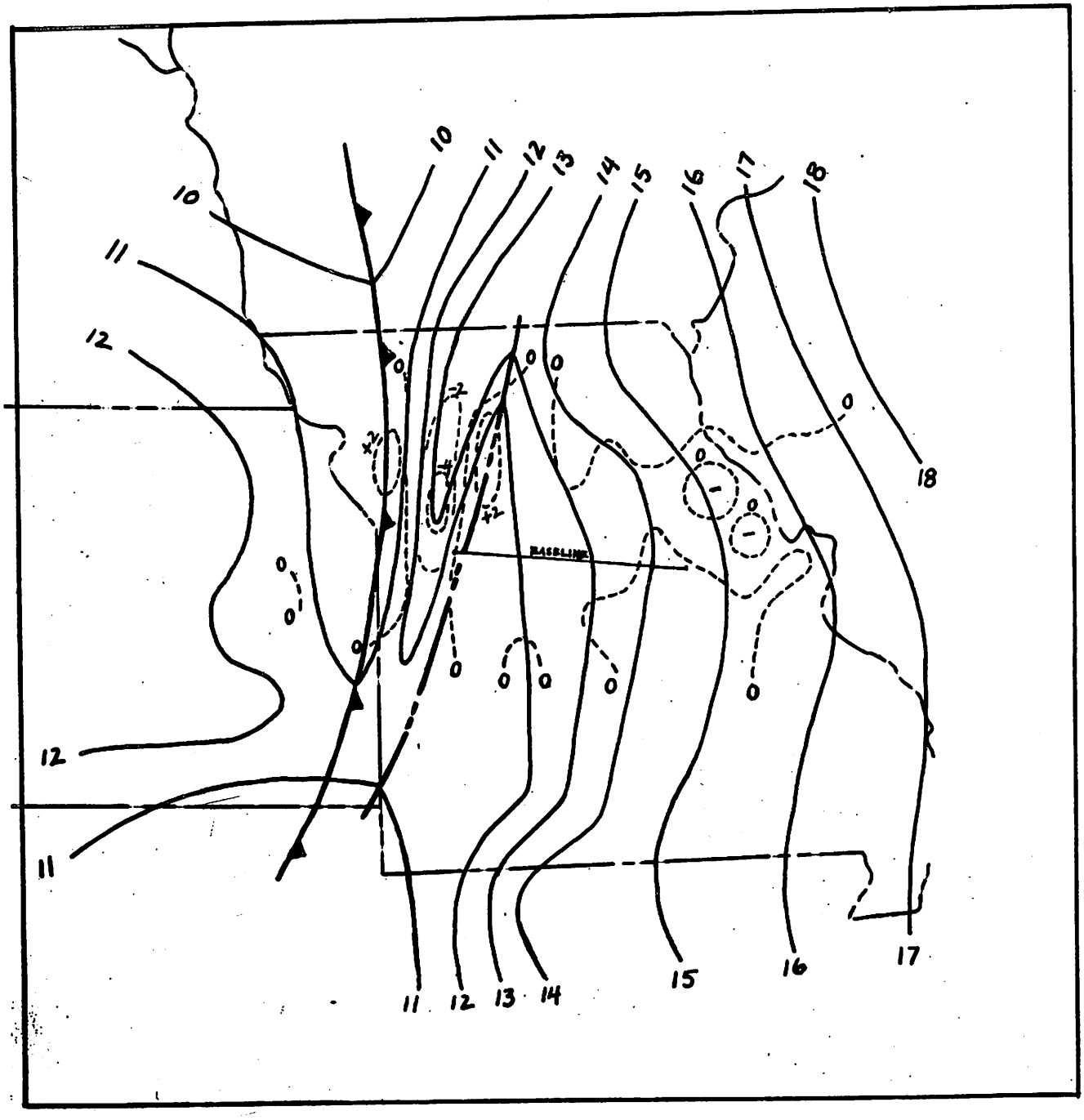


Figure 33. - Sea level chart, 2130 EST, June 22, 1947.

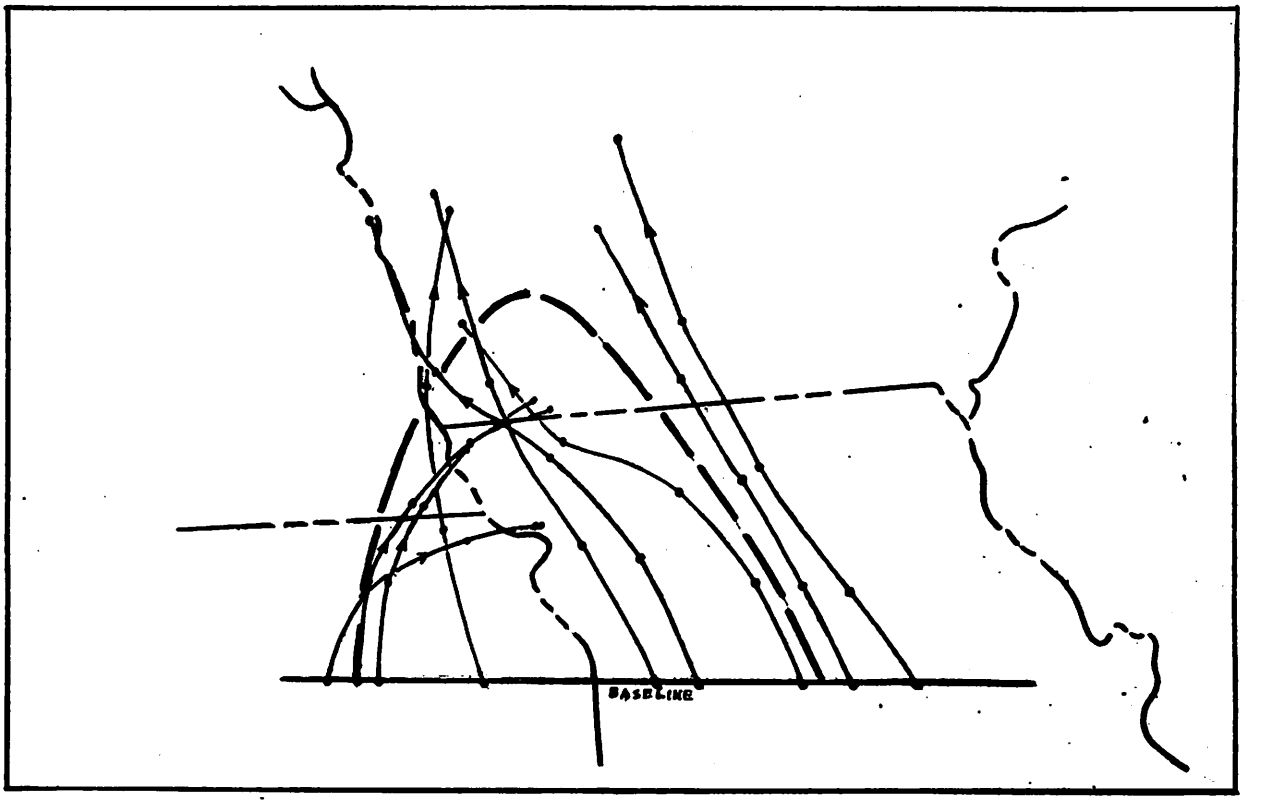


Figure 34. - Trajectories beginning at 1530 CST, June 22, 1947. Dots at 1 1/2 hour intervals. Dashed line shows area of convergence, 1530-2130 CST.

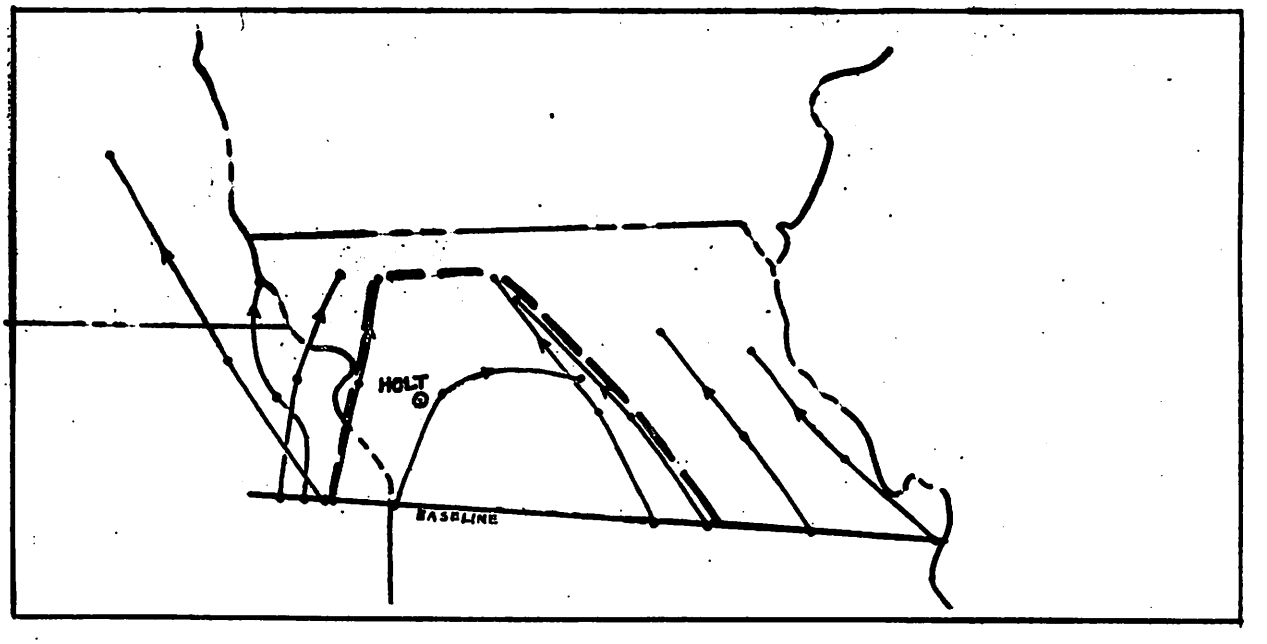


Figure 35. - Trajectories beginning at 1830 CST, June 22, 1947. Dots at 1 1/2 hour intervals. Dashed line shows area of convergence, 1830-2130 CST.

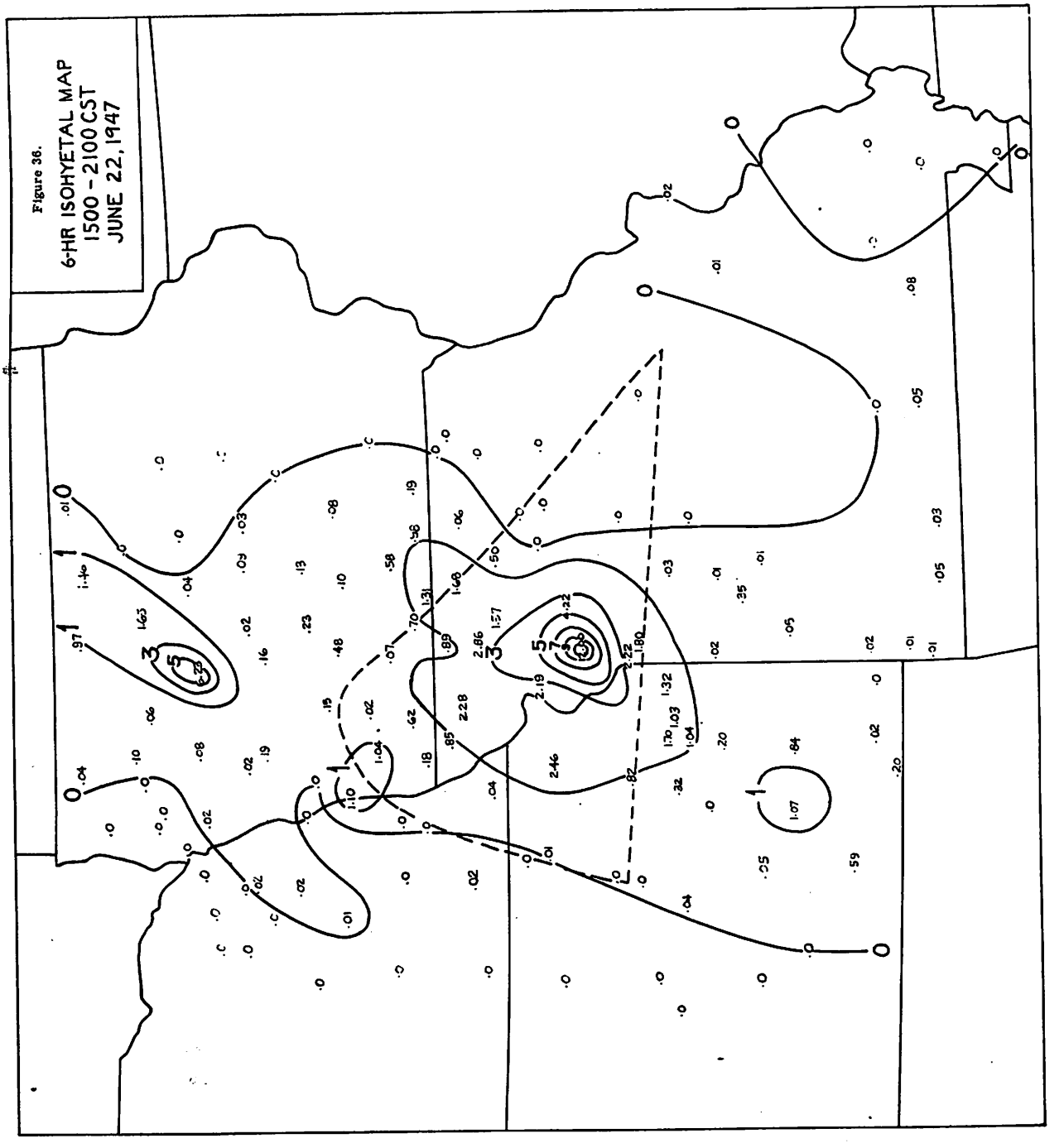


Figure 36.

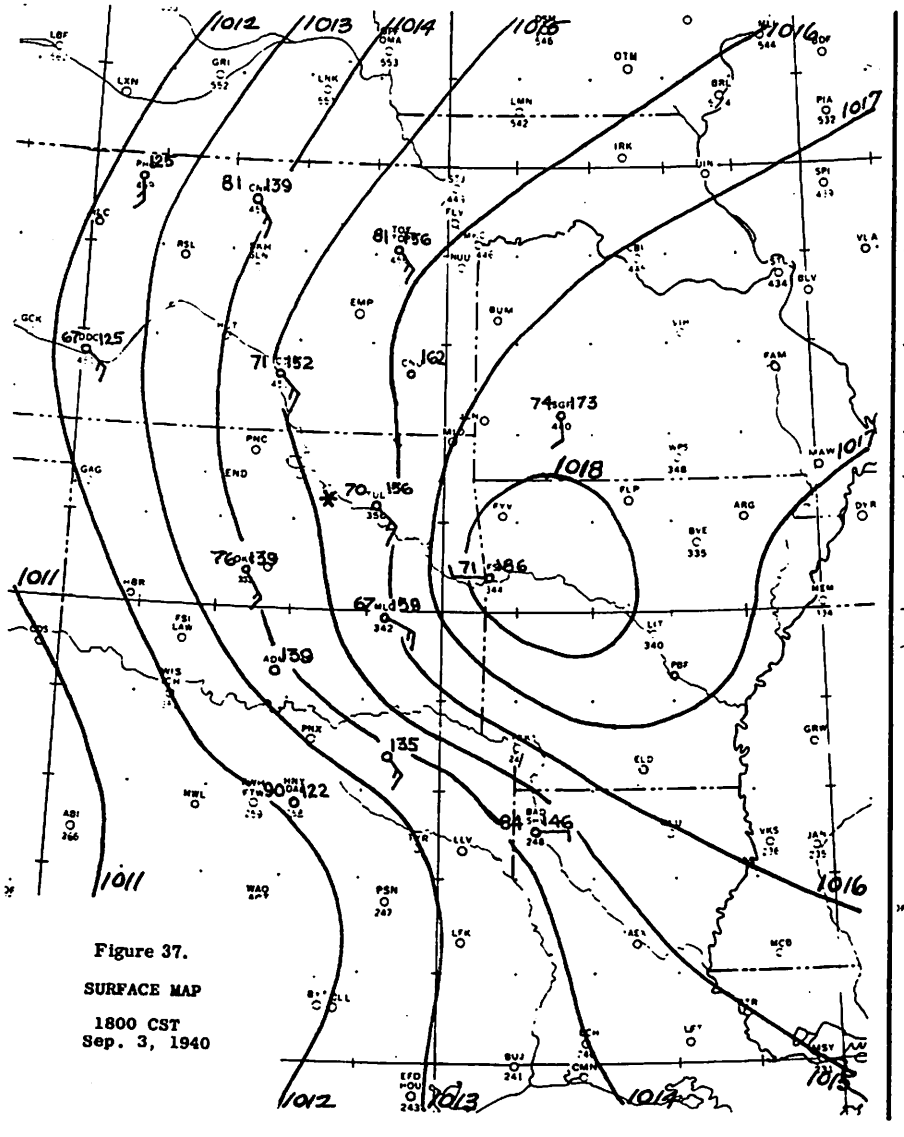

Figure 37.

SURFACE MAP

1800 CST
Sep. 3, 1940

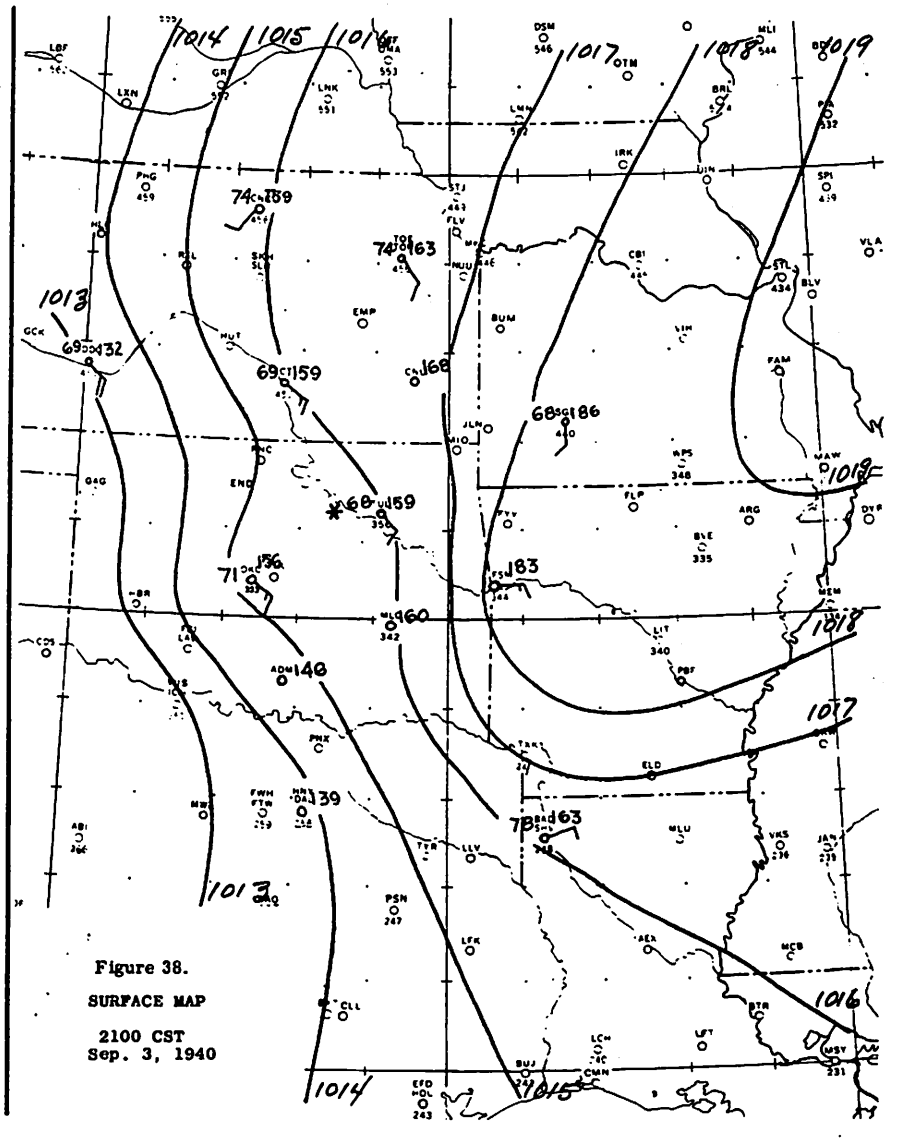

Figure 38.

SURFACE MAP

2100 CST
Sep. 3, 1940

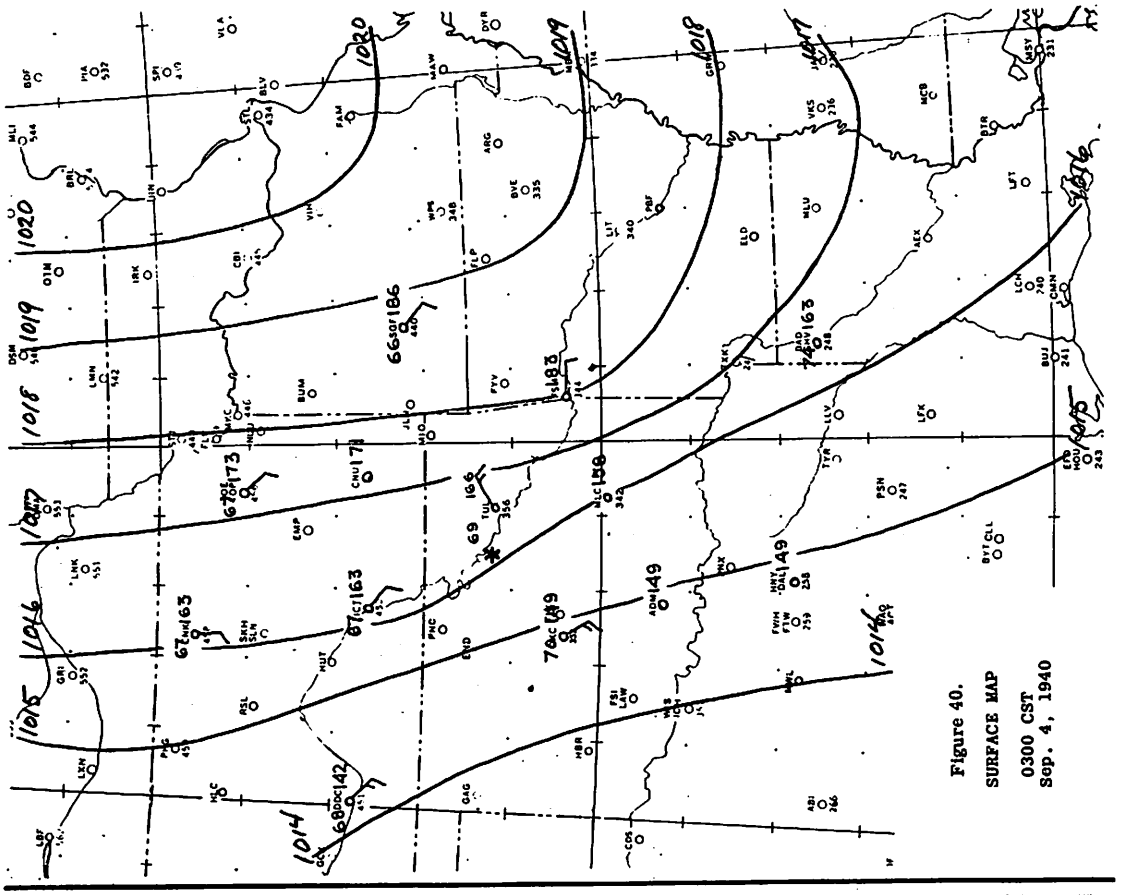

Figure 40.
SURFACE MAP
0300 CST
Sep. 4, 1940

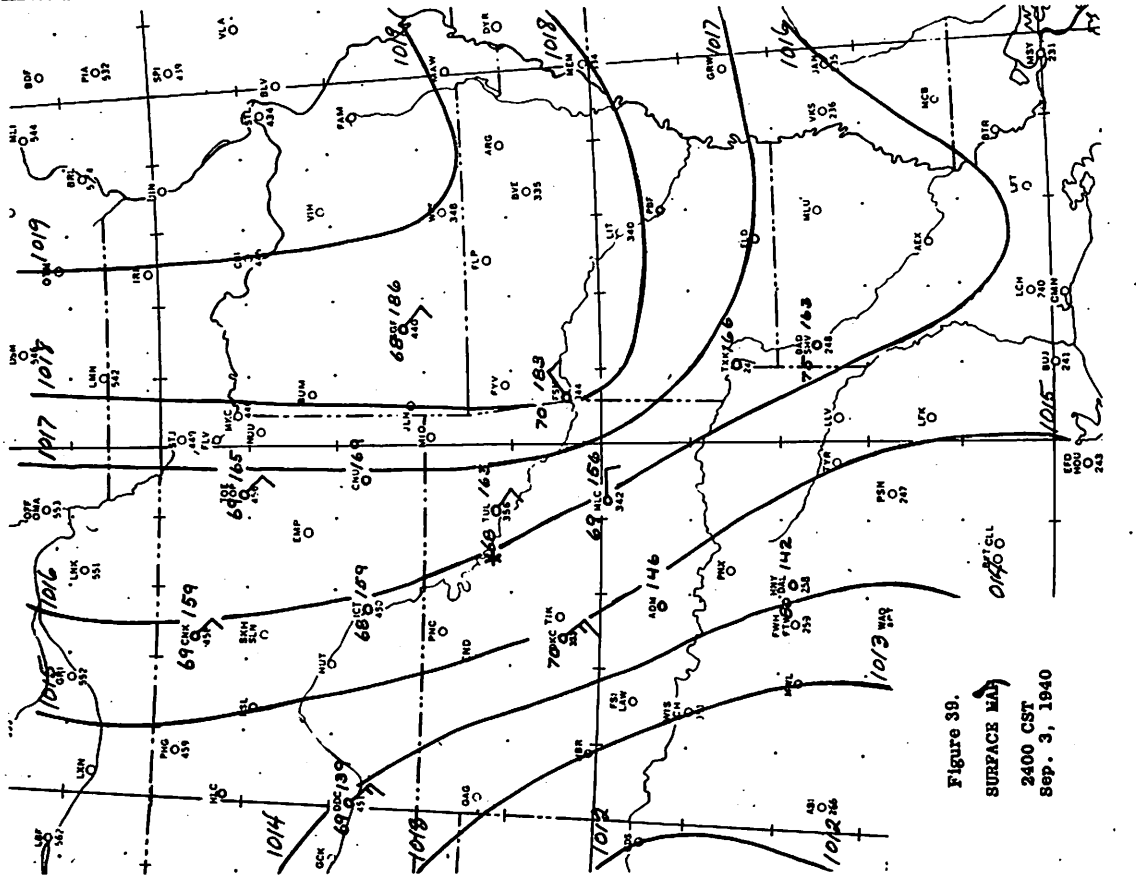

Figure 39.
SURFACE MAP
2400 CST
Sep. 3, 1940

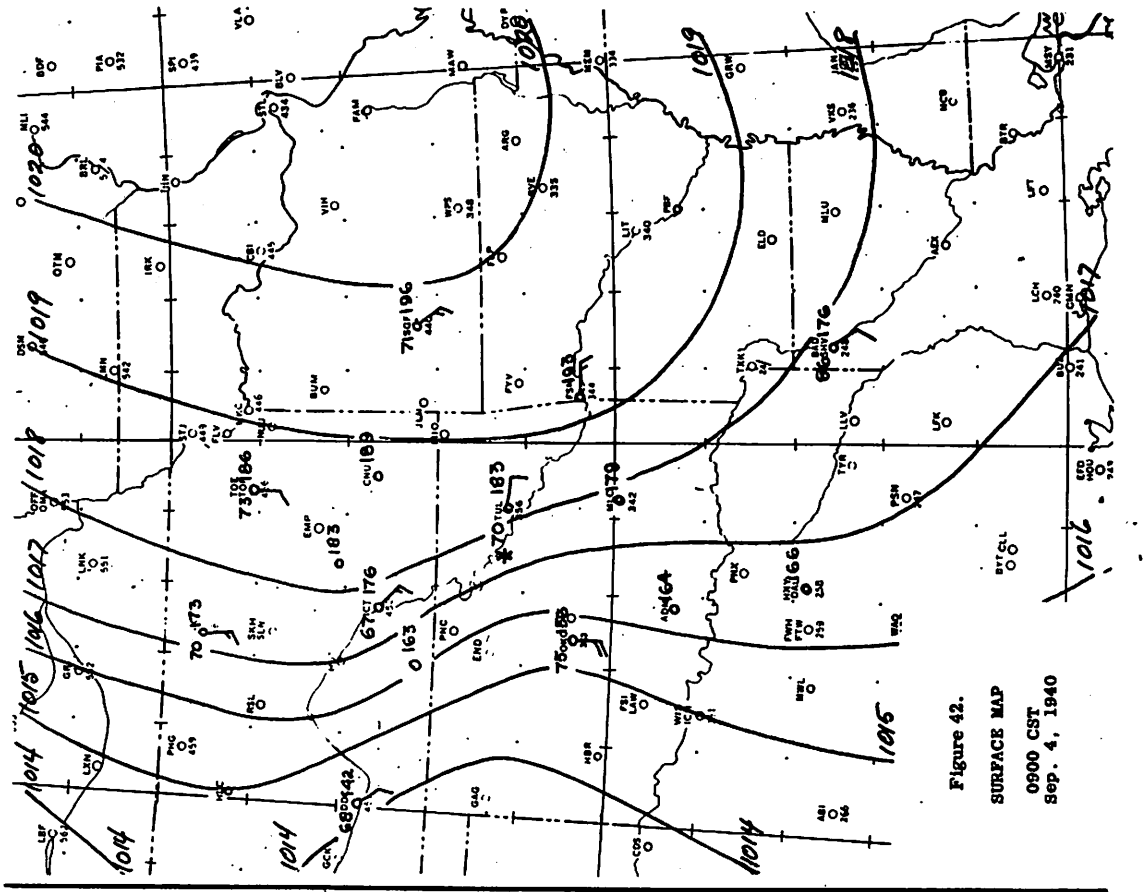

Figure 42.
SURFACE MAP
0900 CST
Sep. 4, 1940

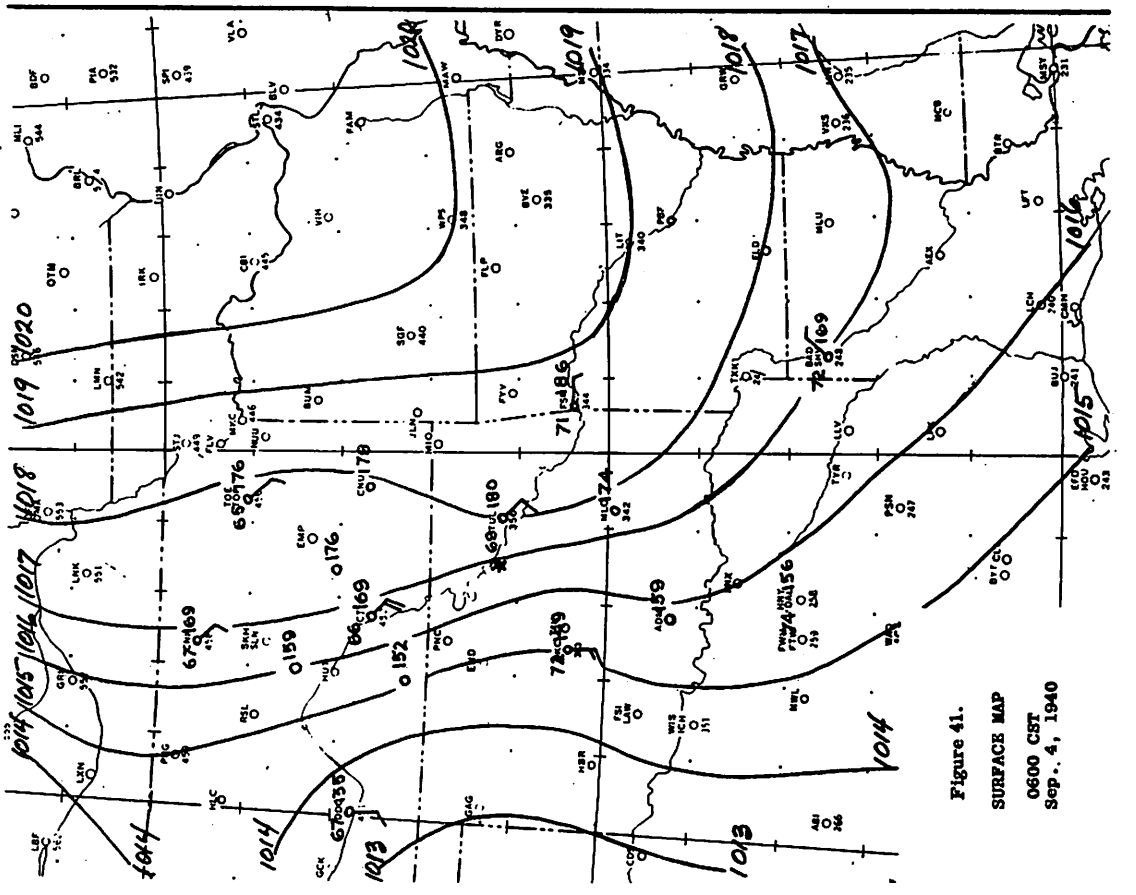

Figure 41.
SURFACE MAP
0600 CST
Sep. 4, 1940

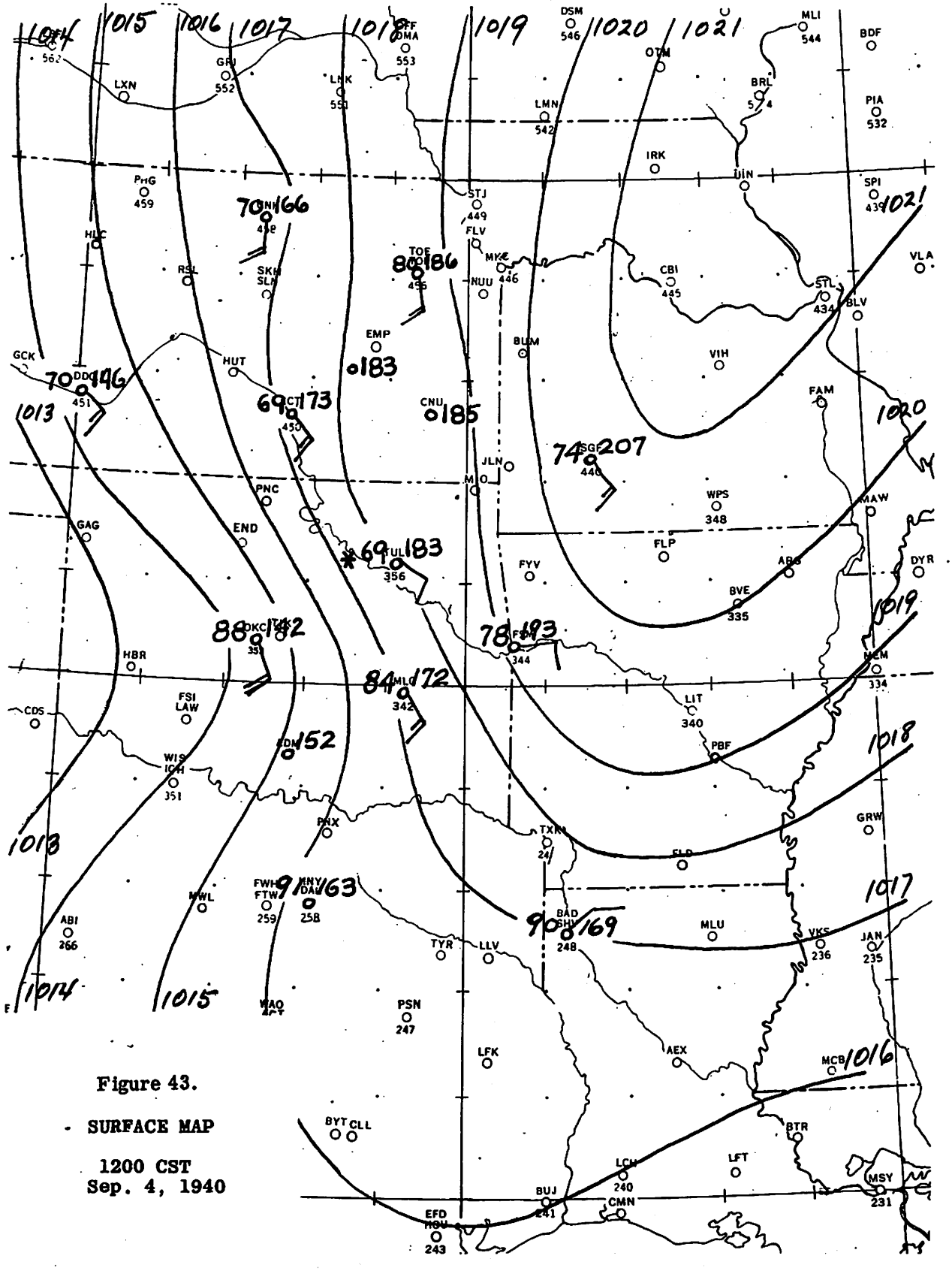


**Figure 43.**

**- SURFACE MAP**

**1200 CST**
**Sep. 4, 1940**

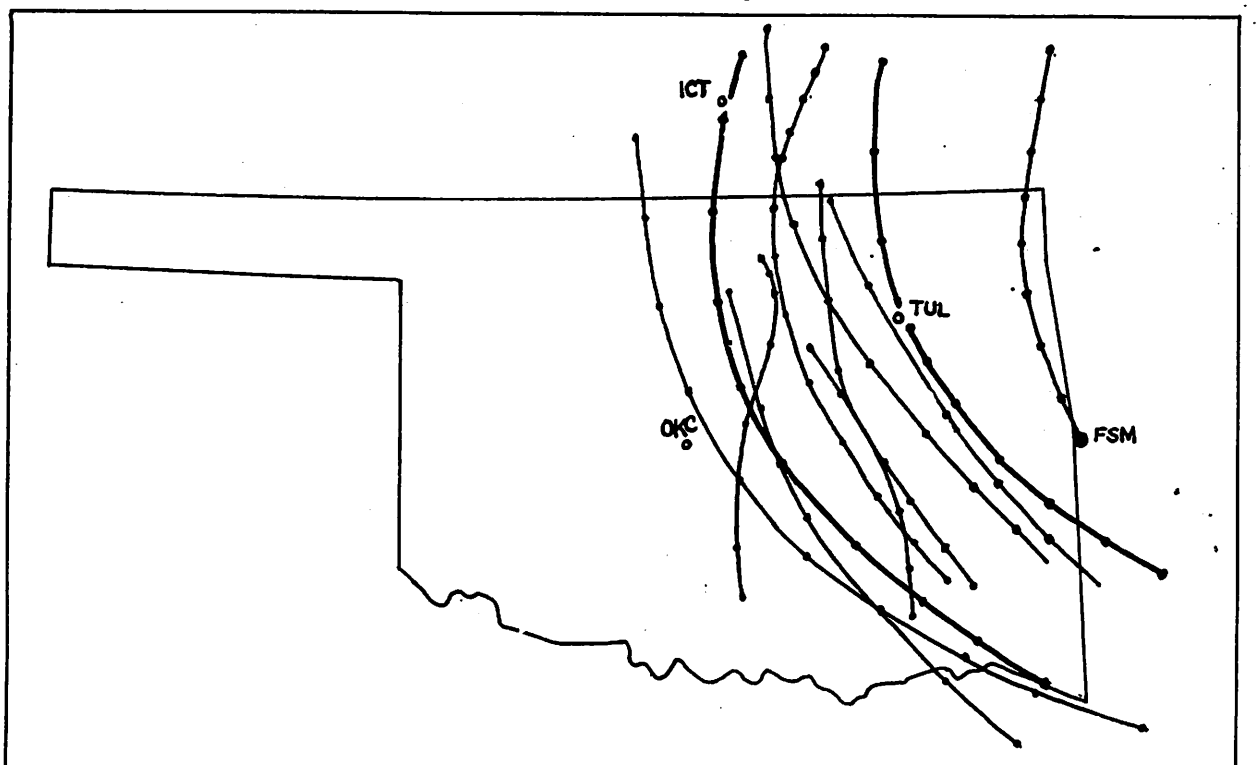


Figure 44. - Composite of trajectories beginning at 1900 and 2200 CST, Sept. 3 and 0200 and 0500 CST, Sept. 4, 1940. Dots are at 1-hour intervals. Heavy lines are lateral boundaries of inflow area.

Figure 45. - Showing location of maximum shear, lateral boundaries, inflow area, L, and $V_n$.

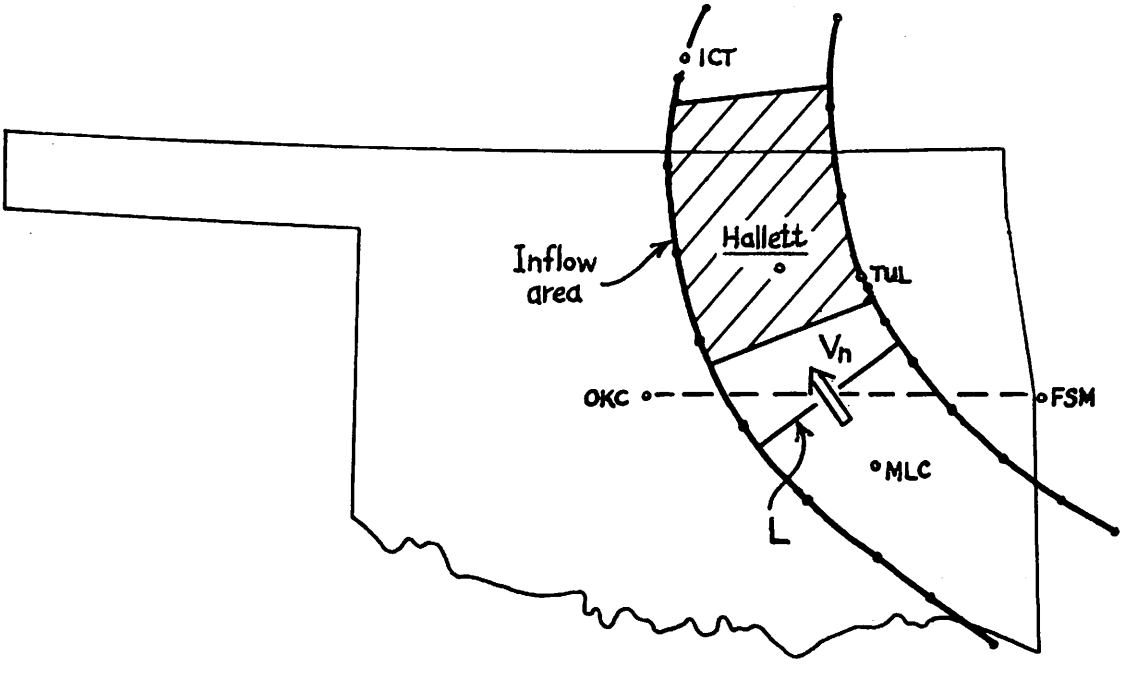

# PART 3. TEST OF METHOD FOR 24-HOUR FORECASTS

C. S. Gilman and K. R. Peterson

Hydrologic Services Division, U. S. Weather Bureau, Washington, D. C.

[Manuscript received April 17, 1959; revised November 19, 1959]

## 1. INTRODUCTION

Parts 1 and 2 have shown that (1) cyclonicity in the horizontal pressure field is an indicator of horizontal convergence (2) there is a volumetric control on the quantity of moisture entering a given region, and (3) with the aid of dynamic trajectories, a consideration of these factors can provide a short-range quantitative precipitation forecast. The present paper concerns the application and field tests of the procedures extended to a 24-hour period. The tests were set up to see whether, using prognostic maps of the surface pressure field and the surface to 500-mb. precipitable water, it was possible to forecast rainfall over the United States east of 105°W. with sufficient accuracy and within a reasonable length of time to be of synoptic value.

Although the primary goal of the experiment was to forecast precipitation amounts of 1 inch or more, 1/2 inch and lesser amounts were also forecast.

The forecast tests were made in three phases. Phase A was conducted during the late winter and the spring 1957 by a single meteorologist working for about one hour a day. During this time, it was necessary for the forecaster to compute the precipitable water field. The meteorologist visualized the changes that were taking place in the pressure field and the locations of the areas of maximum cyclonicity in 12 to 24 hours. He was intimately familiar with the concepts discussed in Parts 1 and 2 as they had been developed up to that time. Little emphasis was given to initial anticyclonic vorticity of the wind or to the rapid replacement of anticyclonic pressure fields by linear or cyclonic fields.

Forecasts were made at the National Meteorological Center (NMC), Suitland, Md. on working days and were interrupted on several occasions. A copy of the forecast was given to a neutral party during the forenoon. The forecaster consulted only the data up to 1230 GMT and the forecast was for the period 1230 GMT today to 1230 GMT tomorrow.

Phase B was conducted by a team of three meteorologists during April 1958 at the National Meteorological Center and during May 1958 at Washington National Airport. While the synoptic experience of each varied, all three had a thorough knowledge of the principles involved in the technique. Two hours were spent making the forecast for a total of 6 man-hours. A forecast was made every working day. (The data available and the forecast period were the same as phase A, except that the period began and ended at 1200 GMT.) By this time precipitable water charts were being prepared by the NMC on a routine

basis. Usually, the first hour was spent in preparing a 12-hour surface prognostic chart and the second hour was spent in constructing trajectories, determining the volume of moisture, and making the precipitation forecast.

Phase C was conducted at Washington National Airport during March 1959 by two meteorologists from the Hydrometeorological Section and one meteorologist from the Airport who was trained in the technique during part of Phase B. Three forecasts were made on each working day and on those week-ends when significant precipitation was expected.

The first forecast was made within an hour after arriving on duty. No formal prognostic maps and no trajectories were prepared. The latest surface map available was for 0900 GMT.

The second forecast was made within an hour after the first forecast had been made. During this time, preliminary 12-hour prognostic surface isallobars were drawn and trajectories were constructed where necessary. The latest surface map available was again for 0900 GMT.

The final forecast was prepared using the 1200 GMT surface map. The preliminary prognostic isallobars and trajectories were modified on the basis of the later information. The final forecast was completed within three hours after 1200 GMT map time.

## 2. DETERMINING WHERE PRECIPITATION WILL OCCUR

A map showing the trajectories of all the surface air particles for the next 24 hours would readily delineate regions of surface convergence. However, since it is time-consuming to construct trajectories over the entire map, the cyclonicity of the surface isobars is used to determine the general regions of convergence. Typical convergence-producing isobaric configurations are shown in figures 1-4. They are observed cases of some of the theoretical patterns of cyclonicity given in Part 1.

Figure 1, a typical example of geostrophic wind shear, occurred at 1830 GMT on April 24, 1957. The region of maximum shear is shown by the dashed lines. The shaded areas enclose the 1-inch isohyets for the 24-hour period 12 hours each side of the isobaric pattern. It can be seen that the precipitation occurred in the vicinity of and downstream from the region of shear.

Figure 2 shows an example of geostrophic shear and curvature as indicated by the slanting lines. This case was observed at 1800 GMT on March 23, 1958. Again, the shaded region encloses the 1-inch isohyet for the 24-hour period centered at map time. The effect of the curvature is evident in the rainfall north of the warm front. Another contributor to the rainfall in this case was the movement of the strong pressure gradient ahead of the Low into a region formerly having a weaker gradient. This resulted in a greater inflow of moist air from the southeast.

A pressure fall region moving ahead of a surface Low will cause the isobars to the east and south of the Low to turn anticyclonically. This effect is shown in figure 3. The solid lines are isobars for 1800 GMT, April 23,

1958, while the dashed lines are isobars 12 hours later. The turning of the isobars resulted in a turning toward the east of the moist flow originating in the Gulf of Mexico with a resultant decrease of the precipitation than might otherwise be expected.

The development of a region of isobaric curvature is shown in figure 4. The isobars for 0630 GMT, May 15, 1958 indicate only one isobar crossing the stationary front along the Kansas-Oklahoma border. Twenty-four hours later, the flow from the south has increased and three isobars (dashed) cross the front. The 1-inch isohyet is shown by the boundary of the shaded regions downstream from the areas of curvature.

Some other isobaric configurations which are convergence-producing are:

(a) isobaric curvature changing with time from anticyclonic or straight to more cyclonic.

(b) isobaric gradient decreasing with time, resulting in the deceleration and turning to the right of the air parcels.

(c) development of an open trough within a V-shaped trough, thereby bringing about a region of cyclonic shear along the eastern boundary of the trough.

After a close inspection of the isobars on the current map and on the prognostic map, the general areas of convergence are outlined. The convergence regions are more closely located by taking trajectories into them. Goodyear [1] discussed the theory and application of dynamic trajectories. The starting points for taking trajectories are obtained by going upstream 18-24 hours from the general convergence region, using the mean second standard level wind or the mean upstream geostrophic wind. The specific convergence region is determined by a combination of computed trajectories and mental trajectories as shown by the isobars.

Two aids to the computation of trajectories are given in figure 5 and table 1. Figure 5 assumes that both the actual wind and the geostrophic wind have the same direction. It gives 6-hour trajectories between 30° and 40° latitude for "balanced" winds, inertia winds, and variations between these extremes. The wind directions are aligned vertically on the diagram. In use the diagram would be rotated to line-up with the observed direction and with the "0" point over the observation station.

If the actual and geostrophic winds are of equal speeds, the trajectory will lie along the direction of the actual and geostrophic winds and its end point will be at the point designating the wind speed.

If the geostrophic wind is zero, the trajectory will be along the arc labeled by the appropriate initial wind speed.

In between these two conditions the end point of a 6-hour trajectory will lie at the intersection of the lines on the diagram which indicate the initial and geostrophic wind speeds.

A strong pressure gradient which replaces a weak gradient with time causes air parcels imbedded within the current to blow across the isobars toward lower pressure. A table (derived from the equations of frictionless motion) which indicates the terminal point of trajectories after 3, 6, 12, and 24 hours with an increase in the geostrophic wind on a parcel as shown is given in table 1. It is assumed that the actual wind and the geostrophic wind have the same speed and direction initially, and that there is no change in the direction of the geostrophic wind during the time period. In using the table, the increase in the geostrophic wind during the succeeding 12 hours is estimated and the time of the trajectory is selected. The numbers in the body of the table locate the terminal point of the trajectory; the first number is the angle of incurvature (toward lower pressure), while the second number is the amount by which the actual wind exceeds the geostrophic wind at the end point. A trial and error solution is necessary and is accomplished by (1) estimating the increase in geostrophic wind during the chosen time period, (2) laying off the tabular change of angle (toward lower pressure), (3) selecting a point along this line and measuring the geostrophic wind at the end of the time period, and (4) multiplying this wind by the proper tabular value. If the distance from the initial point to the estimated terminal point of the trajectory does not agree with the distance represented by (4) above, another point is selected and the same procedure is followed.

## 3. DETERMINING HOW MUCH PRECIPITATION WILL OCCUR

In order to find out how much precipitation will occur, it is first necessary to determine what area of surface air will blow into the convergence region. This inflow area is set off by trajectories, both mental and computed. Consider figure 6, which is a modification of figure 3 of Part 2.

It can be seen that the inflow area is bounded by the lateral bounding trajectories (within which convergence occurs) and by the lines connecting the beginning and the end points of the 24-hour trajectories within the lateral bounding trajectories.

If the inflow area ($mi.^2$) is multiplied by the mean precipitable water (inches) within the inflow area during the 24-hour period, the product is the inflow volume or moisture transport ($mi.^2$ in.) which will flow into the convergence region.

Some consideration should be given to the flow at levels above the surface, particularly if the direction of flow at 850 mb. over the inflow area is markedly different from the flow at the surface. Such a situation often occurs when a Low at the surface is not open to the south and the moisture appears to be coming from the east. However, usually at 850 mb. much of the moisture still has a southerly component. The amount of moisture at higher standard levels is usually not sufficient to warrent consideration along these lines.

Since the precipitation process is not 100 percent efficient, an efficiency factor is used. Additional research is necessary to determine what a proper efficiency factor should be, but with dew points above 60°F. a study by the Hydrometeorological Section [2] has shown that about 75 percent is a good average value. A factor of 80 percent or higher should be used in cases where

Table 1. - Determination of trajectories for increasing geostrophic wind on parcel, assuming initial wind is geostrophic. Tabular values indicate deflection angle ( degrees, counterclockwise) and length of trajectory expressed as multiple of final geostrophic wind in knots ($V_{gf}$).

| Increase in geostrophic wind on parcel in 12 hours | Hours | | | |
|---|---|---|---|---|
| | 3 | 6 | 12 | 24 |
| 1.5 | $1°/2.7V_{g3}$ | $3°/4.9V_{g6}$ | $8°/9.2V_{g12}$ | $7°/18.1V_{g24}$ |
| 2 | 2/2.4 | 6/4.2 | 14/7.9 | 11/15.3 |
| 3 | 4/2.0 | 12/3.4 | 22/6.7 | 13/14.8 |
| 5 | 7/1.6 | 21/2.5 | 33/6.1 | 15/13.5 |

instability is present or where the isobars and trajectories indicate strong convergence. An approximate measure of instability can be determined from a consideration of the difference between the observed 500-mb. temperature and the surface dew point temperature raised adiabatically-pseudo-adiabatically to 500 mb. A nomogram to obtain this latter temperature from the 1000-mb. temperature and dew point is given in figure 7.

Low-level convergence with most of the moisture concentrated at higher levels results in a small efficiency factor. Ideally, an inspection of individual radiosonde observations will reveal such a situation; however, an inspection of dew points and precipitable water values where dew points are relatively low in comparison with the precipitable water is a dependable indicator. Under such conditions the efficiency factor should be reduced to about 50 percent.

The isohyets are determined by dividing the inflow volume(multiplied by an efficiency)by the area of the convergence (precipitation) region, thereby yielding the average precipitation over the convergence region. The configuration of the isohyets is determined from a general knowledge of isohyetal patterns and from a consideration of the movement of the convergence region.

During phases B and C it was observed that the largest observed isohyet bore some relationship to the magnitude of the forecast inflow volume. Therefore the largest forecast isohyet was determined from table 2. It should be

Table 2. - Relationship between forecast inflow volume and largest observed isohyet

| Inflow volume ($mi.^2$ in.) | Largest isohyet (in.) |
|---|---|
| $50 \times 10^3$ | 0.5 |
| 100 | 1.0 |
| 200 | 2.0 - 3.0 |
| 300 | 4.0 - 5.0 |

Table 3. - Square miles of air blowing through 1 mb. in 24 hours at various latitudes.

| Latitude | mi.$^2$ |
|---|---|
| 25°N. | 35,000 |
| 30 | 30,000 |
| 35 | 26,000 |
| 40 | 23,000 |
| 45 | 21,000 |

emphasized that table 2 is based upon only three months of observation with no statistical study of the data involved.

Once the isohyets have been drawn, a rough check is made to ascertain that the precipitation volume indicated is about the same as the inflow volume (with efficiency factor). The accuracy of the computed inflow and precipitation volumes does not justify precise measurement. The areas can be measured with sufficient accuracy by approximating them as rectangles or triangles. Error analysis shows that volumes of 100,000-200,000 mi.$^2$ in. are accurate only to within about $\pm$ 20,000 mi.$^2$ in.

As an approximation of the inflow area, it is possible to compute the square miles of air blowing through 1 millibar of pressure difference over a 24-hour period. The geostrophic wind equation, where

$$V_g \Delta n = \frac{1}{\rho f} \Delta p,$$

gives table 3. In using table 3, the number of square miles of air flowing through 1 millibar at the latitude of the inflow area is multiplied by the number of isobars crossing the inflow area.

## 4. PROGNOSTIC SURFACE ISALLOBARS

For short-period forecasts (up to 6 hours), primary use was made of the current pressure map, but for the latter parts of the 24-hour period, some weight, and in many cases appreciable weight, had to be given to prognostic pressure maps.

One use of the prognostic chart was to estimate the magnitudes and future locations of critical features of the Laplacian of pressure. For this use, it was necessary that the chart contain more detail than would be shown solely by the location of fronts and high and low pressure centers. There are, in particular, areas of cyclonic geostrophic vorticity not associated with any fronts by the usual definition. Even at fronts it was necessary to estimate the over-all angle that the isobars made across the front at a future time.

In many cases a forecast using considerations of the surface isallobars will show up important features which may not be obvious using other prognostic methods. For example, if surface pressures are forecast to persist over the Southeast and a pressure fall is moving into southern Midwest, the

inflow will be increased, drawing air toward lower pressure and converging downstream from the cyclonic shear of the isallobars.

For making the 12-hour prognostic charts of surface pressure, primary use was made of three considerations: (1) continuity as shown by the 12-hour and 3-hour pressure changes, (2) future areas of differential advection and differential release of latent heat (see Gilman [3] and Appleby [4]), and (3) instability. The procedure followed routinely in phase B was as follows:

Beginning an hour before the final map was available, maps of 12-hour and 3-hour pressure changes were corrected for diurnal effects. Then a provisional 12-hour pressure change map was drawn for the period 1200-0000 GMT, using the three considerations listed above. This pressure change map was used with the latest pressure map (0900 GMT) to obtain a preliminary idea of what areas needed the most emphasis. Preliminary trajectories were drawn if time permitted and if they were thought desirable.

When the final map was available, a final 12-hour prognostic surface-pressure-change map was made. The details of this procedure are given in the next section.

## 5. CHRONOLOGICAL ORDER OF STEPS TAKEN DURING FORECAST PROCEDURE

The following is set up for a two-man operation at an analysis center preparing a 24-hour precipitation forecast within 3 hours after map time (t).

The first step is for both forecasters to examine the isobaric configurations of the surface maps at (t-6) and (t-3), the second standard level winds at (t-6) and the precipitable water map at (t-12) (where t represents map time --the time of the latest surface map available before the forecast is issued and the numbers represent the hours before map time). The forecasters arrive at a tentative decision of where the important precipitation will occur.

After this, one of the forecasters analyzes 3-hour pressure changes on the (t-3) surface map and applies a diurnal correction. During this time, the second forecaster is preparing a forecast of the second standard level winds for map time from the (t-6) winds.

Next, one of the forecasters prepares a preliminary 12-hour surface isallobar prog while the other forecaster supplies him with the following necessary information: (a) 12-hour pressure change maps (corrected for diurnal) for (t-3), (t-6), and (t-12)(also at map time, t, as soon as the map has been plotted); (b) regions of differential advection as determined from the (t-6) surface map and the most recent 500-mb. map (t-6 or t-12); (c) indications of instability as determined from the (t-3) surface map and the latest 500-mb. map (t-6 or t-12).

Also, during this time, the second forecaster begins to construct dynamic trajectories into the regions of expected precipitation.

As soon as the latest surface map is ready, 3-hour pressure changes (corrected for diurnal) are analyzed and are used in conjunction with the

12-hour surface pressure changes at map time to modify the 12-hour prognostic chart as necessary and to arrive at a final prognostic chart.

Upon completion of the prognostic map, both forecasters compute a sufficient number of trajectories to delineate all the regions of significant convergence. While one forecaster continues taking trajectories the other also makes a mental forecast of the precipitable water distribution (a formal forecast is not necessary since this quantity is conservative). He also determines the moisture transport into the regions of convergence and applies an efficiency factor to each value.

As a final step both forecasters place the isohyets within the convergence regions and then make a rapid check to ascertain that the forecast volumes as shown by the isohyets are in agreement with the computed moisture transports.

## 6. FORECAST AND VERIFICATION MAPS

The forecast and verification maps for March 1959 (Phase C), arranged in chronological order, are shown in figures 8 to 32. The solid lines are the forecast 24-hour isohyets while the plotted numbers are the observed precipitation amounts. The term "light" means that scattered amounts of 0.25 inch or more might occur but that no 0.25-inch line was expected. Shower and thunderstorm symbols indicate that convective rainfall was forecast with no general region of heavy rain.

## 7. SUMMARY

A statistical verification was prepared by a meteorologist from the Hydrometeorological Section not connected with quantitative precipitation studies. Using a 40,000 mi.$^2$ grid for the United States east of 105°W., he compared the Hydrometeorological Section and Analysis Center forecast 1-inch isohyets (prepared daily at the NMC). Without reference to observed precipitation, the meteorologist added 1/2 inch isohyets to the Analysis Center forecasts as objectively as possible. The River Services 24-hour precipitation maps were used for verification. Forecasts were compared for 24 days between March 3 and April 1, 1959.

The results are shown as contingency tables in tables 4 and 5. For precipitation of one inch or more, a "hit" was recorded when an average of 1 inch or more was forecast and observed within the same 40,000 mi.$^2$ area. It can be seen that Hydrometeorological Section scored 8 "hits" to the Analysis Center's 2 "hits." The skill scores compared 0.25 to 0.07, respectively. A chi-square test applied to tables 4 and 5 yielded values of 52.5 and 6.7, respectively. The forecasts by Hydrometeorological Section showed a tendency to over-forecast, while those by the Analysis Center indicated a tendency to under-forecast precipitation heavier than 1 inch.

Table 4 shows that 32 area forecasts were made of precipitation equal to or greater than 1 inch. As mentioned, eight of these area forecasts verified correct. In order to investigate how many of these would have verified by

Table 4. - Summary of Hydrometeorological Section forecast vs. observed precipitation (inches) during March 1959

| | | FORECAST | | | |
|---|---|---|---|---|---|
| | | < 1.0 | ≥ 1.0 | Total | |
| OBSERVED | < 1.0 | 1101 | 24 | 1125 | Skill score = 0.25 |
| | ≥ 1.0 | 19 | 8 | 27 | |
| | Total | 1120 | 32 | 1152 | |

chance alone, 32 of the total number of forecast areas (24 days x $\frac{48 \text{ areas}}{\text{day}}$ = 1152) were selected at random and verified. Five separate trials were made with the following results:

| Trial | 1 | 2 | 3 | 4 | 5 |
|---|---|---|---|---|---|
| Number correct of 32 | 0 | 1 | 0 | 1 | 1 |

Although, admittedly, the test is somewhat biased since it fails to take climatology into account, it appears that only 1 forecast is most likely to verify correct by chance. A persistence test also was made to investigate the significance of the forecast results. The 24-hour mean precipitation over each of the grid elements was "forecast" to persist during the succeeding 24 hours. The verification showed no correct forecasts. In order to make a more reasonable persistence test, the mean areal precipitation for the 6 hours preceding the beginning of the verification period was "forecast" to continue for the next 24 hours at four times the 6-hour rate. In this case, all 6-hour amounts of 1/4 inch or more were noted and checked against the succeeding 24-hour precipitation of 1 inch or more. The results of this test also indicated no correct forecasts by persistence. From these results and from the results of Phases A and B, it is believed that the forecasts made by the Hydrometeorological Section, utilizing the principles of cyclonicity and volumetric control, have shown a degree of skill of synoptic value.

In each case, the forecast was issued about 3 hours after the latest surface map became available, while the Analysis Center forecasts were prepared about 6 hours earlier. Short-cuts in the procedure used in the preparation of the surface prognostic chart along with the speed-up which usually accompanies routine daily use could conceivably reduce the time for preparation of the Hydrometeorological Section Forecast to 2 hours. Useful results can be obtained from the application of the principles involved after merely a few minutes consideration, with the most profitable results obtainable after 2-3 hours application.

Table 5. - Summary of Analysis Center forecast vs. observed precipitation (inches) during March 1959

| | | FORECAST | | | |
|---|---|---|---|---|---|
| | | < 1.0 | ≥ 1.0 | Total | |
| OBSERVED | < 1.0 | 1110 | 15 | 1125 | Skill score |
| | ≥ 1.0 | 25 | 2 | 27 | = 0.07 |
| | Total | 1135 | 17 | 1152 | |

It is the opinion of the forecasters that they had not reached a plateau of skill in the subjective use of the techniques employed. Many fairly simple studies could be carried out to improve the procedure. It is felt that the forecasts have shown an improvement during the three phases, especially in selecting areas where several inches of precipitation would fall, that there is much more skill in placing the precipitation area for the first 12 hours than for the last 12, and that the location for the last 12-hour rainfall could be definitely improved by the middle of the period.

## REFERENCES


1. H. V. Goodyear, "A Graphical Method for Computing Horizontal Trajectories In the Atmosphere," Monthly Weather Review, vol. 87, No. 5, May 1959, pp. 188-195.
2. G. Lott and V. Myers, "Meteorology of Flood-Producing Storms in the Mississippi River Basin," Hydrometeorological Report No. 34, U. S. Weather Bureau, Washington, D. C. 1956.
3. C. S. Gilman, "Expansion of the Thermal Theory of Pressure Changes," ScD Thesis, M.I.T., 1949, (unpublished).
4. J. F. Appleby, "Trajectory Method of Making Short-Range Forecasts of Differential Temperature Advection, Instability and Moisture," Monthly Weather Review, vol. 82, No. 11, Nov. 1954, pp. 320-334.

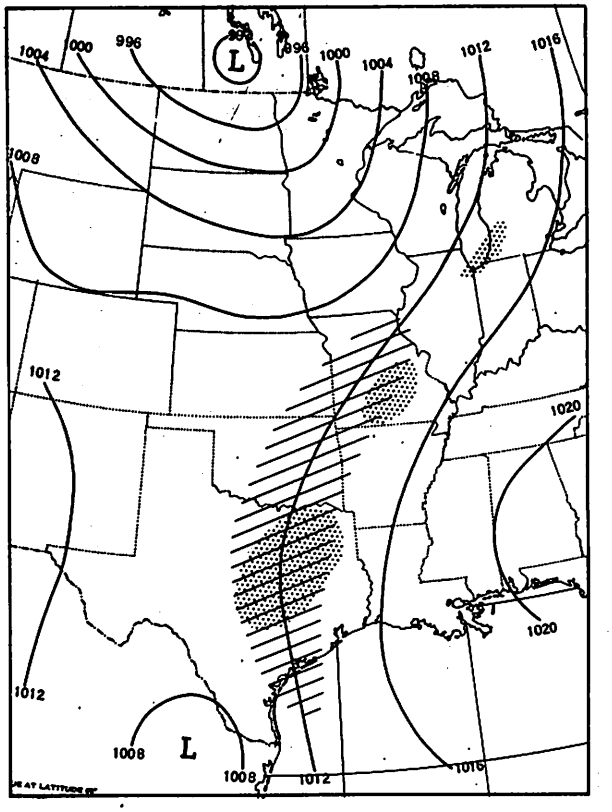


Figure 1. - Surface map, 1830 GMT, April 24, 1957, a typical case of cyclonic isobaric shear. Hatching shows region of cyclonic shear at map time; stippling indicates areas enclosed by 1-in. isohyet for 24 hours ending 0630 GMT April 25, 1957.

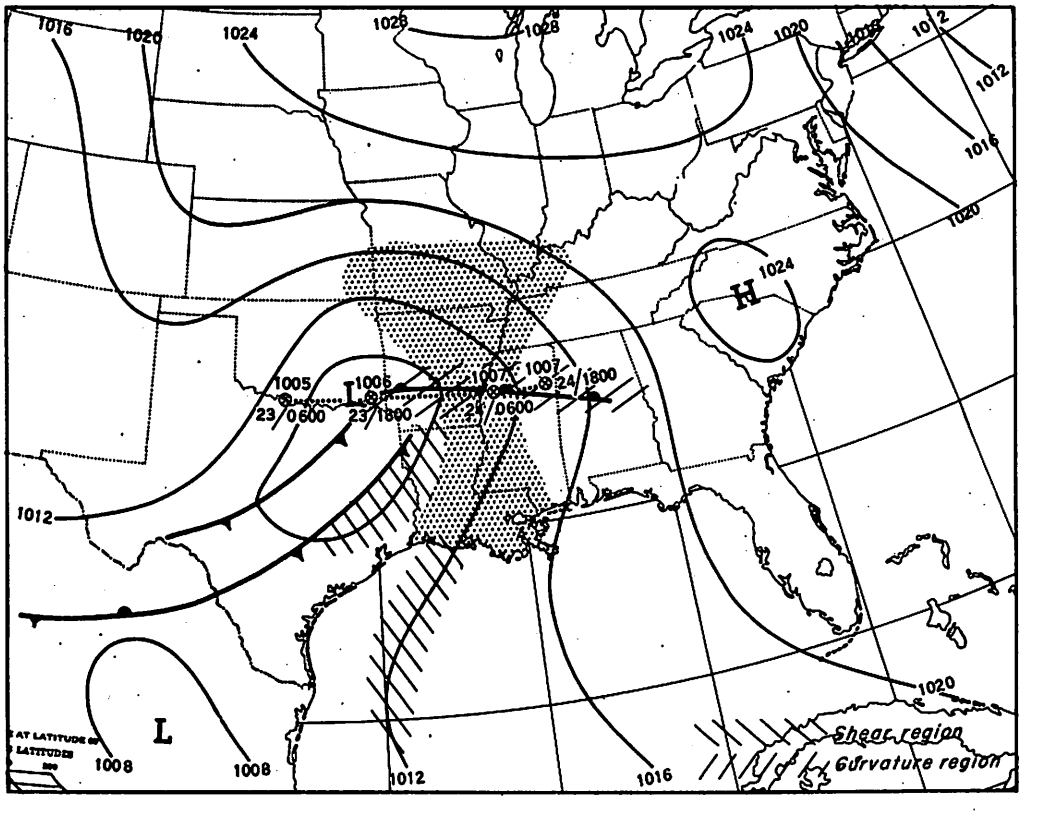


Figure 2. - Surface map, 1800 GMT, March 23, 1958, an example of curvature, shear, and strengthening gradient. Hatching shows regions of shear and curvature; stippling indicates area enclosed by 1-in. isohyet for 24 hours ending 0600 GMT, March 24, 1958.

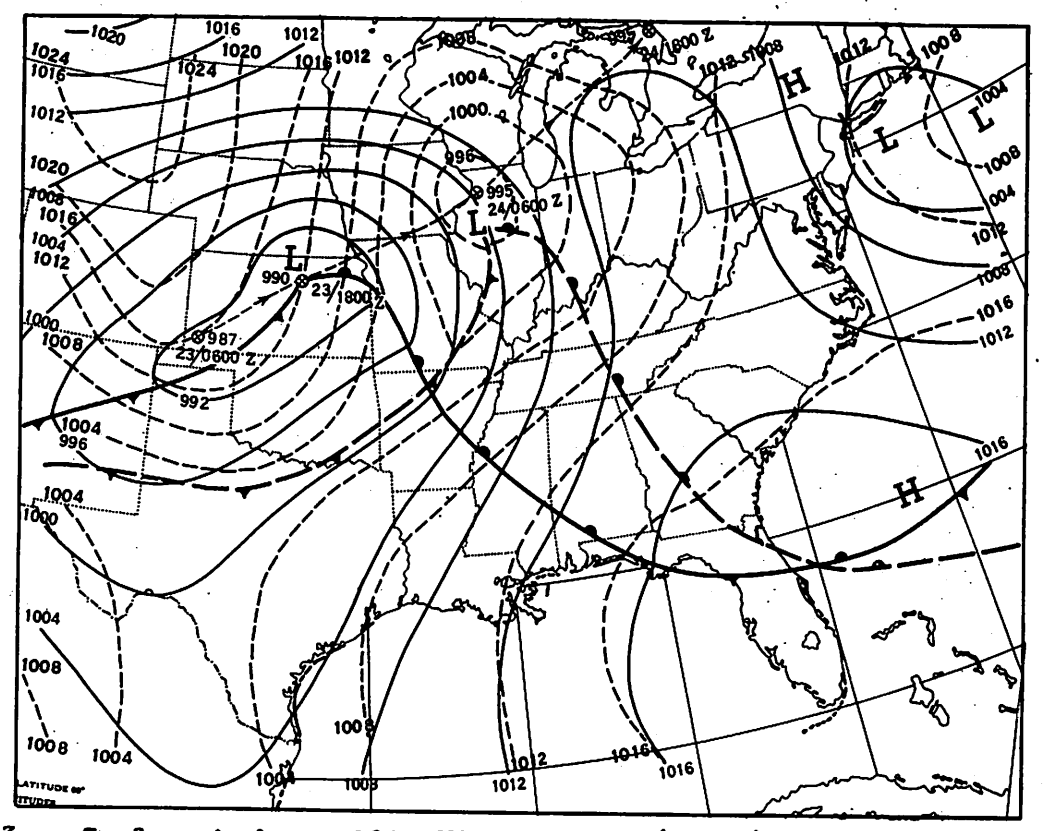


Figure 3. - Surface isobars, 1800 GMT, April 23 (solid) and 0600 GMT, April 24, 1958 (dashed), illustrating effect of pressure fall moving ahead of Low.

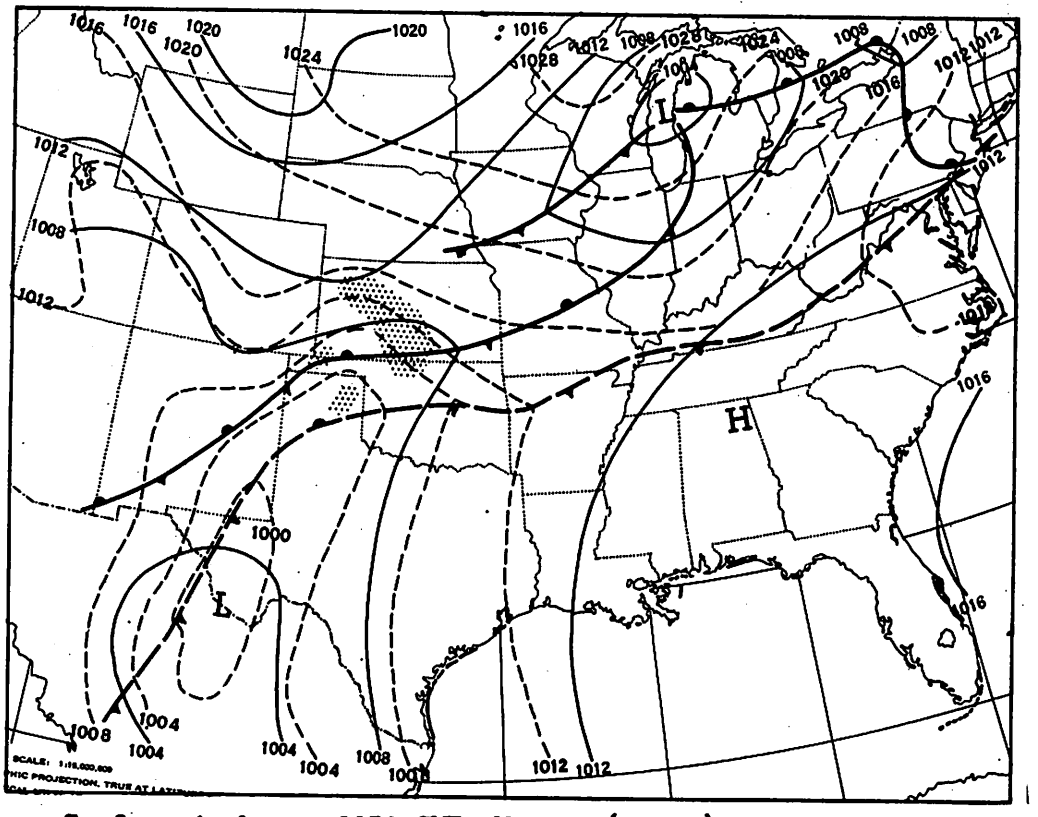


Figure 4. - Surface isobars, 0630 GMT, May 15 (solid) and 0630 GMT, May 16, 1957 (dashed), illustrating development of cyclonic curvature. Stippling indicates area enclosed by 1-in. isohyet for 24 hours ending 0630 GMT, May 16.

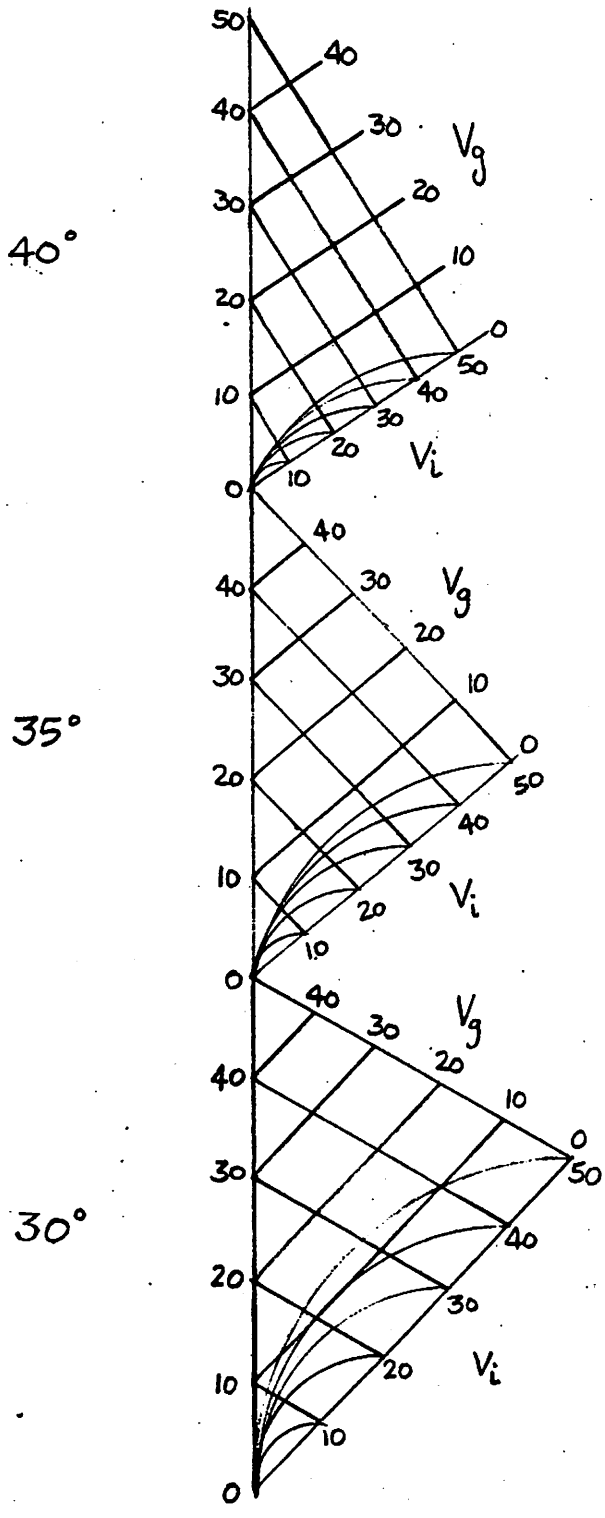


Geostrophic wind and initial wind both have same direction.

Trajectories are for 6 hours.

1. For "balanced" wind, end point is along vertical line.
2. For "inertia" wind, end point is at intersection of $V_g = 0$ and value of $V_i$.
3. For other winds, end point is at intersection of $V_g$ and $V_i$

Figure 5. - Trajectory computer for determining "balanced" winds, "inertia" winds, and winds between these two extremes.

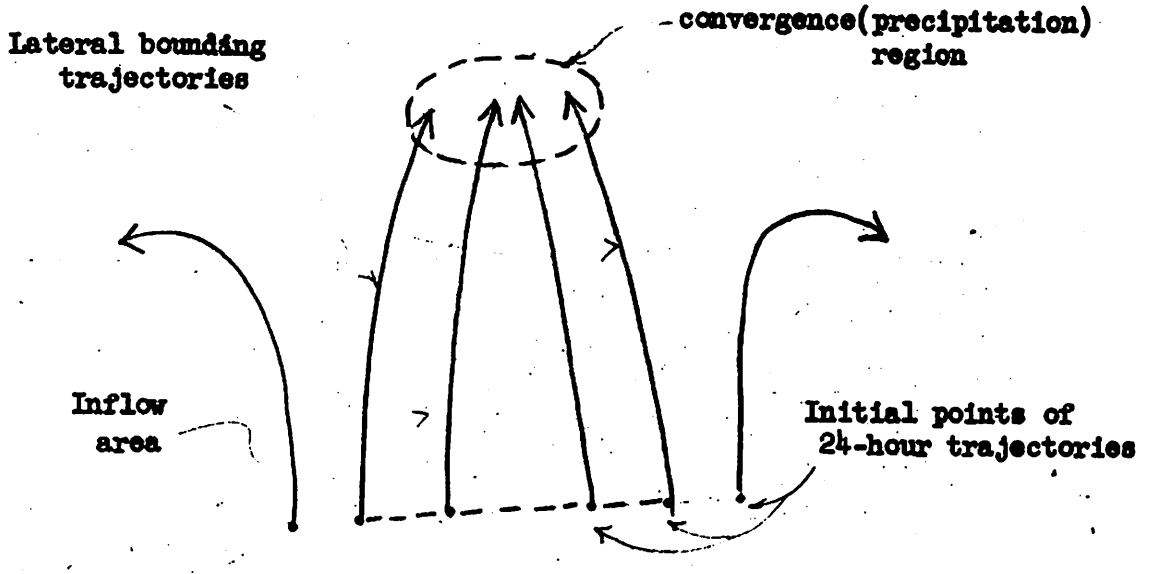


Figure 6.

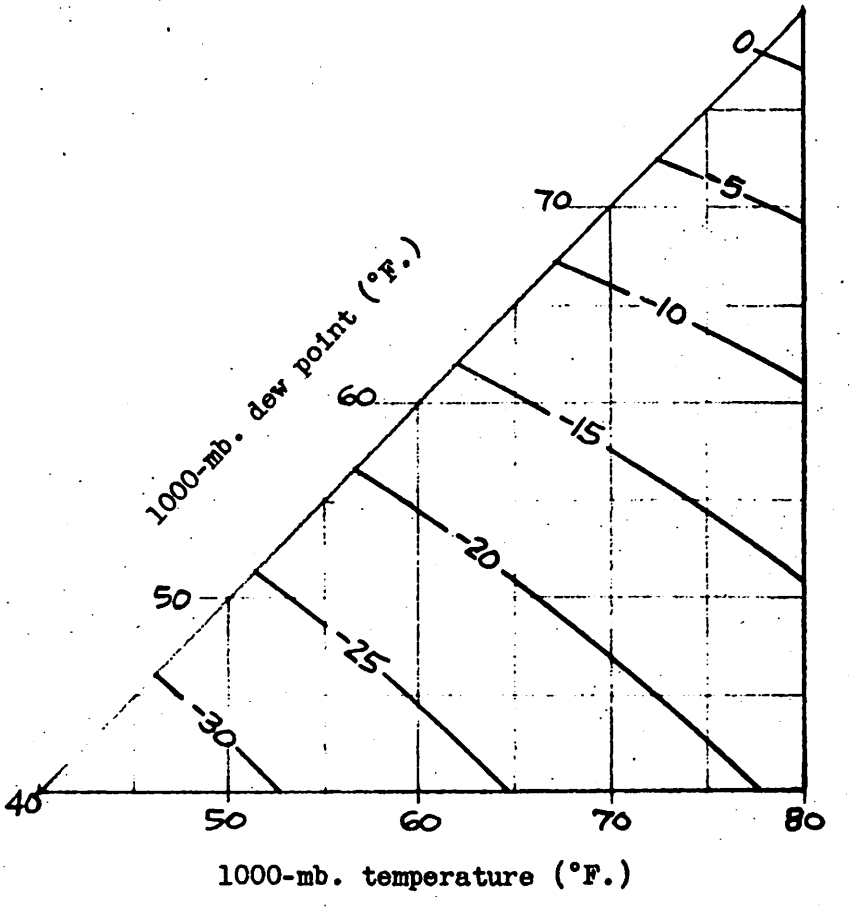


Figure 7. - Temperature (°C.) at 500 mb. of an air parcel lifted adiabatically - pseudoadiabatically from 1000 mb. to 500 mb.

Figures 8-31. - (Following in chronological order)
Forecast and observed precipitation, March 1959. Forecast shown by solid lines (24-hr. isohyets) and shower or thunderstorm symbols to indicate convective rainfall with no general region of heavy rain. Plotted numbers are observed 24-hr. rainfall, with stippling showing areas of more than 1 inch.

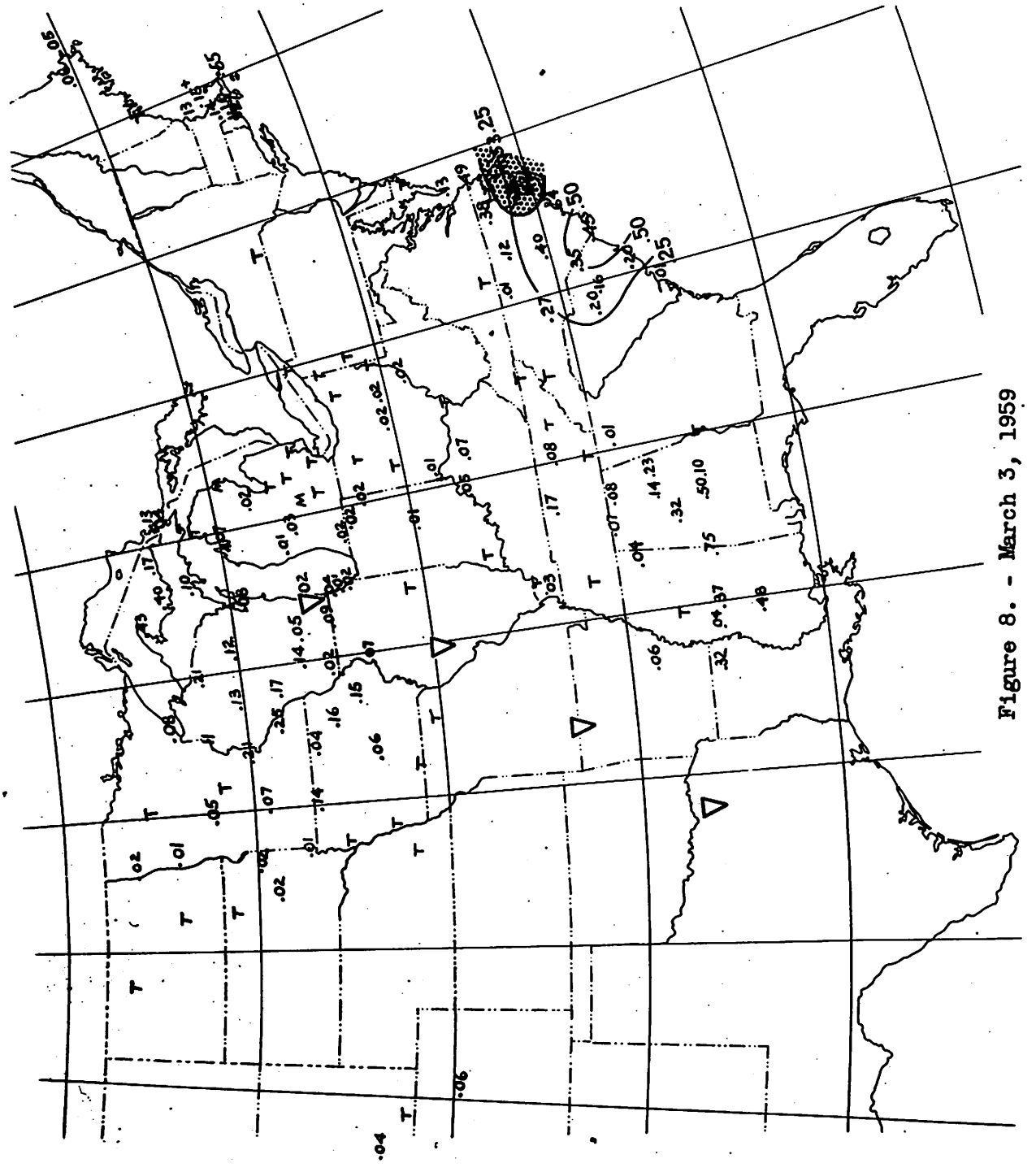

Figure 8. - March 3, 1959

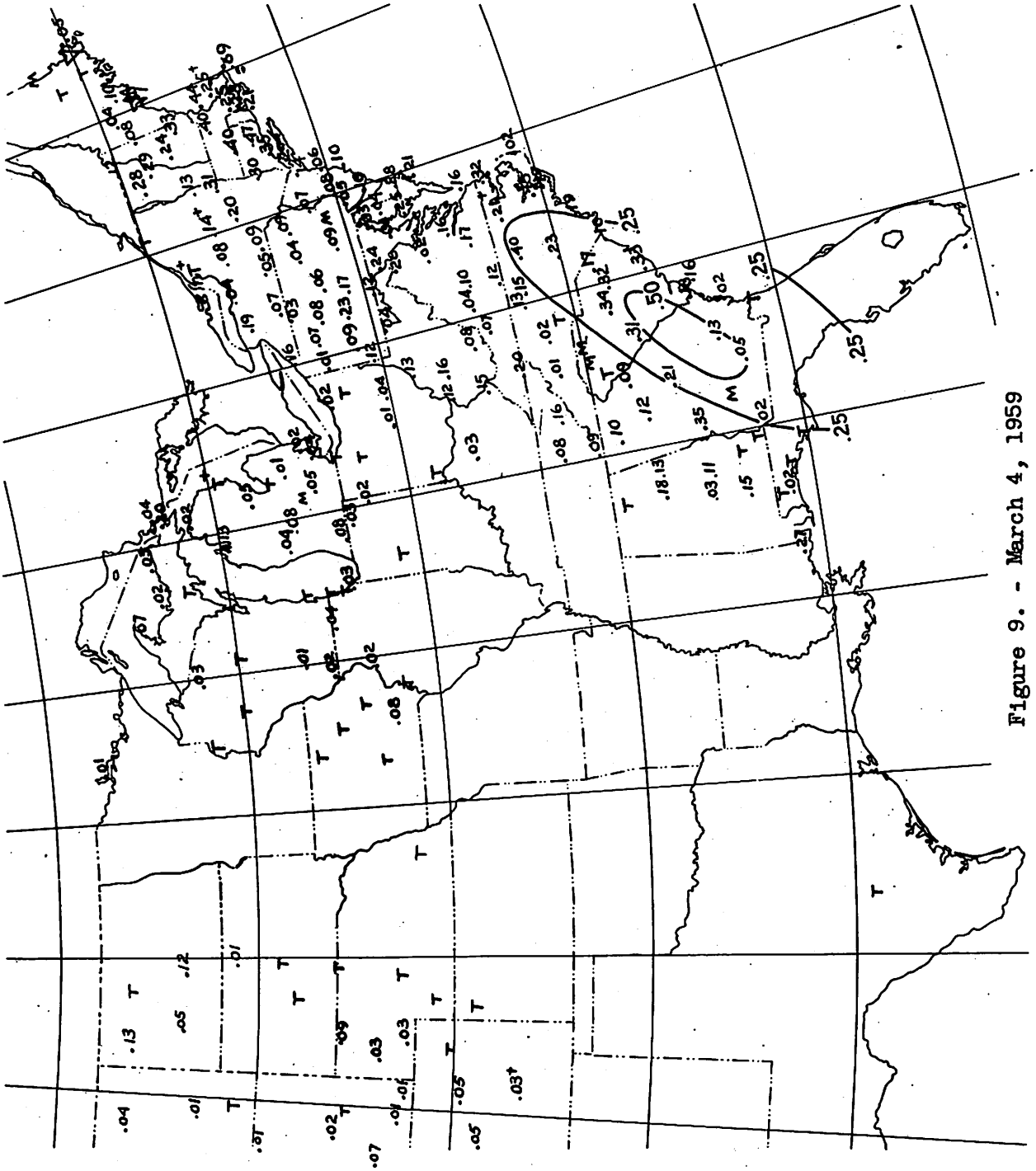

Figure 9. - March 4, 1959

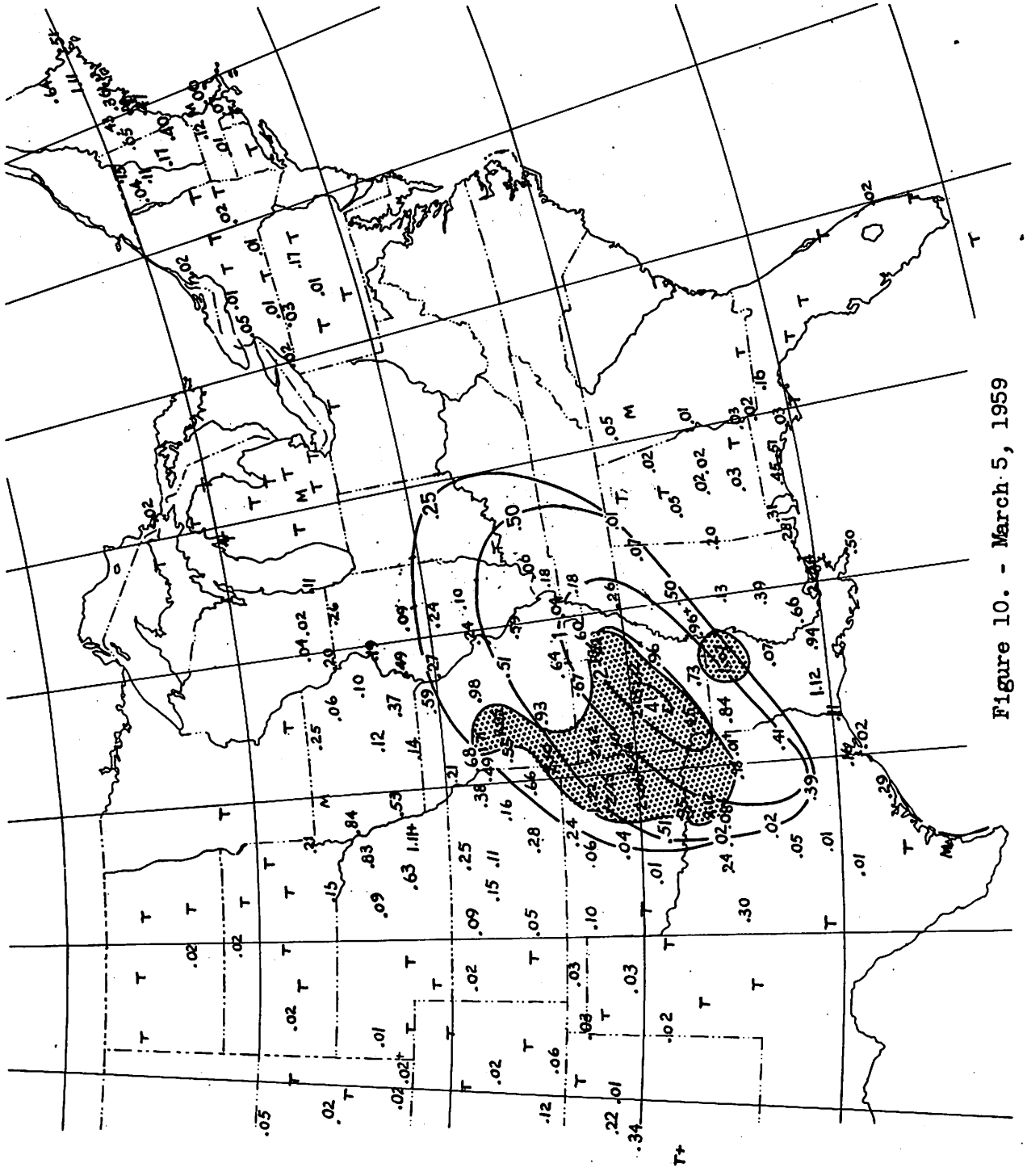

Figure 10. - March 5, 1959

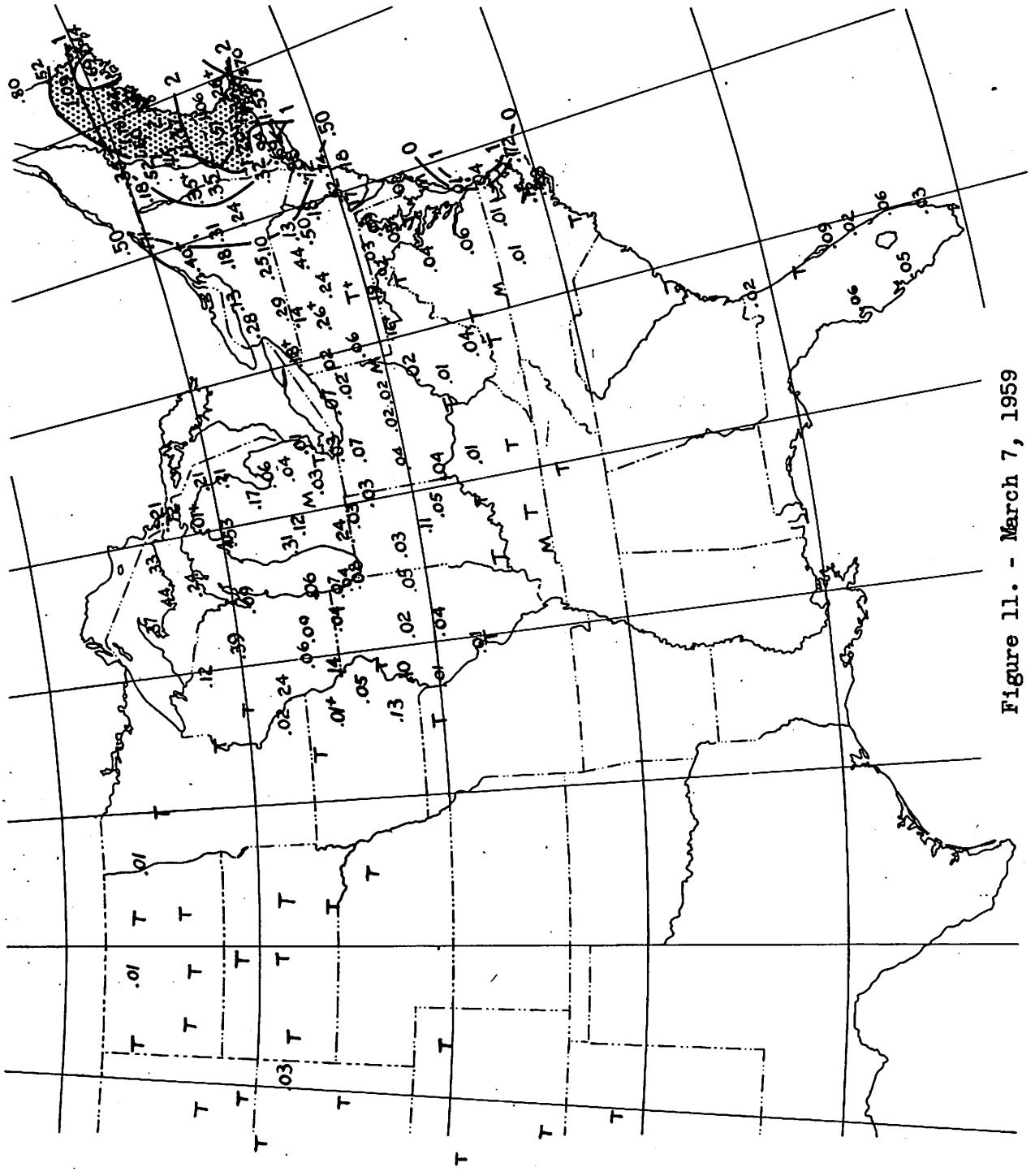

Figure 11. - March 7, 1959

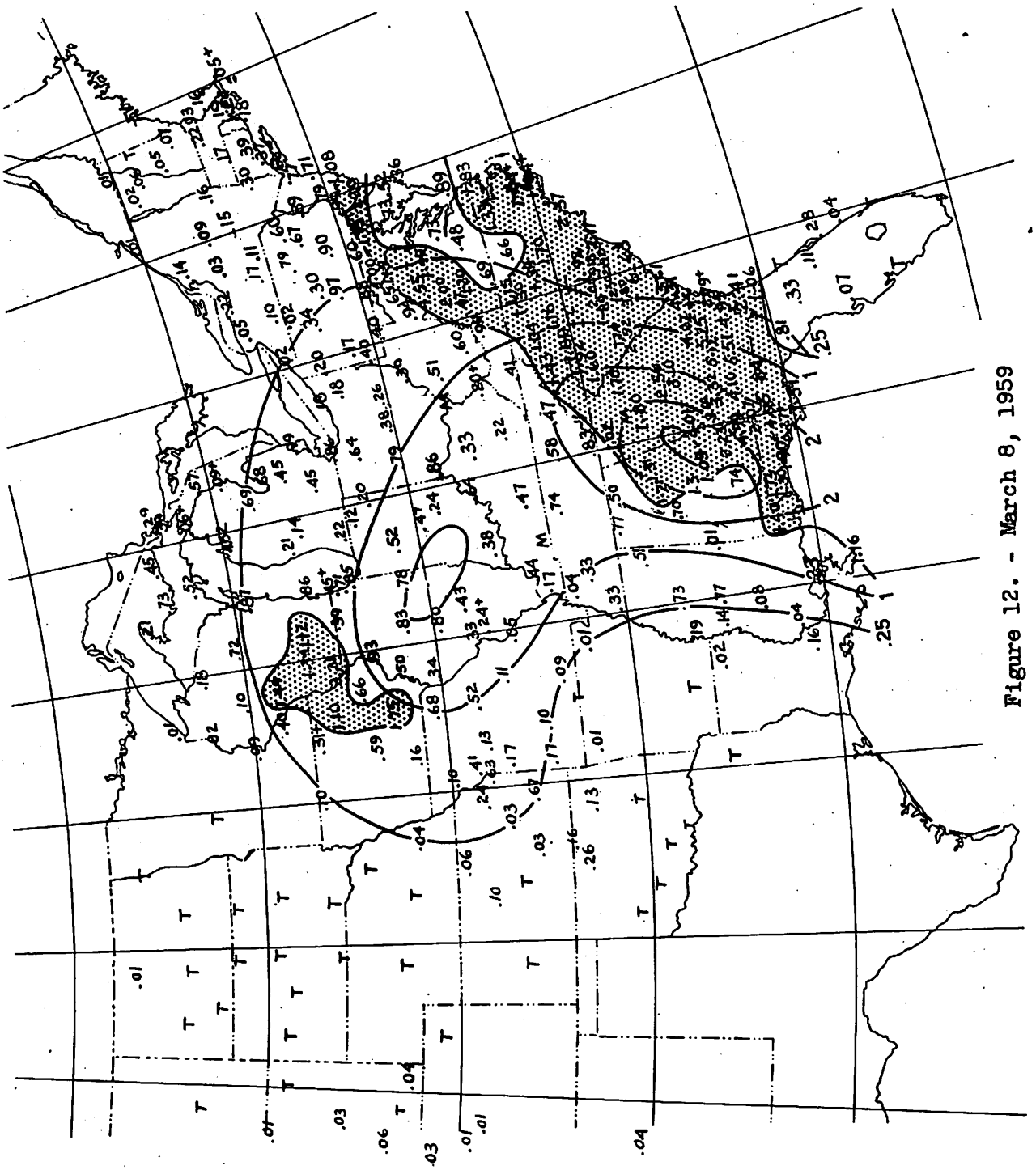

Figure 12. - March 8, 1959

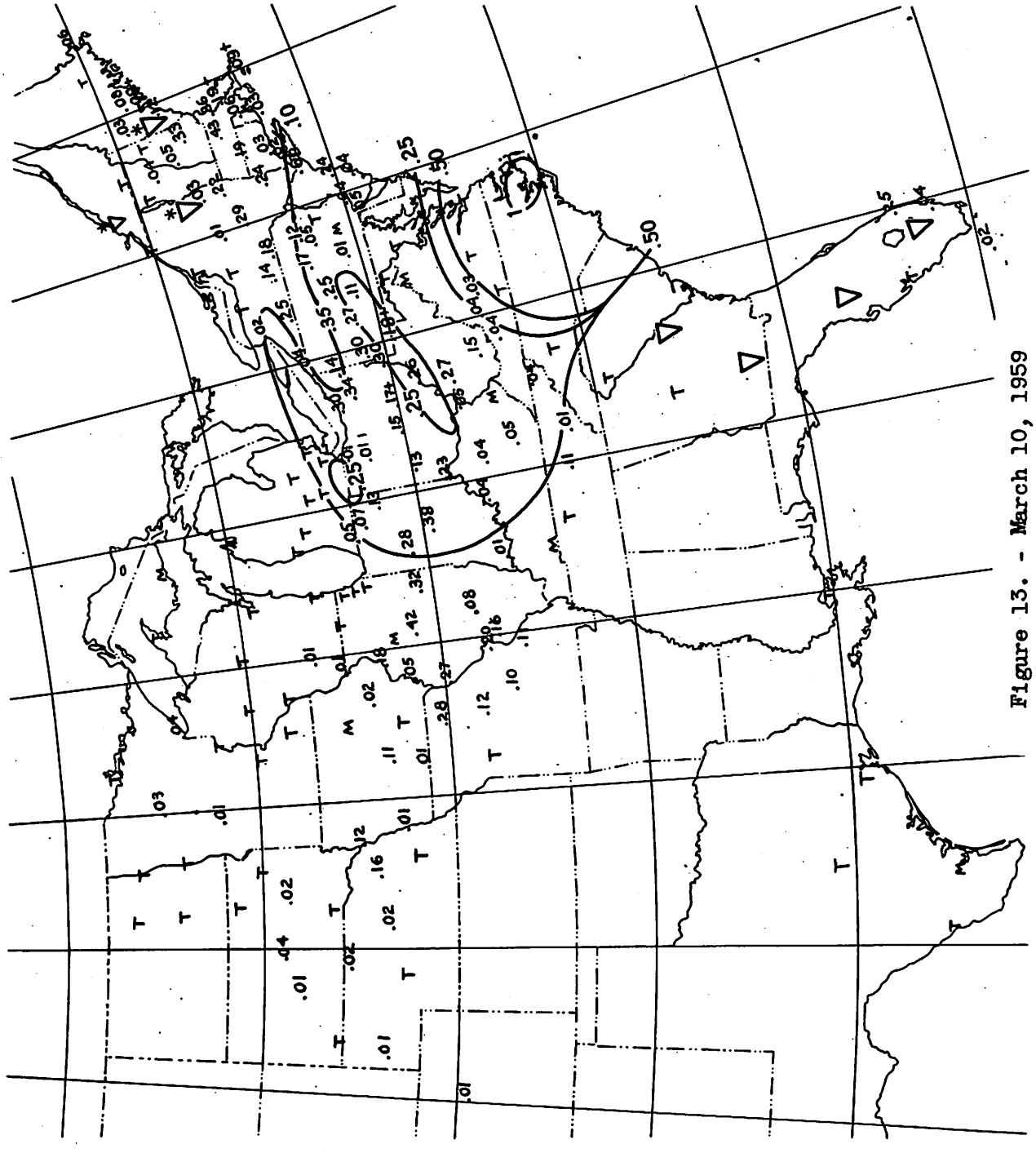

Figure 13. - March 10, 1959

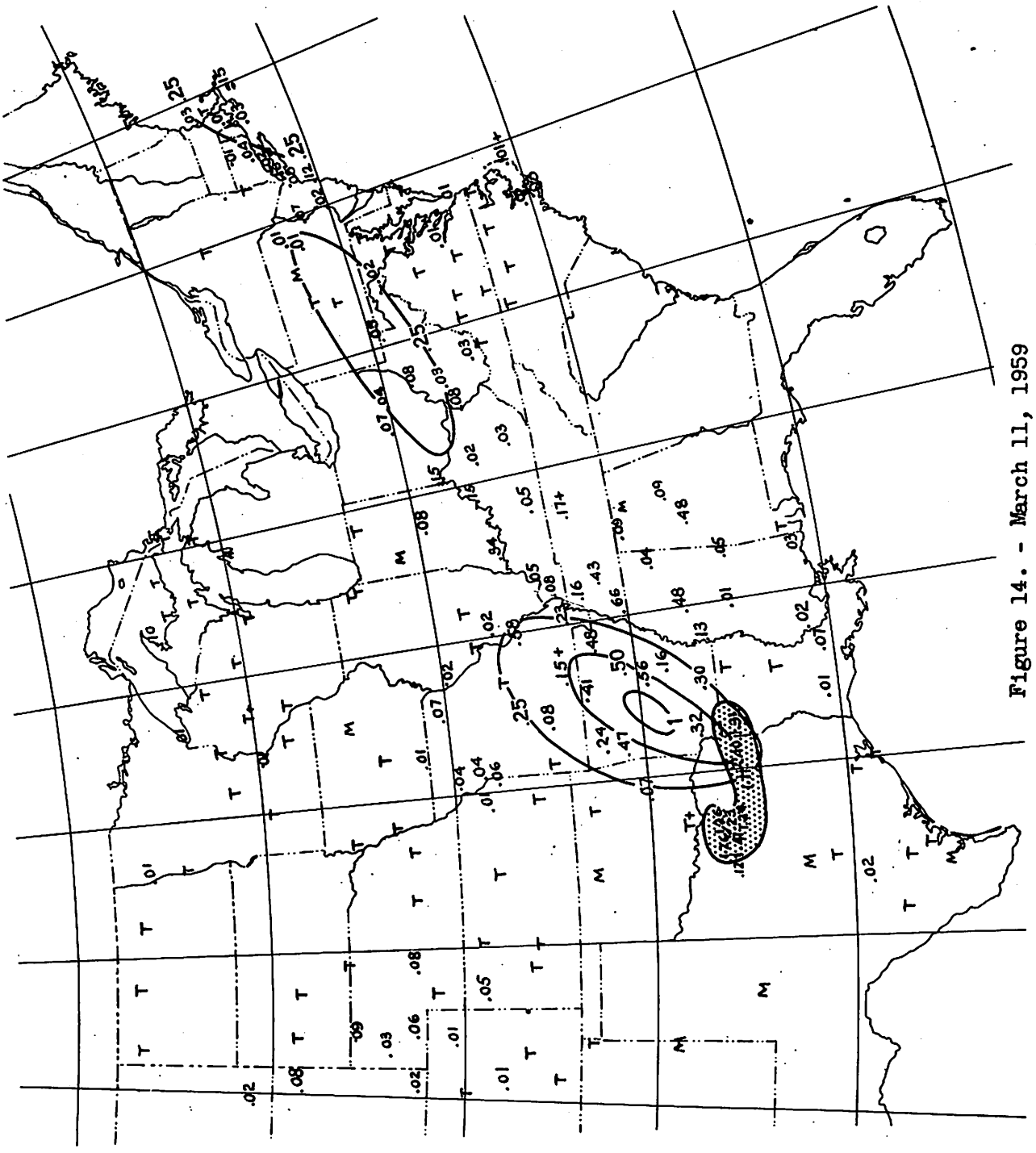

Figure 14. - March 11, 1959

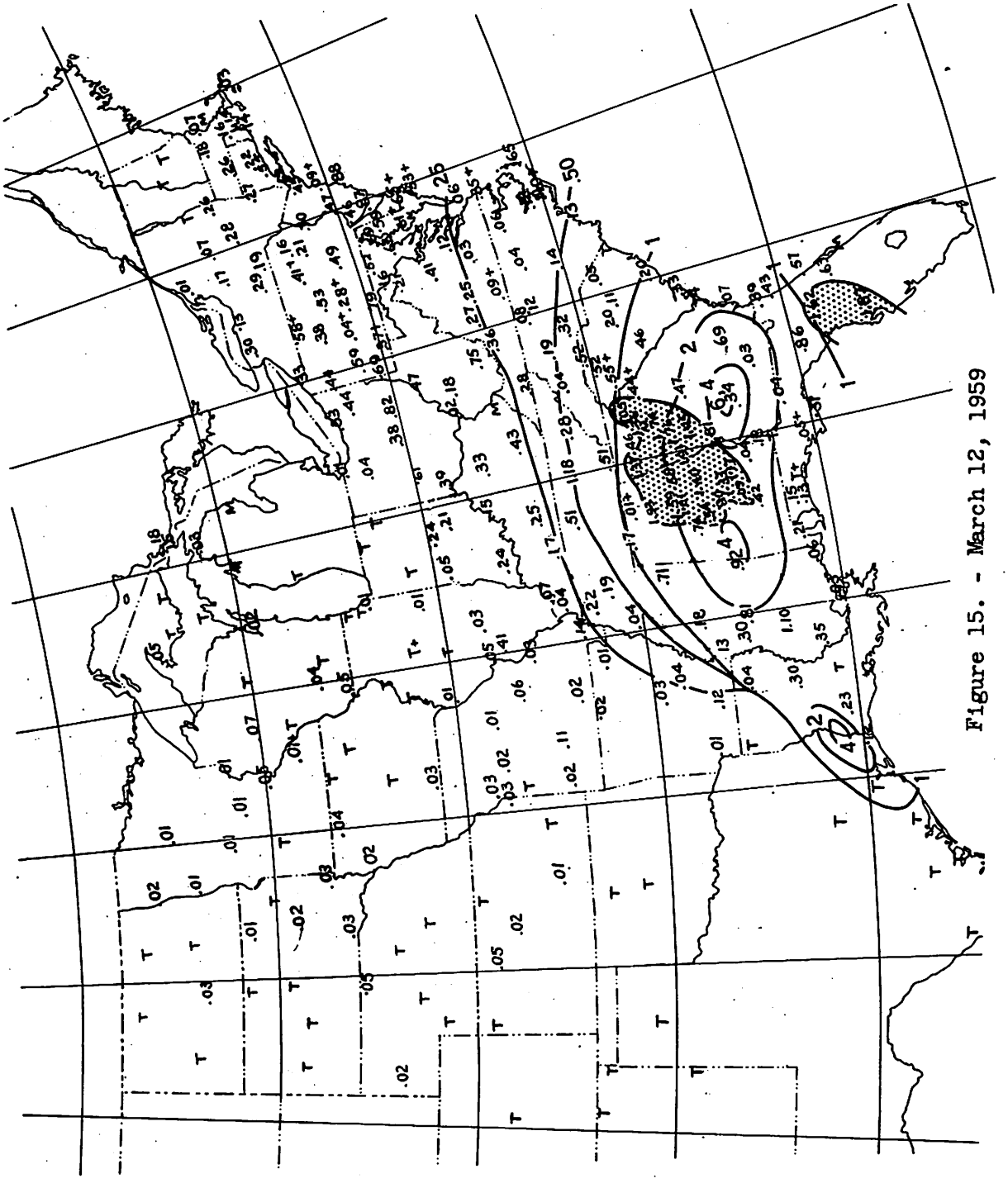

Figure 15. - March 12, 1959

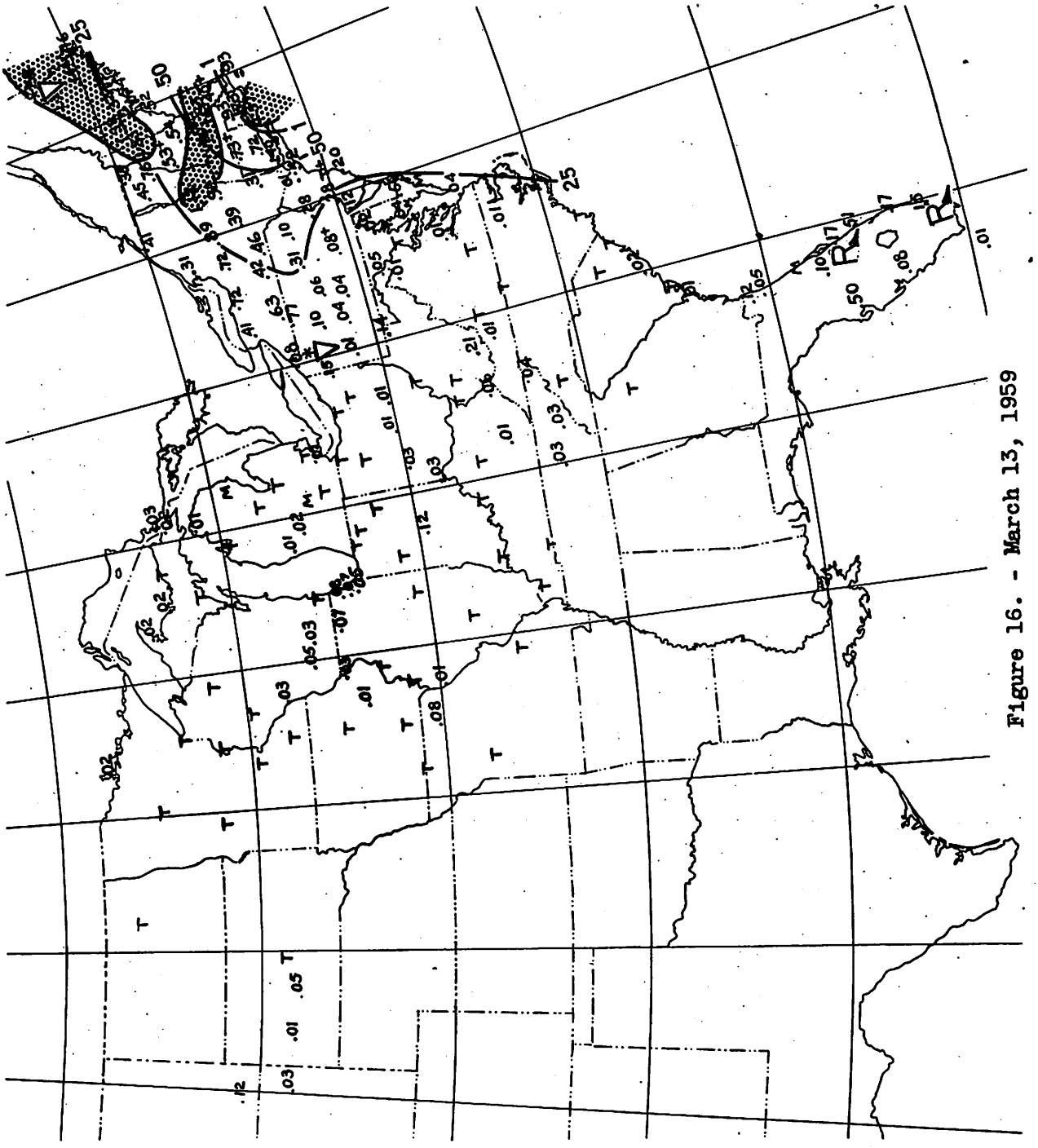

Figure 16. - March 13, 1959

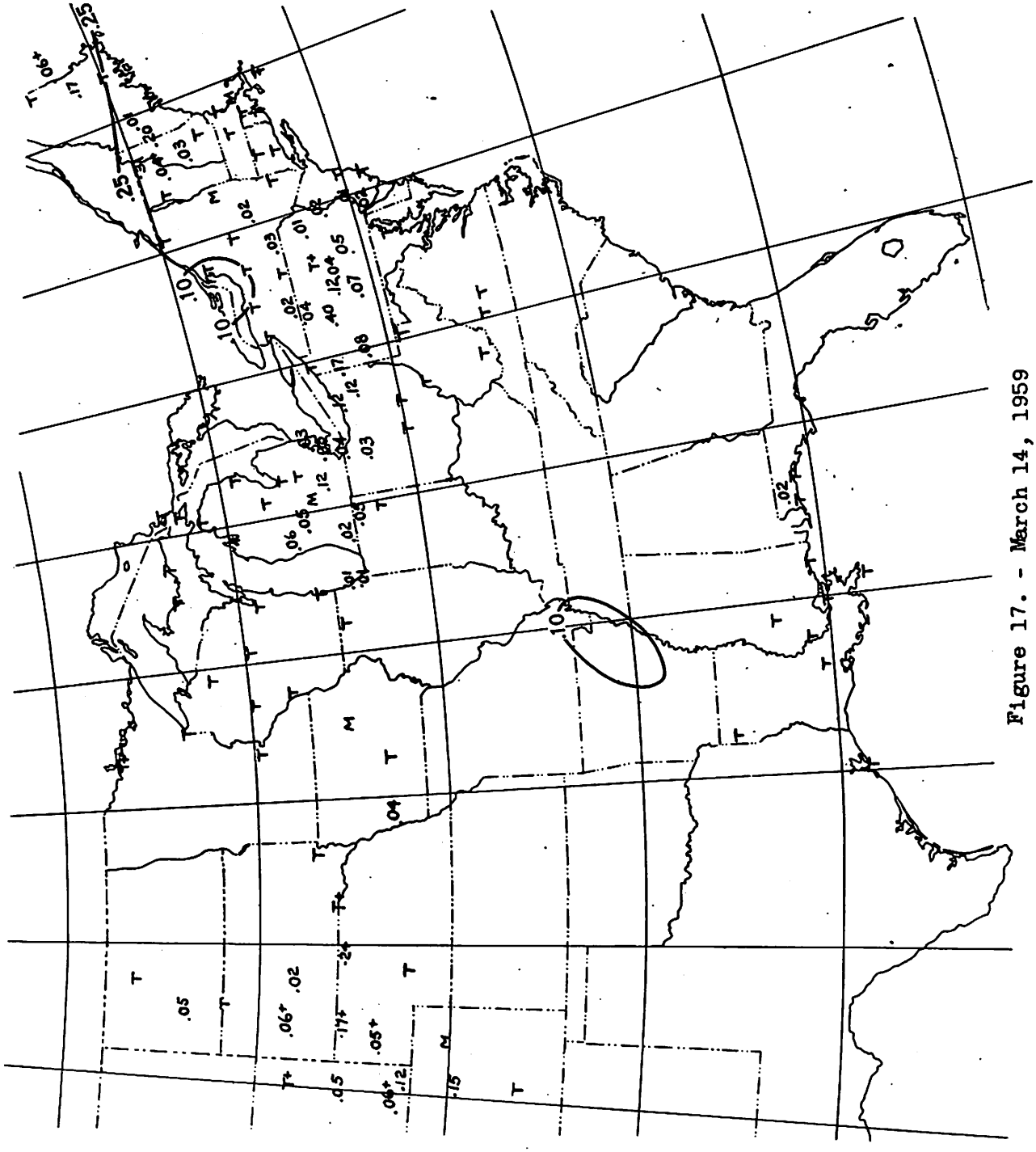

Figure 17. - March 14, 1959

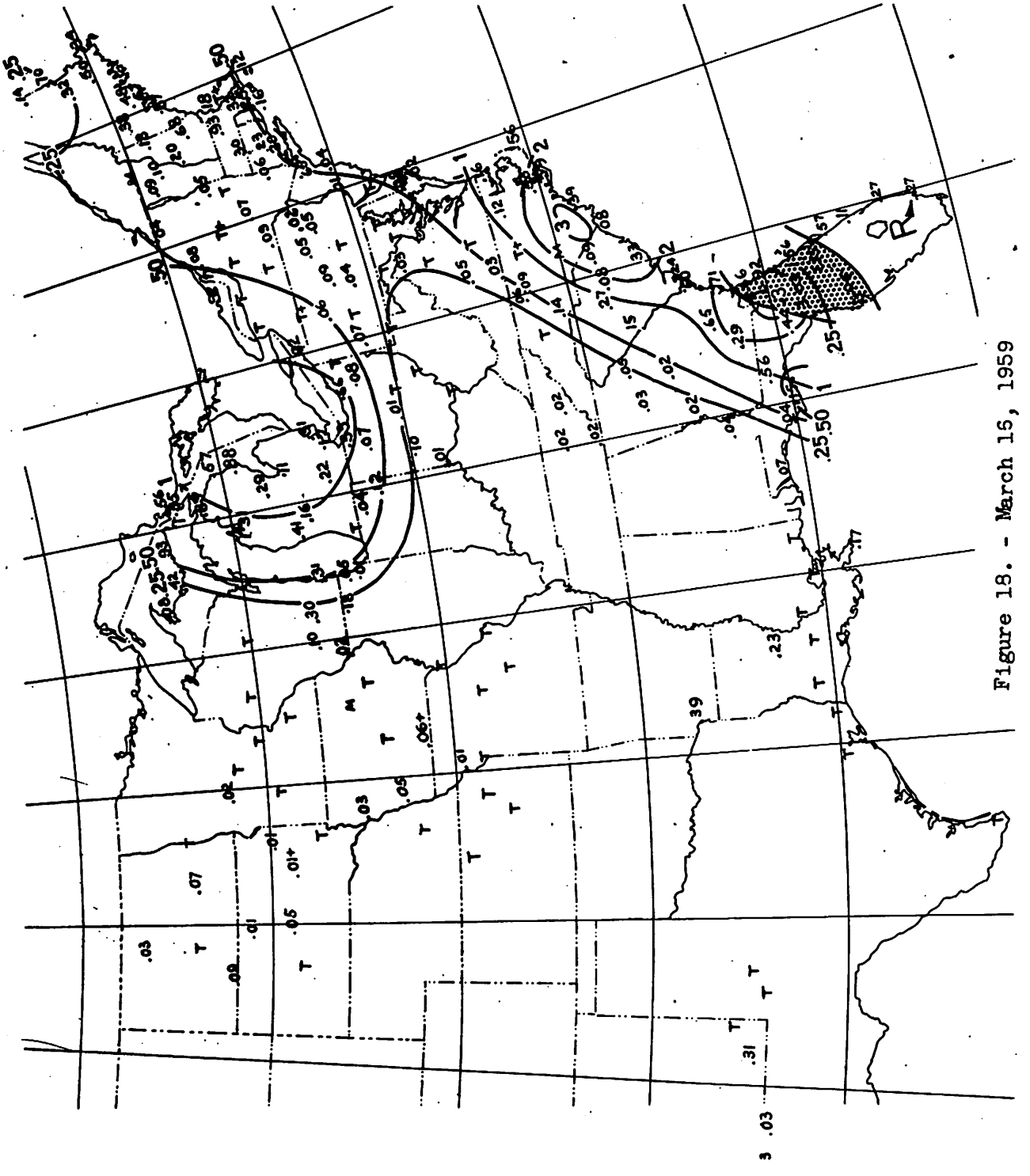

Figure 18. - March 15, 1959

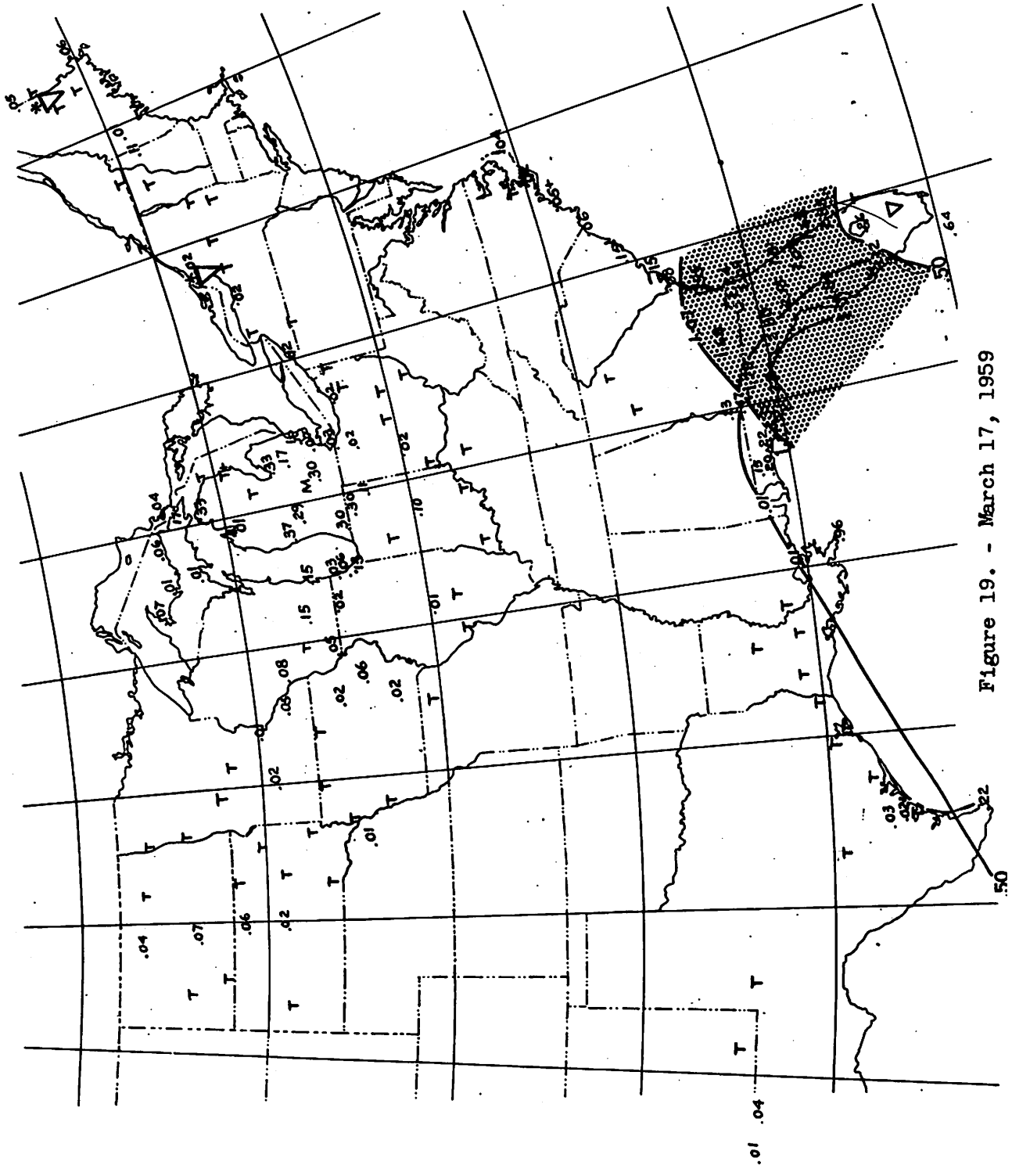

Figure 19. - March 17, 1959

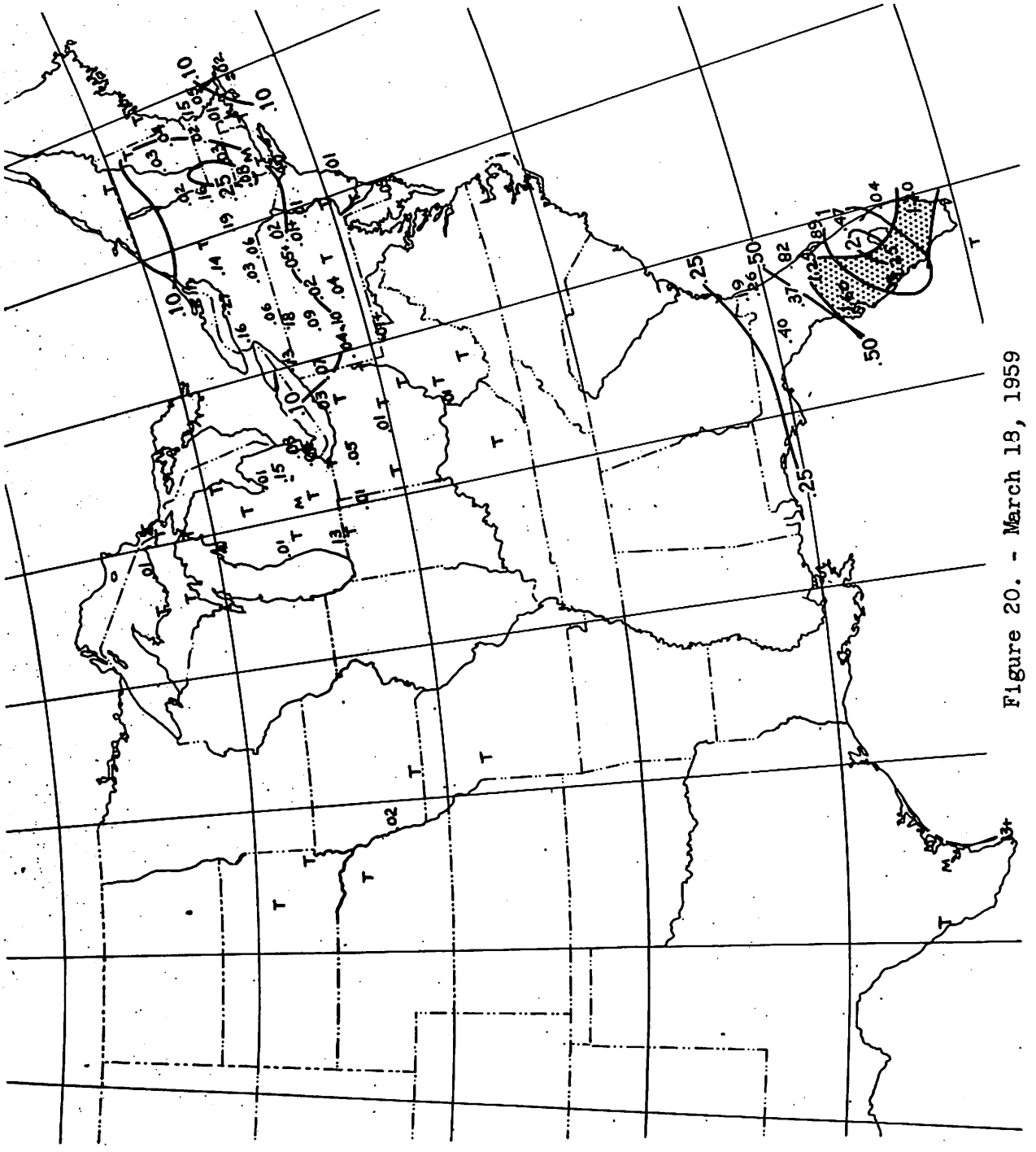

Figure 20. - March 18, 1959

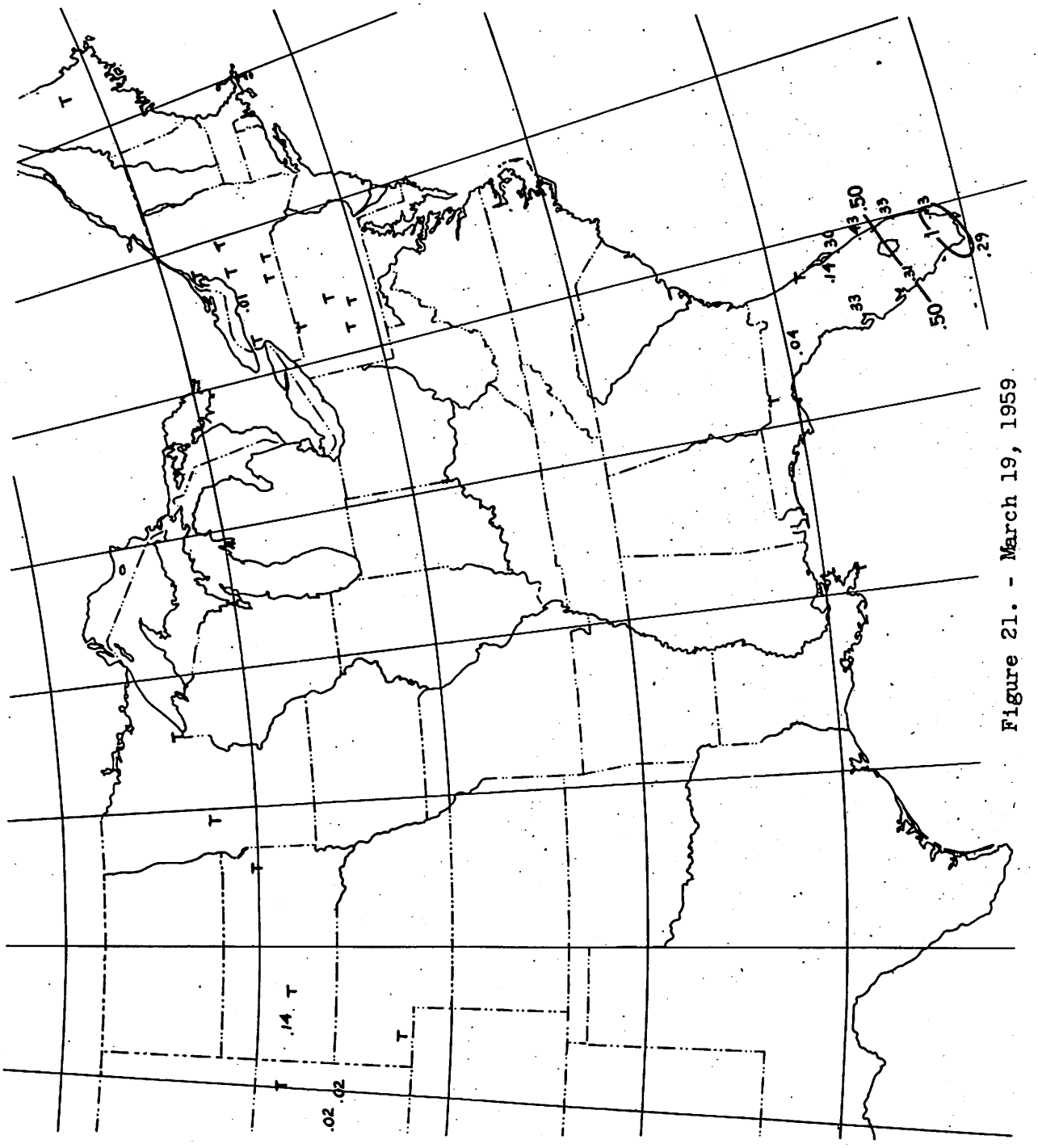


Figure 21. - March 19, 1959

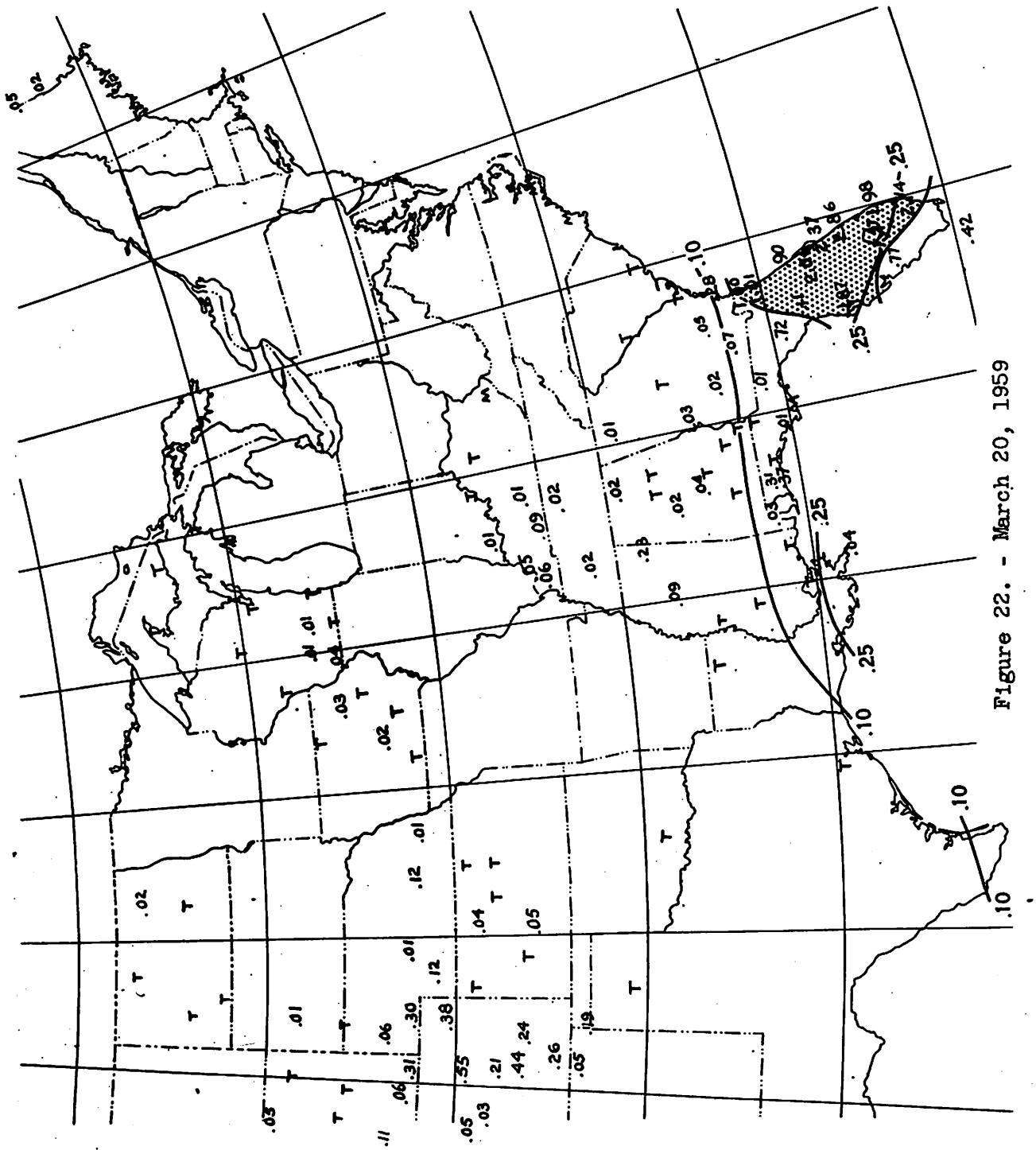

Figure 22. - March 20, 1959

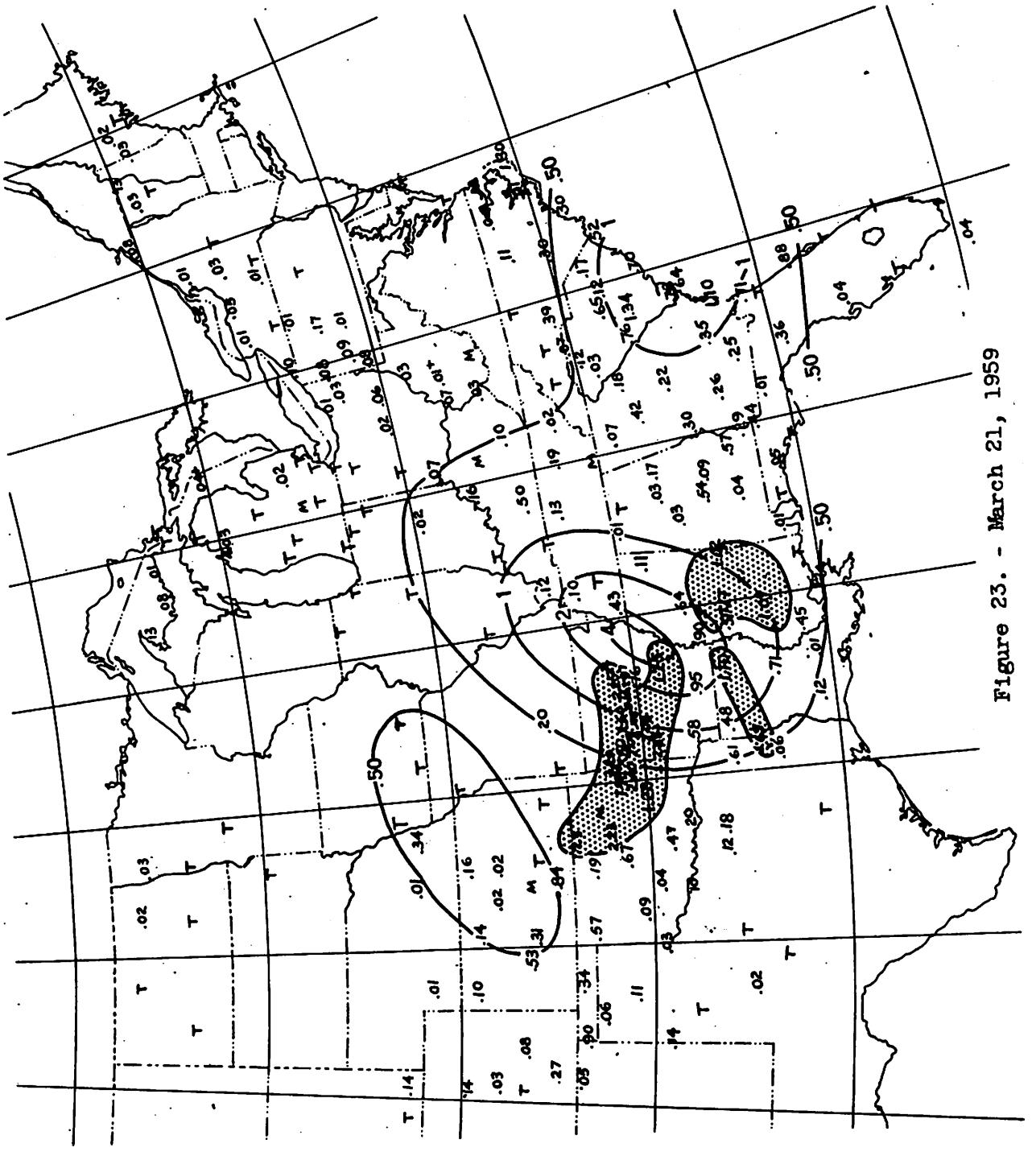

Figure 23. - March 21, 1959

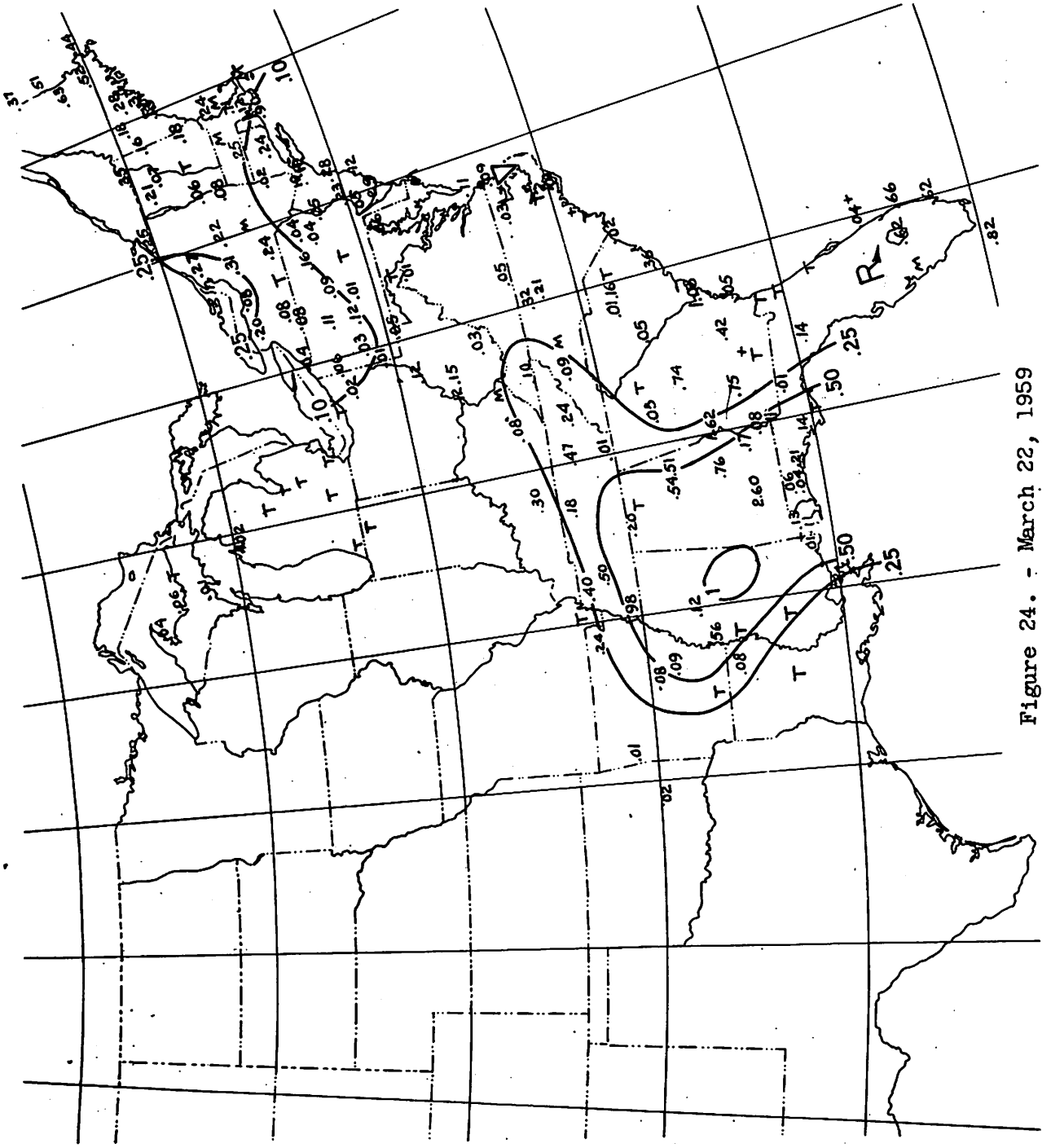

Figure 24. - March 22, 1959

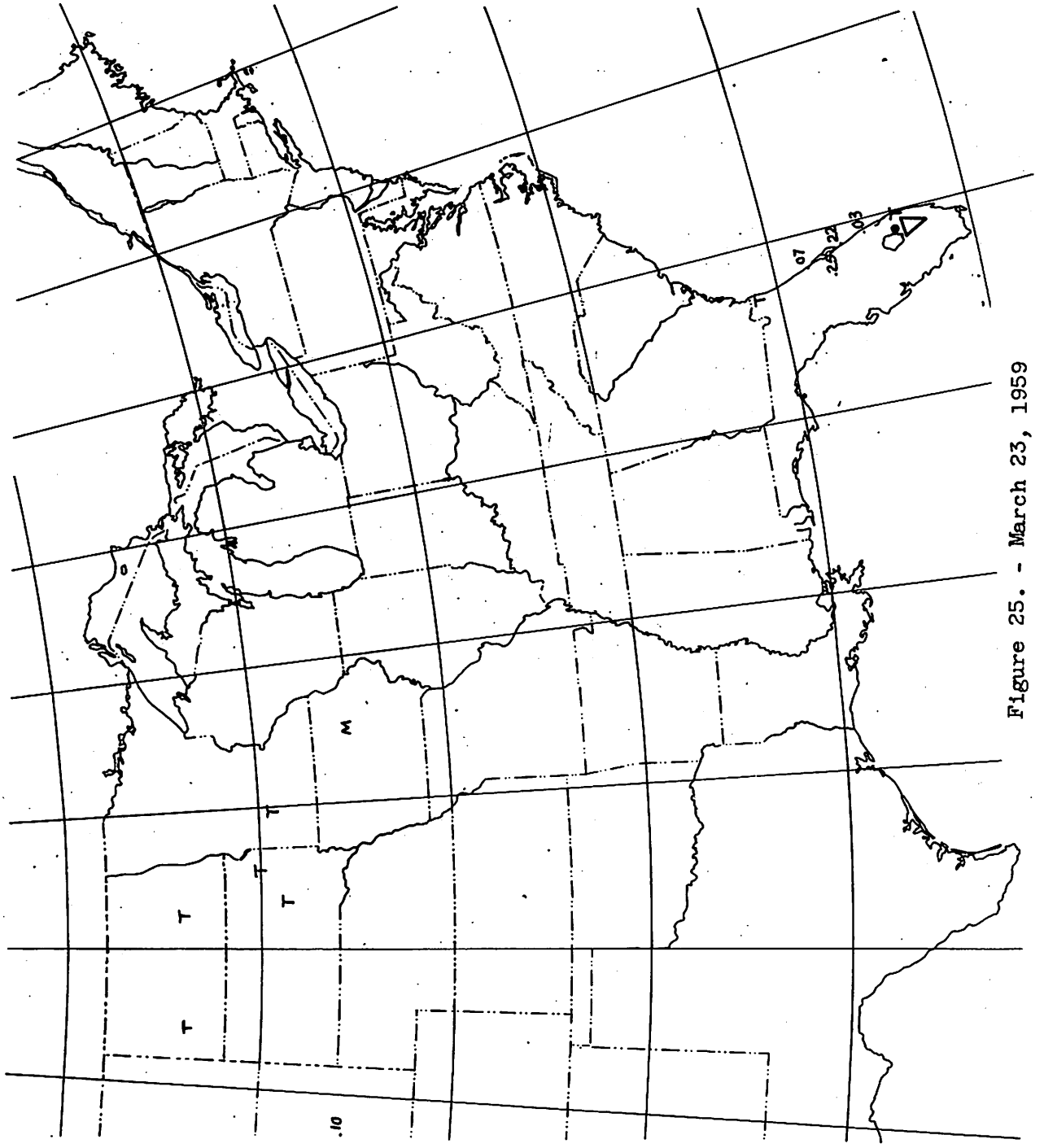


Figure 25. - March 23, 1959

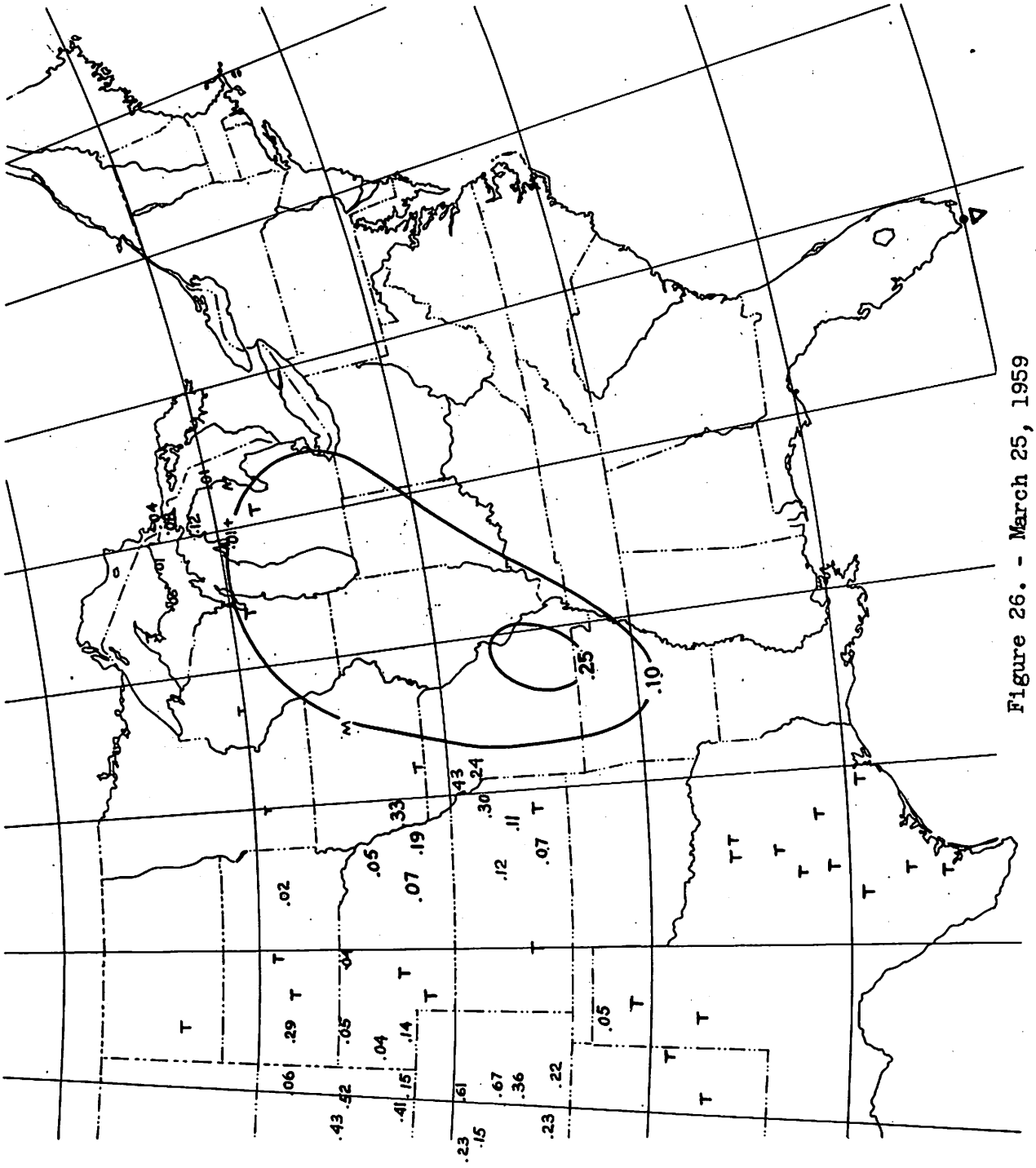

Figure 26. - March 25, 1959

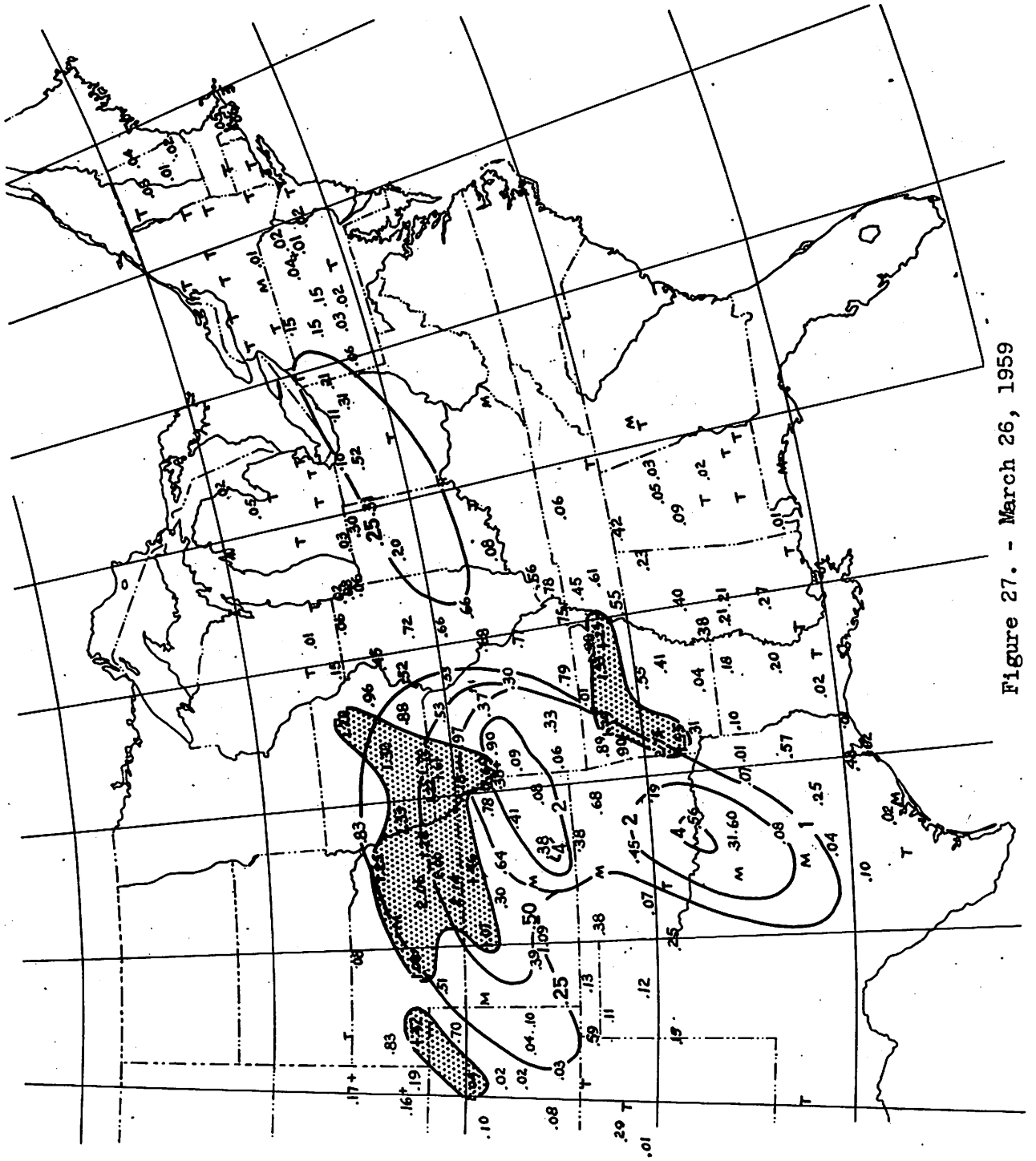

Figure 27. - March 26, 1959

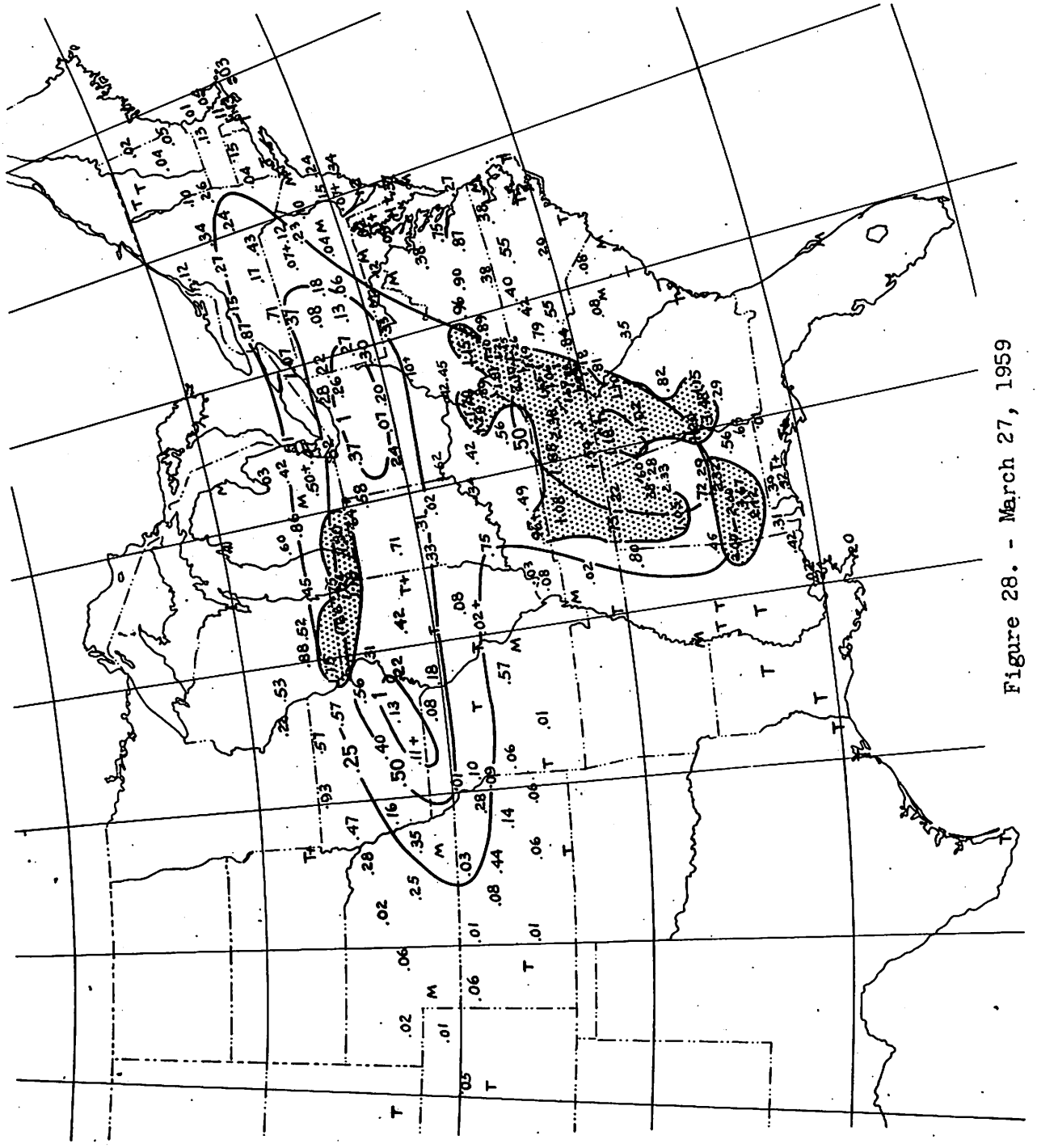

Figure 28. - March 27, 1959

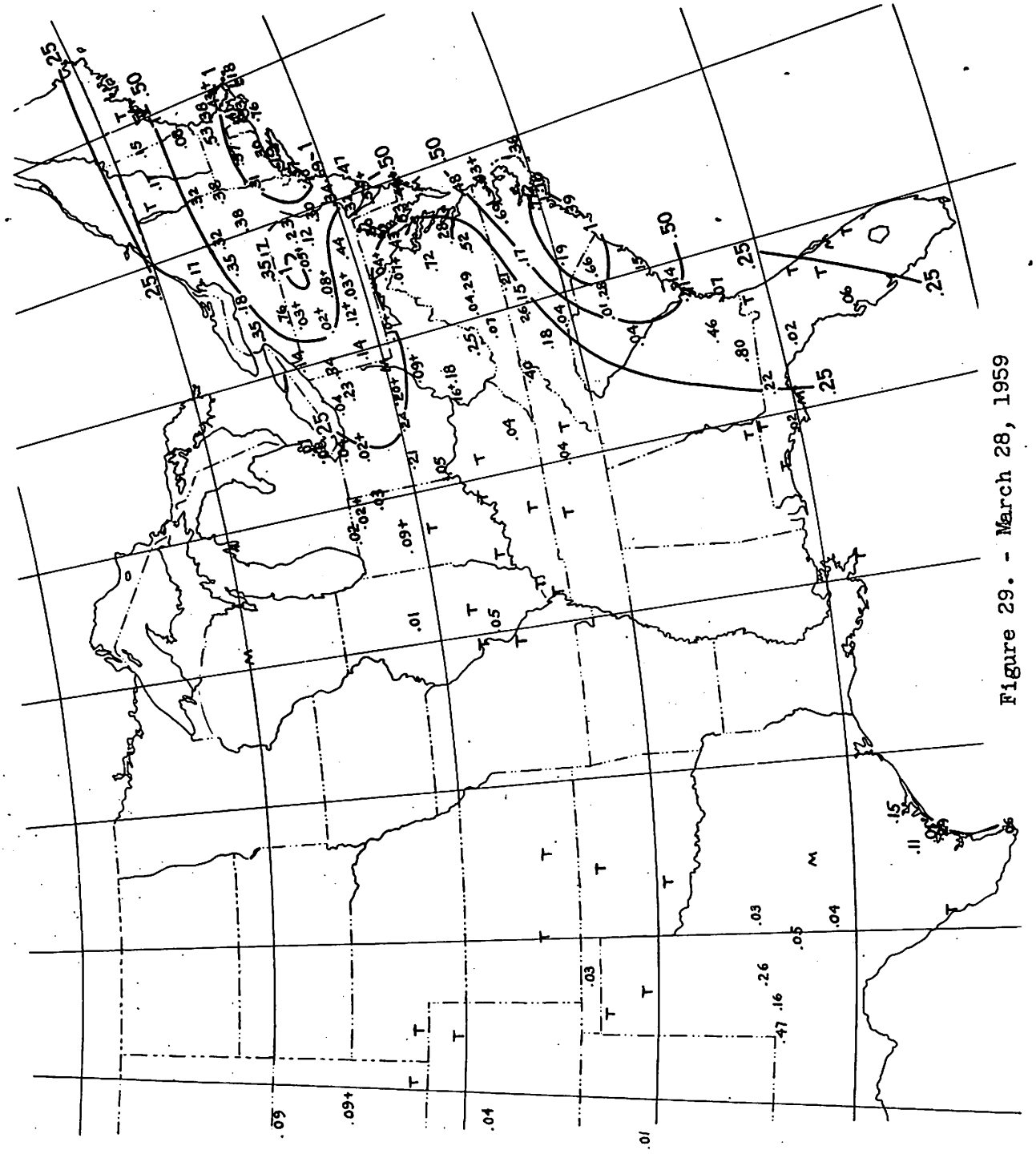

Figure 29. - March 28, 1959

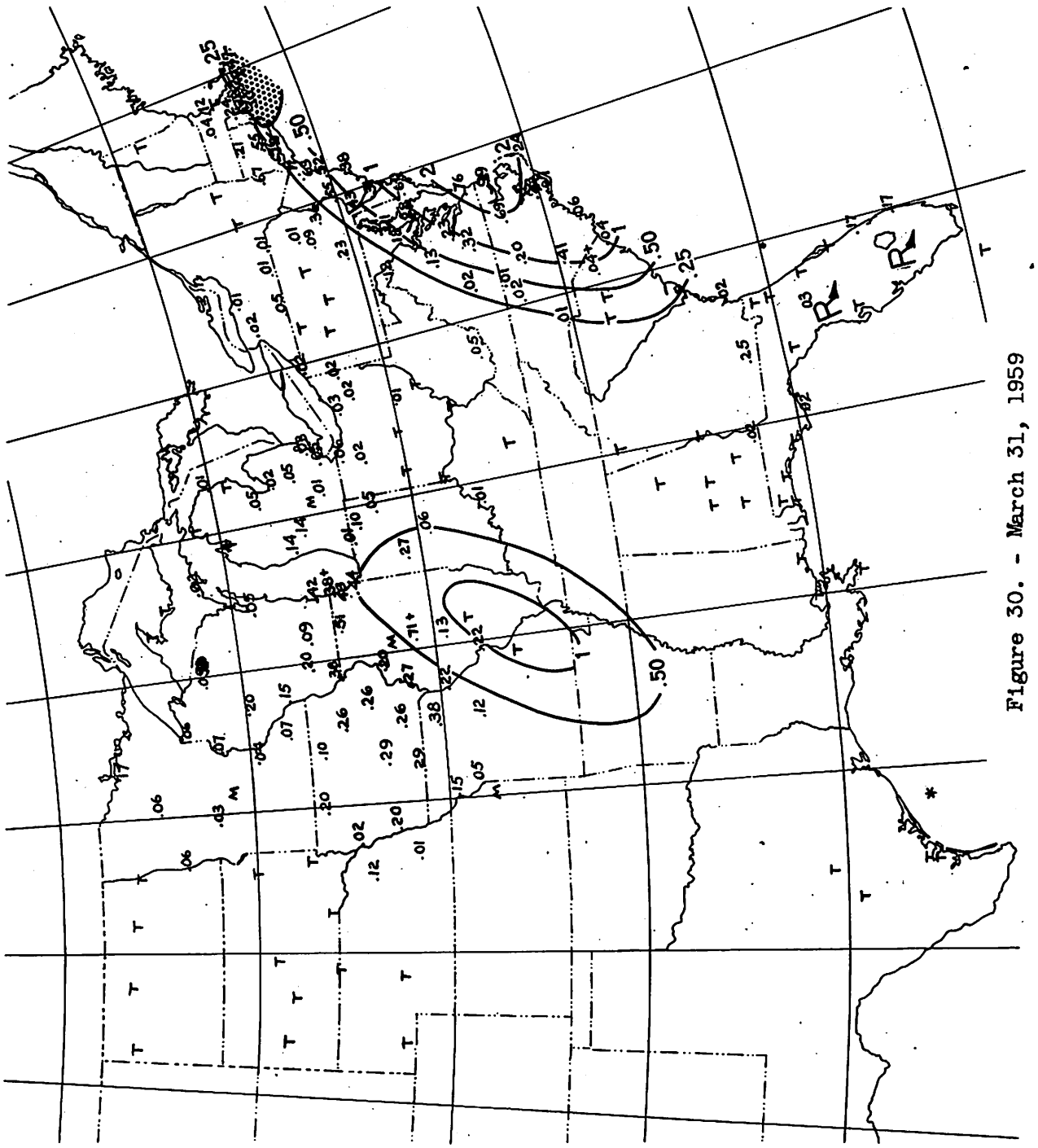

Figure 30. - March 31, 1959

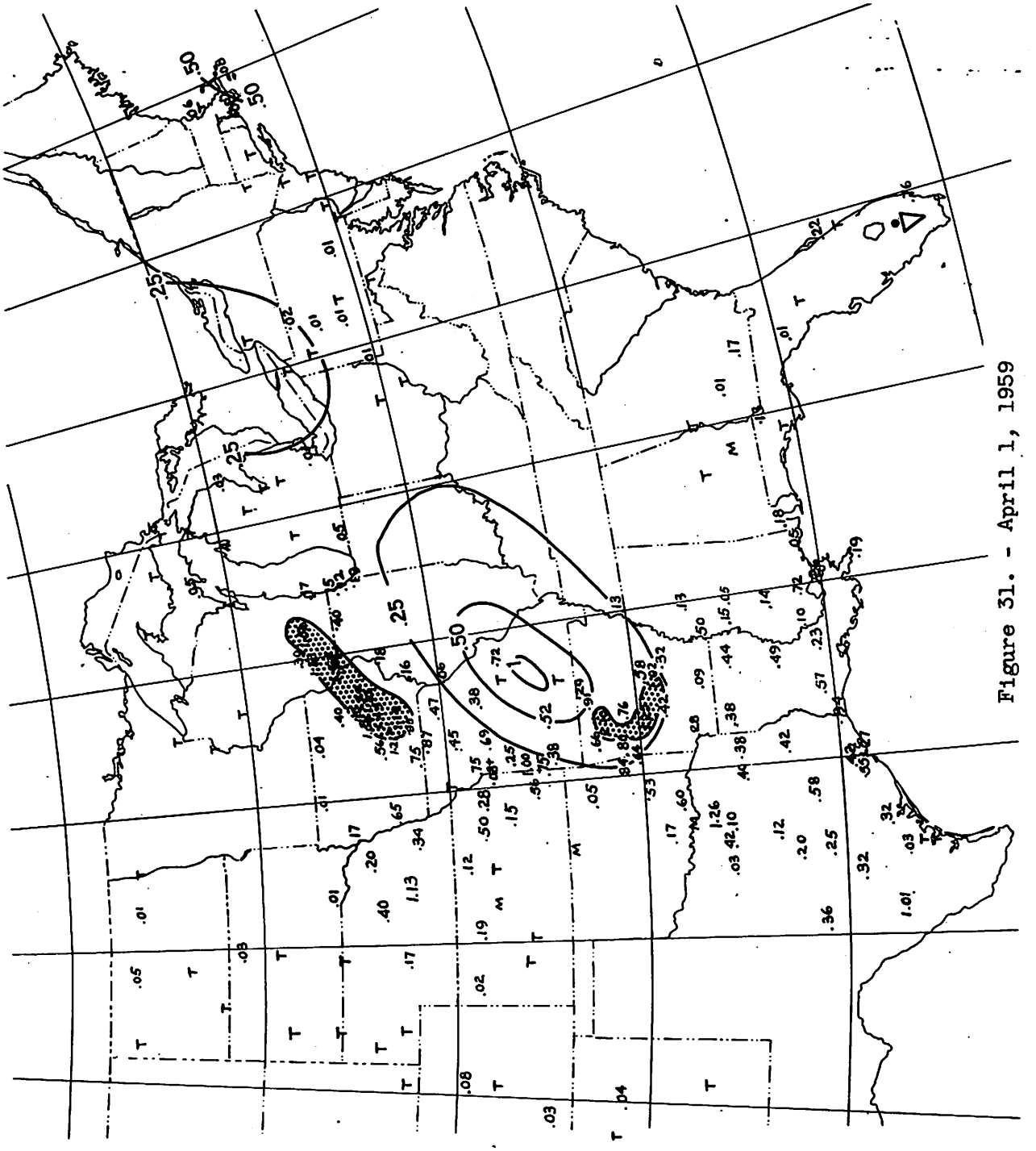

Figure 31. - April 1, 1959

# PART 4. QUANTITATIVE ESTIMATES OF PRECIPITATION IN HURRICANES USING OBSERVED SEA LEVEL PRESSURE MAPS

K. R. Peterson and S. Molansky

Hydrologic Services Division, U. S. Weather Bureau, Washington, D. C.

[Manuscript received February 25, 1959; revised November 13, 1959]

## 1. INTRODUCTION

The most important single factor contributing to the loss of life and property during the passage of most tropical storms is flooding. Although the storm surge plays a major role at the coast, rainfall has a significant effect and is the sole contributor to flooding inland. A knowledge beforehand of the expected rainfall would be of valuable assistance in preparation for a hurricane, such as evacuation of regions expected to be flooded and in the operation of proposed coastal protective works.

Quantitative precipitation forecasts in hurricanes are currently restricted to climatological considerations. Schoner [1] has developed a procedure based upon the climatological means of precipitation over 100-mile squares. Such methods give a useful broad-scale outlook. However, a precipitation forecast based upon dynamic principles and capable of locating the rainfall more closely would eliminate many unnecessary hurricane preparations and would be a decided forecasting improvement.

This paper presents an application of the techniques given in Parts 1-3 to hurricane situations for 3 to 9 hour precipitation forecasts, given a perfect forecast of the surface pressure field. The main purpose is to offer a comparison of these precipitation forecasts with the actual observed precipitation. A secondary purpose is to present a subjective evaluation by the authors of the strengths and weaknesses of the techniques used.

Since the "forecasts" were made about 3 years after the events had taken place, precautions were necessary to minimize any subconscious knowledge of the precipitation pattern. Every effort was made to prevent any consultation of the pattern for several months before the forecast was made. In particular, it is difficult to see how the forecaster could, under the precautions taken, have had any detailed knowledge of the 6-hour breakdown of the amounts since the verifying isohyetal maps were prepared after the forecasts had been completed.

### Hurricanes selected

Five hurricanes were selected for study, namely, Connie 1955, Hazel 1954, Edna 1954, Carol 1954, and Alice 1954 and are discussed in the order given. Forecasts for four of the hurricanes were prepared by the first author. In

order to investigate the possibility of a bias in the application of the techniques, the second author, who was heretofore unfamiliar with the forecasting technique and only received a short briefing, prepared forecasts for hurricane Edna.

Data

The data used in the study consisted of: (1) Sea level pressure maps at 3 hour intervals. Specially prepared maps were used for hurricane Alice and for most of hurricanes Hazel and Connie, while maps prepared at the National Meteorological Center were used for hurricanes Carol and Edna and for the initial forecasts of Hazel and Connie. (2) Wind data obtained from second standard level winds and from available ship winds (increased by 10 percent). (3) Precipitable water data computed from radiosonde observations. (4) Isohyetal maps prepared from Weather Bureau Hourly Precipitation Data. In hurricane Alice, a bucket survey conducted by the Albuquerque District Office of the Corps of Engineers was used to supplement the regular observational network.

## 2. FORECAST PROCEDURE

Hurricane Alice was investigated after it had passed inland and lost its symmetry. In this respect, it was similar to hurricane Diane 1954 and therefore the same forecast techniques as reported in Part 2 were applied. This investigation is, in part, a test of those techniques.

The remaining hurricanes were studied when their pressure patterns were approximately symmetrical. Because of this symmetry, it was difficult and in some cases impossible to locate regions of maximum shear and curvature in the isobars. Therefore, the methods used in Part 2 were not applicable directly and a different technique had to be devised. The following procedure was developed.

Trajectories

Beginning with the map 1-1/2 hours before the forecast period, trajectories were constructed, spaced at 60-n.mi. intervals, 90° azimuth clockwise from the instantaneous hurricane path. Applying the procedures developed by Goodyear [2], trajectories were taken at increments of 1-1/2 hours, using 3-hourly surface maps. Occasionally, because of a strong gradient, it was necessary to take trajectories at 3/4-hour intervals. At the first 60-n.mi. point, the gradient was usually so strong that trajectories had to be computed at 30-minute or 15-minute intervals. Because of the length of time required and because the procedures have been developed with the idea in mind of synoptic application, this first trajectory was omitted in most cases.

Some trajectories were also taken 45°, 60°, 135° azimuth clockwise from the hurricane path. The trajectories begun at 45° and 60° tended to curve rapidly inward toward the hurricane center while those at 135° traveled northward with little indication of convergence. If one direction is chosen, it appears that trajectories started 90° azimuth clockwise from the hurricane path and taken at 60-n.mi. intervals provide the most information concerning the location of convergence regions.

Precipitation area

An inspection of the trajectories will locate the region of convergence, around which is drawn the boundary of the precipitation area. It is assumed that all significant precipitation will fall within this boundary. The boundary is determined somewhat subjectively. Beginning near the hurricane center at initial map time, it passes through the points on the trajectories which are 1-1/2 hours downstream from the starting points. This represents the lower boundary. The upstream and right lateral boundaries set off the trajectories along the line of non-divergence. An inspection of the diagrams will show that this part of the boundary is the least subjective. The left lateral boundary is placed 30 to 60 n.mi. beyond the end points of the 7-1/2 hour trajectories. Since the maximum convergence generally occurred near the end points and since, from observation, the heaviest rainfall in a hurricane does not usually occur at the boundary of the precipitation area, the forecasters felt justified in extending the left boundary as indicated.

Inflow volume

The inflow volume is determined from equation (1) of Part 2. In this case, L is the distance from the hurricane center to the right-hand limit of the precipitation area.

Efficiency

An efficiency of 75 percent has been applied to all cases. See Parts 2 and 3 for further details on this factor.

Isohyets

The isohyets are placed within the precipitation area so that the heaviest precipitation is forecast to occur where the trajectories indicate the greatest convergence. The remaining isohyets are spaced according to an average hurricane isohyet spacing. As a final step, the precipitation volume as represented by the isohyets is checked against the computed precipitation volume.

Hurricane Connie is discussed in detail; the other hurricanes are discussed only briefly but include maps and summaries.

## 3. HURRICANE CONNIE 1955

Hurricane Connie crossed the coast near Morehead City, N.C. at about 1000 EST, August 12, 1955. A track of the pressure center, based upon hourly surface pressure analyses is shown in figure 1. The center moved slowly northward after crossing the coast, but accelerated somewhat and recurved toward the northwest after passing farther inland. During the late evening of the 13th, hurricane Connie passed over Lake Erie into Canada.

Immediately prior to the first forecast from 1200-1800 EST, August 12, hurricane Connie passed inland and was traveling in a general northward direction. Trajectories were taken at 60-n.mi. intervals to the right of the storm path. From the pattern of the trajectories, two 3-inch isohyetal

centers were placed as shown in figure 2. The forecast moisture transport within the designated inflow area was 117,000 mi.$^2$ in. The observed isohyetal map (fig. 3) indicates a good forecast, patternwise, although the 1-inch center in New Jersey and Long Island was not forecast, while only one maximum center occurred, whereas two were forecast. (The southernmost forecast maximum was based partly upon the trajectory pattern and partly upon a subjective drawing of the isohyets near the hurricane center.) The observed precipitation volume, within the 0.5-inch isohyet was 85,000 mi.$^2$ in.

During the second forecast from 1800-2400 EST, the hurricane was filling slowly as it traveled northward through eastern North Carolina and Virginia. Trajectories were taken in two directions from the storm path, one set 90° to the right and a second set 60° to the right of the storm path. Both sets of trajectories were used to delineate the inflow area and to place the isohyets (figs. 4a and 4b). The forecast precipitation volume was 121,000 mi.$^2$in. The two 2-inch centers were positioned where the trajectories indicated the greatest convergence. The 1-inch isohyet was placed around these centers and extended southward to account for the rainfall expected in the vicinity of the hurricane center. The precipitation volume was made equal to the computed (adjusted) moisture transport.

The verifying isohyetal map (fig. 5) shows that the forecast was good. The predicted 1-inch isohyet covered a somewhat larger area and was forecast about 40 n.mi. too far south. Only one 2-inch isohyet occurred and this was about half-way between the forecast 2-inch isohyets. One-inch amounts fell in extreme southeastern New York State but were not forecast. The observed precipitation volume within the 0.5-inch isohyet was 63,000 mi.$^2$in.

During the third forecast from 0000-0600 EST, August 13, hurricane Connie filled slowly but still maintained much of its intensity as it began to recurve north-northwestward up Chesapeake Bay. Trajectories were taken at 60-n. mi. intervals 90° to the right of the storm path. These trajectories indicated a region of maximum convergence centered over northeastern Maryland and southeastern Pennsylvania (fig. 6). The adjusted moisture transport was 116,000 mi.$^2$ in., slightly less than for the previous 6-hour forecast. The inflow area was also less, being only 69,200 mi.$^2$, with an average precipitation of 1.7 inches.

The verifying isohyetal map (fig. 7) indicates that the 1-inch isohyet was well placed but that only one 3-inch amount was observed. The observed volume of precipitation within the 0.5-inch line was 86,000 mi.$^2$in. The average rainfall within this isohyet was 1.4 in. Both of these values are smaller than the forecast values.

During the fourth and final forecast period from 0600-1200 EST, August 13, hurricane Connie filled considerably, but still maintained much of its circulation and symmetry. The center passed through Maryland and central Pennsylvania, recurving slowly toward the northwest. As before, trajectories were taken at 60-n.mi. intervals to the right of the hurricane path. These trajectories indicated a somewhat less organized pattern of convergence than had been encountered previously. On this basis, three maximum isohyetal centers were placed as shown in figure 8. The adjusted moisture transport was 98,500 mi.$^2$in., again, slightly less than the previous 6-hour forecast. The average forecast rainfall over the inflow area was 1.2 inches.

The verifying isohyetal map (fig. 9) indicates that the larger 1-inch isohyet was generally well placed. The 2-inch isohyet between Pennsylvania and New Jersey verified well, except for some heavier rain to the north. The 2-inch isohyets in southwestern Pennsylvania and over Lake Erie were overforecast; but amounts over 1 inch occurred in both regions. The observed precipitation volume within the 0.5-inch isohyet was 83,300 mi.$^2$in. and the average rainfall over the area covered by the same isohyet was 1.2 inches.

## 4. HURRICANE CAROL 1954

Hurricane Carol was notable for its unexpected acceleration over water after passing 15 miles to the east of Hatteras, N.C. The storm passed over the eastern tip of Long Island Sound and crossed the New England coast near the Connecticut-Rhode Island border at 1000 EST, August 31, 1954. Although the total storm rainfall was not unusually heavy (5-6-in. amounts in southeastern Connecticut and central Massachusetts) most of the rainfall at a particular station occurred in short intervals of time (4-6 hours), thereby causing local flooding. Hurricane Carol was chosen for study partly to see if the forecasting technique could predict these short bursts of rainfall.

Precipitation forecasts for hurricane Carol were prepared for three 6-hour periods beginning 0000 EST, 0600 EST, and 1200 EST, August 31, 1954. The forecasts and verifications are shown in figures 10-15. The inflow and precipitation volumes are summarized in table 1.

## 5. HURRICANE EDNA 1954

Within 11 days after hurricane Carol, the northeastern United States was subjected to hurricane Edna which followed a track and acceleration of forward movement somewhat similar to that of its predecessor. While Edna penetrated the United States mainland only briefly, first while crossing Cape Cod and finally a short distance east of Eastport, Maine, substantial rainfall was recorded from the Delmarva peninsula northeastward along and to the left of the track.

Precipitation forecasts for hurricane Edna were prepared for three 6-hour periods beginning 0000 EST, 0600 EST, and 1200 EST, September 11, 1954. The forecasts and verifications are shown in figures 16-21. The inflow and precipitation volumes are summarized in table 1.

## 6. HURRICANE HAZEL 1954

Hurricane Hazel crossed the coast near Wilmington, N.C. during mid-morning of October 15, 1954. The center moved at 45 knots during the late morning and afternoon as it passed through the Carolinas and Virginia in a generally north-northeast direction. As the storm approached and passed Washington, D. C. its forward speed increased to 50-60 knots. By 1930 EST the initial center had filled over central Pennsylvania and a second center formed about 100 n.mi. to the north-northwest of the first center. The second center moved off into Canada on the morning of the 16th.

Three forecasts were made for hurricane Hazel, the first two being 6-hour forecasts, 0600-1200 EST and 1200-1800 EST, October 15, 1954. The third

forecast was for the 3 hours 1800-2100 EST. The first forecast was prepared using the procedure for a symmetrical hurricane. Trajectories were taken at 45°, 90°, and 135° azimuth clockwise from the hurricane path. By the time of the second forecast, the hurricane had become definitely asymmetrical and the remaining forecasts were prepared similar to the method used with Diane 1955 (Part 3). These forecasts along with the verifications are shown in figures 22-27. The inflow and precipitation volumes are summarized in table 1.

## 7. HURRICANE ALICE 1954

Hurricane Alice crossed the coast south of Brownsville, Tex. on the morning of June 25, 1954. The center slowly weakened and had dissipated by the evening of June 26, after having closely followed the Rio Grande River during most of its overland travel.

The rainfall associated with hurricane Alice was notable in that the heavier precipitation occurred about 300 n.mi. inland long after the storm had crossed the coast, and that this rainfall reintensified during the 26th and 27th and to a lesser extent on the 28th, resulting in serious flooding along the Rio Grande.

Quantitative precipitation forecasts were prepared at 6-hour intervals from 0600-1200 CST June 26, 1954 through 1800-2400 CST June 27, 1954 and are shown with observed precipitation maps and sea level pressure maps in figures 28-48. Dynamic trajectories were initiated 1-1/2 hours before the beginning of the forecast period and were taken at 1-1/2 hour intervals. Table 2 summarizes the inflow and precipitation volumes for each period.

## 8. SUMMARY

Quantitaive precipitation forecasts have been made for five hurricanes. Four of the hurricanes had circular symmetry of the isobars for part or all of the forecast periods, thereby making it difficult to locate regions of maximum shear and curvature. A technique has been developed to prepare precipitation forecasts for such storms. Considering the fact that each forecast was made without a knowledge of the verifying isohyetal map, the forecasts are believed to show some promise. The major precipitation almost always occurred within the forecast precipitation boundary. Some lighter rain fell outside of the boundary and perhaps could have been forecast if more trajectories had been constructed. Table 1 lists for these four hurricanes (1) the factors which determine the precipitation volume, (2) the forecast precipitation volume, (3) the observed precipitation volume, and (4) the forecast and observed mean rainfall amounts. It is apparent that the computed and observed precipitation volumes show considerable variance for many of the forecasts, while the mean rainfall amounts are generally much closer. The probable reason for this is that on the occasions when the precipitation volume was over- or under-forecast, the forecast precipitation area was also over- or under-forecast by the same amount. This over- or under-forecasting could be due to a number of causes, namely:

1. Lack of data - an insufficient number of wind, pressure, and radiosonde observations over the ocean.

2. Data inaccuracies in ship winds and pressures which lead to errors in trajectories because of incorrect initial winds and geostrophic winds.

3. Computational errors. Aside from errors due to interpolation, the following error sources are important:

   (a) The 10 percent factor introduced into the ship winds as an approximation of the second standard level wind, and

   (b) Too long a time increment in constructing trajectories in cases where the geostrophic wind is not constant.

4. Taking only one baseline (90° to the right of the hurricane path) at one initial time (3 hours before forecast time).

5. Trajectory errors - assumption of no friction in trajectory construction and the difficulty of determining trajectories near the hurricane center.

6. Neglecting topography.

7. Insufficient knowledge of the efficiency of the precipitation process.

In general, of these sources of error, perhaps the most important is the error due to the efficiency. A study is planned to determine the efficiency in an objective manner. In day-to-day forecasting it would be necessary to prepare 3-hour, 6-hour, and 9-hour prognostic surface charts. Another study has been initiated to minimize this problem.

Also listed in table 1 are the means, the ranges, the standard deviations, and the coefficients of variation of the factors making up the forecast precipitation volume. Hurricane Alice 1954 has been omitted from these computations since it was not a symmetrical hurricane during the time forecasts were made. Also, the last forecast for Hazel has been omitted because of asymmetry. The last row in the table shows that the normal wind, $V_n$, has the greatest variation, while the precipitable water, W, has the least.

Hurricane Alice lost most of its isobar symmetry after passing inland and thereafter forecasts were prepared in the same manner as for the storms presented in Part 2. The inflow and precipitation volumes and related quantities for each forecast are summarized in table 2. It is believed that the results of these forecasts, made without a knowledge of the verifying isohyetal maps, help to substantiate the procedure set forth in Part 2.

The following general comments are applicable to the forecasts for hurricane Alice.

1. Center of maximum precipitation forecast too far west (by about 10-20 miles).

2. Area of central isohyets in good agreement.

3. Outer isohyets (especially 0.5 in.) over-forecast.

4. Forecast precipitation volume over-forecast by about 15-35 percent.

Provided that a surface map in the vicinity of the hurricane could be rapidly prepared and that reliable surface prognostic maps were available, the authors believe that the forecasting technique could be applied in sufficient time to be of synoptic value, although revision of the method for application to an initial map 4-1/2 or 5 hours before the beginning of the forecast would provide more time for careful consideration.

## REFERENCES

1. R. W. Schoner, "Frequency and Distribution of Areal Rainfall Averages Associated with Tropical Storms Entering the Coast of the United States (Texas to Maine)," Weather Bureau Manuscript, July 1957.
2. H. V. Goodyear, "A Graphical Method for Computing Horizontal Trajectories in the Atmosphere," Monthly Weather Review, vol. 87, No. 5, May 1959, pp. 183-195.

Table 1. - Summary of the parameters, inflow volume, and precipitation volume for the four symmetrical hurricanes studied

| Hurricane | Time (EST) | Date | L | θ | $\overline{V}_n$ | W | $I_v \times 10^{-3}$ | $P_v \times 10^{-3}$ | $\overline{I}$ | $\overline{P}$ |
|---|---|---|---|---|---|---|---|---|---|---|
| Hazel 1954 | 06-12 | Oct. 15 | 260 | 17 | 56 | 1.9 | 120 | 175 | 1.3 | 1.7 |
| | 12-18 | | 218 | 10 | 55 | 1.8 | 85 | 165 | 2.0 | 1.1 |
| Connie 1955 | 12-18 | Aug. 12 | 260 | 0 | 50 | 2.0 | 117 | 85 | 1.5 | 1.6 |
| | 18-24 | | 306 | 14 | 45 | 2.0 | 121 | 63 | 1.0 | 1.4 |
| | 00-06 | Aug. 13 | 318 | 20 | 43 | 2.0 | 116 | 86 | 1.7 | 1.4 |
| | 06-12 | | 326 | 12 | 38 | 1.8 | 99 | 83 | 1.2 | 1.2 |
| Carol 1954 | 00-06 | Aug. 30 | 269 | 5 | 42 | 2.0 | 26 | 24 | 1.0* | 1.1* |
| | 06-12 | | 269 | 17 | 38 | 2.0 | 52 | 67 | 1.8* | 1.8* |
| | 12-18 | | 276 | 11 | 40 | 1.8 | 61 | 44 | 1.7* | 1.6* |
| Edna 1954 | 00-06 | Sept. 11 | 267 | 22 | 43 | 2.1 | 22 | 28 | 2.1* | 2.1* |
| | 06-12 | | 270 | 16 | 48 | 2.1 | 34 | 58 | 2.3* | 2.0* |
| | 12-18 | | 330 | 11 | 43 | 1.7 | 29 | 83 | 2.0* | 2.0* |
| Mean | | | 281 | | 45 | 1.9 | | | | |
| Range | | | 112 | | 18 | 0.4 | | | | |
| Standard Deviation | | | 33 | | 6.0 | 0.13 | | | | |
| Coefficient of Variation | | | 0.12 | | 0.13 | 0.07 | | | | |

L = Distance (n.mi.) from hurricane center to lateral convergence boundary 90° azimuth clockwise from hurricane path.

θ = Angle (in degrees) which $\overline{V}_n$ makes with L.

$\overline{V}_n$ = Mean wind (kt.) along L.

W = Mean precipitable water (in.) over inflow volume.

$I_v = 0.75L\overline{V}_n \cos\theta W_p t$ Adjusted forecast inflow volume ($mi.^2 in.$) for 6 hours. (Includes 75 percent efficiency factor.)

$P_v$ = Observed precipitation volume ($mi.^2 in.$) for 6 hours within 0.5-inch isohyet.

$\overline{I}$ = Forecast mean precipitation (in.).

$\overline{P}$ = Observed mean precipitation (in.)

* = Mean value within 1-inch isohyet; other values are means within 0.5-inch line.

Table 2. - Summary of the parameters, inflow volume, and precipitation volume for hurricane Alice, 1954

| Time (CST) | Date | L | $\overline{V}_n$ | W | $I_v \times 10^{-3}$ | $P_v \times 10^{-3}$ | $\overline{I}$ | $\overline{P}$ |
|---|---|---|---|---|---|---|---|---|
| 06-12 | June 26 | 60 | 37 | 2.1 | 210 | 108 | 1.1 | 0.8 |
| 12-18 | | 70 | 32 | 2.0 | 202 | 158 | 1.2 | 1.4 |
| 18-24 | | 97 | 35 | 2.0 | 216 | 195 | 1.4 | 0.9 |
| 00-06 | June 27 | 122 | 38 | 2.0 | 264 | 288 | 1.6 | 1.3 |
| 06-12 | | 90 | 32 | 1.8 | 256 | 190 | 0.9 | 0.6 |
| 12-18 | | 67 | 30 | 1.6 | 156 | 162 | 1.0 | 0.6 |
| 18-24 | | 75 | 30 | 1.6 | 176 | 143 | 0.9 | 0.9 |

$L$ = Length (n.mi.) of upstream inflow boundary

$\overline{V}_n$ = Mean wind (kt.) along L

$W$ = Mean precipitable water (in.) over inflow volume

$I_v$ = $0.75\ L\ \overline{V}_n W_p t$ Adjusted forecast inflow volume ($mi.^2 in.$) for 6 hours. (Includes 75 percent efficiency factor.)

$P_v$ = Observed 6-hour precipitation volume ($mi.^2 in.$)

$\overline{I}$ = Forecast mean precipitation (in.).

$\overline{P}$ = Observed mean precipitation (in.).

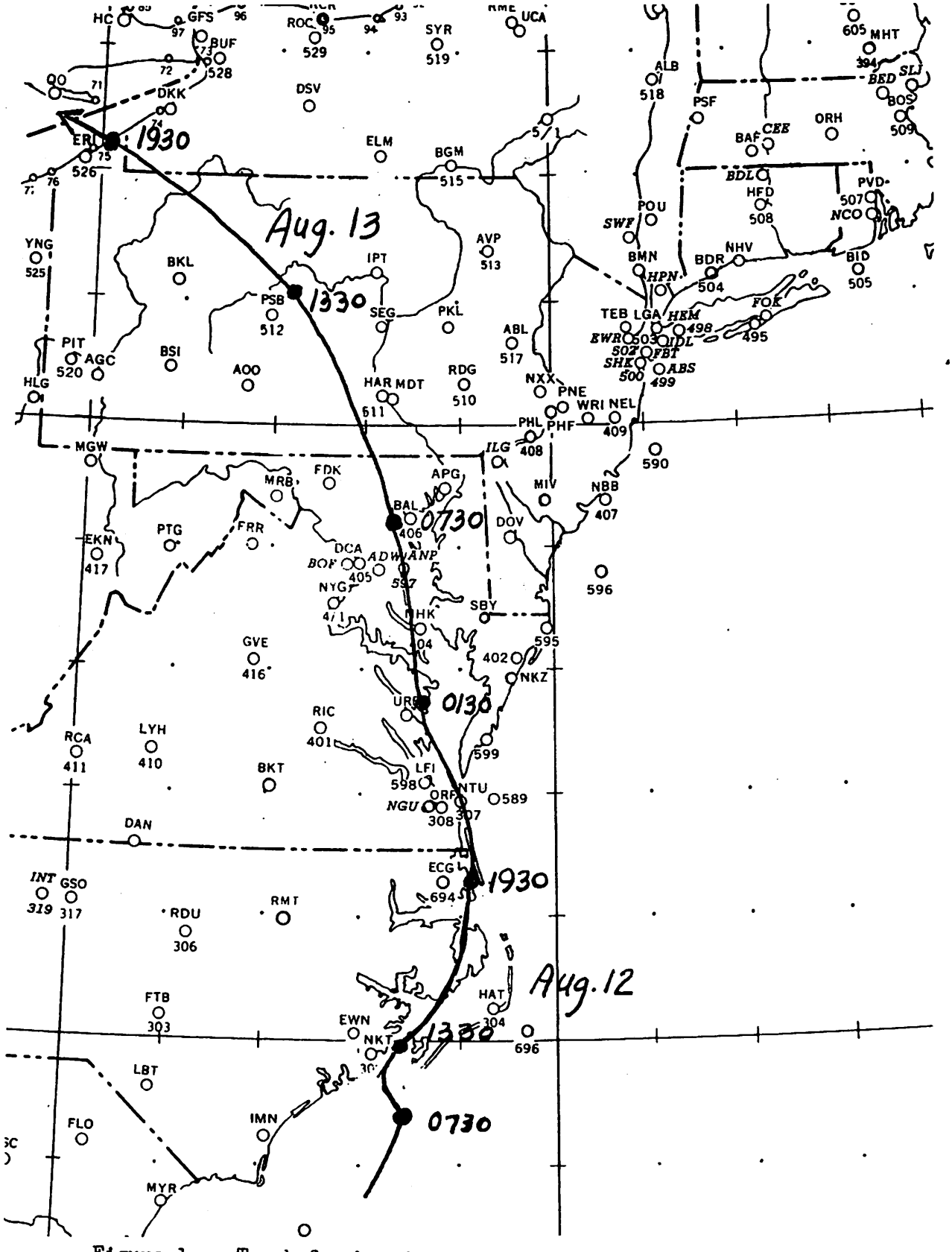


Figure 1. - Track for hurricane Connie, August 1955. Time: EST

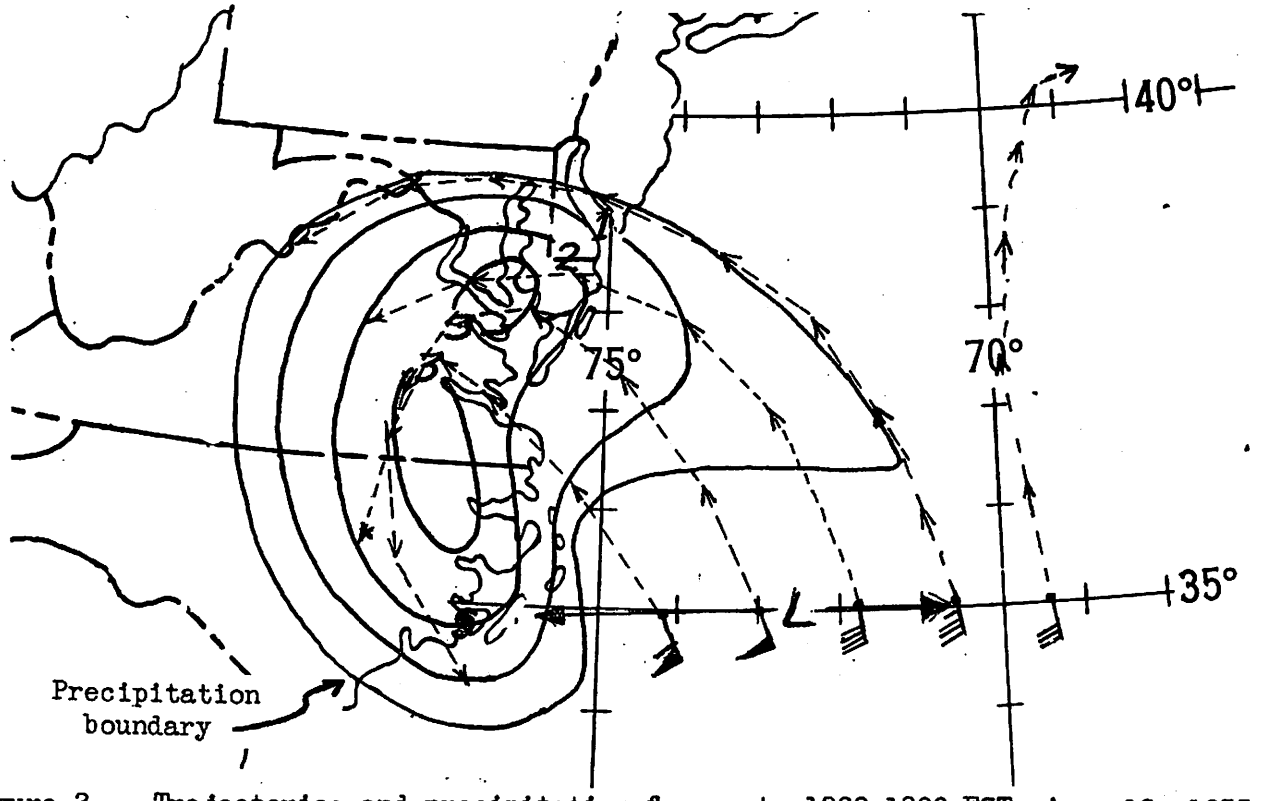


Figure 2. - Trajectories and precipitation forecast, 1200-1800 EST, Aug. 12, 1955.

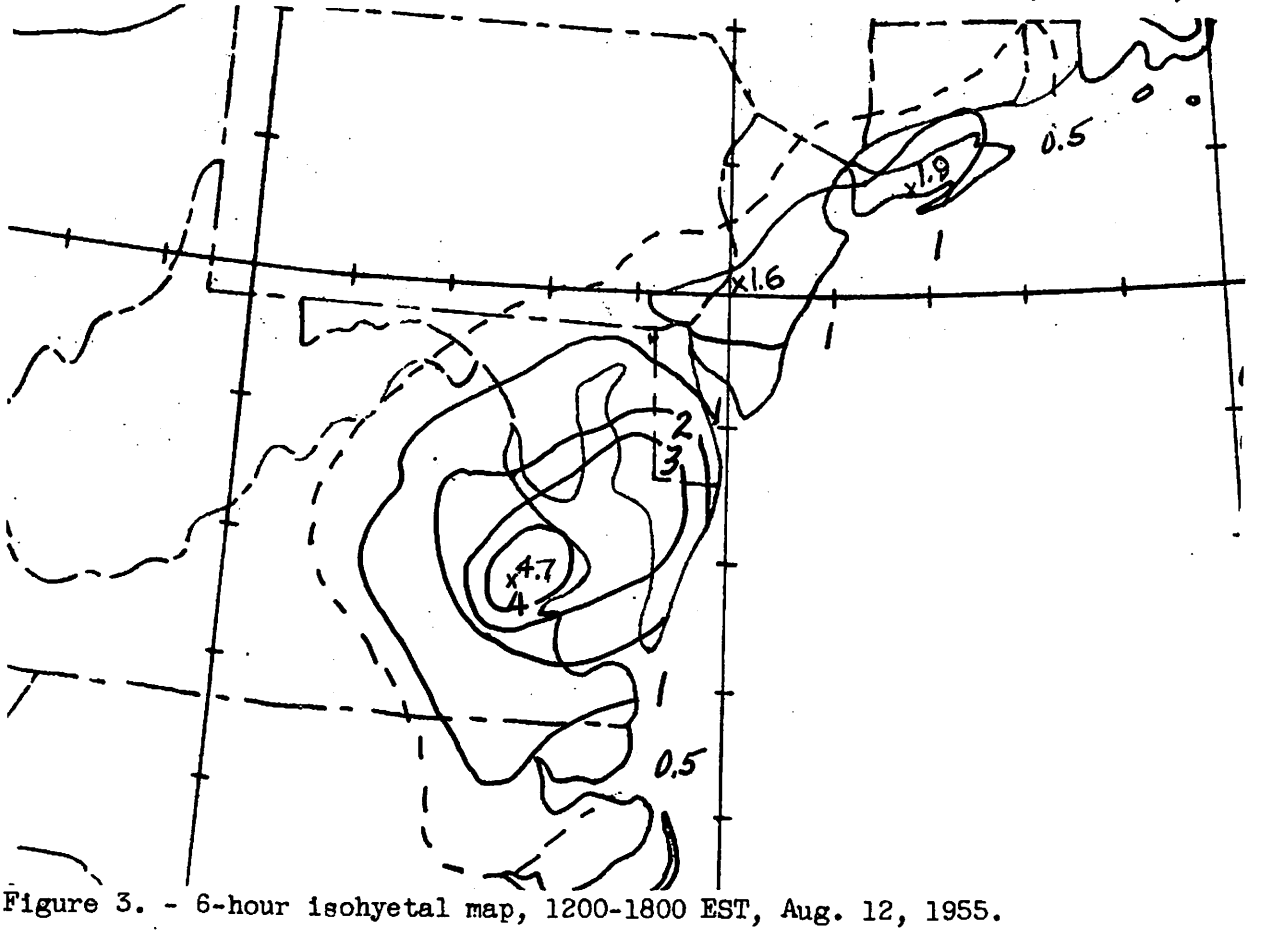


Figure 3. - 6-hour isohyetal map, 1200-1800 EST, Aug. 12, 1955.

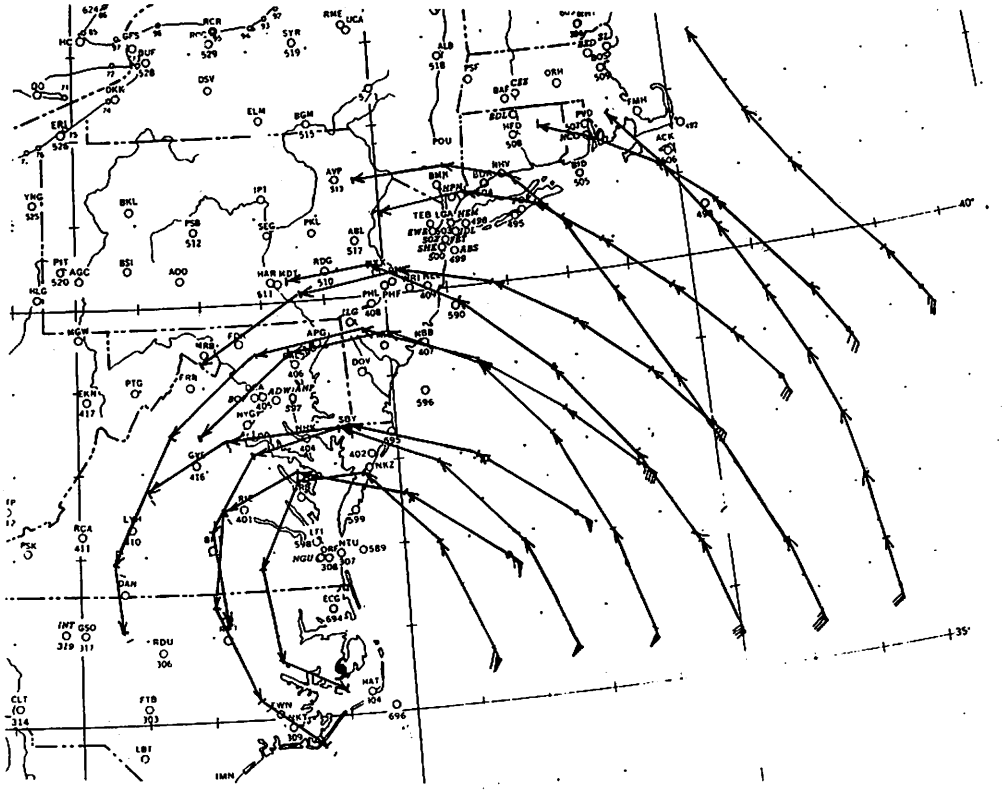

Figure 4a. - Dynamic trajectories 60° and 90° to right of hurricane path, 1630-2400 EST, August 12, 1955.

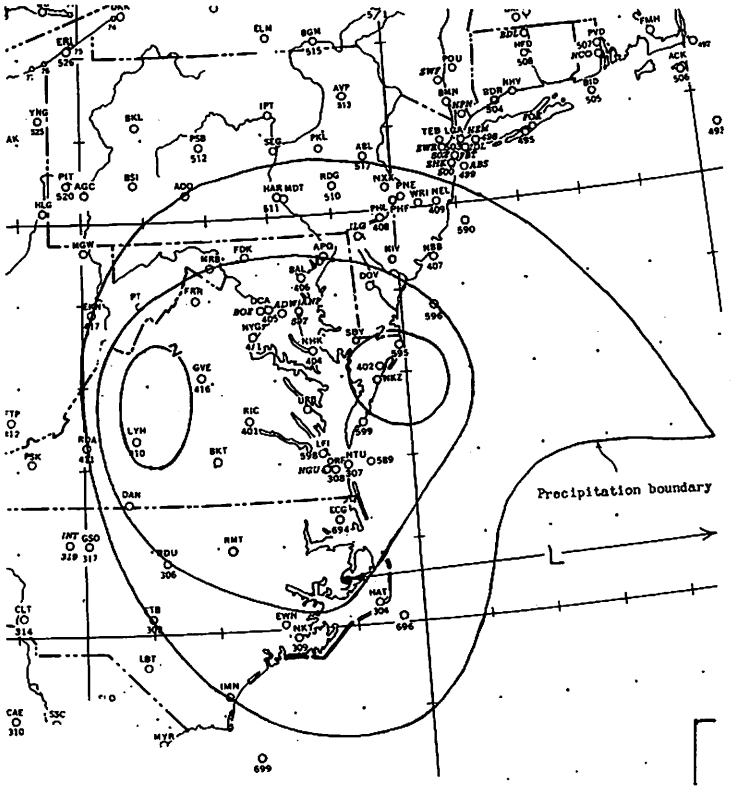


Figure 4b. - Forecast isohyets, 1800-2400 EST, Aug. 12, 1955.

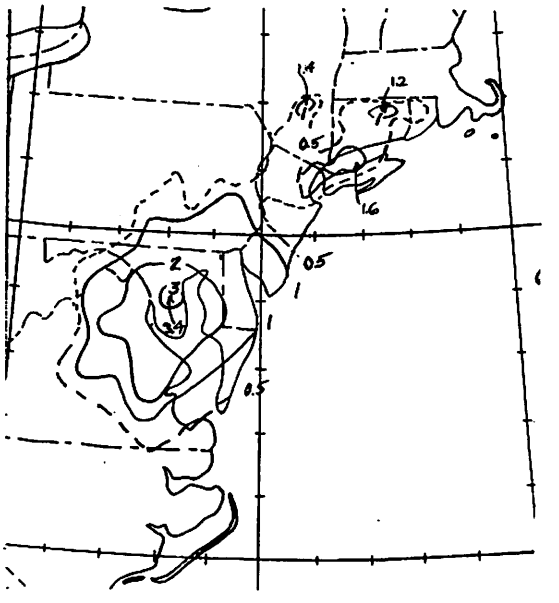

Figure 5. - 6-hour isohyetal map, 1800-2400 EST, Aug. 12, 1955.

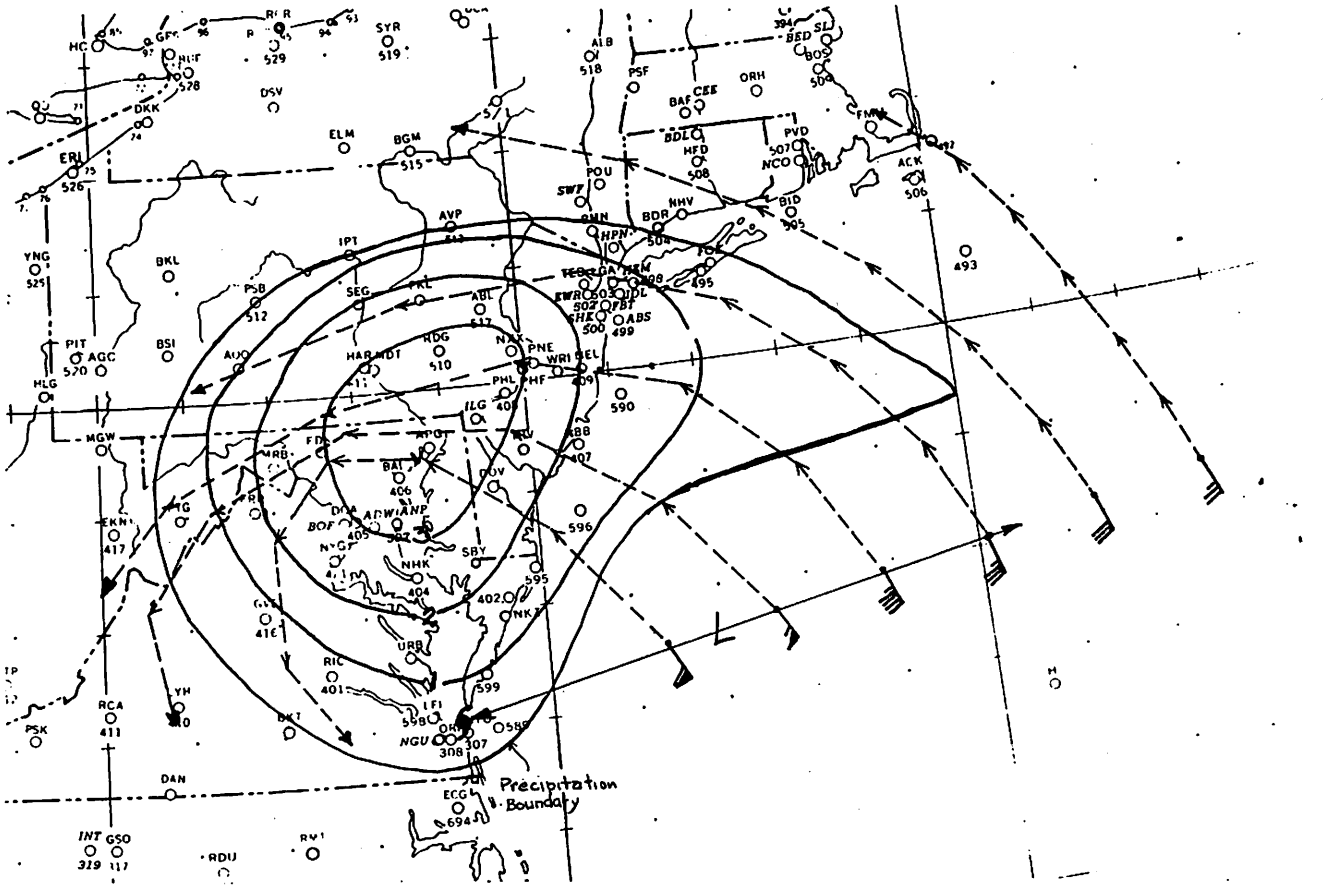


Figure 6. - Trajectories and precipitation forecast, 0000-0600 EST, Aug. 12, 1955

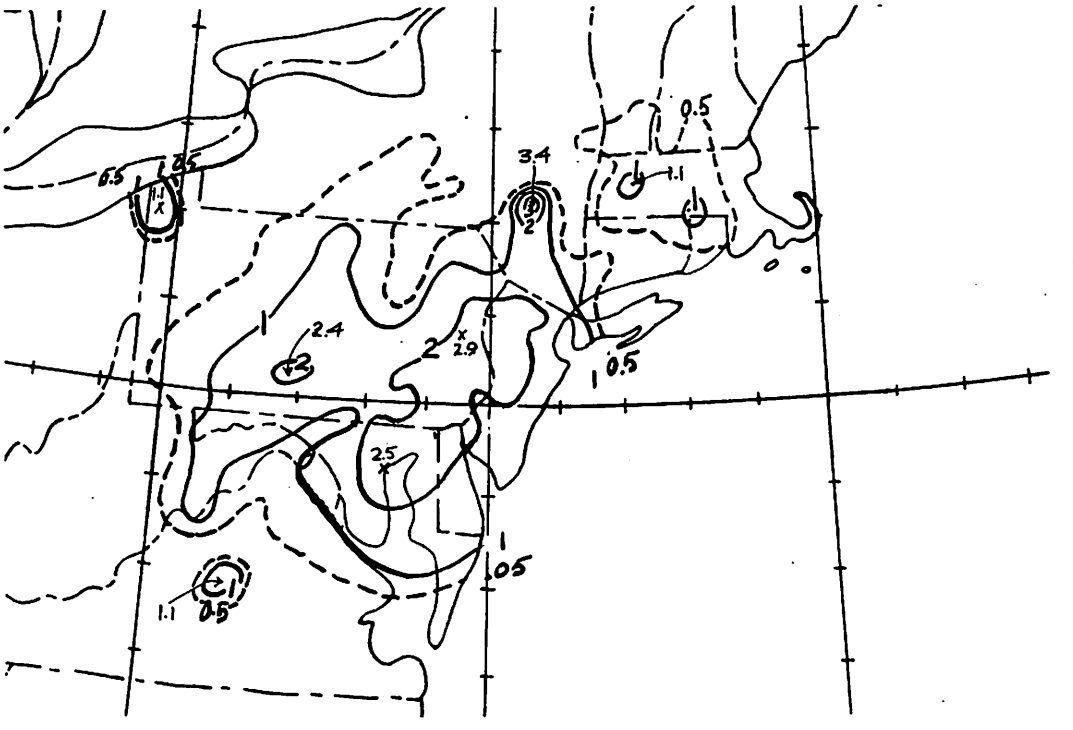


Figure 7. - 6-hr. isohyetal map, 0000-0600 EST, Aug. 13, 1955

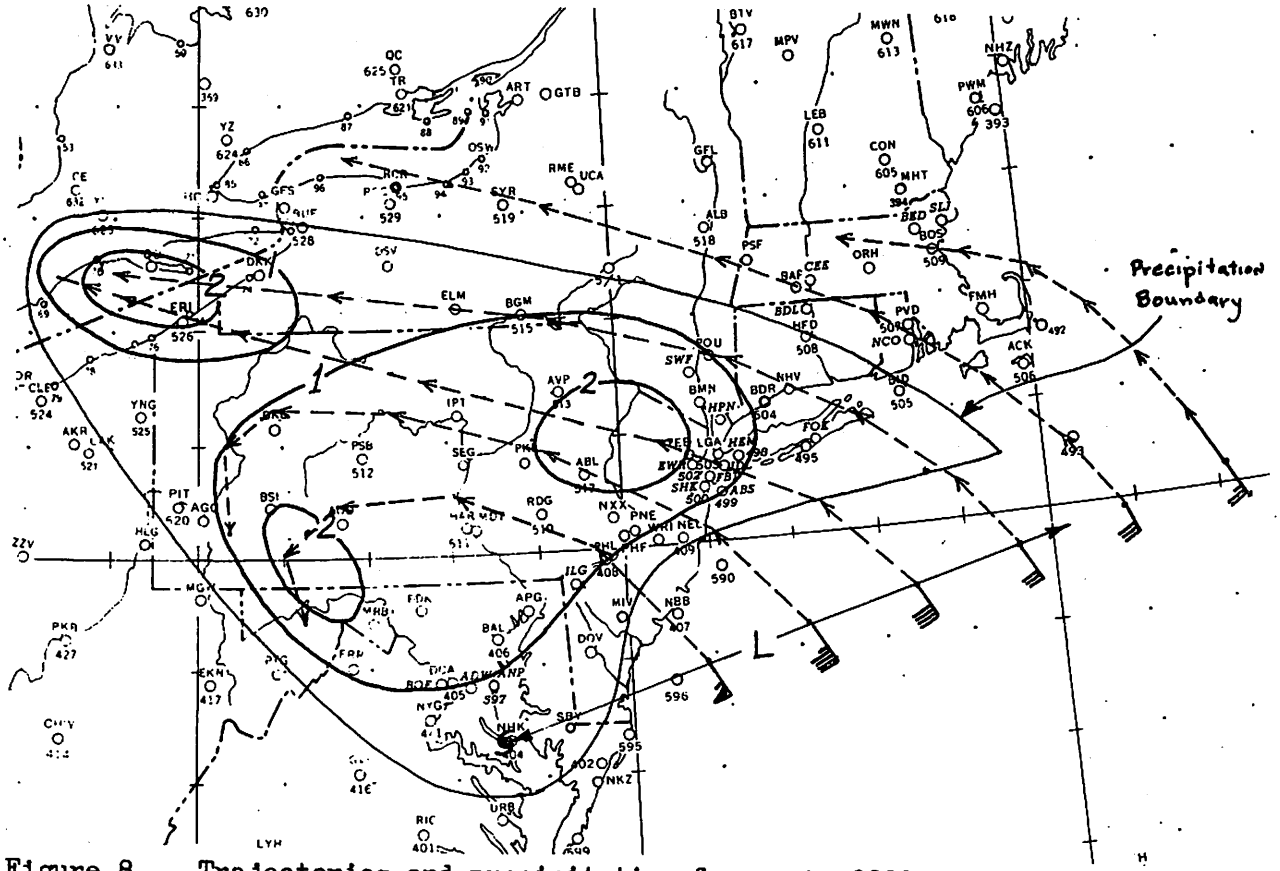


Figure 8. - Trajectories and precipitation forecast, 0600-1200 EST, Aug. 13, 1955

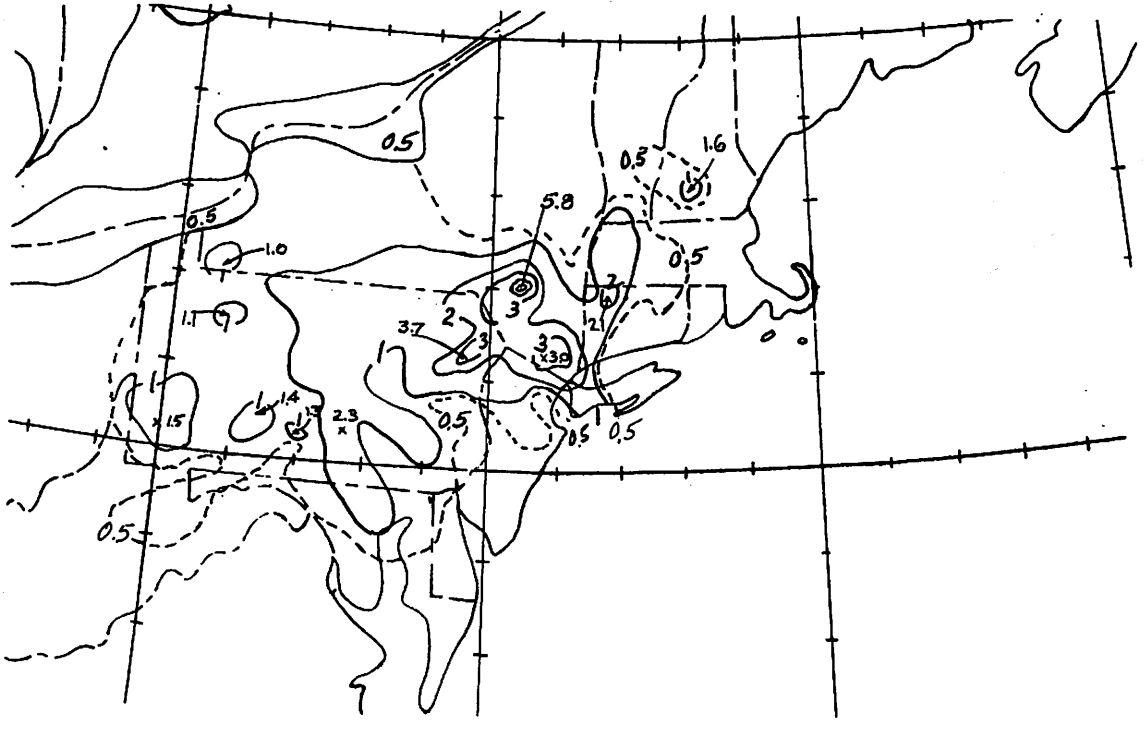


Figure 9. - 6-hr. isohyetal map, 0600-12-- EST, Aug. 13, 1955

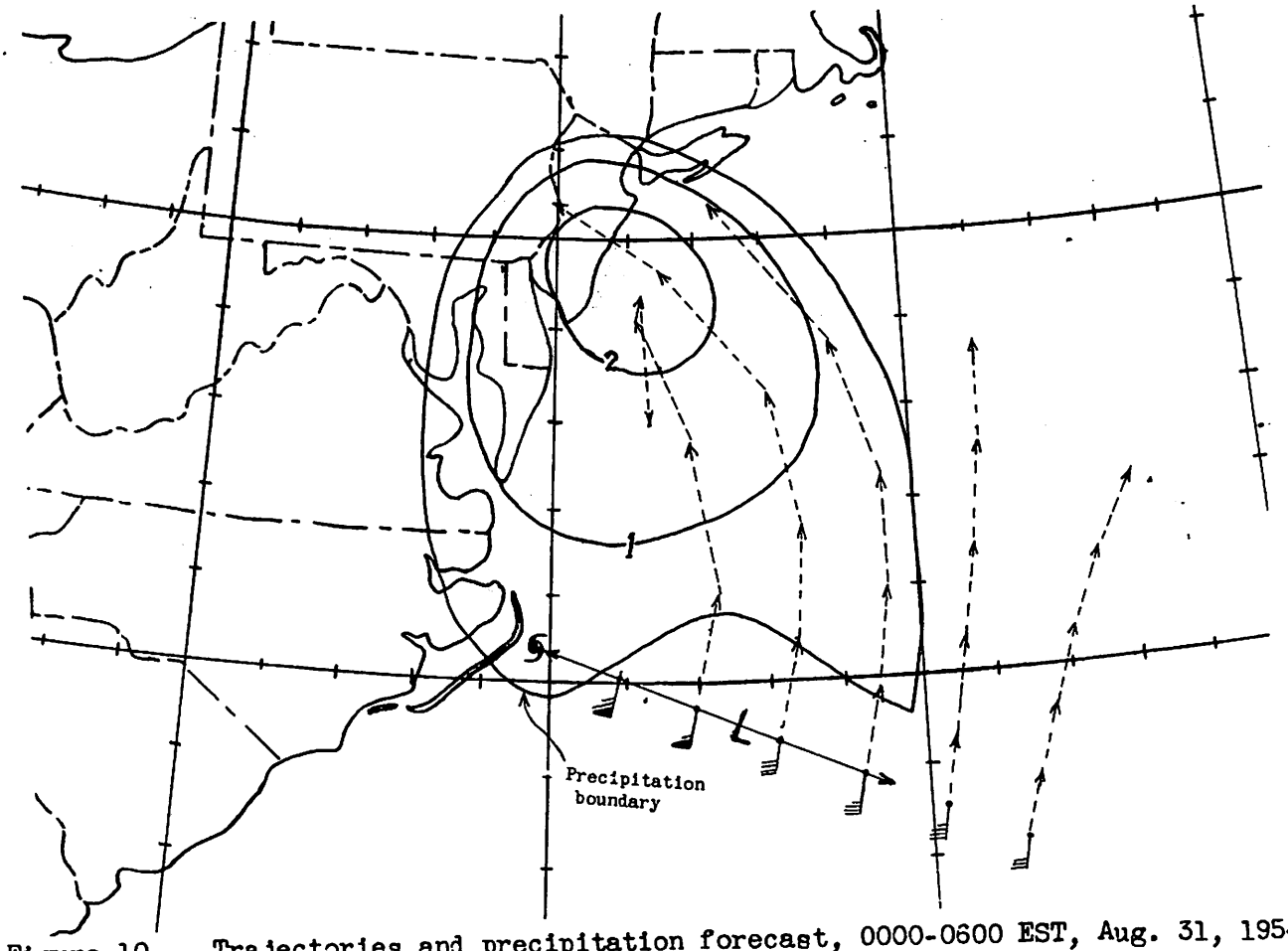


Figure 10. - Trajectories and precipitation forecast, 0000-0600 EST, Aug. 31, 1954

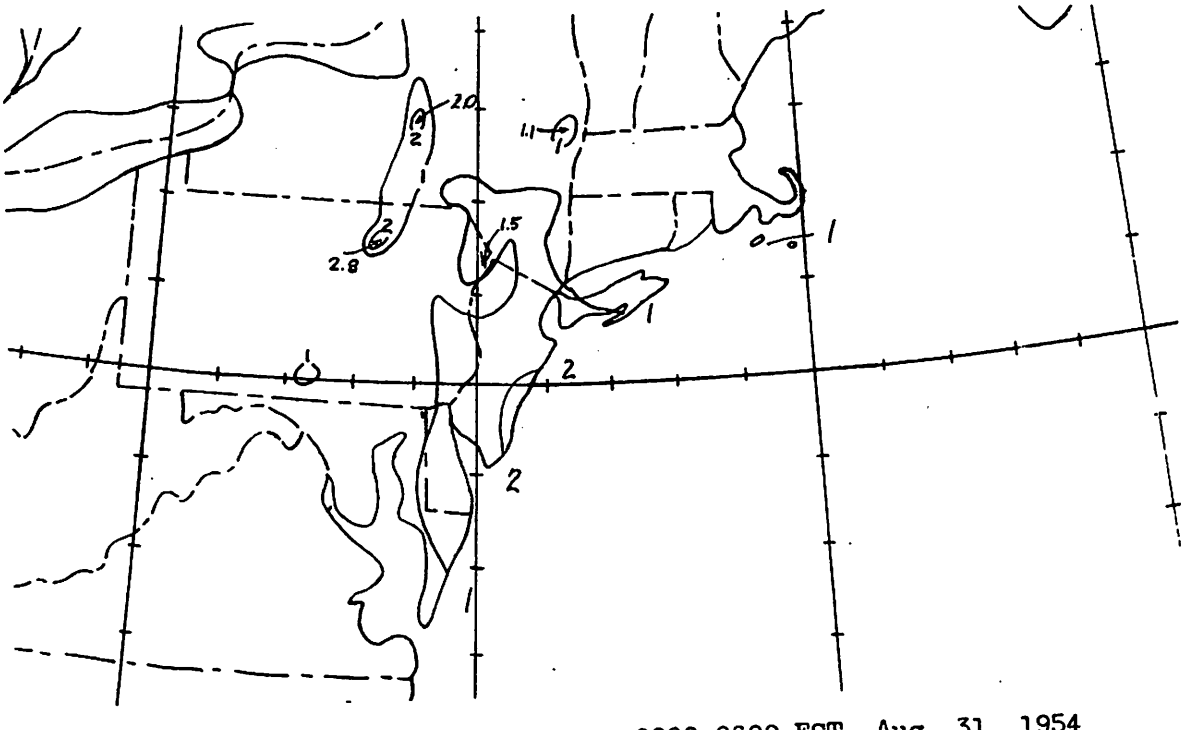


Figure 11. - 6-hr. isohyetal map, 0000-0600 EST, Aug. 31, 1954

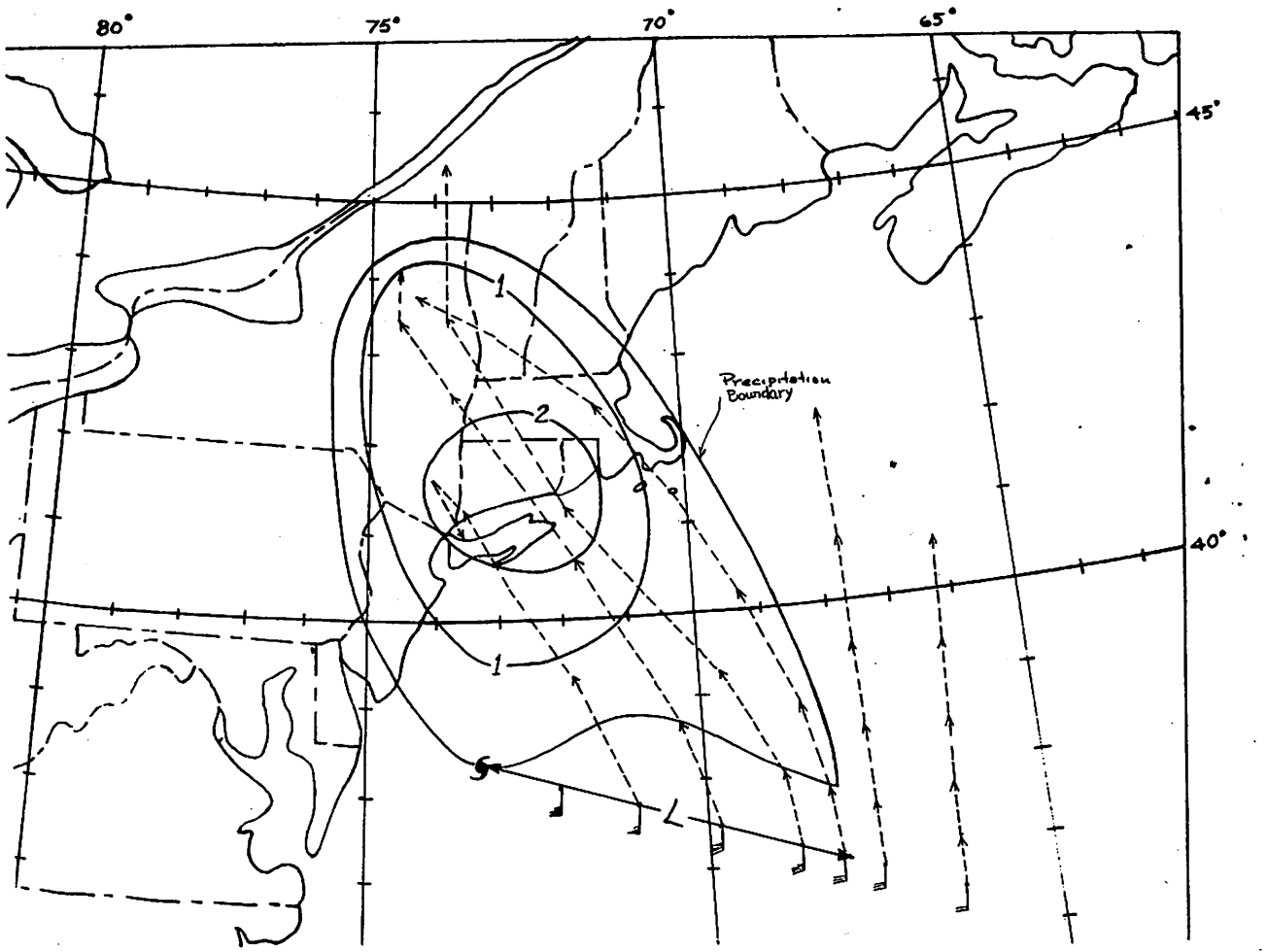


Figure 12. - Trajectories and precipitation forecast, 0600-1200 EST, Aug. 31, 1954

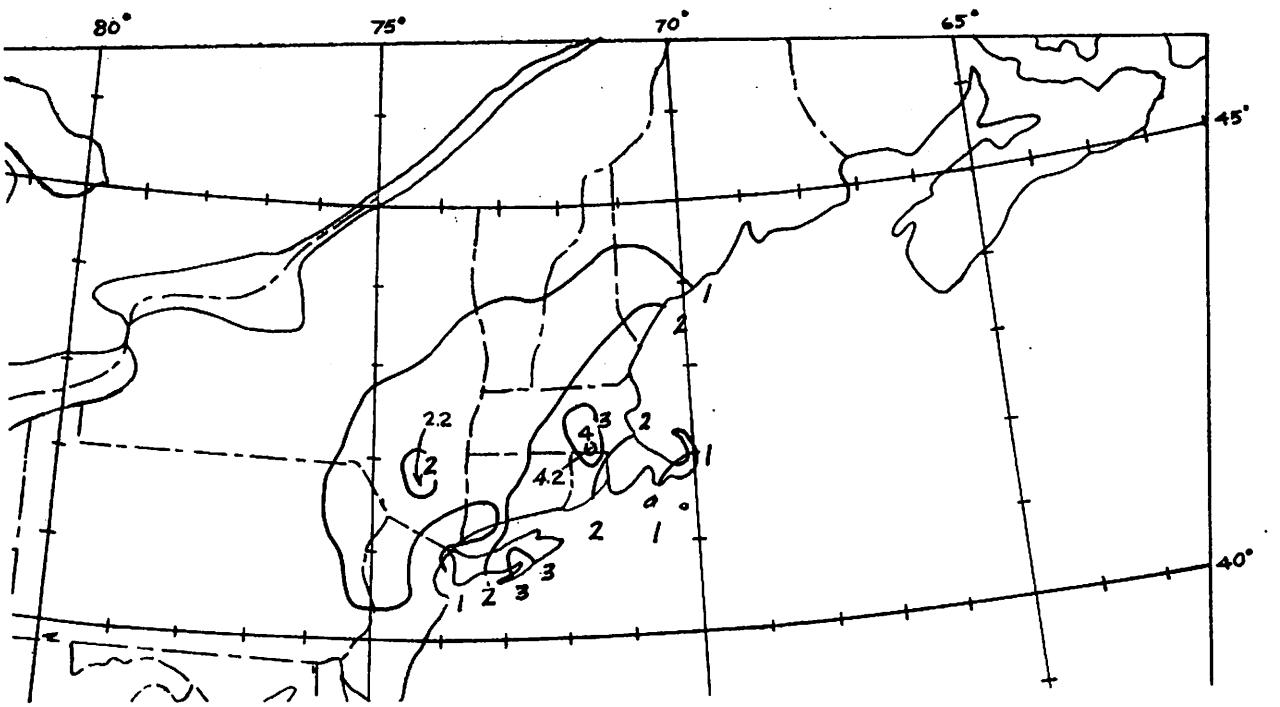


Figure 13. - 6-hr. isohyetal map, 0600-1200 EST, Aug. 31, 1954

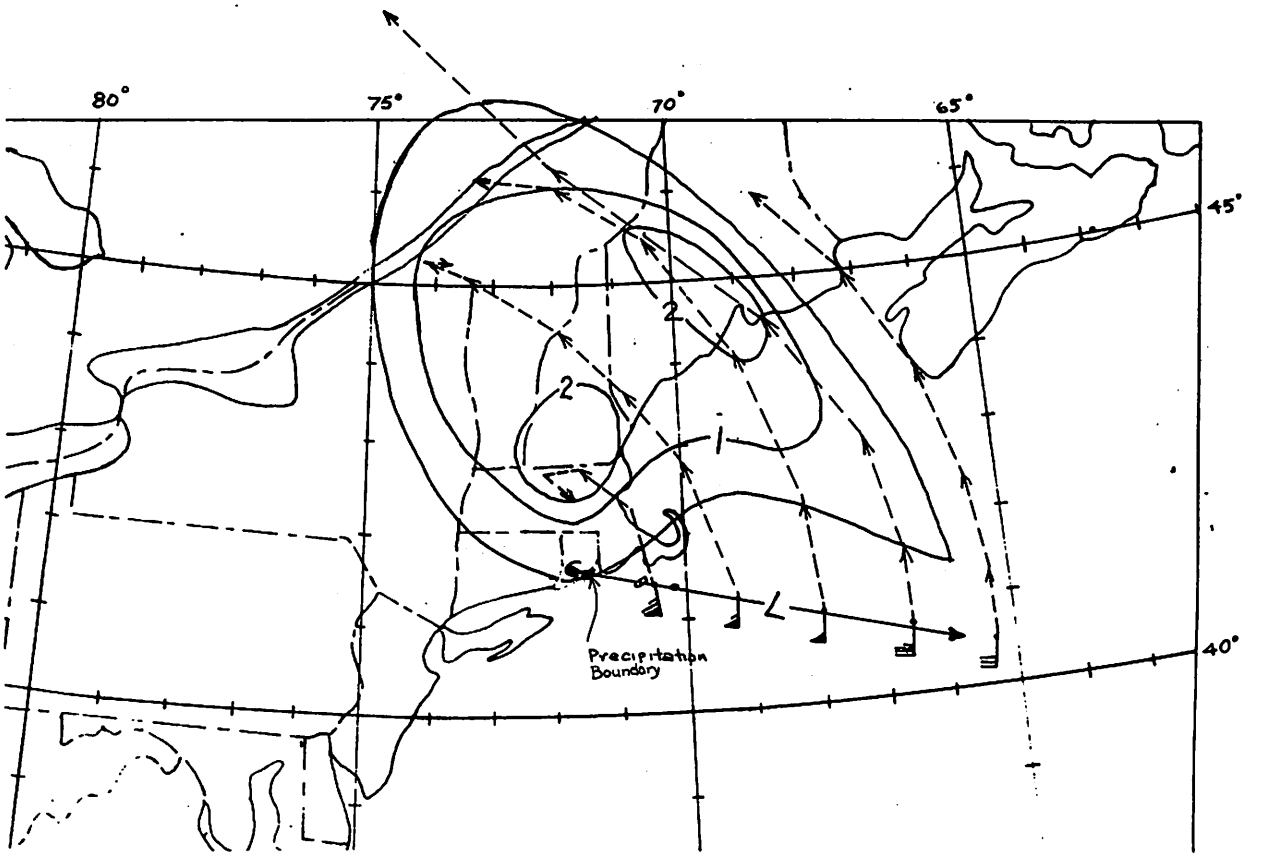


Figure 14. - Trajectories and precipitation forecast, 1200-1800 EST, Aug. 31, 1954

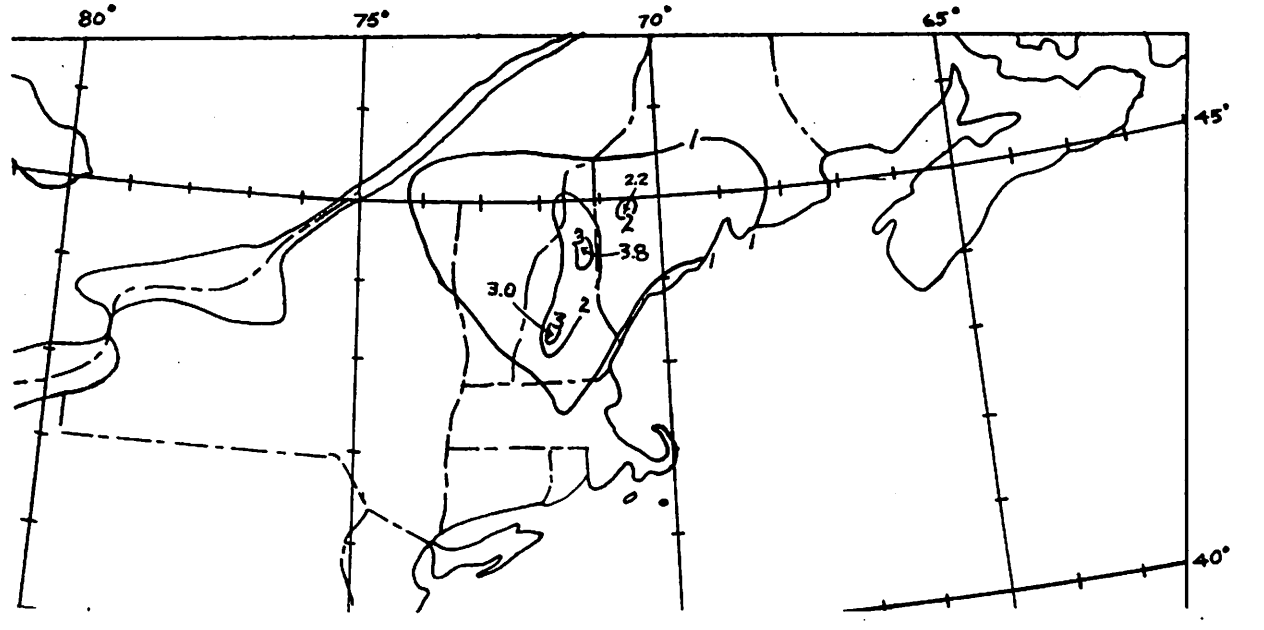


Figure 15. - 6-hr. isohyetal map, 1200-1800 EST, Aug. 31, 1954

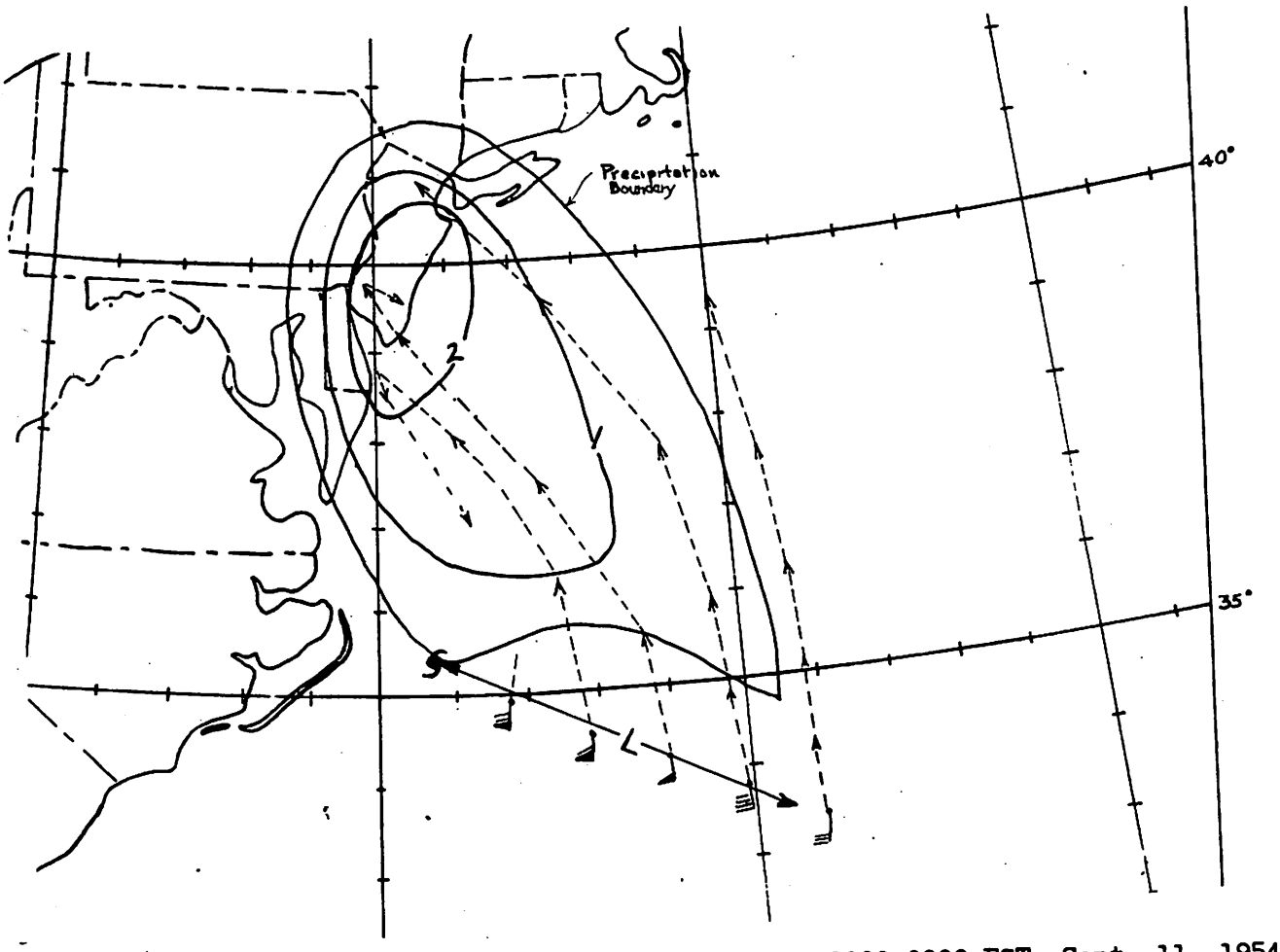


Figure 16. - Trajectories and precipitation forecast, 0000-0600 EST, Sept. 11, 1954

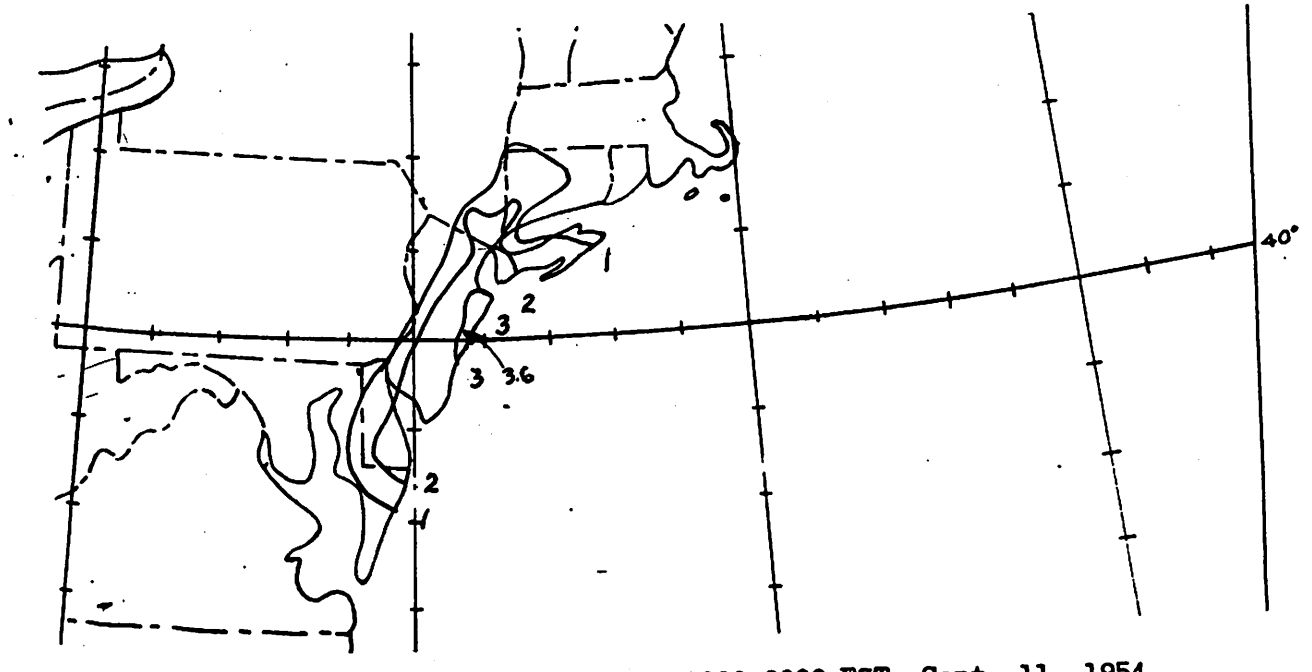


Figure 17. - 6-hr. isohyetal map, 0000-0600 EST, Sept. 11, 1954

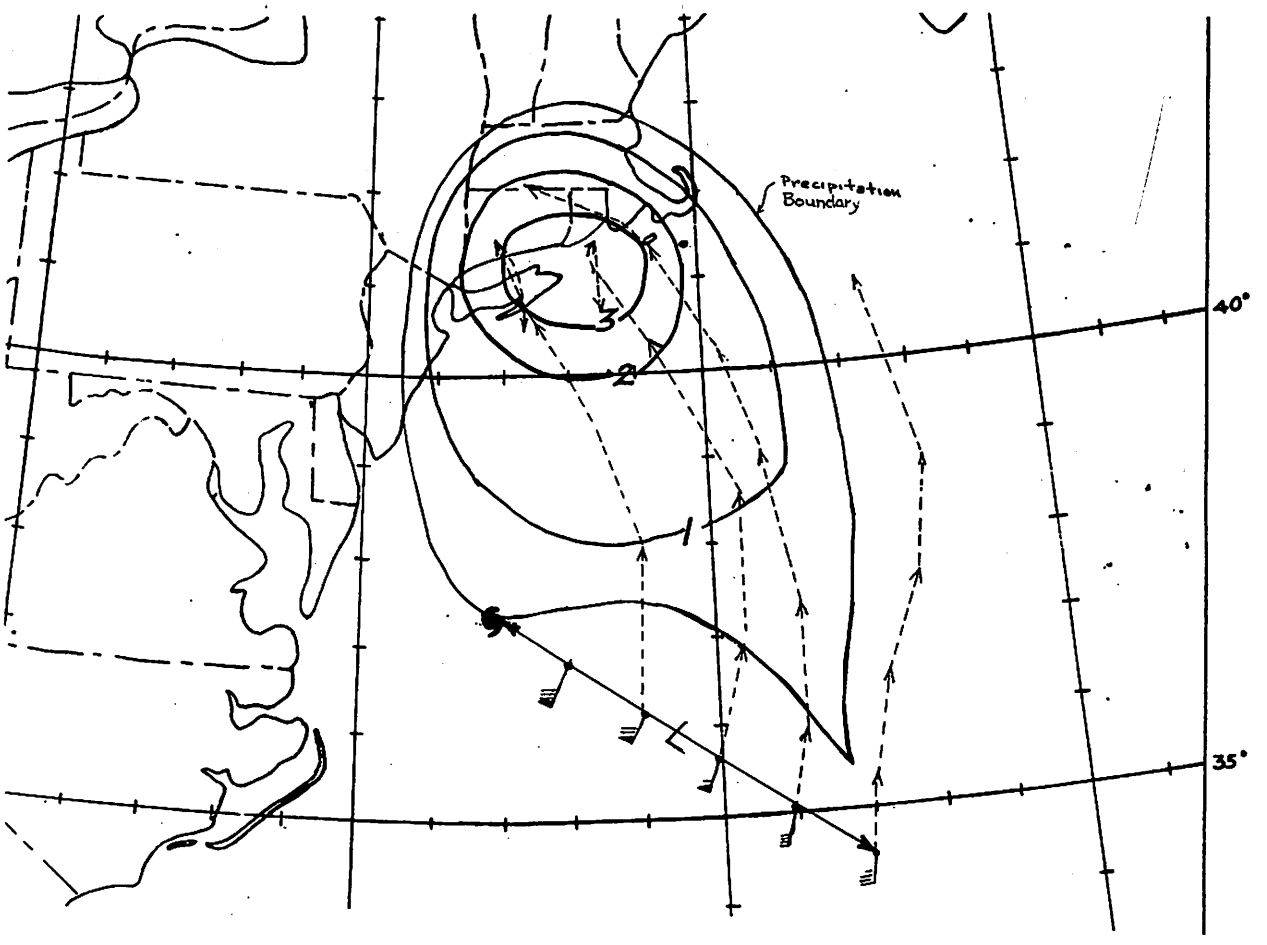


Figure 18. - Trajectories and precipitation forecast, 0600-1200 EST, Sept. 11, 1954

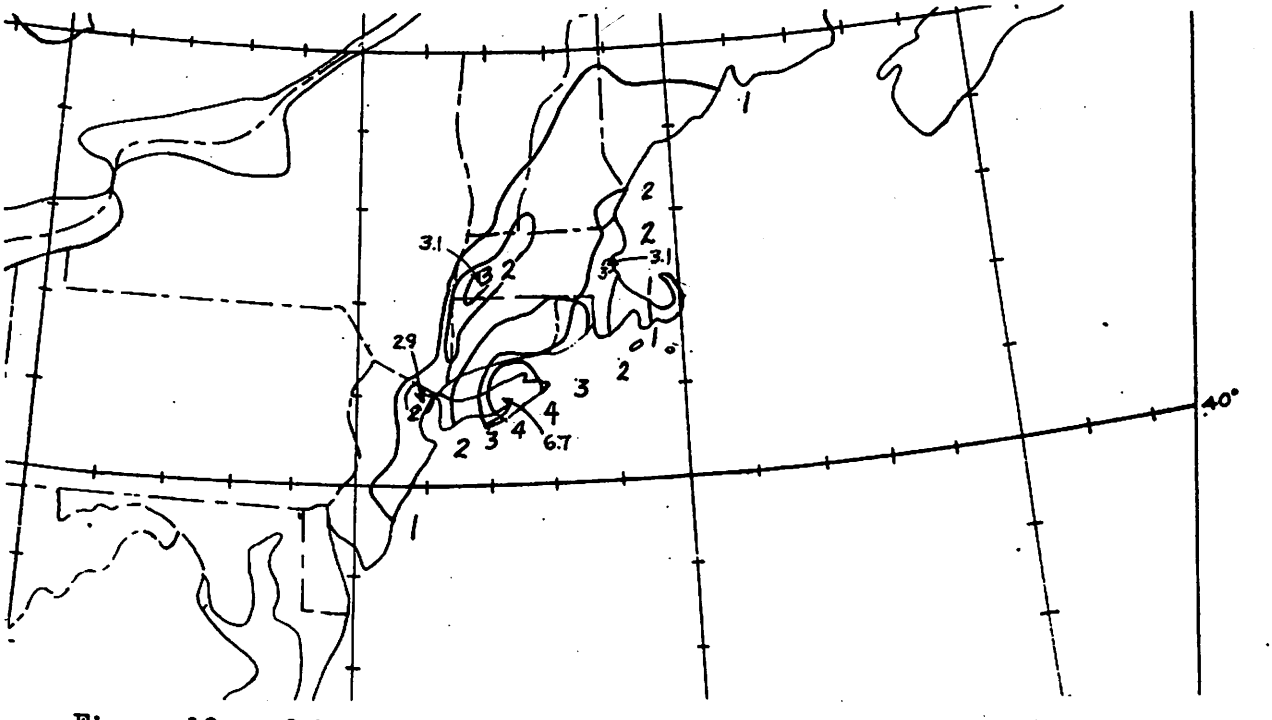


Figure 19. - 6-hr. isohyetal map, 0600-1200 EST, Sept. 11, 1954

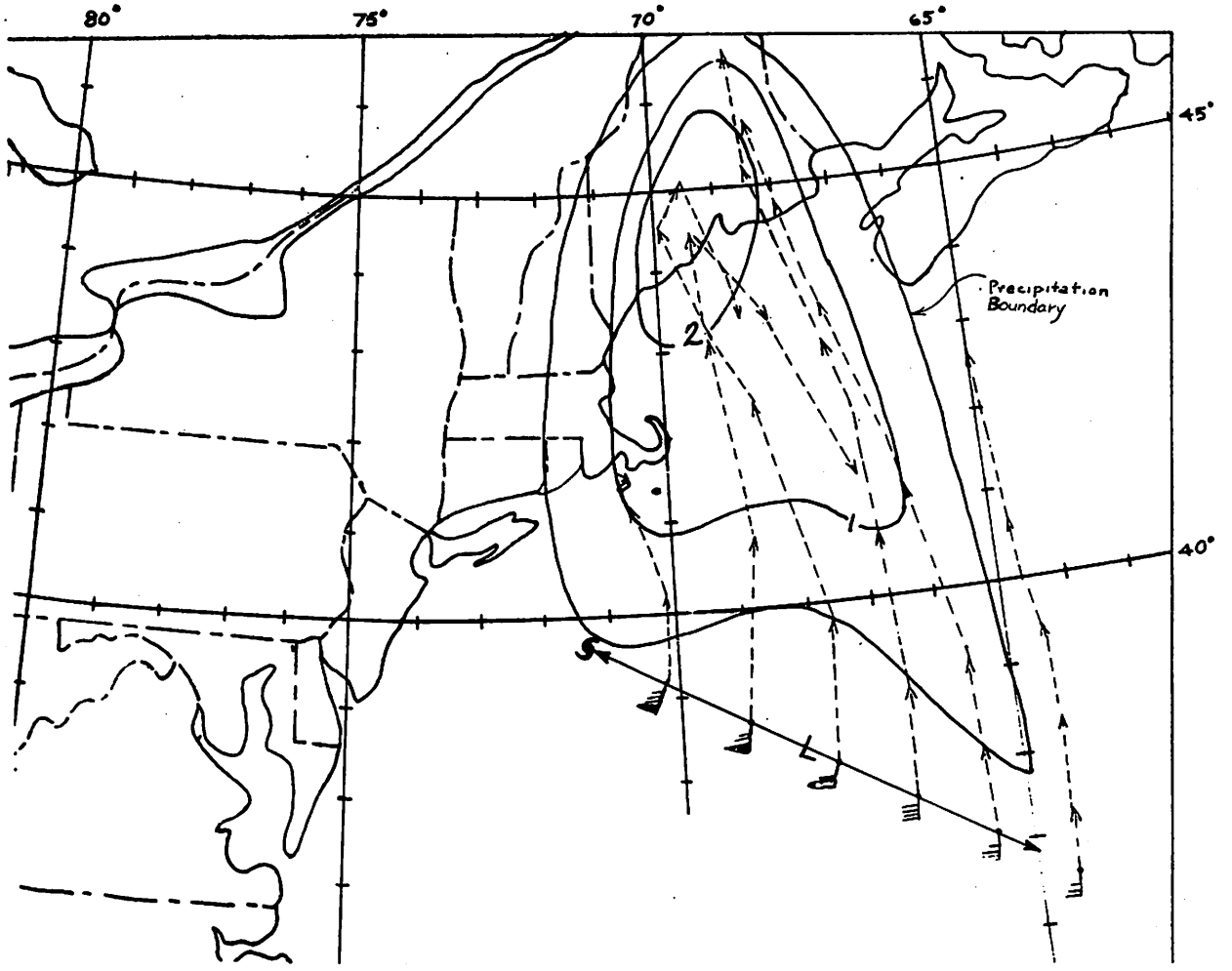


Figure 20. - Trajectories and precipitation forecast, 1200-1800 EST, Sept. 11, 1954

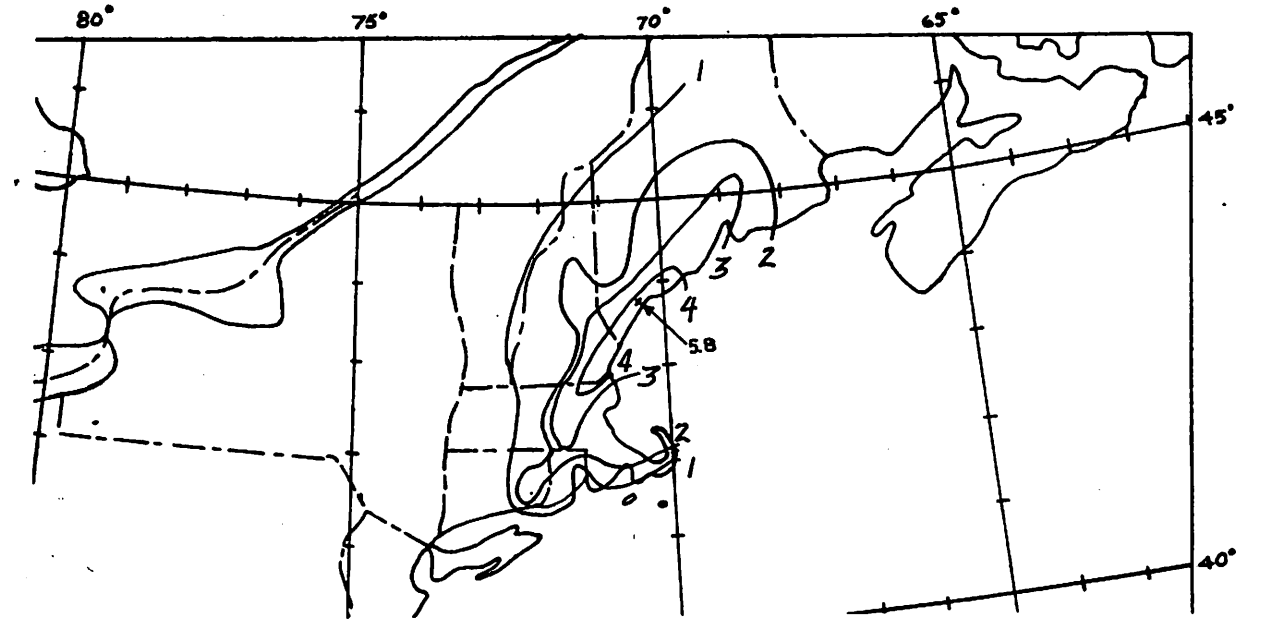


Figure 21. - 6-hr. isohyetal map, 1200-1800 EST, Sept. 11, 1954

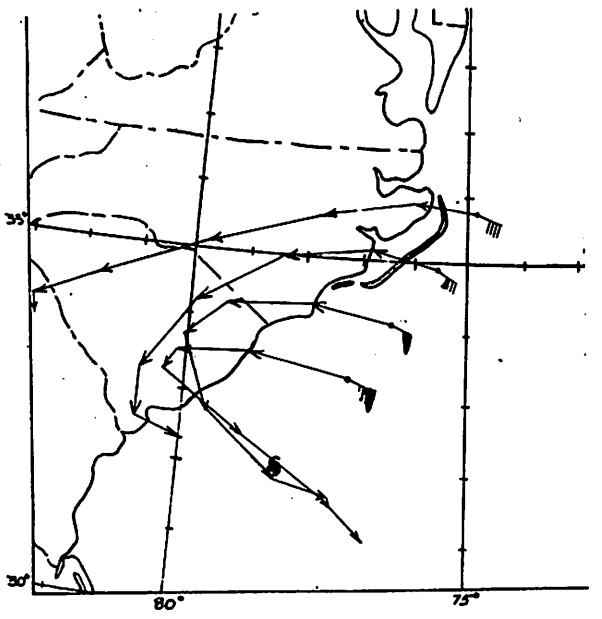


Figure 22a. - Dynamic trajectories 45° to right of hurricane path, 0430-1200 EST, Oct. 15, 1954

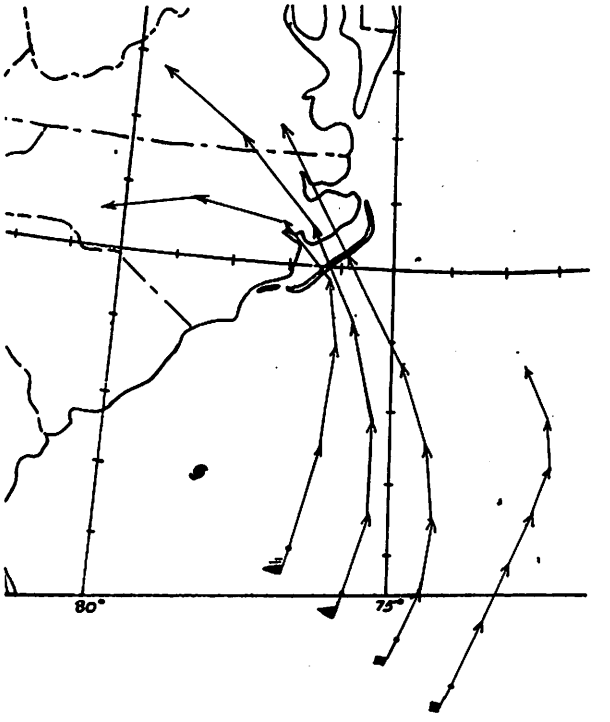


Figure 22b. - Dynamic trajectories 90° to right of hurricane path

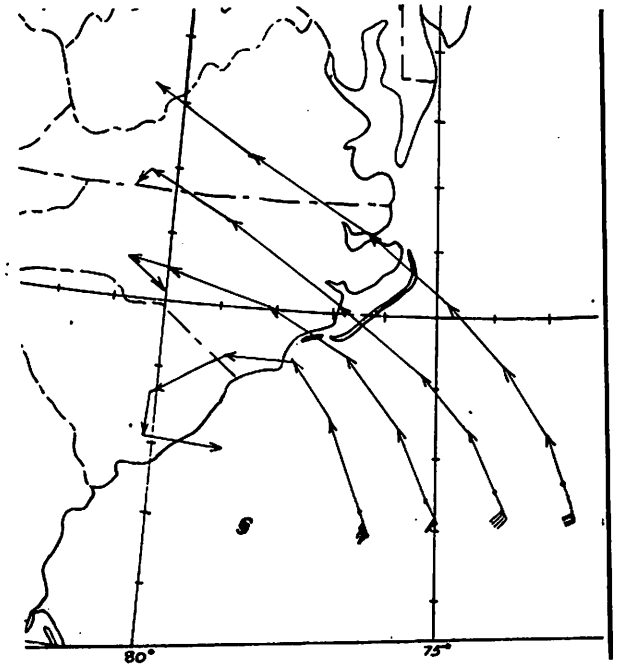


Figure 22c. - Dynamic trajectories 135° to right of hurricane path

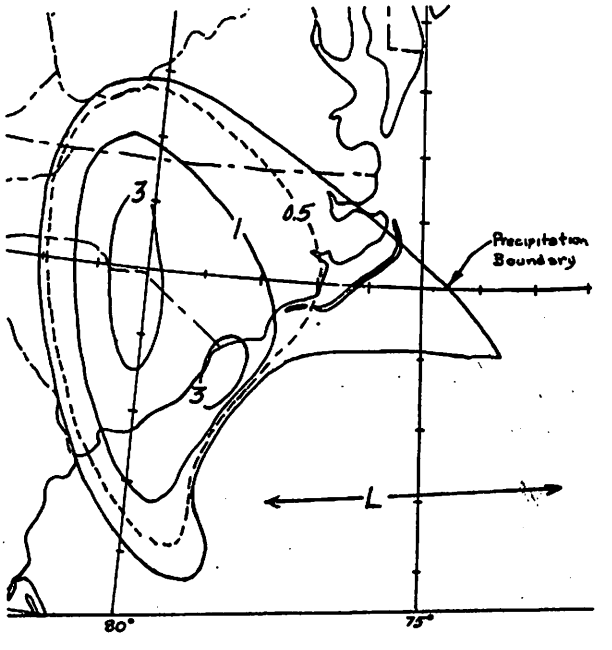


Figure 22d. - Forecast isohyets, 0600-1200 EST, Oct. 15, 1954

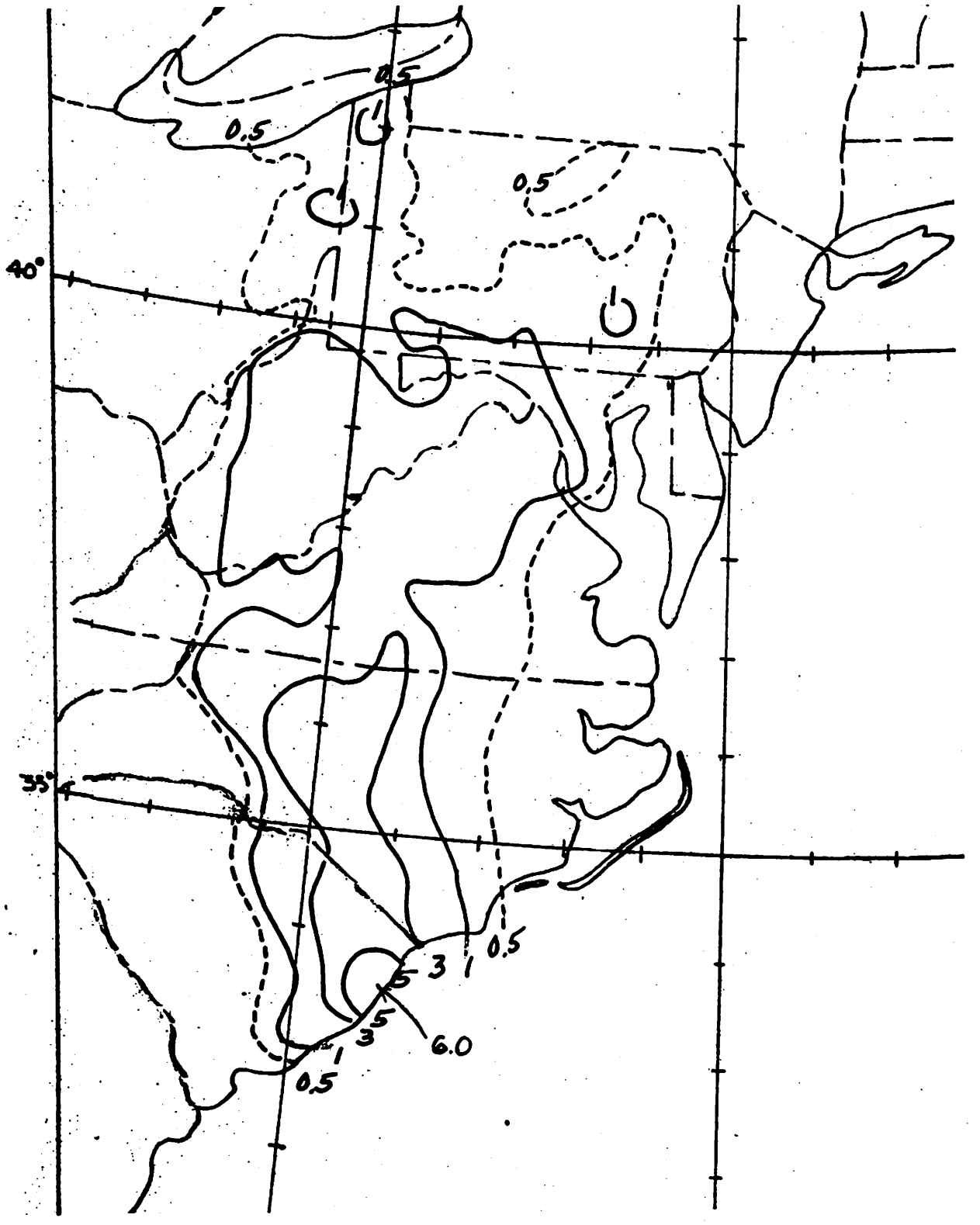


Figure 23. - 6-hour isohyetal map, 0600-1200 EST, October 15, 1954.

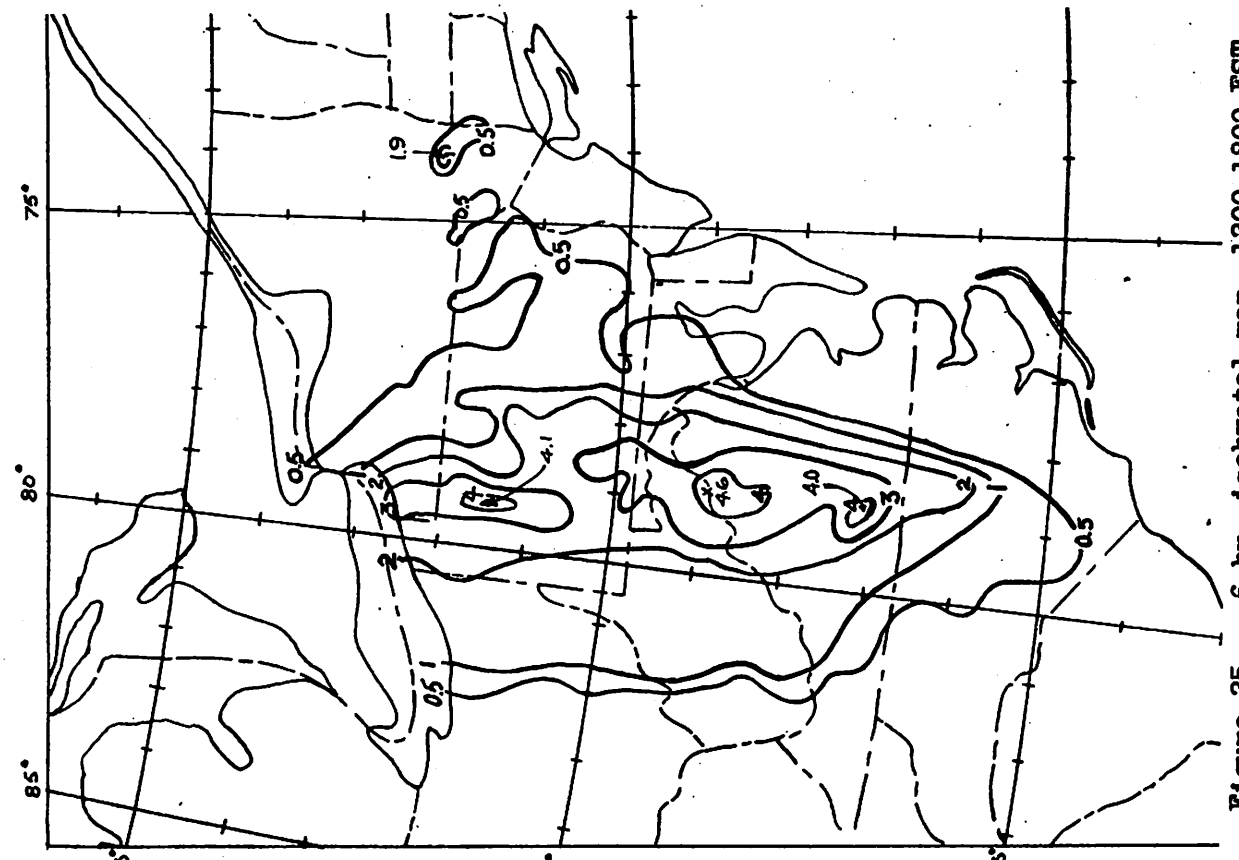


Figure 25. - 6-hr. isohyetal map, 1200-1800 EST, Oct. 15, 1954

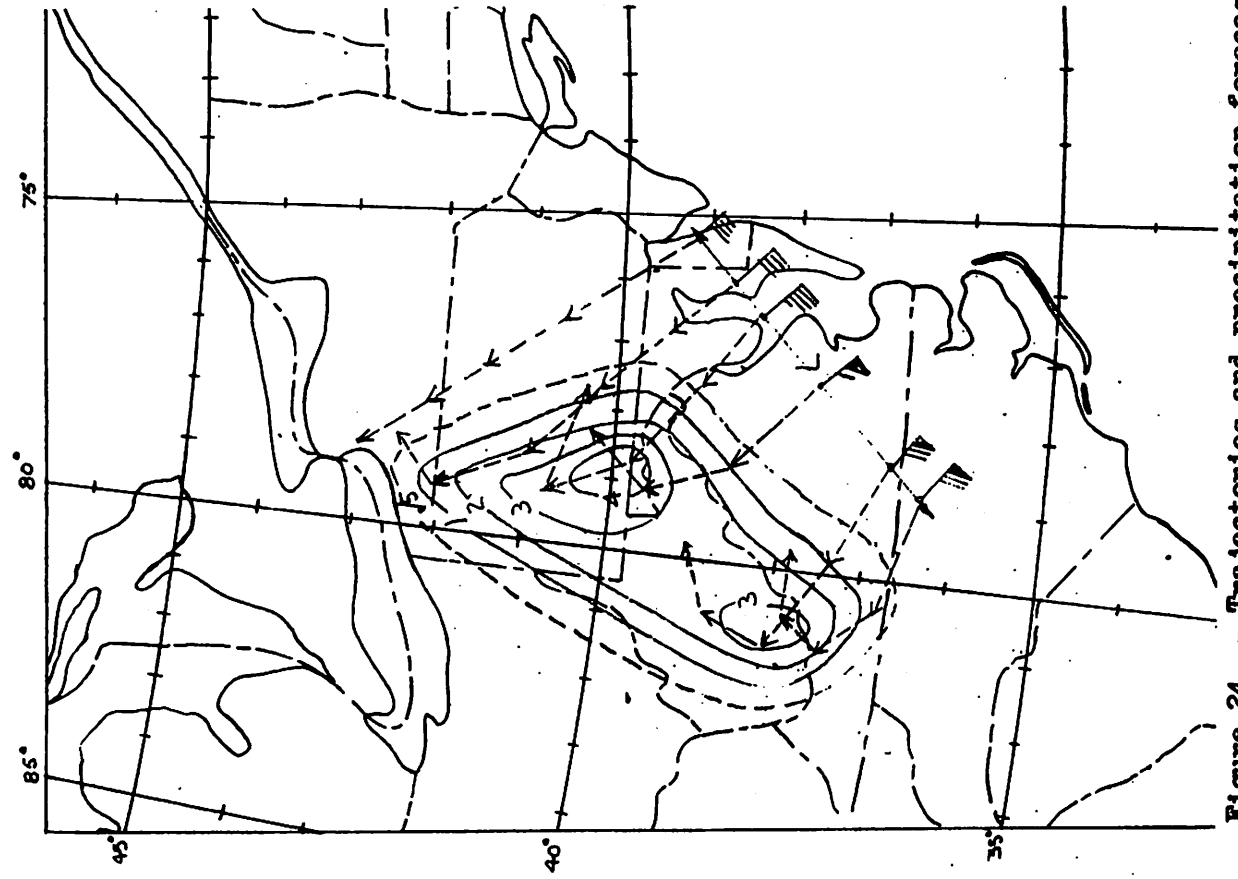


Figure 24. - Trajectories and precipitation forecast, 1200-1800 EST, Oct. 15, 1954

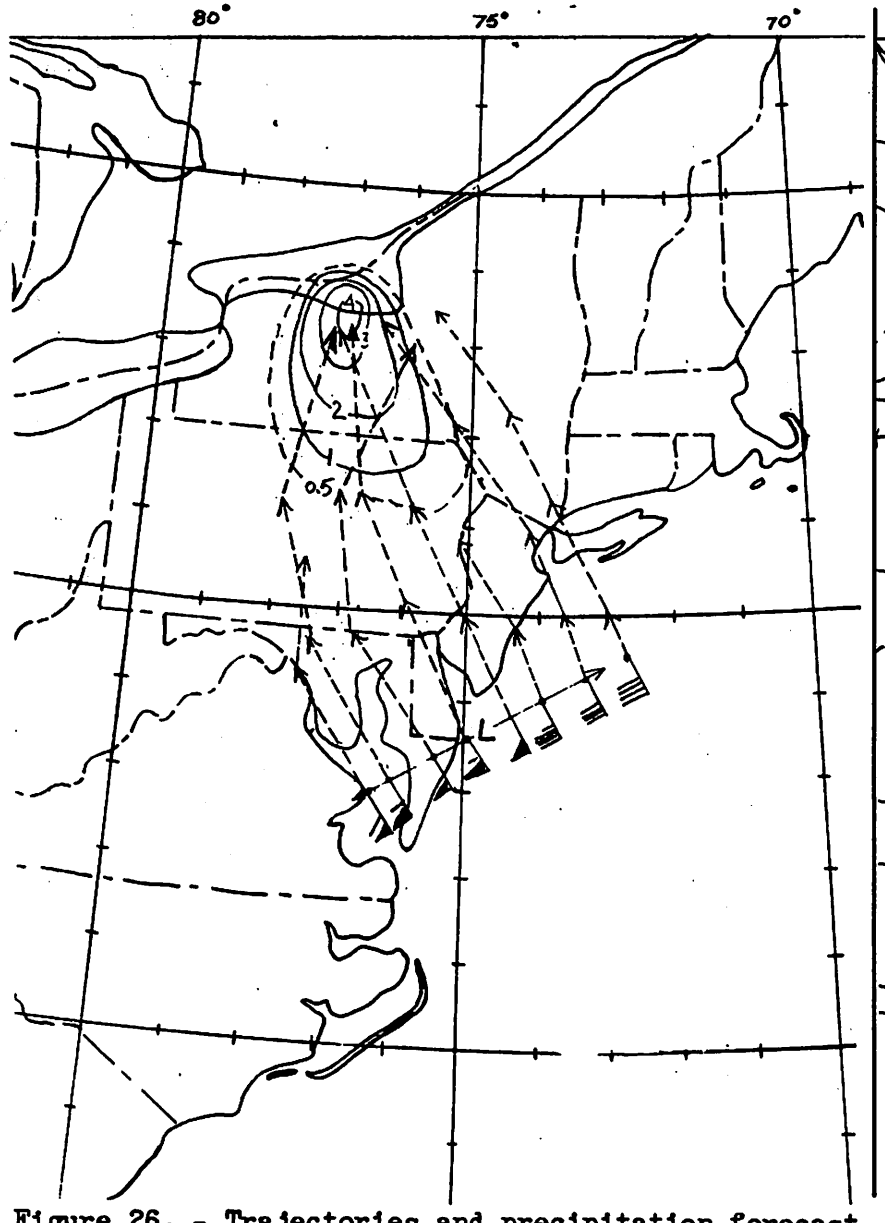


Figure 26. - Trajectories and precipitation forecast, 1800-2400 EST, Oct. 15, 1954

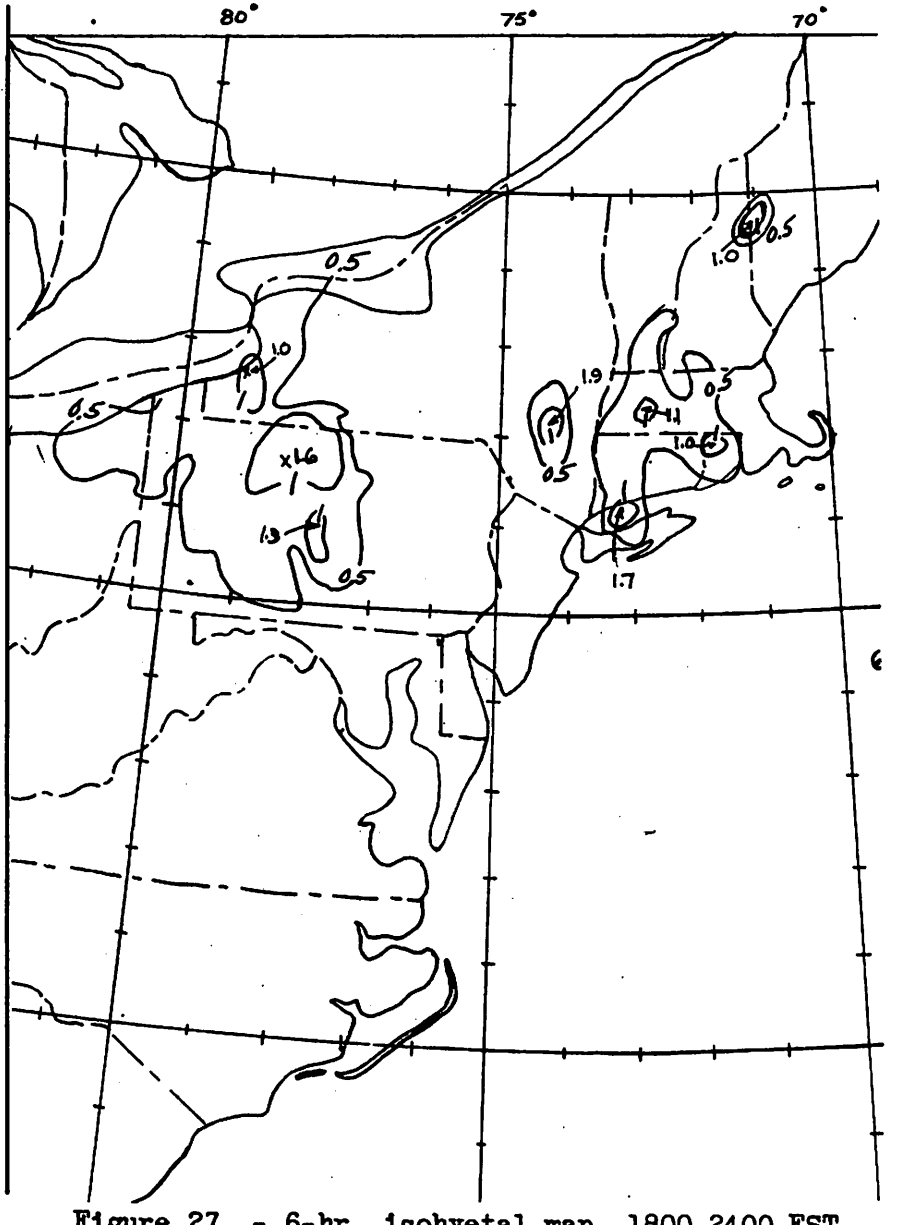


Figure 27. - 6-hr. isohyetal map, 1800-2400 EST, Oct. 15, 1954

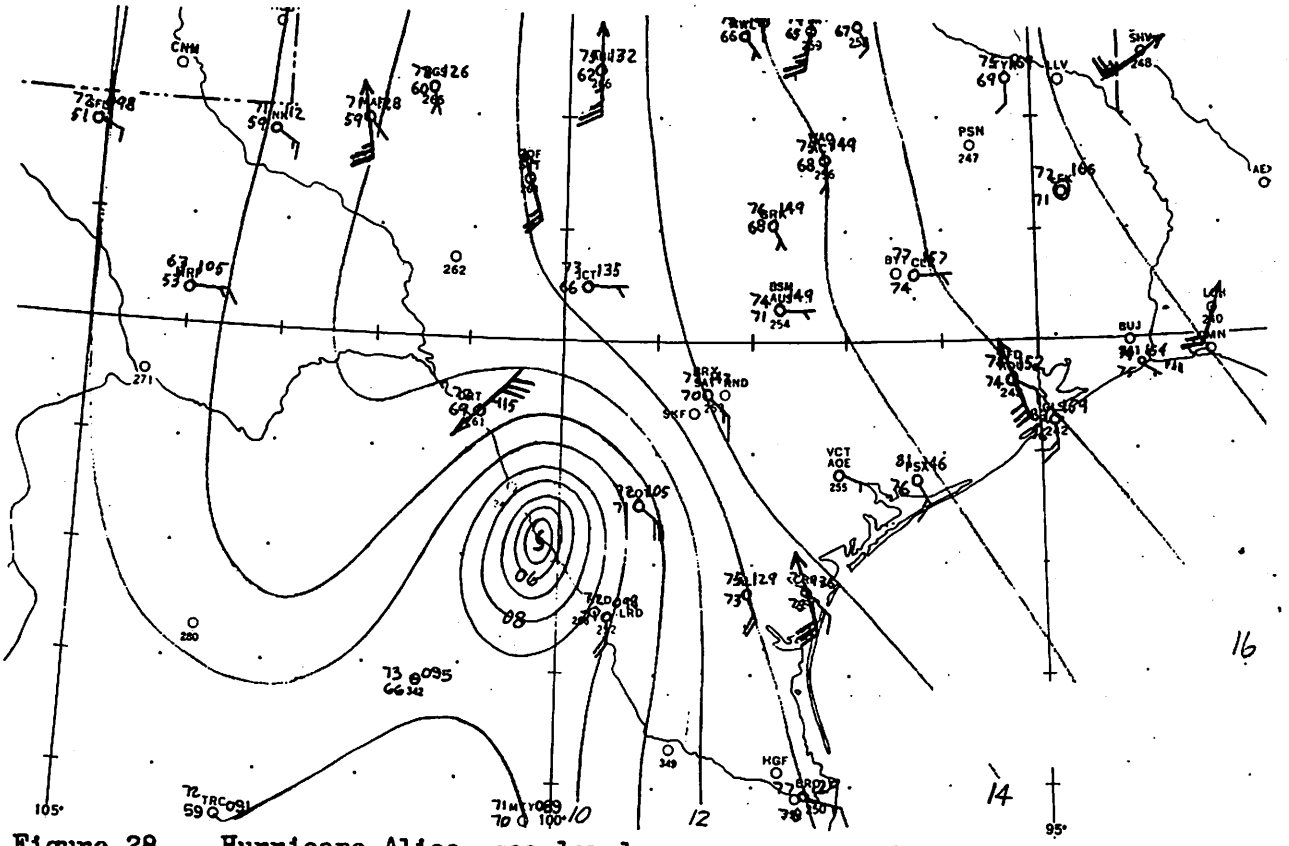

Figure 28. - Hurricane Alice, sea level pressure map, 1330 CST, June 26, 1954

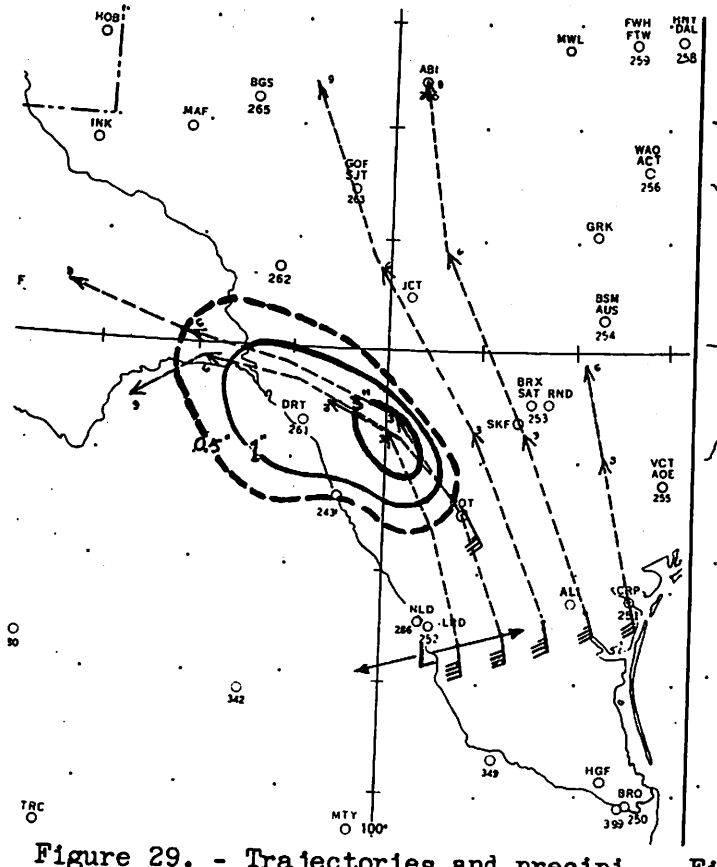

Figure 29. - Trajectories and precipitation forecast, 0600-1200 CST, June 26, 1954

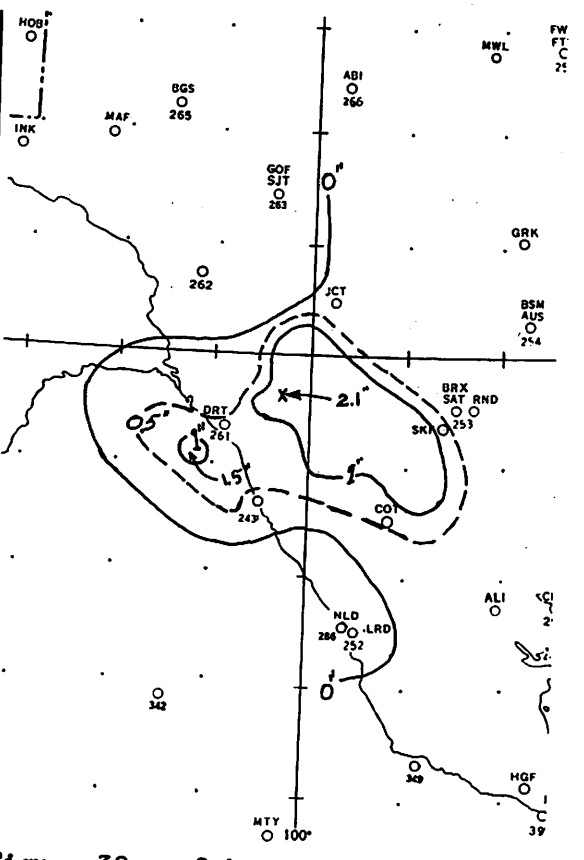

Figure 30. - 6-hr. isohyetal map, 0600-1200 CST, June 26, 1954

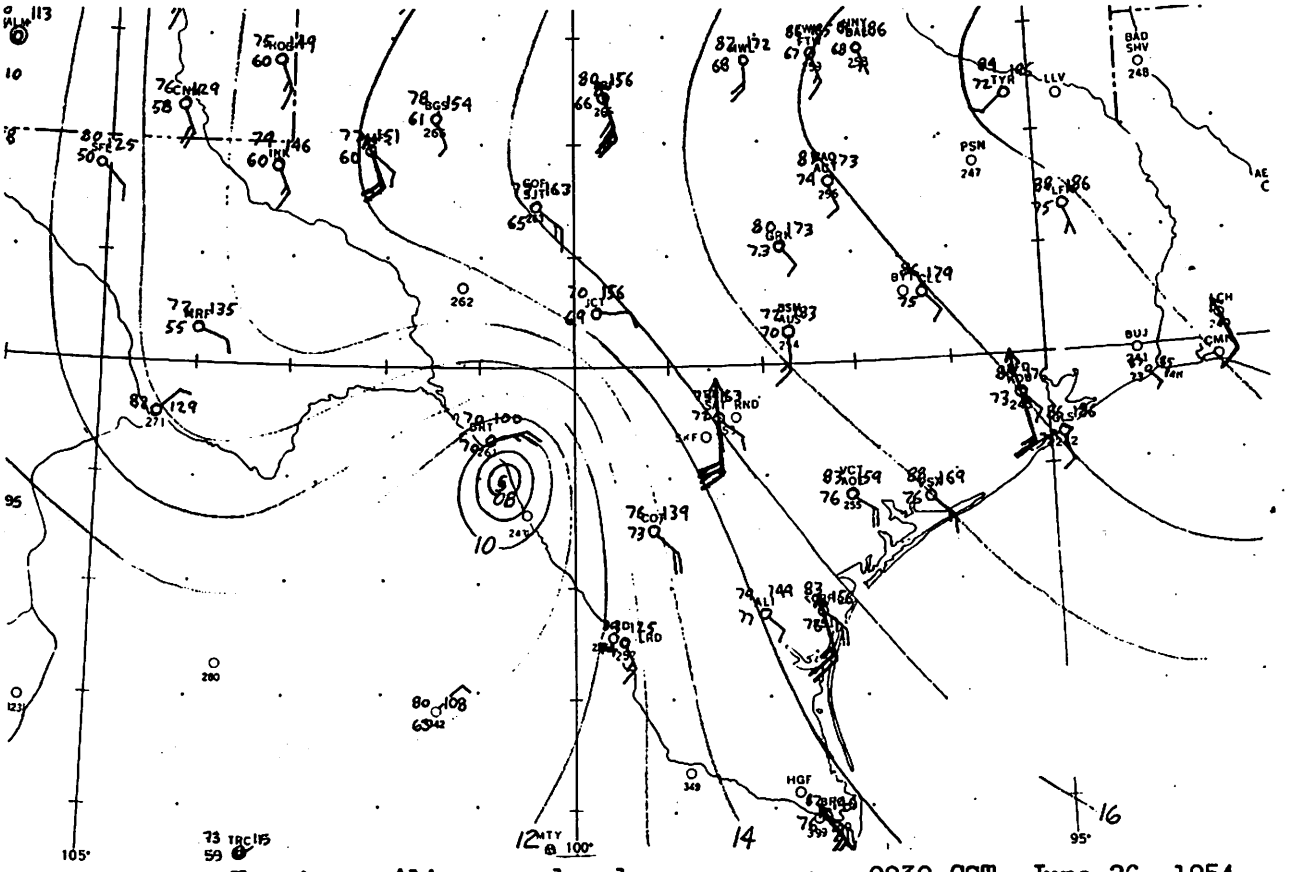

Figure 31. - Hurricane Alice sea level pressure map, 0930 CST, June 26, 1954

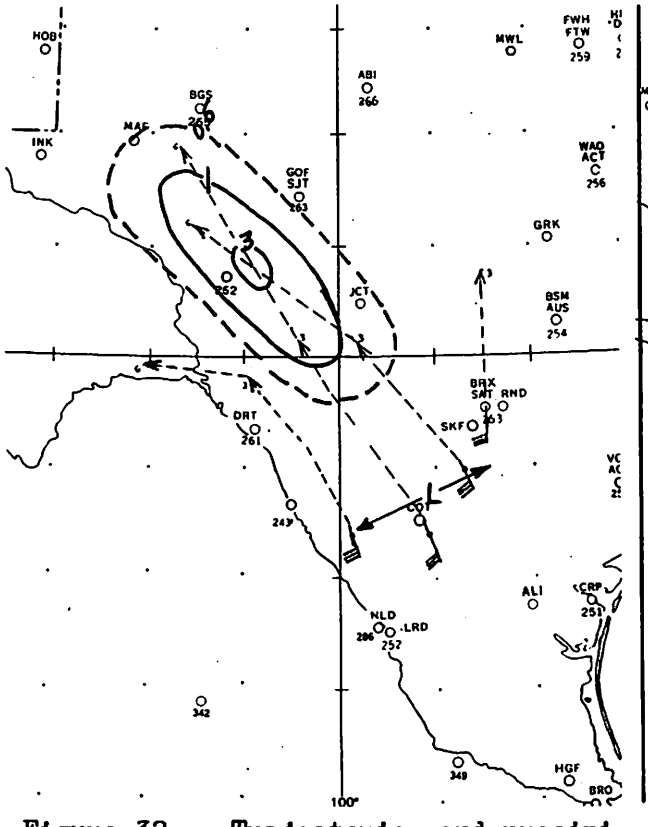

Figure 32. - Trajectories and precipitation forecast, 1200-1800 CST, June 26, 1954

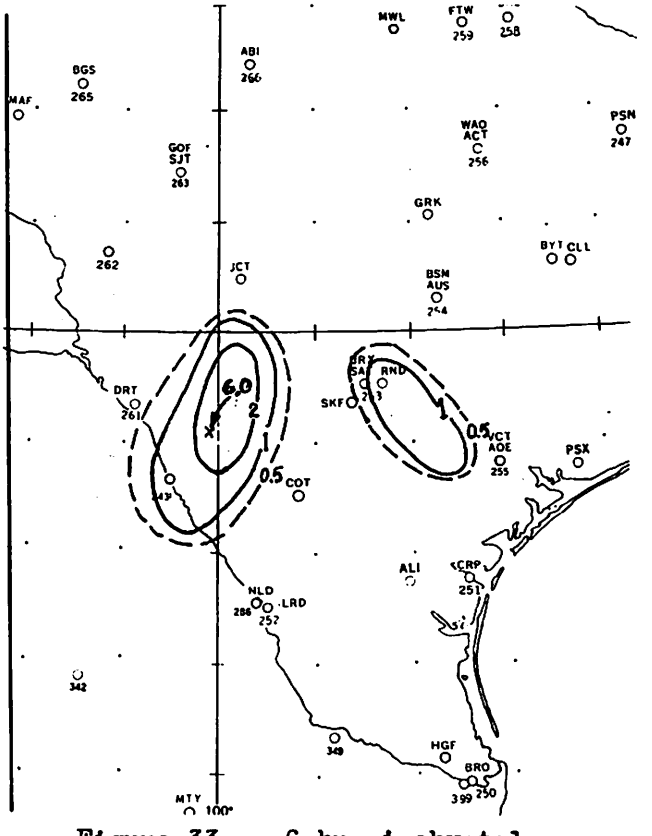

Figure 33. - 6-hr. isohyetal map, 1200-1800 CST, June 26, 1954

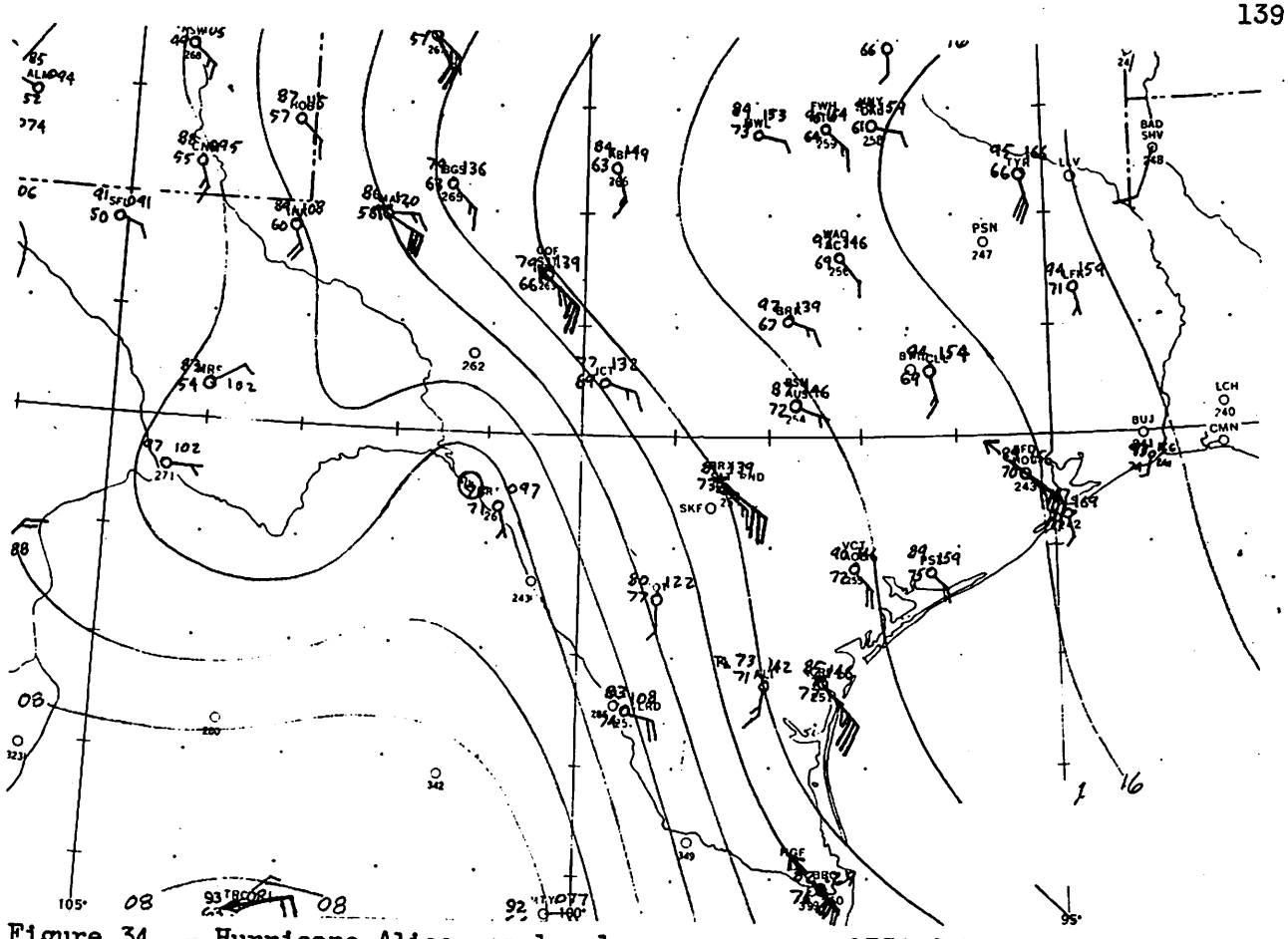

Figure 34. - Hurricane Alice sea level pressure map, 1530 CST, June 26, 1954

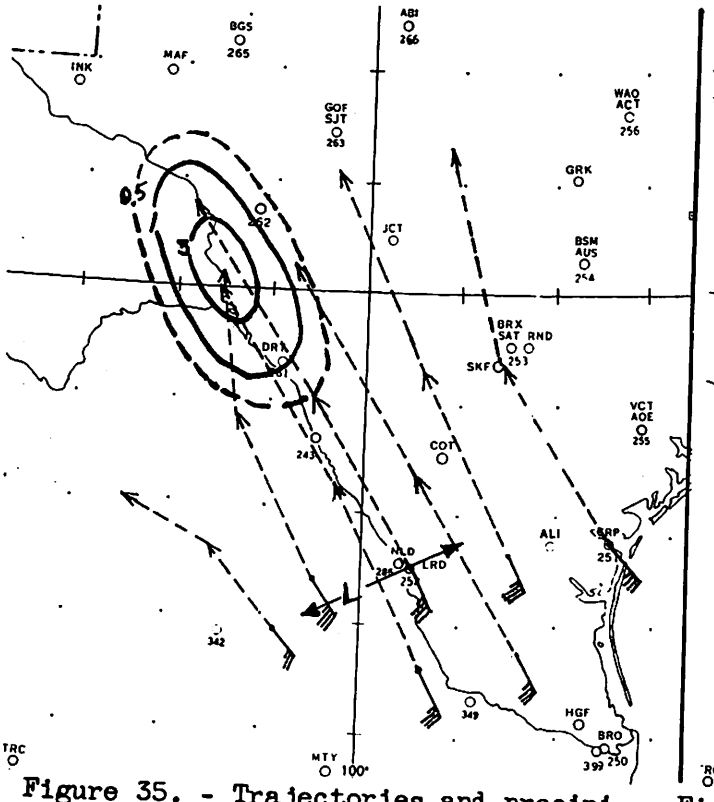

Figure 35. - Trajectories and precipitation forecast, 1800-2400 CST, June 26, 1954

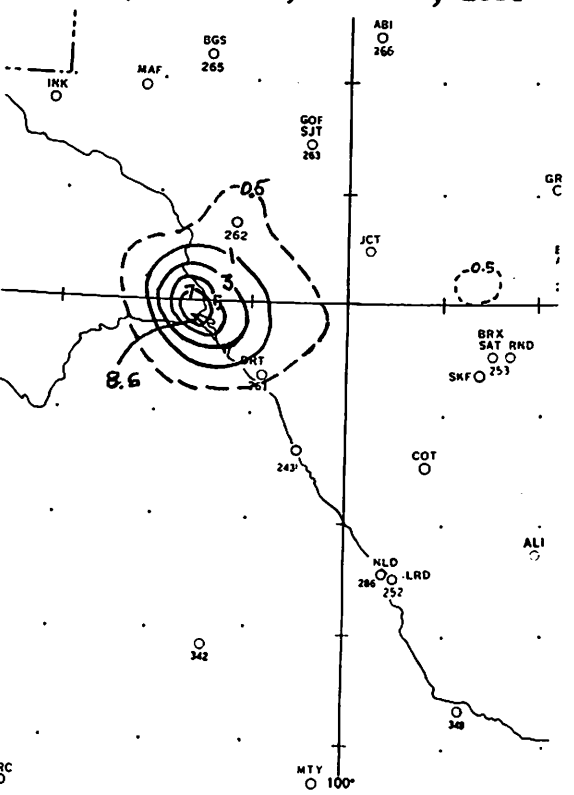

Figure 36. - 6-hr. isohyetal map, 1800-2400 CST, June 26, 1954

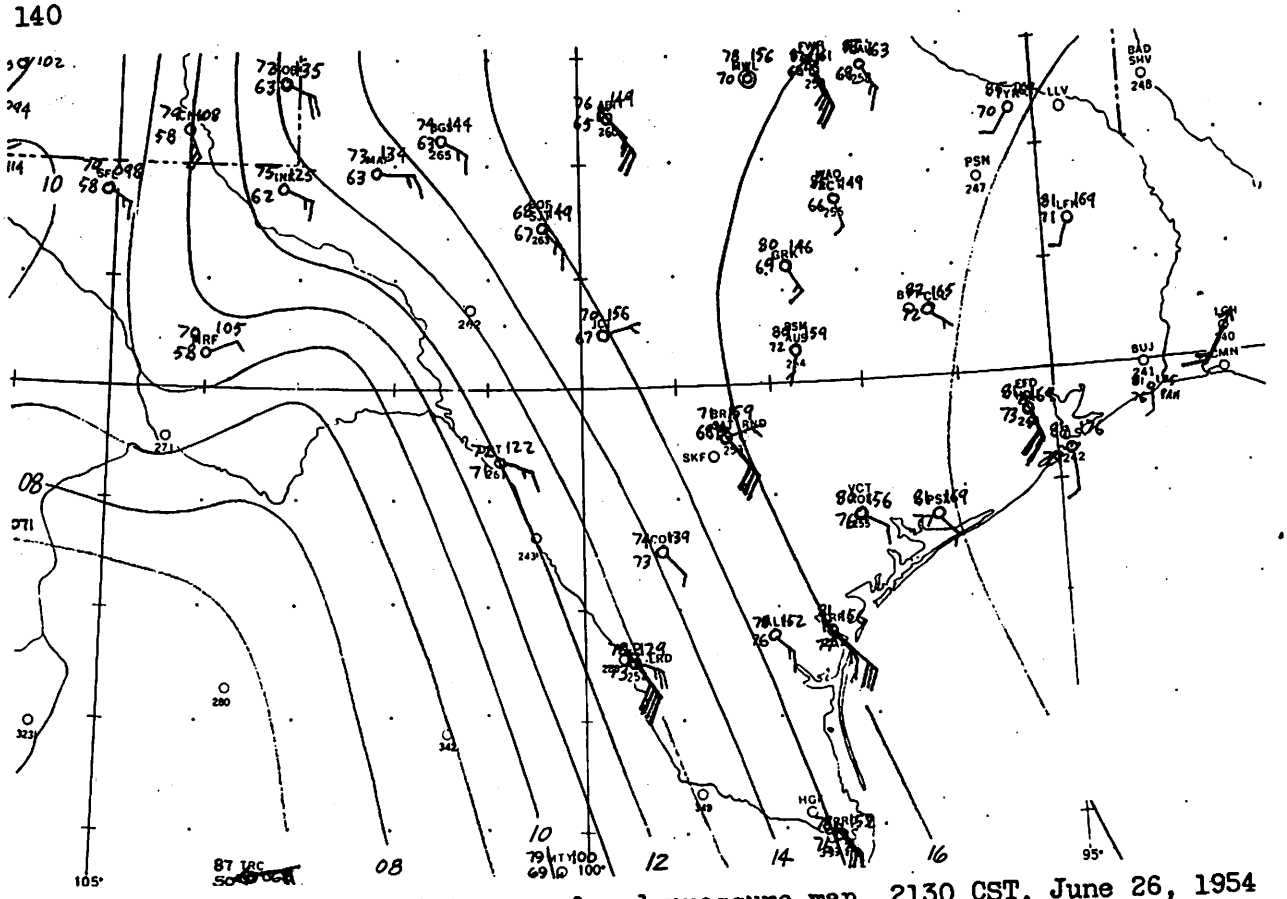

Figure 37. - Hurricane Alice sea level pressure map, 2130 CST, June 26, 1954

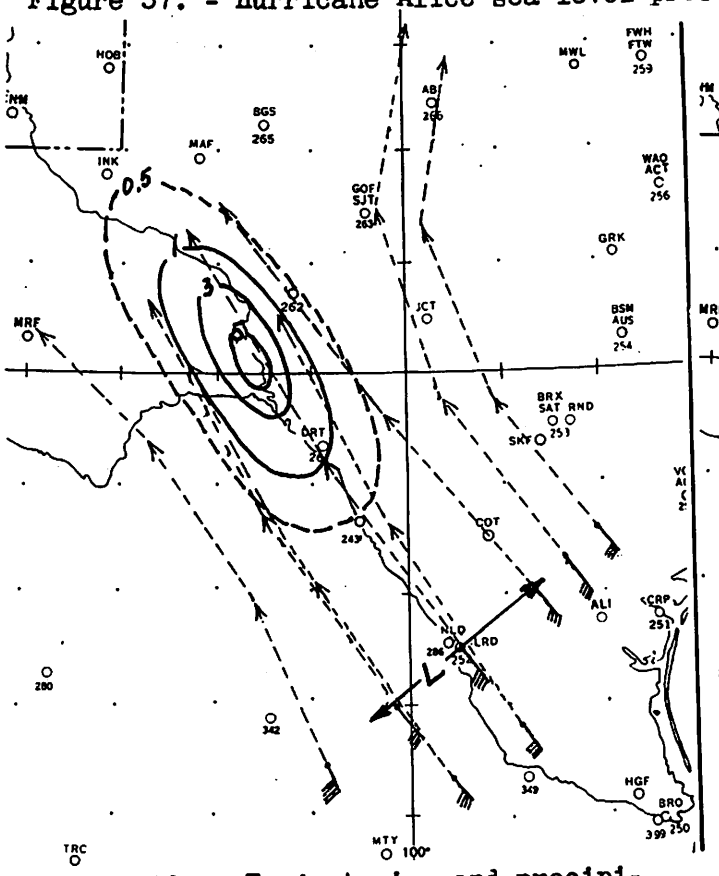

Figure 38. - Trajectories and precipitation forecast, 0000-0600 CST, June 27, 1954

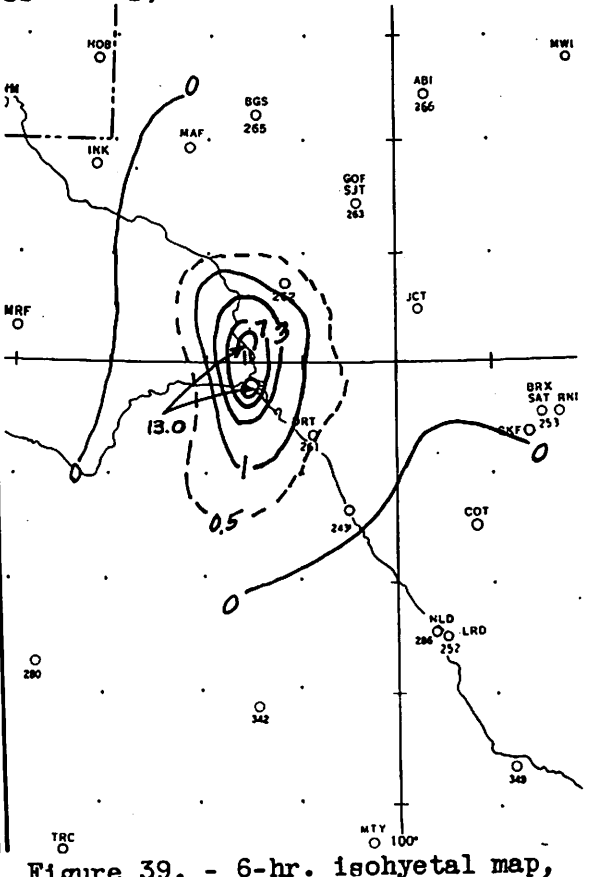

Figure 39. - 6-hr. isohyetal map, 0000-0600 CST, June 27, 1954

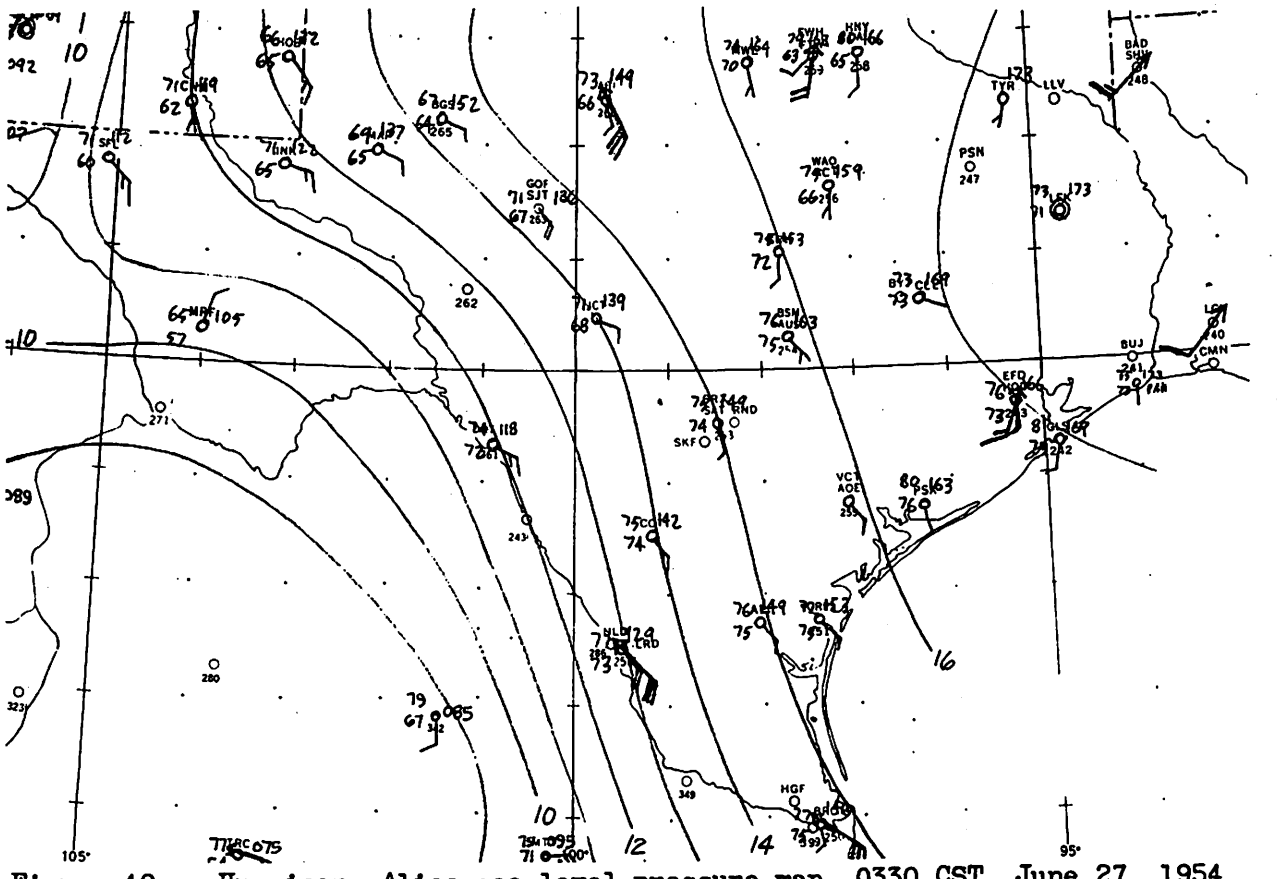

Figure 40. - Hurricane Alice sea level pressure map, 0330 CST, June 27, 1954

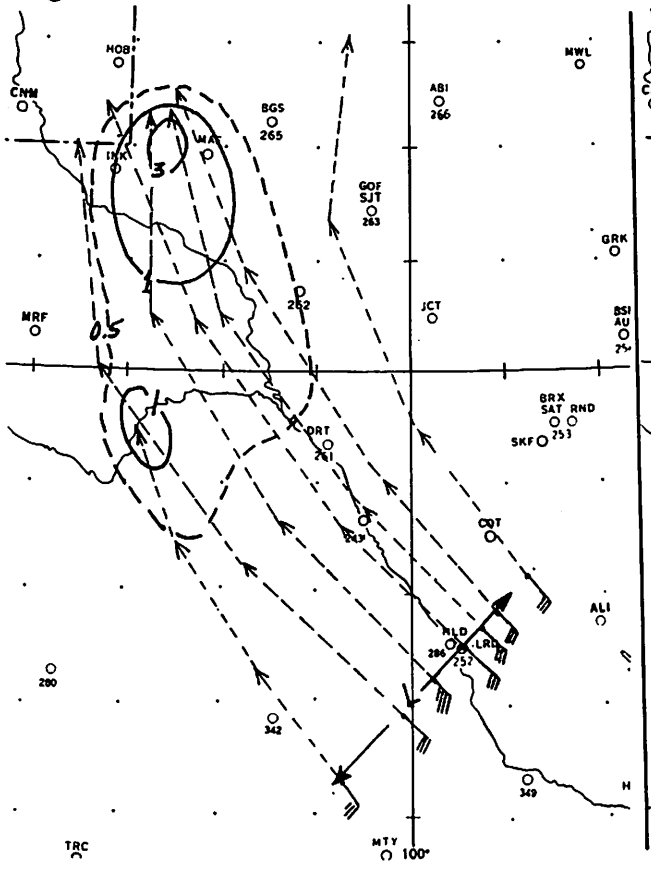

Figure 41. - Trajectories and precipitation forecast, 0600-1200 CST, June 27, 1954

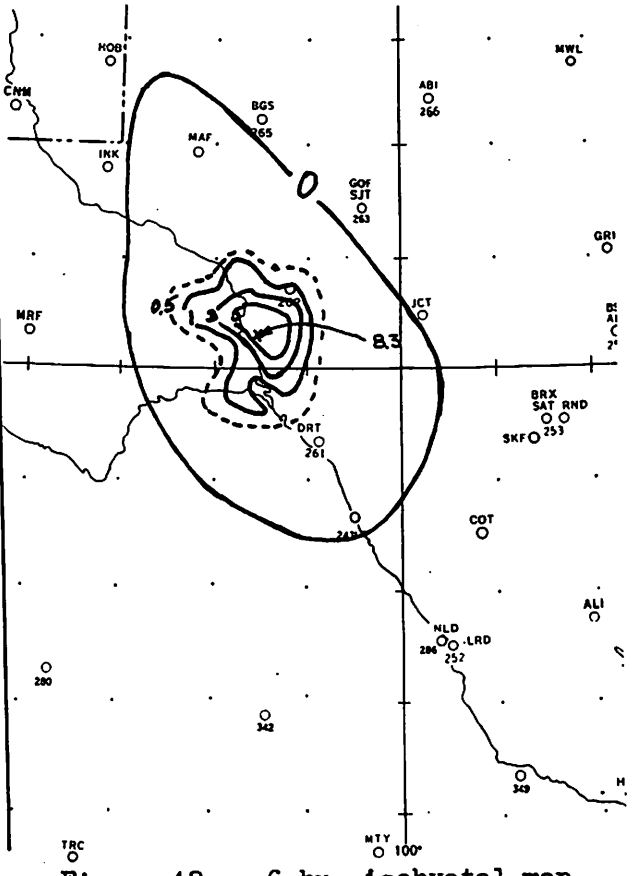

Figure 42. - 6-hr. isohyetal map, 0600-1200 CST, June 27, 1954

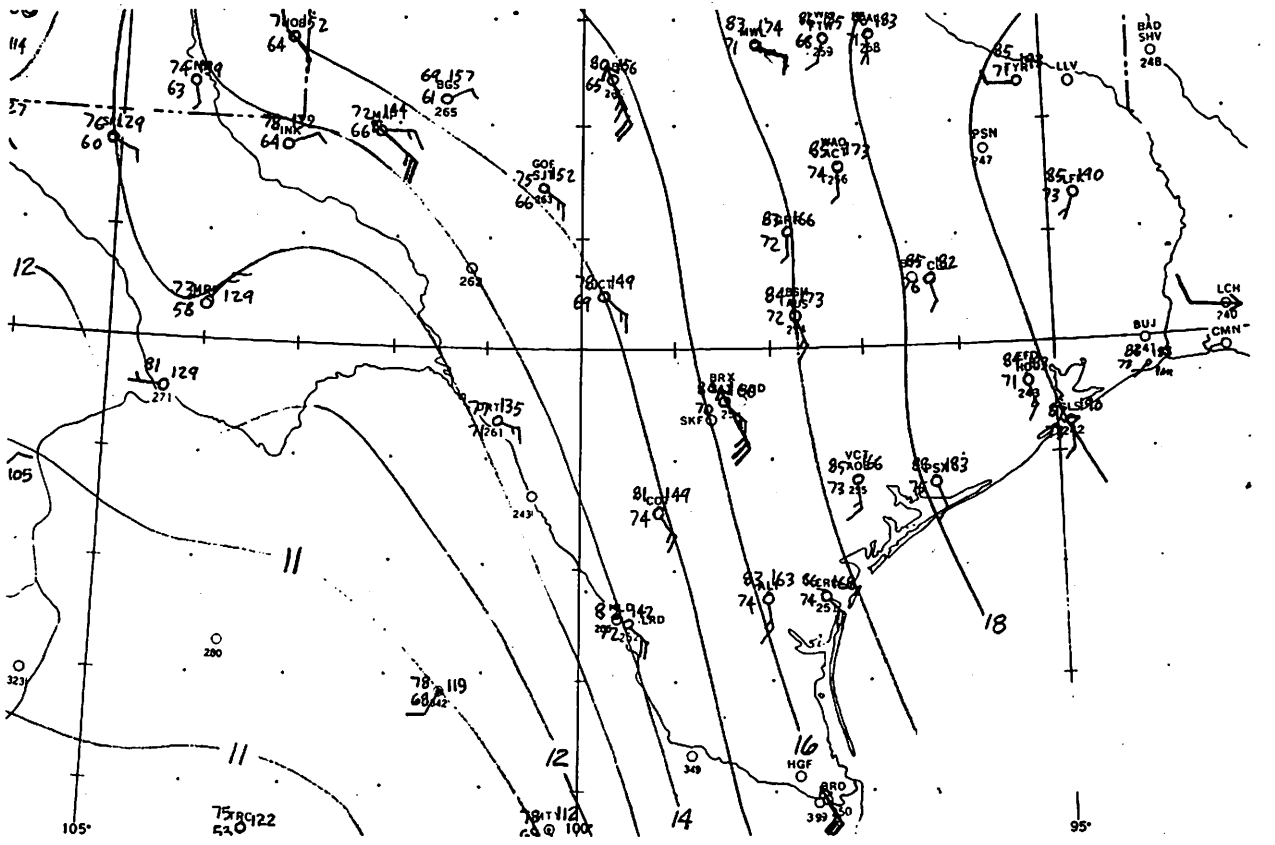

Figure 43. - Hurricane Alice sea level pressure map, 0930 CST, June 27, 1954

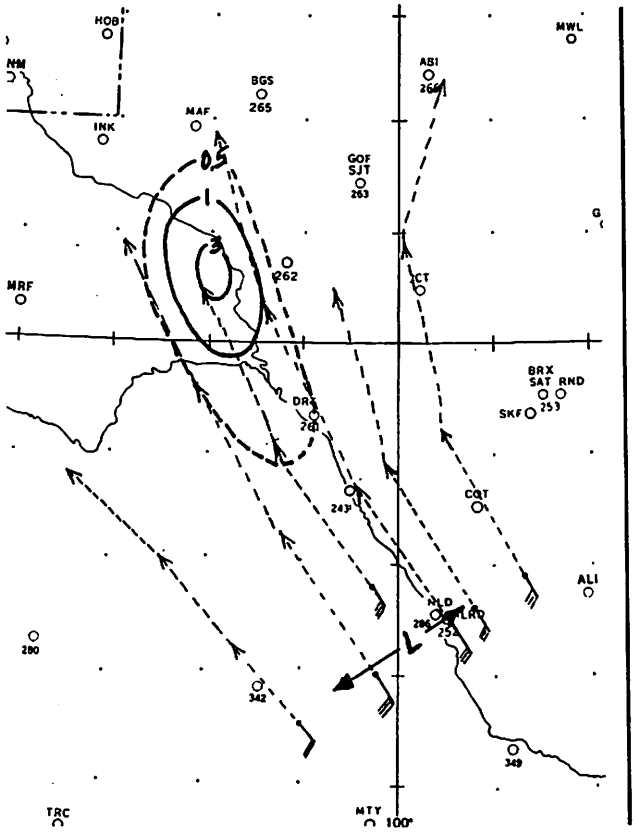

Figure 44. - Trajectories and precipitation forecast, 1200-1800 CST, June 27, 1954

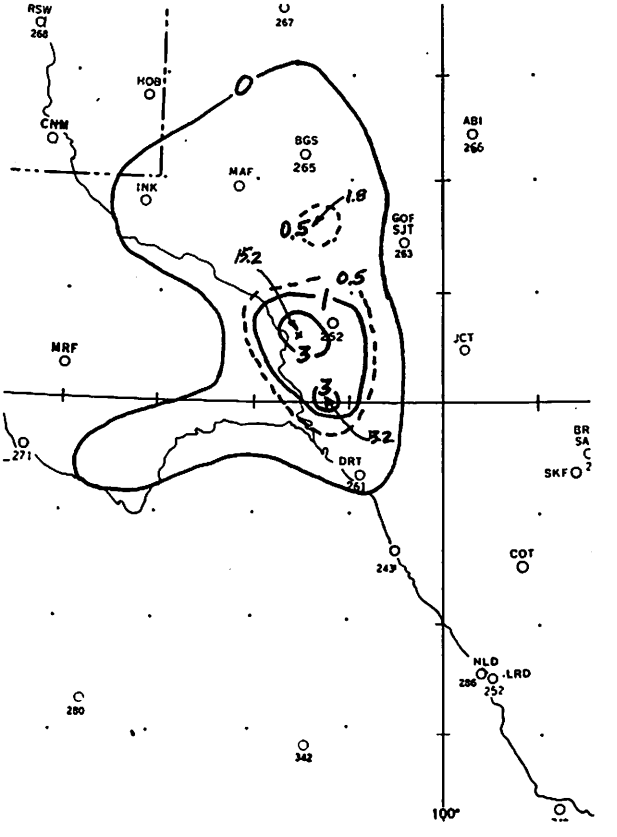

Figure 45. - 6-hr. isohyetal map, 1200-1800 CST, June 27, 1954

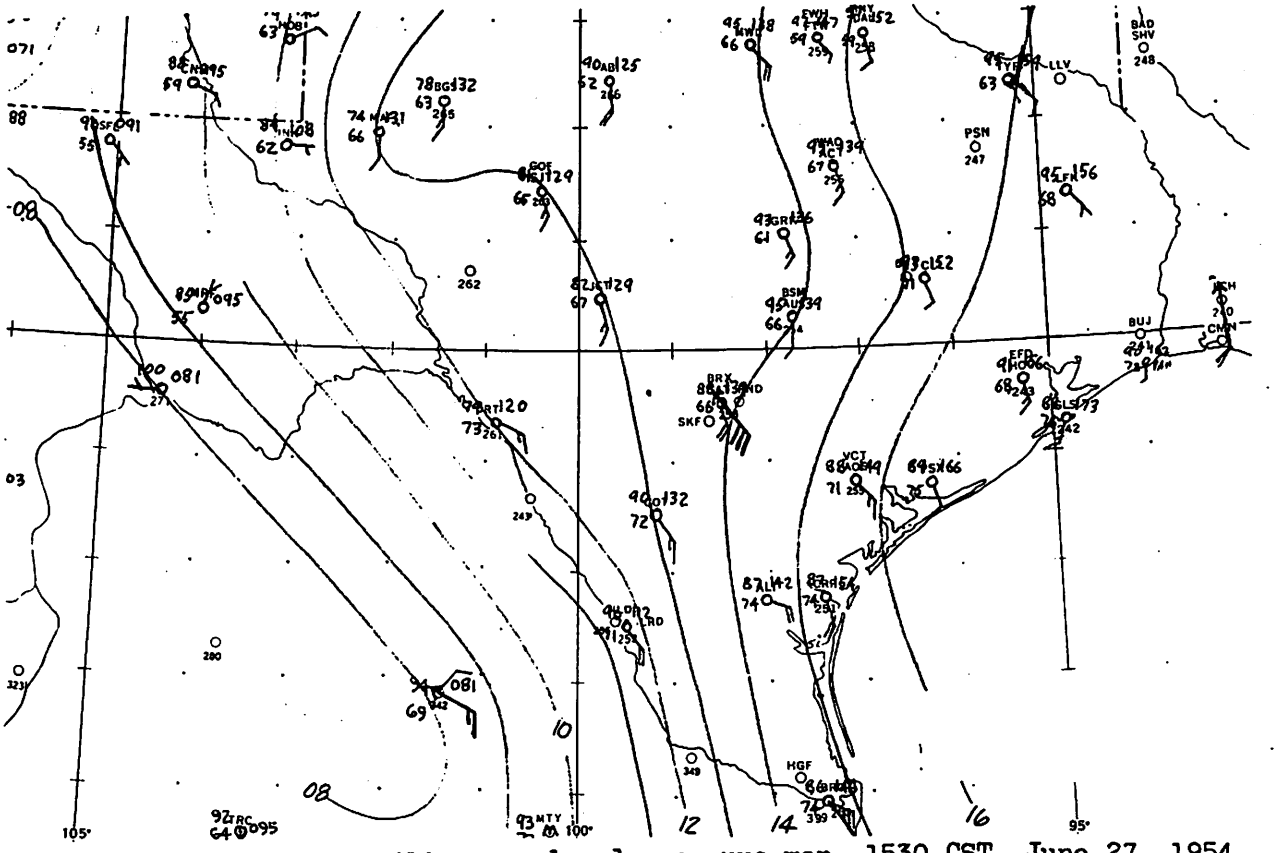

Figure 46. - Hurricane Alice sea level pressure map, 1530 CST, June 27, 1954

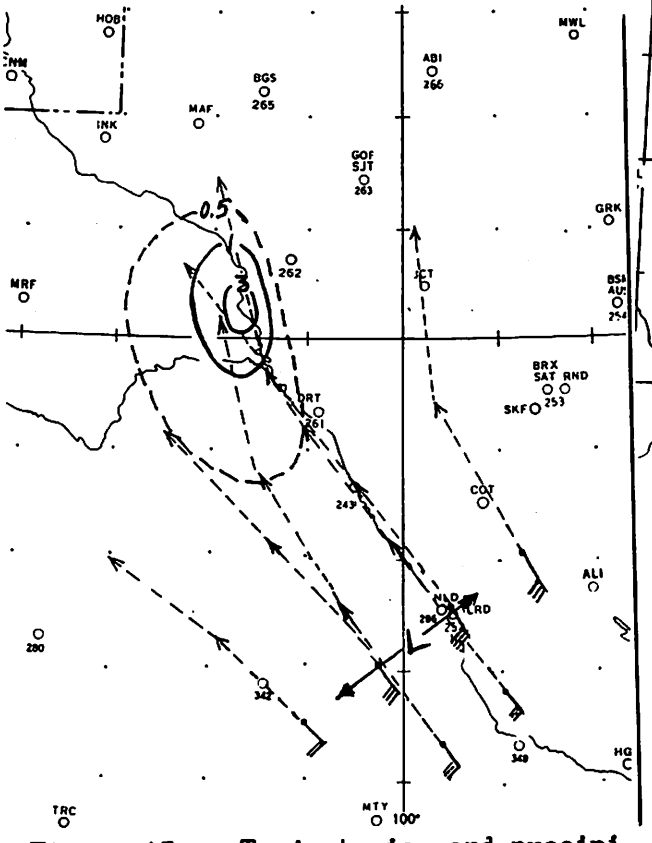

Figure 47. - Trajectories and precipitation forecast, 1800-2400 CST, June 27, 1954

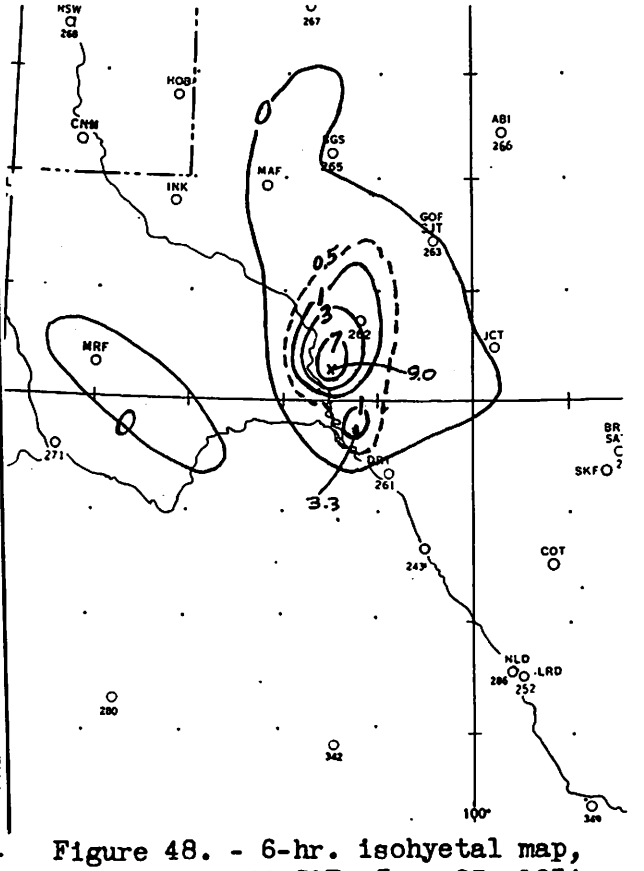

Figure 48. - 6-hr. isohyetal map, 1800-2400 CST, June 27, 1954